Technische Universität München

Fakultät für Chemie

Metabolism from the early evolution of life to complex environments - A new pathway for carbon fixation in deeply-branching bacteria and adaptions of human bacterial pathogens

---

Thomas Maximilian Steiner

Vollständiger Abdruck der von der Fakultät für Chemie der Technischen Universität München zur Erlangung eines

Doktors der Naturwissenschaften (Dr. rer. nat.)

genehmigten Dissertation.

Vorsitzender:	Prof. Dr. Tom Nilges
Prüfer der Dissertation:	1. apl. Prof. Dr. Wolfgang Eisenreich
	2. Prof. Dr. Thomas Brück
	3. Priv.-Doz. Dr. Wolfgang Fischer

Die Dissertation wurde am 28.09.2021 bei der Technischen Universität München eingereicht und durch die Fakultät für Chemie am 10.03.2022 angenommen.

The presented PhD. work was carried out at the Faculty of Chemistry of the Technische Universität München at the Lehrstuhl für Biochemie as well as the Bayerisches NMR Zentrum - Strukturelle Membranbiochemie between March 2017 and August 2021 under the supervision of apl. Prof. Dr. Wolfgang Eisenreich.

Parts of this work have been published:

Steffens L.*, Pettinato E.*, Steiner T. M.*, Mall A., König S., Eisenreich W., Berg I. A. High CO_2 levels drive the TCA cycle towards autotrophy. **Nature** 592, 748-788 (2021), 10.1038/s41586-021-03456-9.

Kunze M.*, Steiner T.*, Chen F., Huber C., Rydzewski K., Stämmler M., Heuner K., Eisenreich W. Metabolic adaption of *Legionella pneumophila* during intracellular growth in *Acanthamoeba castellanii*. **International Journal of Medical Microbiology** 311 (4), 151504 (2021), 10.1016/j.ijmm.2021.151504.

Steiner T. M.*, Lettl C.*, Schindele F., Goebel W., Haas R., Fischer W., Eisenreich W. Substrate usage determines carbon flux *via* the citrate cycle in *Helicobacter pylori*. **Molecular Microbiology** 116 (3), 841-860, (2021), 10.1111/mmi.14775.

Further publications not related to this work:

Steiner T. M., Eisenreich W. Isotopologue profiling of infectious diseases in **Encyclopedia of Infection and Immunity**, Nima Rezai, Amsterdam, Elsevier, 4, 372 (2022), 10.1016/B978-0-12-818731-9.00149-X.

Steiner T.*, Chen F.*, Rydzewski K., Morguet C., Achatz F., Eisenreich W., Heuner K. Metabolic plasticity of *Francisella tularensis* subsp. *holarctica* (wild type), *Francisella novicida* and F*rancisella* sp. strain W12-1067. **German Journal of Microbiology** 2 (1), 19 (2022), 10.51585/gjm.2022.1.0012.

Steffens L.*, Pettinato E.*, Steiner T. M.*, Eisenreich W., Berg I. A., Tracking the reversed oxidative tricarboxylic acid cycle in bacteria. **Bio-protocol** 12 (6), e4364 (2022), 10.21769/BioProtoc.4364.

Spier A., Connor M. G., Steiner T., Carvalho F., Cossart P., Eisenreich W., Wai T., Stavru F. Mitochondrial respiration restricts *Listeria monocytogenes* infection by slowing down host cell receptor recycling. **Cell Reports** 37 (6), 109989 (2021), 10.1016/j.celrep.2021.109989.

Geisberger T., Diederich P., Steiner T., Eisenreich W., Schmitt-Kopplin P., Huber C. Evolutionary steps in the analytics of primordial metabolic evolution. **Life** 9 (2), 50 (2019).

*These authors contributed equally as first authors.

"Nature doesn't ask your permission; it doesn't care about your wishes, or whether you like its laws or not. You're obliged to accept it as it is, and, consequently all its results as well"

Fyodor Dostoevsky

Table of contents

Abstract

Bacteria are the most diverse domain of life. This diversity arises through the different ecological niches they are able to colonize. Adaptability herein is based on adjusting their metabolic demands to the available nutrients in the respective niche, as the environment dictates the possibilities as well as necessities of cellular metabolism. Subsequently, similar environments should produce similar metabolic phenotypes. Therefore, by recreating the putative ecological niche of an organism one can study its metabolism, even when studies in the actual environment are not possible.

For the direct assessment of active metabolism, meaning the intracellular fluxes of metabolites, stable isotope labelling today is the benchmark technology. Herein an isotopically enriched tracer is added to growing bacteria and afterwards stable metabolic products are isolated. Analysis of their respective isotopologue composition allows statements about the activity and flux in specific metabolic pathways.

One of the most important but inaccessible bacterial metabolic phenotypes is the metabolism of the earliest cellular organism. Understanding the metabolism of this organism bridges the gap between abiotic reactions producing the first biomolecules and the emergence of cellular life. The first organism probably emerged at hydrothermal vents and was dependent on autotrophic carbon fixation. Recently the reverse oxidative tricarboxylic acid (roTCA) cycle was discovered as a new pathway for CO_2-fixation. To get more insights into the driving force of this pathway and its relevance for the first cellular organism, it was studied in *Hippea maritima*. This bacterium lives in association with hydrothermal vents and thereby presents a suitable surrogate system for the investigation of carbon fixation under conditions similar to the early earth. Labelling experiments with $^{13}CO_2$ together with protein quantification showed that the cycle requires high cellular levels of citrate synthase as well as high partial pressures of CO_2 to operate efficiently. This is necessary to allow the thermodynamically unfavourable citrate cleavage, as acetyl-CoA has to be removed from the equilibrium through carboxylation to pyruvate. Based on these results, the roTCA cycle at the moment is the most plausible carbon fixation pathway in the earliest cellular organism. It is energetically highly efficient, its intermediates act as precursors for a variety of cellular building blocks and its activity is correlated with an increased CO_2-concentration that was present on the primordial earth.

While during early evolution efficient CO_2-fixation was the essential trait to sustain life, most organisms today are heterotrophs and therefore require a complex mixture of nutrients to survive. To extend and thereby generalize the connection between environment and bacterial metabolism, two heterotrophic bacteria were further studied in this work; despite both being heterotrophs, these organisms still show great disparities in their life style. On the one hand, *Legionella pneumophila* is mostly found in fresh-water and soil, while replication only occurs inside a variety of host cells like amoeba and also human alveolar macrophages. On the other hand, *Helicobacter pylori* is exclusively found in the human stomach in the extracellular environment of gastric epithelial cells, where it has experienced a prolonged coevolution with the human host.

To study the metabolic capabilities of *H. pylori*, it was cultivated in a complex medium, that resembles its ecological niche during infection, with the addition of a variety of ^{13}C-labelled tracers. This revealed an adaptive TCA cycle fully operating in the closed oxidative direction with rapid equilibrium fluxes between oxaloacetate—succinate and α-ketoglutarate—citrate. ^{13}C-Profiles of

the four-carbon intermediates in the TCA cycle, especially of malate, together with the observation of an isocitrate lyase activity by *in vitro* assays, suggested carbon fluxes *via* a glyoxylate bypass. In conjunction with the lack of enzymes for anaplerotic CO_2 fixation, the glyoxylate bypass could be relevant to fill up the TCA cycle with carbon atoms derived from acetyl-CoA.

L. pneumophila employs a biphasic life-style, wherein after an initial replicative phase, virulence factors are expressed in the transmissive phase upon the shortage of nutrients. This biphasic behaviour suggests also metabolic adaptions during the life cycle. The growth-phase dependent metabolism of *L. pneumophila* was therefore analysed during growth in *Acanthamoeba castellanii*. During the whole infection cycle *L. pneumophila* incorporated amino acids from its host into the bacterial proteins. However, partial bacterial *de novo* biosynthesis from exogenous ^{13}C-serine and, at minor rates, from ^{13}C-glucose could be shown for bacterial alanine, aspartate, glutamate, and glycine. Usage of serine increased during the post-exponential phase of intracellular growth, whereas glucose was utilized by the bacteria throughout the infection cycle and not only late during infection as assumed on the basis of earlier *in vitro* experiments. The early usage of ^{13}C-glucose by the intracellular bacteria suggests that glucose availability could serve as a trigger for replication of *L. pneumophila* inside the vacuoles of host cells.

Taken together, studies in surrogate systems of the respective niche allow to investigate bacterial metabolic adaptions to vastly different environments. The work in *H. maritima* demonstrated how sensitive the cellular metabolism reacts to changes in the growth environment on the molecular level, namely the CO_2-partial pressure. Similarly, the heterotrophic organisms studied in this work showed idiosyncratic adaptions to their respective ecological niches. While *L. pneumophila* potentially uses glucose as a signalling molecule instead of a nutrient source as common in many bacteria, *H. pylori* does not depend on CO_2-fixation anymore in its central metabolic network, demonstrating its immense deviations from the earliest cellular organisms.

L. pneumophila and *H. pylori* also represent human pathogens. Regarding pathogenic bacteria, the connection between environment and metabolism could be utilised to develop new treatment strategies. These are desperately needed due to rising antibiotic resistance. However, in pathogens this interplay between environment and metabolism is further complicated by the fact that they inhabit a living niche, which they also interact with through virulence factors. As the environment controls the metabolism of the pathogen, which is again connected to the expression of virulence factors, a different nutritional environment should provoke differences in virulence. Therefore, modulation of the host metabolism – representing the environment – should influence bacterial virulence to yield a promising way to battle bacterial infections.

Kurzzusammenfassung

Bakterien bilden die vielfältigste Domäne des Lebens. Diese Vielfalt ergibt sich aus der Vielzahl von ökologischen Nischen, die sie besiedeln können. Ihre Anpassungsfähigkeit beruht dabei auf der Anpassung ihrer Stoffwechselbedürfnisse an die in der jeweiligen Nische verfügbaren Nährstoffe, denn die Umwelt diktiert sowohl die Möglichkeiten als auch die Notwendigkeiten des zellulären Stoffwechsels. Folglich sollten ähnliche Umgebungen ähnliche metabolische Phänotypen erzeugen. Die Nachbildung der vermeintlichen ökologischen Nische eines Organismus ermöglicht daher Studien zum Stoffwechsel, selbst wenn Studien in der tatsächlichen Umgebung nicht möglich sind.

Für die direkte Analyse des aktiven Stoffwechsels, d. h. der intrazellulären Stoffflüsse, ist die Markierung mit stabilen Isotopen heute die maßgebliche Technologie. Dabei wird ein isotopenangereicherter "Tracer" Bakterienkulturen während des Wachstums zugesetzt und anschließend werden stabile Stoffwechselprodukte isoliert. Die Analyse der jeweiligen Isotopenzusammensetzung erlaubt Aussagen über die Aktivität und den Fluss in bestimmten Stoffwechselwegen.

Einer der wichtigsten, aber unzugänglichen bakteriellen Stoffwechselphänotypen ist der Stoffwechsel des ersten zellulären Organismus. Das Verständnis des Stoffwechsels dieses Organismus schließt die Lücke zwischen abiotischen Reaktionen, welche die ersten Biomoleküle hervorgebracht haben, und der Entstehung des zellulären Lebens. Der erste Organismus entstand wahrscheinlich an hydrothermalen Quellen und war auf autotrophe Kohlenstofffixierung angewiesen. Kürzlich wurde der reverse oxidative Tricarbonsäurezyklus (roTCS) als neuer Weg zur CO_2-Fixierung entdeckt. Um mehr Einblicke in die Triebkraft dieses Weges und seine Bedeutung für den ersten zellulären Organismus zu erhalten, wurde er in *Hippea maritima* untersucht.

Dieses Bakterium lebt in der Umgebung von hydrothermalen Quellen und stellt damit ein geeignetes Surrogatsystem für die Untersuchung der Kohlenstofffixierung unter ähnlichen Bedingungen wie auf der frühen Erde dar. Markierungsexperimente mit $^{13}CO_2$ zusammen mit der Quantifizierung von Proteinen zeigten, dass der Zyklus hohe zelluläre Mengen von Citrat-Synthase sowie hohe Partialdrücke von CO_2 benötigt, um effizient zu funktionieren. Dies ist notwendig, um die thermodynamisch ungünstige Citratspaltung zu ermöglichen, da Acetyl-CoA durch Carboxylierung zu Pyruvat aus dem Gleichgewicht entfernt werden muss. Auf Grundlage dieser Ergebnisse ist der roTCS-Zyklus derzeit der plausibelste Kohlenstofffixierungsweg im frühesten zellulären Organismus. Er ist energetisch hocheffizient, seine Zwischenprodukte dienen als Vorstufen für eine Vielzahl von Zellbausteinen und seine Aktivität korreliert mit einer erhöhten CO_2-Konzentration, die auf der Urerde vorhanden war.

Während in der frühen Evolution effiziente CO_2-Fixierung die wesentliche Eigenschaft zur Erhaltung des Lebens war, sind die meisten Organismen heute heterotroph und benötigen zum Überleben eine komplexe Mischung von Nährstoffen. Um den Zusammenhang zwischen Umwelt und bakteriellem Stoffwechsel zu erweitern und damit zu verallgemeinern, wurden in dieser Arbeit zwei Bakterien näher untersucht, die zwar beide heterotroph sind, aber dennoch große Unterschiede in ihrer Lebensweise zeigen.

Einerseits kommt *Legionella pneumophila* hauptsächlich in Süßwasser und im Boden vor, während die Replikation nur in Wirtszellen wie Amöben und auch menschlichen Alveolarmakrophagen stattfindet. *Helicobacter pylori* hingegen ist ausschließlich im menschlichen Magen in der

extrazellulären Umgebung von Magenepithelzellen zu finden, wo es eine lange Koevolution mit dem menschlichen Wirt erlebt hat.

Um die metabolischen Fähigkeiten von *H. pylori* zu untersuchen, wurde das Baktrium in einem komplexen Medium kultiviert, das seiner ökologischen Nische während der Infektion ähnelt, und es wurden verschiedene ^{13}C-markierte Tracer hinzugefügt. Diese Experimente zeigten einen adaptiven TCS-Zyklus, der geschlossener in oxidativer Richtung mit schnellen Gleichgewichtsflüssen zwischen Oxalacetat-Succinat und α-Ketoglutarat-Citrat arbeitet. ^{13}C-Profile der C$_4$-Zwischenprodukte im TCS-Zyklus, insbesondere von Malat, zusammen mit der Beobachtung einer Isocitrat-Lyase-Aktivität durch *in-vitro*-Assays, ließen auf Kohlenstoffflüsse über einen Glyoxylat-Bypass schließen. In Verbindung mit dem Fehlen von Enzymen für die anaplerotische CO_2-Fixierung könnte der Glyoxylat-Bypass von Bedeutung sein, um den TCS-Zyklus mit Kohlenstoffatomen aus Acetyl-CoA aufzufüllen.

L. pneumophila zeigt eine biphasische Lebensweise, bei der nach einer anfänglichen Replikationsphase in der folgenden transmissiven Phase bei Nährstoffmangel Virulenzfaktoren exprimiert werden. Dieses biphasische Verhalten lässt auch auf metabolische Anpassungen während des Lebenszyklus schließen. Daher wurde der wachstumsphasenabhängige Stoffwechsel von *L. pneumophila* während des Wachstums in *Acanathamoeba castellanii* analysiert. Während des gesamten Infektionszyklus baute *L. pneumophila* Aminosäuren aus seinem Wirt in die bakteriellen Proteine ein. Für Alanin, Aspartat, Glutamat und Glycin konnte jedoch eine partielle bakterielle *de novo*-Biosynthese aus exogenem ^{13}C-Serin und in geringerem Umfang aus ^{13}C-Glukose nachgewiesen werden. Die Verwendung von Serin nahm während der postexponentiellen Phase des intrazellulären Wachstums zu, während Glukose von den Bakterien während des gesamten Infektionszyklus verwendet wurde und nicht nur zu späteren Zeitpunkten der Infektion, wie aufgrund früherer *in-vitro*-Experimente angenommen. Die frühe Verwendung von ^{13}C-Glukose durch die intrazellulären Bakterien deutet darauf hin, dass die Verfügbarkeit von Glukose als Auslöser für die Replikation von *L. pneumophila* in den Vakuolen der Wirtszellen dienen könnte.

Insgesamt ermöglichen Studien in Surrogatsystemen der jeweiligen Nische die Untersuchung der bakteriellen metabolischen Anpassungen an sehr unterschiedliche Umgebungen. Die Arbeiten an *H. maritima* haben gezeigt, wie empfindlich der zelluläre Stoffwechsel auf molekularer Ebene auf Veränderungen in der Wachstumsumgebung reagiert, in diesem Fall den CO_2-Partialdruck. In ähnlicher Weise zeigten die in dieser Arbeit untersuchten heterotrophen Organismen idiosynkratische Anpassungen an ihre jeweiligen ökologischen Nischen. Während *L. pneumophila* möglicherweise Glukose als Signalmolekül statt als Nährstoffquelle nutzt, wie es bei vielen Bakterien üblich ist, ist *H. pylori* in seinem zentralen Stoffwechselnetz nicht mehr auf CO_2-Fixierung angewiesen, was seine immensen Abweichungen von den frühesten zellulären Organismen zeigt.

L. pneumophila und *H. pylori* sind darüber hinaus menschliche Krankheitserreger. Bei den pathogenen Bakterien könnte der Zusammenhang zwischen Umwelt und Stoffwechsel genutzt werden, um neue Behandlungsstrategien zu entwickeln.

Diese werden aufgrund der zunehmenden Antibiotikaresistenz dringend benötigt. Bei Krankheitserregern wird dieses Wechselspiel zwischen Umwelt und Stoffwechsel jedoch noch dadurch verkompliziert, dass Sie eine lebendige Nische bewohnen, mit der sie auch durch Virulenzfaktoren interagieren. Da die Umwelt den Stoffwechsel des Erregers steuert, der wiederum mit der Expres-

sion von Virulenzfaktoren zusammenhängt, sollten andere Nährstoffe in der Umwelt zu Unterschieden in der Virulenz führen. Daher sollte die Modulation des Wirtsstoffwechsels - der die Umwelt repräsentiert - die bakterielle Virulenz beeinflussen und einen vielversprechenden Weg zur Bekämpfung bakterieller Infektionen eröffnen.

List of abbreviations

2-OG	2-oxoglutarate	FT-IR	Fourier-transform infrared
3-PG	3-phosphoglycerate		
A. castellanii/Ac	*Acanthamoeba castellanii*	GAP	glyceraldehyde-3-phosphate
ATP	adenosine triphosphate	GAS	glyoxylate shunt – anaplerosis – succinyl-CoA synthetase
BB	*Brucella* broth		
cagA	cytotoxin associated gene A	GC	gas chromatography
		H. maritima	*Hippea maritima*
CCM	central carbon metabolism	*H. pylori*	*Helicobacter pylori*
		HUVEC	human umbilical vein endothelial cells
Ccp	carbon catabolite protein		
CoA	coenzyme A	KDPG	2-keto-3-desoxy-phosphogluconate
Cra	catabolite repressor/activator		
		KEGG	Kyoto encyclopedia of genes and genomes
Csr	carbon storage regulator		
		Lag P	lag phase
C. trachomatis	*Chlamydia trachomatis*	LamA	*Legionella* amylase A
		LC	liquid chromatography
D. acetivorans	*Desulfurella acetivorans*	LCV	*Legionella* containing vacuole
DAMM	danger associated molecular motif	*L. monocytogenes*	*Listeria monocytogenes*
DNA	desoxyribonucleic acid	*L. pneumophila*	*Legionella pneumophila*
E4P	erythrose-4-phosphate	LUCA	last universal common ancestor
E. coli	*Escherichia coli*		
ED	Entner Doudoroff	MFA	metabolic flux analysis
EMP	Embden Meyerhof Parnas	*M. leprae*	*Mycobacterium leprae*
FCS	fetal calve serum	MS	mass spectrometry

mTORC1	mechanistic target of rapamycin complex 1	TCA	tricarboxylic acid
M. tuberculosis	*Mycobacterium tuberculosis*	TP	transmissive phase
NADH	nicotinamide adenine dinucleotide	VacA	vacuolating toxin A
NADPH	nicotinamide adenine dinucleotide phosphate	WT	wild type
NMR	nuclear magnetic resonance		
OAA	oxaloacetate		
P. aeruginosa	*Pseudomonas aeruginosa*		
PAMP	pathogen associated molecular pattern		
PEP	phosphoenolpyruvate		
PHB	polyhydroxybutyrate		
PPP	pentose phosphate pathway		
R5P	ribulose-5-phosphate		
RP	replicative phase		
roTCA cycle	reverse oxidative TCA cycle		
rTCA cycle	reverse TCA cycle		
S. aureus	*Staphylococcus aureus*		
S. flexneri	*Shigella flexneri*		
S. pneumoniae	*Streptococcus pneumoniae*		
S. typhimurium	*Salmonella typhimurium*		
T4SS	type 4 secretion system		

1 Introduction

1.1 Bacteria as the most adaptive domain of life

". . .Lying huddled together and wriggling, just as if you saw with your naked eye a whole tubful of very little eels and water, the eels moving about in swarms; and the whole water seemed to be alive with the multitudinous animalcules. For me this was among all the marvels that I have discovered in nature the most marvellous of all, and I must say that, for my part, no more pleasant sight has yet met my eye than this of so many thousands of living creatures in one small drop of water, all huddling and moving, but each creature having its own motion." (1). In 1674, Antonie van Leeuwenhoek had the first glimpse into the microbial world through his self-built microscope (2). During ~350 years following his discovery, unicellular microorganisms and especially bacteria have been recognised as the oldest, most diverse and most prevalent kingdom of life (3).

The first unicellular organism, the last universal common ancestor (LUCA) living about 3.5 billion years ago, is thought to have been a bacterial cell (4, 5). Today, bacteria account for about 70 Gt of organic carbon thereby being responsible for about 15 % of all organic carbon on the earth (6). In the human body, there are equally as many bacterial cells as human cells (~37 trillion) (7). Their unrivalled ability to adapt through evolution has allowed them to subdue basically any niche on earth as their habitat. Bacteria have been found in potentially life-hostile environments covering temperature ranges from –20 to 110°C, enduring pH-values from 0.7-11 and thriving in salinities up to e. g. five mol/L of NaCl (8). Fig. 1 gives an overview of extreme habitats, where bacteria have been isolated from. Not only do they inhabit every ecological niche on earth but even more so they shaped the overall ecology of the globe. Free oxygen has only been present on earth for about 2.4 billion due to the activity of photosynthetic cyanobacteria (9).
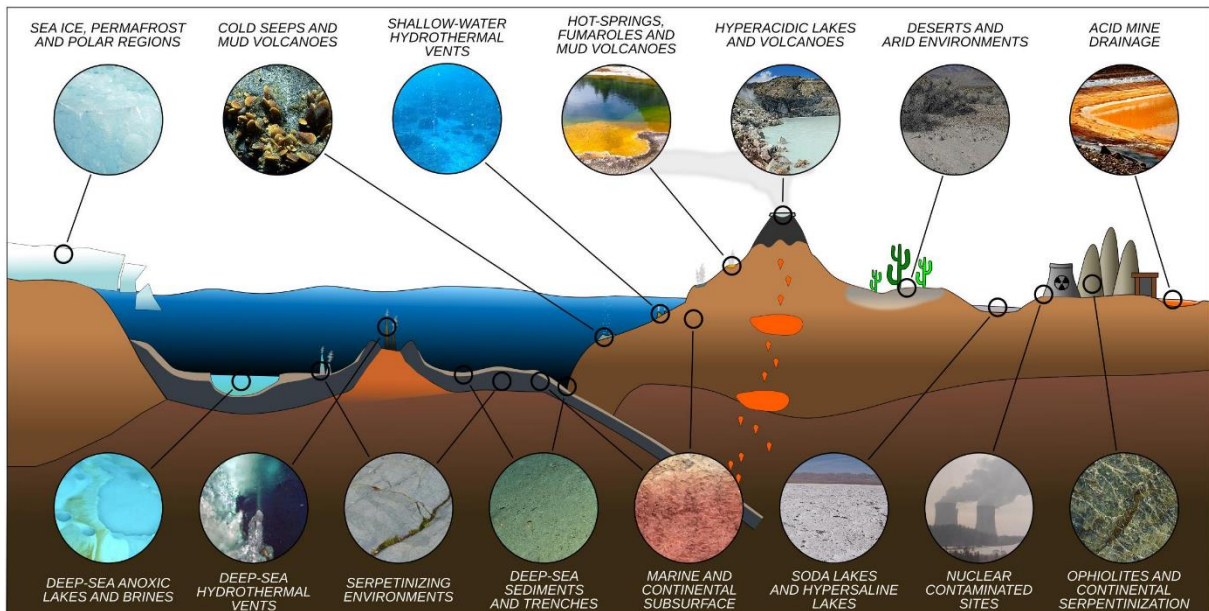

Figure 1 Schematic overview of potentially uninhabitable environments, bacteria have been isolated from (8).

Although higher animals are often considered the pinnacle of evolution, bacteria might be even more astounding in terms of the countless variations they produced from supposedly unicellular simplicity.

They are the most diverse kingdom of life, whereby the full extent of species in this domain has not been captured yet (10). While theoretical estimations suggest up to a trillion different bacterial species (11, 12), a census-based approach proposes 2.2-4.3 million species (13). Regardless of the actual number there is a wide gap between these estimations and the ~10.000 bacterial species known today (11).

"Nothing in biology makes sense except in the light of evolution" as Theodosius Dobzhansky put it (14). One of the main reasons for this unrivalled flexibility of bacteria is metabolic adaption. Metabolism represents the interface between an organism and its environment, as the organism can only use the nutrients available in the respective niche to produce energy and the building blocks for cellular material (15). Without the ability to adapt to a specific set of nutrients in an ecological niche, cell growth and thereby further adaptions would not be possible. Therefore, the environment dictates the possibilities as well as necessities of cellular metabolism (Scheme 1, A).

A   Environment ⟶ Metabolism

B   Environment ⟶ Metabolism
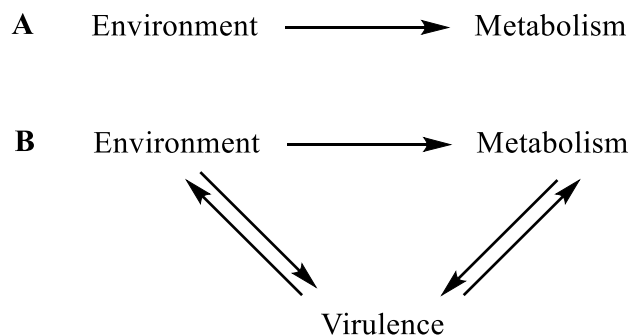
Virulence

Scheme 1 The environment shapes the metabolism of cellular life (A). In pathogenic bacteria this relation is complicated by virulence factors that interact with the environment as well as metabolism (B).

Subsequently, similar environments should produce similar metabolic phenotypes. Therefore, by recreating the putative ecological niche of an organism, one can study its metabolism, even when studies in the actual environment are not possible. Similarly, the metabolism from organisms originating from the same environment should be convergent.

Based on this, insights into metabolic phenotypes that are not directly accessible to experimental investigations can be obtained. In this regard some of the most important but inaccessible bacterial metabolic phenotypes are the metabolism of the earliest cellular organism, which most likely was a bacterium, and the actual metabolism of bacterial pathogens during human infection.

To answer the question about the origin life, information about the metabolism of the last universal common ancestor (LUCA) is crucial as it will bridge the gap between abiotic formation of biomolecules and the emergence of cellular life (4, 5). However, this putative organism does not exist anymore. Hence, investigations about its metabolism are only possible by studying present organisms that live under similar conditions (see section 1.3).

Likewise, the actual metabolism of pathogens during infections cannot be directly assessed, as this would require measurements within the human body while simultaneously not disturbing the organism. Nevertheless, in the face of rising antibiotic resistance, better insights into bacterial metabolism are desperately needed. In terms of pathogens the unidirectional relationship between environment and metabolism is further complicated by the fact that pathogens can modify their

ecological niche through virulence factors, which are also influenced by metabolism (Scheme 1, B) (see section 1.4)

In order to understand the connection between environment and bacterial metabolism, surrogate systems for the analysis of these otherwise inaccessible metabolic phenotypes will be used. In terms of carbon fixation under conditions similar to the early earth, the thermophilic bacterium *Hippea maritima* (see section 1.6) is studied. Further, two bacteria with highly different life styles are investigated in environments that recreate their respective ecological niche. The metabolic capabilities of *Helicobacter pylori* are analysed in a nutrient-rich medium mimicking environments during human infections (section 1.7). The growth-phase dependent metabolism of *Legionella pneumophila* is studied during infection of *Acanthamoeba castellanii* as a model for human macrophages infected by the intracellular pathogen (section 1.8). Studying these two heterotrophic organisms extends the connection between the ecological niche and the resulting metabolic capabilities to different environments. Additionally, as *H. pylori* and *L. pneumophila* represent human pathogens, a better understanding of their metabolism could lead to new strategies for treating infections.

All sections focus on metabolic pathways comprising the central carbon metabolism. Therefore, before dealing with specific chapters about the organisms and their ecological niches under study, relevant pathways of the core metabolism are introduced in the next section.

1.2 Metabolic pathways comprising the central carbon metabolism

Despite of the so far inextricable complexity of the metabolome (16), all metabolites are built from precursors, which arise through metabolic pathways that are similar in most organisms throughout all domains of life; this set of reactions is referred to as the central carbon metabolism (CCM) (15, 17). These reactions comprise only about a hundred compounds and form the basis to fulfil the demands for energy and biomass during cell growth. In terms of heterotrophs, input substrates like glucose and amino acids are connected to essential metabolic precursors for other metabolites *via* a "minimal walk", meaning the least amounts of enzymatic steps necessary to connect all essential molecules to the input substrates (18). Similarly, autotrophs mostly produce acetyl coenzyme A (acetyl-CoA) from inorganic precursors, which is further shuttled into all parts of the CCM. The following sections briefly discusses the main metabolic pathways comprising the CCM.

A central hub of carbon metabolism generally is a pathway for sugar degradation and production. The first degrading pathway to be discovered, referred to as glycolysis or more specifically the Embden-Meyerhof-Parnas-pathway, is central to many organisms. Its elucidation and isolation of the individual enzymes was completed by 1940 through studies in yeast as well as muscle tissue (19). This pathway allows the degradation of the C_6-sugar glucose into two C_3-units of pyruvate *via* ten enzyme-catalysed steps. Overall, the sequence can be divided into a preparatory phase, consuming two molecules of adenosine triphosphate (ATP) and a pay-off phase yielding four ATP. The preparatory phase uses phosphorylation and rearrangement reactions to produce two molecules of glyceraldehyde-3-phosphate (GAP). Subsequently in the pay-off-phase, GAP is oxidized to pyruvate, wherein oxidation of GAP to 3-phosphoglycerate provides NADH (15). Since its initial discovery it continues to be the most extensively studied metabolic pathway, mainly due to its importance in cancer cell metabolism (20).

Simultaneously starting in the 1930s, another main catabolic pathway for sugars was investigated, which is known as the pentose phosphate pathway (PPP). In contrast to glycolysis, it operates in a non-linear fashion, which made its elucidation more laborious and time-consuming. The first draft was presented in 1955 (21) but discoveries about specific enzymes and reaction mechanisms continued until the early 2000s (22). However, similar to glycolysis it can be divided into two distinct phases namely the oxidative PPP and the non-oxidative PPP. The oxidative PPP is linked to glycolysis as they both use glucose-6-phosphate as a starting material; however, its outcome greatly differs. The PPP mainly produces NADPH as a reducing equivalent. The other product, ribulose-5-phosphate, is further converted through the non-oxidative PPP, which is again intertwined with glucose, as it utilizes fructose-6-phosphate as well as GAP. The non-oxidative PPP comprises a variety of reversible sugar interconversions catalysed by transketolases and transaldolases. These enzymes allow exchange of C_2- and C_3-units between different sugars, yielding erythrose-4-phosphate, ribose-5-phosphate and sedoheptulose-7-phosphate, which serve as metabolic precursors for aromatic amino acids, the RNA backbone and lipopolysaccharides in the case of bacteria (15, 22).

Glycolysis and the PPP were thought to completely explain cellular sugar catabolism, but in the 1940s evidence accumulated for an additional pathway – the Entner-Doudoroff pathway (ED pathway) (23). Although, mostly found in gram-negative bacteria, it was found in all domains of life (24).

It shows similarities to glycolysis, as overall again two molecules of pyruvate are produced from one molecule of glucose. Still, the intermediates are different. Glucose-6-phosphate is initially oxidized to 6-phospho-gluconolactone and further transformed to the central intermediate of this pathway, 2-keto-3-desoxy-6-phosphogluconate (KDPG). This molecule can be split up into pyruvate and GAP, which is again transformed to pyruvate in analogy to glycolytic reactions. The ED pathway allows the usage of additional carbon sources like aldol sugars but in comparison to glycolysis has an overall lower net yield in terms of ATP (one vs two per molecule of glucose). This is partly compensated by the reduced protein expression that is necessary for operation of the ED pathway. As reactions in glycolysis operate close to equilibrium, they require a 3.5-fold excess of protein compared to the ED pathway, which uses the early formation of pyruvate from KDPG as a strong driving force, thereby reducing the necessary protein concentrations for its activity (25).

After discovery of the three main sugar degradation pathways, research in the late 1960s yielded gluconeogenesis as a pathway to sugar synthesis (26). This pathway reverses most enzymatic steps in glycolysis while replacing three enzymes that operate unidirectional under physiological conditions. Namely, pyruvate is transformed to PEP *via* oxaloacetate as an intermediary step. Further, dephosphorylating reactions from fructose-1,6-bisphosphate to fructose-6-phosphate as well as from glucose-6-phosphate to glucose are carried out by the respective phosphatases (15). Using this pathway allows production of sugars during autotrophic growth as well as during growth on substrates like fatty acids.

In terms of degrading pathways pyruvate, the end-product of glycolysis as well as the ED pathway, is further transformed to acetyl-CoA. This decarboxylation reaction happens in a multi-enzyme complex and produces NADH. Alternatively, in anaerobic organisms, ferredoxin is used as an electron acceptor (15). Acetyl-CoA plays a central role in metabolism as it serves as a building block for fatty acids and other biomolecules and is necessary for protein acetylation, an important posttranslational modification (15, 27, 28). Finally, it allows complete oxidation of carbon atoms originating from glucose through entering the Krebs cycle (15).

The central carbon metabolism is completed by the Krebs cycle or tricarboxylic acid (TCA) cycle (29). Although it was already noted in the early 1930s that carbohydrates are completely oxidized to CO_2, the pathway was unclear. Krebs and others elucidated an elegant cyclic reaction sequence thereby providing the final oxidative steps from acetyl-CoA to CO_2. Alongside this cycle produces precursor molecules for amino acids, porphyrins and pyrimidines as well as GTP, NADH, and $FADH_2$ (15, 30). The cycle is initiated by the condensation of acetyl-CoA with oxaloacetate to form citrate - the central intermediate of this cycle. Through rearrangement reactions and two decarboxylation steps, the acetyl-moiety is completely oxidized, leaving behind succinate as a C_4-intermediate that is readily oxidized to regenerate oxaloacetate.

Like other enzymes in the CCM, the enzymes of the TCA cycle show homology across bacteria, archaea and eukaryotes and are generally highly efficient, suggesting a long-lasting evolution. Still, there are several variations observed either as incomplete topologies or through bypassing the canonical enzymes (31). The most prominent bypass to the TCA cycle was also discovered by Hans Krebs together with one of his coworkers, Hans Kornberg and is known as glyoxylate bypass or glyoxylate shunt (32). This pathway avoids decarboxylation reactions by utilising the isocitrate-lyase reaction, which generates succinate and glyoxylate from isocitrate.

Glyoxylate is subsequently combined with acetyl-CoA to produce malate, which can again be converted to oxaloacetate. This cycle avoids loss of carbon thereby allowing for example growth solely on acetate, which can enter gluconeogenesis *via* this pathway. Occurrence of this pathway is widely distributed through plants, fungi and bacteria but there are no reports of it being active in mammals (33). The pathways comprising the CCM together with amino acids produced from its intermediates are summarized in Fig. 2.
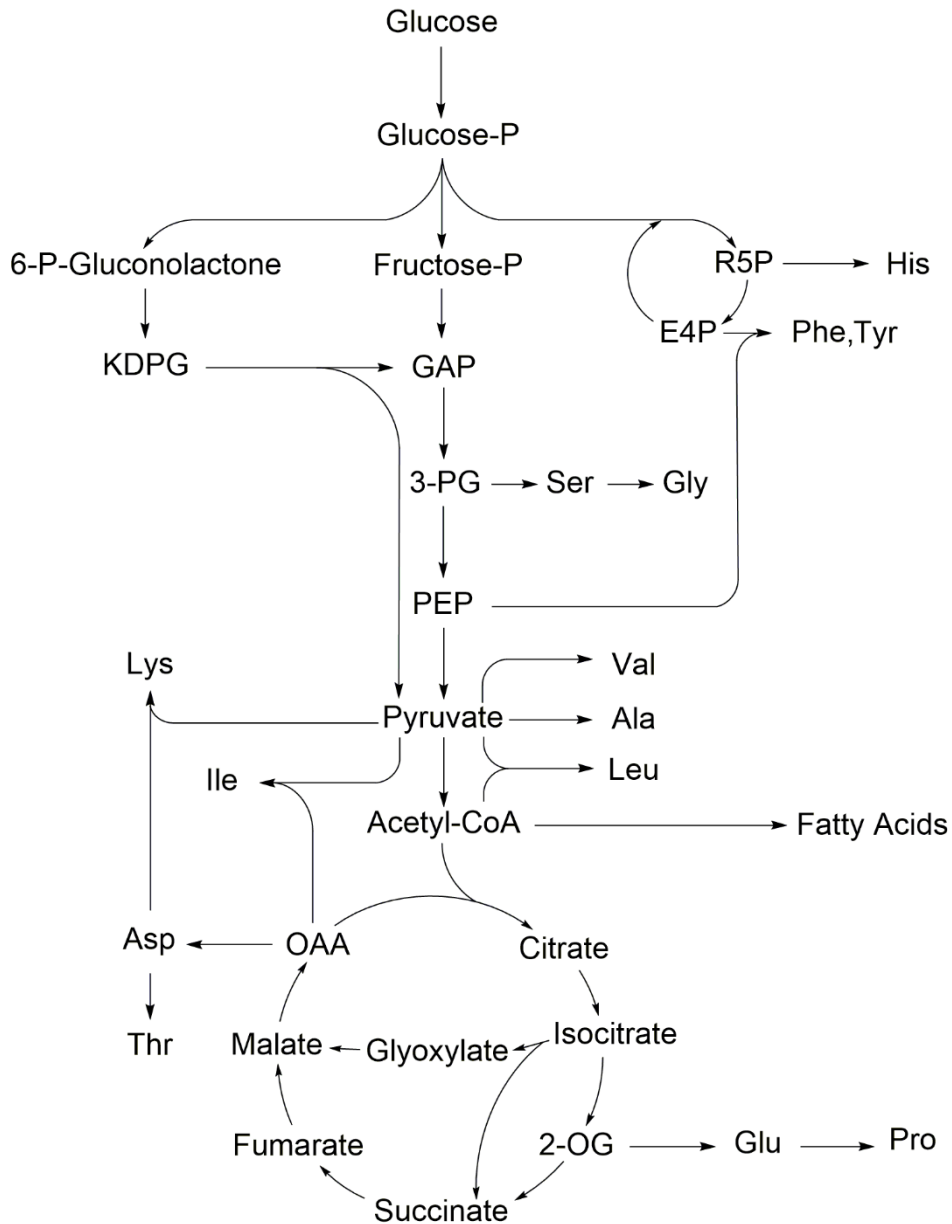
Figure 2 Overview of the central carbon metabolism and connections to amino acid biosynthesis. P: Phosphate; R5P: Ribulose-5-phosphate; E4P: erythrose-4-phosphate; KDPG: 2-keto-3-desoxy-phosphogluconate; GAP: glyceralde-hyde-3-phosphate; 3-PG: 3-phosphoglycerate; PEP: phosphoenolpyruvate; OAA: oxaloacetate; 2-OG: 2-oxo-glu-tarate.

The pathways presented here form a metabolic blueprint for all domains of life but the actual functions vary for example due to alternative enzymes, multitasking pathways and metabolic redundancies (34, 35). Additionally, new pathways and connections between known pathways are

still being discovered, although mostly due to serendipity. New pathways are often attributed to adaptions to specific ecological niches. Looking at the plethora of microorganisms, it is hard to estimate to which extent metabolism is already discovered especially talking into account that only a minority of microorganisms has been cultivated and an even smaller number was characterized extensively.

Most studies focus on a small set of model organisms (36). Therefore, the discovery of novel pathways is mostly propelled by studies of so far uncultured microorganisms. Especially the field of microbial CO_2-fixation pathways has become more diverse since initial reports about the omnipresent Calvin-Benson cycle in plants and phototrophic bacteria as the most important CO_2 fixation pathway as well as the reductive acetyl-CoA pathway and the reverse TCA cycle (rTCA) (37-39). This trinity of fixation pathways was greatly expanded by discoveries of the 3-hydroxypropionate (3-HP) pathway, the 3-hydroxypropionate/4-hydroxybutyrate (3-HP/4-HB) pathway, the dicarboxylate/4-hydroxybutyrate (DC/4-HB) pathway and most recently by the reverse oxidative TCA (roTCA) cycle and the reductive glycine pathway (40-44). These discoveries were possibe through studies in so far uncharacterized bacteria. Especially the roTCA cycle shows that even a well characterised reaction like the citrate synthase can yield surprises. This enzyme can act in the citrate cleaving direction in *Desulfurella activorans*. Hence, the reverse oxidative TCA cycle functions without the usage of an ATP-dependent citrate lyase, which is employed in the rTCA (45).

Other recent discoveries of new metabolic pathways tightly interconnected with the CCM include the ethylmalonyl-CoA pathway (46) and the methylaspartate cycle (47) as alternatives to the glyoxylate cycle or the β-hydroxyaspartate cycle for growth on glycolate (48). Variations and new combinations of known pathways have also been shown. In *Mycobacterium tuberculosis* and generally in cyanobacteria, absence of 2-oxoglutarate dehydrogenase in the TCA cycle is compensated by a two-step reaction; 2-oxoglutarate is first reduced to succinate semialdehyde and subsequently oxidized to succinate (49, 50). Regarding sugar metabolism, an interesting case was observed in *Pseudomonas putida*. The bacterium uses a combination of the three pathways for sugar catabolism outlined above, termed the EDEMP cycle: although most glucose is oxidized to gluconate in the ED pathway, a portion of GAP also enters the PPP and is used for gluconeogenesis to newly synthesize glucose-6-phosphate for oxidation (51). These few examples show that the concept of biochemical unity breaks down when looking at the constant evolution and adaption of microorganisms as discussed above (35). These variations in metabolic pathways reflect the range of niches colonized by bacteria that require fine-tuned metabolic adaptions. As explained above carbon fixation, probably the oldest and therefore most-evolved aspect of cellular carbon metabolism, comprises a multitude of pathways that all yield the same or at least similar products in the form of acetyl-CoA, glycolate or GAP. The different pathways as well as their relevance for the origin of life will be discussed in more detail in section 1.3.

In addition to identification of new metabolic pathways, the interplay between metabolism and other cellular functions receives more and more attention. This represents a conceptual shift from metabolism being just a vehicle driven by intra- and extracellular signals to metabolism sitting at the crossroad of multiple cellular functions and thereby providing as well as receiving input for other cellular processes (52). This interplay becomes especially important during infections. Here, the host also represents an ecological niche for the respective pathogen, compulsorily leading to

metabolic adaptions by the microorganism. Interaction and manipulation of the host are supposed to increase nutrient availability in general and also to fulfill the specific demands of growth substrates by the respective pathogen (53-56). Additionally, in contrast to abiotic niches, the host can actively react to the infection e. g. through nutritional deprivation to fight infections. This metabolic interplay between host and pathogen will be elucidated in more detail in section 1.4 (55, 57).

1.3 Carbon fixation as the essential trait at the origin of cellular life

When looking at the phylogenetic tree of life, all three domains converge at one point thereby suggesting a putative last universal common ancestor (LUCA). Understanding the metabolism of this organism could help to bridge the gap between abiotic reactions providing initial biomolecules and the emergence of cellular life. Looking at early cellular metabolism, autotrophic carbon fixation is the essential metabolic trait to sustain life (58-60). Biotic carbon fixation produces an unnatural ratio of $^{12}C/^{13}C$ due to slightly faster reaction rates of the lighter isotope based on the kinetic isotope effect (61, 62). This carbon fractionation due to life is constant for over 3.5 billion years (63) and can even be traced back more than 4 billion years using gas inclusions in rock samples (64-66). This prolonged biotic carbon fractionation clearly shows the importance of carbon fixation for the emergence and progression of cellular life.

Some of the oldest samples containing isotopically light carbon inclusions have been found in association with sea-floor and shallow-water hydrothermal vents (66, 67). Based on these findings different kind of approaches converge on hydrothermal vents as a suitable environment for the origin of life. Top-down approaches to generate a putative physiology for LUCA based on genome reconstruction project its ecological niche to have been geochemically active and rich in H_2, CO_2, iron, and nickel – conditions present at hydrothermal vents (4). Similarly, phylogenomic studies show that clades associated with hydrothermal vents are the deepest branches so far in the tree of life (5). Chemical bottom-up approaches to the origin of life have yielded a variety of biomolecules like thioesters, amino acids, dipeptides and fatty acids when simulating conditions at hydrothermal vents (68-71).

Taken together, carbon fixation in organisms that live in association with hydrothermal vents provides the most suitable and promising surrogate system to obtain insights into the metabolism of LUCA. However, this niche imposes several constraints on an organism. Most importantly, it has to be able to strive under elevated temperatures (> 50°C) as well as function without oxygen. So far eight different CO_2-fixation pathways have been discovered as already mentioned above. Looking at the constraints imposed by the putative environments around hydrothermal vents, the 3-HP/4HB-bicycle, the 3-HP cycle as well as the Calvin-Benson cycle can be dismissed as they have only been reported in aerobic organisms. The reductive glycine pathway has so far only been demonstrated in *Desulfovibrio desulfuricans*, which is not associated with hydrothermal vents and has an optimal growth temperature of only 34-37°C (44). Additionally, one of the key enzymes in this pathway - formate dehydrogenase – has been shown to be irreversibly inactivated at elevated temperatures (72). Therefore, this pathway is probably not suitable for conditions similar to the early earth.

The four remaining pathways (table 1) have been reported in anaerobic, thermophilic organisms and all yield acetyl-CoA, formed from two molecules of CO_2, to feed the CCM. Looking at the overall free energy difference in the production of acetyl-CoA, the roTCA cycle is so far the energetically most efficient pathway. This is achieved by replacing the ATP-dependent citrate lyase used in the rTCA by a reversible citrate synthase thereby saving one molecule of ATP per molecule of acetyl-CoA (43). In contrast to all other fixation routes, the roTCA cycle does not depend on a pathway-specific enzyme. Instead, it uses the widely distributed enzymes of the TCA cycle, which are of central importance to almost all organisms today.

1.3 Carbon fixation as the essential trait at the origin of cellular life

Table 1 (adapted from (45)) Comparison of CO_2-fixation pathways that could have been operated by the earliest cellular organism. roTCA cycle: reverse oxidative tricarboxylic acid cycle; rTCA cycle: reverse tricarboxylic acid cycle; WL-pathway: Wood-Ljungdahl pathway; DC/4-HB-pathway: Dicarboxylate/4-Hydroxybutyrate-pathway.

Pathway	Estimated $\Delta G'^0$ (kj/mol)	Pathway-specific enzyme
roTCA cycle	-50.9	-
rTCA cycle	-53.5	ATP-dependent citrate lyase
WL-pathway	-77.3	CO dehydrogenase/acetyl-CoA synthase
DC/4-HB-pathway	-152.3	4-hydroxybutyryl-CoA dehydratase

The roTCa cycle was first demonstrated in *D. acetivorans* and *Thermosulfidibacter takaii* that both grow optimally at elevated temperatures ($> 52°C$) in the absence of oxygen (43, 60, 73, 74). These characteristics make the roTCA cycle a premier candidate for the oldest carbon fixation pathway. Despite depending on enzymes common to almost all anaerobic organisms, its discovery occurred only recently in 2018. This raises the question about its driving force and prevalence
, as one would expect a highly efficient, ancient CO_2-fixation pathway to be widely distributed in nature. To shine light on this potential contradiction, in this work the roTCA cycle is studied in depth in *Hippea maritima*. This organism is presented in detail in section 1.6.

## 1.4 Metabolism in the context of antibiotic resistance and infections

"Bacterial *in vivo* metabolism is one of the most fundamental aspects of virulence of pathogenic bacteria yet our understanding of it is relatively limited (75)." Similar to metabolism of the earliest cellular organisms, actual bacterial *in vivo* metabolism of human pathogens is rather inaccessible. According to a recent report, the five most prevalent classes of bacterial pathogens (mycobacteria, chlamydia, gonococci, pneumococci and meningococci) accounted for about 456 million cases of bacterial infections in 2017. Additionally, these numbers do not take into account 2.4 billion cases of respiratory infections and diarrhoeal diseases, which are also often caused by bacterial pathogens (76). The burden of bacterial infectious diseases is aggravated by the rising number of antibiotic-resistant pathogens. According to estimations, about 700.000 people died due to infections with resistant pathogens in 2017, while this number could increase to ten million in 2050 (77).

Many antibiotic compounds used today target similar cellular functions like peptidoglycan biosynthesis or the DNA gyrase. Further, the current way of antibiotic research tends to often identify compounds that are similar to the ones already discovered (78). Therefore, new targets are desperately needed. Relieve of the antibiotic burden could also lower selective advantages through the uptake of resistance gens in nature, as these genes generally compromise other cellular functions, making resistant pathogenic bacteria less competitive in an environment without antibiotics (79). Metabolism and especially carbon metabolism could provide an alternative target for antibiotic development due to several reasons. (i) There is accumulating evidence that metabolic activity is related to virulence or controls virulence. This will be explained in more detail below. (ii) The identification and disturbance of metabolic bottlenecks could lead to attenuated growth without killing the bacteria, thereby reducing the chance of resistance formation as no selection pressure is applied, which would provoke evolution. (iii) Bacteria partially rely on different metabolic pathways compared to their human host. These biorthogonal pathways could be exploited as there are potentially no harmful effects for the host (75). (iv) Recent reports link metabolic alterations to increased susceptibility to known antibiotics (80-83). (v) Antibiotic resistance due to horizontal gene transfer from globally present resistance genes ("resistome") could be reduced as enzymes especially in the CCM are highly conserved in nature (84). (vi) Although, metabolic pathways are highly conserved, the carbon substrates used by pathogens during infection are highly specific. This is again a testament to metabolic adaption to the environment as pathogens are only able to replicate within specific niches of the host. This could allow for selective therapy in contrast to today's broad-band antibiotics. (vii) Pathogens manipulate the host during infection to access nutrients. Therefore, antibacterial therapy could also be done through treatment of the host cell to cut off crucial nutrients and thereby avoiding bacterial replication (85).

Taken together, targeting the central carbon metabolism of pathogens as well as the host offers a promising route to new antibiotics with an overall lower risk of resistance formation compared to current broad-band antibiotics. Still, this could lead to metabolic adaption as a new mechanism of resistance in addition to target modification, drug inactivation and inhibition of drug import, which have already been reported (86).

As mentioned in section 1.1, the connection between metabolism and environment is complicated through virulence in pathogenic bacteria. The extent of this triangle relationship is not yet known and potentially specific for each pathogen. Still, general trends can be extracted, when comparatively discussing different pathogens. Although these interrelations (scheme 2) have considerable overlap, for simplification the next section is split into interactions between metabolism and virulence (blue arrows) as well as virulence factors influencing the host for metabolic purposes (red arrows).
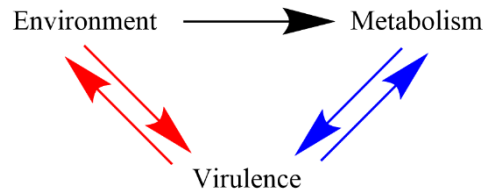
Scheme 2 Interrelation between the environment, namely the host cell, metabolism and virulence in pathogenic bacteria. Metabolism and virulence are interrelated to ensure that expression of virulence factors correlates with the metabolic state of the pathogen (blue arrows). Virulence factors modulate the host cell environment to meet the metabolic demands of the pathogen (red arrows).

Connection between metabolism and virulence

Pathogens are generally heterotrophs with preferred carbon sources (53) due to genome reduction, which leads to decreased metabolic abilities (87). This is often attributed to adaptions to the host as a replicative niche leading to a pathogen-specific sub-set of usable carbon sources, although pathogens might encounter up to 100 potential carbon sources during infection (88).

Due to this specificity, disturbance of specific enzymes for metabolite uptake or turnover severely impacts the colonization of the host by arresting growth and virulence subsequently. These liable enzymes are not restricted to a specific part of the metabolism or a class of substrates. Many examples have already been found for mutants with defects in substrate uptake (89-92), sugar degradation as well as gluconeogenesis (93-99), the TCA cycle (100-102), branched chain or aromatic amino acid biosynthesis (103, 104) and purine biosynthesis (105, 106).

Besides solely controlling bacterial growth during infection, the availability or absence of metabolites can also trigger the expression of virulence genes as indicated in scheme 2. The metabolic composition in the surroundings of a bacterium herein works as an anatomic sign post telling the bacterium, if it is in an environment suitable for infection (107). Subsequently, virulence factors are expressed when metabolite levels are above or beyond a certain threshold (108-112). Similar to the growth substrates during infection, these metabolites are again pathogen-specific, which underlines adaption to the respective niche in the host.

Besides metabolism regulating virulence gene expression, these two traits can also be directly connected on the genetic level as genes for metabolic enzymes have been found in pathogenicity islands. These are genomic islands, found only in pathogenic strains of a class of bacteria that are exclusively expressed during infection (113-115). Further transcriptional master regulators can control virulence as well as metabolic genes simultaneously. As the production of virulence factors puts an additional energetic and metabolic burden on the pathogen, expression of these traits has to be regulated in respect to the metabolic state of the cell.

A prominent example is PrfA in *L. monocytogenes*; on the on side it activates hexose-phosphate transporters upon infection and is sensitive to glycerol or glutathione levels, but on the other side it also regulates expression of the toxin listeriolysin, one of the major virulence factors of *Listeria* (104, 116-118). CodY, a global regulator in many gram-positive bacteria responds to metabolic queues like low levels of branched chain amino acids during infection through upregulation of branched chain amino acid synthesis and expression of virulence genes (119-121).

The carbon storage regulator Csr, the carbon catabolite control protein Ccp as well as the catabolite repressor Cra repress the usage of other carbon sources, when glucose or in general a preferred carbon source is available and subsequently redirect metabolism, when this carbon source is no longer available, while they also control the expression of virulence factors (122-130). Owing to this simultaneous transcriptional control of virulence and metabolism, bacterial transcriptomic profiles before and after infection revealed tight regulation and remodelling of metabolism due to infection (104, 106, 131-133).

In terms of regulator proteins, metabolism and virulence are closely connected *via* a genetic regulation circuit as explained above, but this feedback loop can be even tighter through the action of moonlight proteins, meaning proteins that directly participate in a metabolic pathway and additionally have active or regulatory functions in virulence (134, 135). Generally, these moonlighting functions are observed when a metabolic protein is expressed at a different location than the cytosol. In this regard, enzymes of the central carbon metabolism were shown to work as adhesins, transporters or to combat reactive oxygen and nitrogen species when expressed on the cell surface (136-139). Similarly, within the host cell or in association with secretion systems, these proteins can act as virulence factors (140-142).

Taken together, metabolism is tightly connected to virulence of bacterial pathogens, as the availability of carbon substrates is crucial for replication as well as expression of virulence traits during infection. While bacteria try to manipulate their replicative niche during infection to fulfil their specific metabolic demands by expressing virulence factors, the host cell simultaneously combats this effort leading to a kind of chess match at the cellular level (scheme 2, red arrows) (107). This perpetual interplay demands increasingly complex strategies by the pathogen, which will be discussed in the next section.

Connection between virulence and the host environment during infections

As mentioned before, pathogens often require specific nutritional conditions for replication during infection, but these often stand in contrast to the environment they face. The host cytosol is already considered as a nutrient-poor environment and intracellular pathogens residing within a vacuole additionally have to transport nutrients across the vacuolar membrane. Further immune response reactions can aggravate nutrient deprivation (56, 107, 143-153). Although immune reactions, similar to the metabolic demands, are specific for each pathogen due to different pathogen associated molecular patterns (PAMPs) being presented to the host cell (154), there are general strategies observed in host cells upon encountering pathogens.

According to a recent work, recognition of so-called danger associated metabolic modifications (DAMMs) triggers immune response (151). These can be for example alterations in the glycolytic

flux, mitochondrial integrity or oxidative phosphorylation activity of the host cell, leading to inflammasome activation (155, 156). Amino acid deprivation is another defense-mechanism by immune cells upon infection that specifically targets bacterial carbon substrates. Especially tryptophan availability is often restricted through activation of indolamine-2,3-dioxygenase, which converts tryptophan to formylkynurenin (157). Further, expression of immunoresponsive gene 1 allows for the production of itaconate, which exerts antibacterial effects e. g. through inhibition of isocitrate lyase in the glyoxylate bypass (158, 159).

To combat these adverse conditions and exploit host nutrients during infection pathogens have evolved a plethora of strategies for which the term "nutritional virulence" was introduced (160, 161). This covers a plethora of cellular reactions of the bacterium starting already at the point of nutrient uptake (145).

Herein, bacteria can either manipulate host transporter systems (162-164) or use high affinity uptake systems for substrates that are essential to their growth like specific amino acids (92, 165, 166). Besides just consuming common substrates available from the host, pathogens can use alternative carbon substrates. There is already a quite diverse pallet of carbon substrates used by pathogens during infection, which constantly keeps expanding (56). Besides glucose or amino acids as general carbon sources, also very specific compounds like sialic acid, sorbitol or a glycosylamine composed of fructose and asparagine were demonstrated to be metabolised by certain pathogens during infection (85, 167-169).

Bacteria can also increase carbon substrate availability by various mechanisms e. g. degradation of macromolecules or manipulation of autophagy. In terms of macromolecules degradation and further metabolisation of sphingomyelin, collagen or fatty acids from lipid droplets have been shown (170-172). Regarding autophagy, a controlled degradation process to regulate homeostasis in the host cell, some bacteria circumvent it to avoid lysis of their subcellular compartments, while others actively provoke it e. g. to increase the availability of amino acids (173-175).

Finally, the host metabolism can be directly manipulated through virulence factors to increase substrate availability. In this context, up- as well as down-regulation of host glycolysis as well as fatty acid synthesis were demonstrated depending on the nutrient demands of the respective pathogen (176-182).

Another emerging paradigm for bacterial metabolism during infection is the concept of a bipartite metabolism (56, 93, 148). For several pathogens, it has been shown that they use a combination of carbon substrates simultaneously during colonization of the host; this stands in contrast to diauxic growth in broth observed for example in *Escherichia coli* where different substrates are consumed successively. In contrast, a bipartite metabolism conveys several advantages for pathogens during host colonization (93-95, 102, 183). (i) The metabolic demands can be quickly adapted to changing environments during infections. (ii) Utilisation of multiple substrates alleviates the metabolic burden on the host cell thereby avoiding or at least dampening the inflammatory response (56). Taken together, "not surprisingly, it has transpired that host–pathogen interactions are fundamentally regulated by an interplay between host and microbial metabolic pathways and the levels of metabolites in infection microenvironments (149)." The variety of interplays between the host cell as an ecological niche and bacterial virulence and metabolism requires species-specific analysis of a pathogen in an environment that resembles the actual infection. This work studies the metabolism

of *Helicobacter pylori* and *Legionella pneumophila*, which will be presented in more detail in section 1.7 and 1.8.

The reasons mentioned above make clear, why knowledge about the actual bacterial metabolism is crucial in respect to antibiotic resistance as well as the origin of life. Additionally, on-going discoveries constantly expand the metabolic map suggesting it to be far from complete (184). For the direct assessment of active metabolism, meaning the intracellular fluxes of metabolites, stable isotope labelling today is the benchmark technology. The next section provides a summary of the historic development and todays applications of this technology with a focus on the metabolism of bacteria.

1.5 Isotopes as tracers in metabolic research

1.5.1 Historic development

Isotopes have a longstanding tradition as tracers in biological research. This concept was first introduced by Rudolf Schoenheimer in 1935 with his seminal study about the incorporation of deuterated fatty acids into rat fat storage (185). Although there were earlier studies tracing the fate of specific compounds *in vivo* like the usage of lead-isotopes (186) or phenyl-labelled fatty acids (187), Schoenheimer was the first to use the concept of labelling a biological compound without significantly changing its metabolic and physiologic properties. ""In the new approach, the fate of the molecule into which the isotope had been incorporated was studied, not simply the isotope itself (188)." As Schoenheimer wrote already in 1935: "The number of possible applications of this method appears to be almost unlimited". Research on this subject quickly expanded in parallel with the availability of stable as well as radioactive isotopes of the core set of biologically relevant elements, namely hydrogen, carbon, nitrogen, oxygen, phosphorus and sulfur (189-195).

In terms of carbon metabolism, due to the available instrumentation and limited scope of labelled carbon precursors, studies were mainly focussed on carboxylation reactions and following the metabolic fate of molecules carrying a labelled carboxyl-group. Despite these limitations carbon isotopes quickly contributed to break-through discoveries. $^{14}CO_2$ was a crucial tool in the elucidation of the Calvin-Benson-Bassham-cycle in photosynthesis, which represents the most important CO_2-fixation pathway in the global carbon cycle today (37, 196). Supplying $^{13}CO_2$ to heterotrophic bacteria led to the discovery of the Wood-Werkmann reaction, meaning the carboxylation of pyruvate to oxaloacetate also known as an anaplerotic reaction. This changed the perception that only autotrophs are able to assimilate CO_2 (197, 198). The knowledge about CO_2-fixation in the central metabolism of heterotrophic bacteria quickly expanded and as Hans Krebs put it:" The facts so far available suggest that the significance of carbon dioxide assimilation, by way of carboxylation of pyruvic acid, lies in the fact that this reaction is an essential link in the synthesis of indispensable cell constituents (199)."

Krebs himself used carbon isotopes to investigate intermediates in the tricarboxylic acid cycle named after him and experiments with ^{14}C-acetate were crucial in the elucidation of the glyoxylate bypass of the Krebs cycle (29, 32). Amongst a variety of studies, $^{14}CO_2$ also helped to elucidate the role of CO_2 as a reducing agent in methanogenesis and its participation in the Urea cycle (200, 201).

In the late 1960s, the metabolic map was seen as kind of complete but contained only a very limited number of pathways compared to today (16). Subsequently, research on metabolic pathways declined and isotopes were mainly used in environmental studies or as standards in analytical chemistry (202). Regarding isotopes in metabolism, they were intensively used in nutritional research and for studies in mammalian tissue. This led for example to the discovery of numerous breath tests, allowing a non-invasive diagnosis of several diseases (203).

After several decades with low interest in metabolic pathway research, improvements in the main techniques for analysis of isotopes in biomolecules – nuclear magnetic resonance spectroscopy (NMR spectroscopy) and mass spectroscopy-based applications (MS) – laid the foundation for metabolomics as a field of research in the late 1990s, following the already established genomics,

proteomics and transcriptomics (204-207). The new instrumentation allowed for unbiased analysis of whole cell extracts (208) and made an instant impact by revealing the huge unexplored space of biochemical intermediates and pathways thereby leading to re-emerging interest in metabolism (209). The number of studies based on metabolic analysis kept expanding since then (207, 210); subsequently in contrast to the readily comprehensible metabolic map from the early 1970s (16), the KEGG database currently comprises 16000 metabolites connected *via* more than 8700 reactions and is still expanding (211).

Similar to the pure detection of metabolites in biological samples, the improvements in MS and NMR also greatly advanced the usage of stable isotope tracers in metabolic research (204). Therefore, these techniques in combination with isotopes are now used regularly in many fields of research, e. g. geobiochemistry (212), *in vivo* metabolic analysis of mammalian tissue (213), metabolic pathways in cancer cells (214) or in nutritional research (215).

Looking at bacterial metabolism, new studies emerged, which greatly expanded the palette of metabolic pathways and at least for microorganisms again and again disproved the concept of biochemical unity, as the diversity of ecological niches occupied by bacteria mentioned above directly translates to their metabolic diversity (35). Looking at CO_2-fixation pathways specifically, it was a long-standing opinion that there were only three pathways, namely the Calvin-Benson-cycle, the reductive TCA cycle and the Wood-Ljungdahl-pathways (37-39, 216). Since the early 1990s, five new fixation pathways have been discovered, for which the usage of elegant labelling strategies in newly cultivated microorganisms was crucial (40-43). These experiments will be discussed in more detail in section 1.5.2.

In the context of microorganisms relevant for biotechnology, ^{13}C-metabolic flux analysis (^{13}C-MFA) emerged as a tool to quantitatively evaluate metabolic fluxes in bacteria thereby facilitating metabolic engineering (217-219). Flux here means the "rate of metabolite interconversion in biochemical pathways" (220). Similar to reaction rates in chemistry, fluxes cannot be measured directly, but can be calculated based on quantification of extracellular metabolites and evaluation of the labelling patterns of several intracellular metabolites, when microorganisms are cultivated in the presence of e. g. ^{13}C-labelled substrates. By inducing additional constraints on the possible flux *via* ^{13}C-labelling patterns, they can be mathematically determined (220-222). This technique allowed the elucidation of general metabolic capabilities of many model organisms such as *E. coli* or *Chlostridium acetobutylicium* (223, 224).

^{13}C-MFA is generally performed under controlled conditions, meaning usually only one carbon source with a defined portion of the labelled substrate is supplied to bacteria growing in chemostat cultures to ensure constant growth conditions. Additionally, the metabolic network has to be known at least for the most part to allow flux calculation and all products and educts of the network have to be quantified (217, 225). Therefore, ^{13}C-MFA analysis is generally performed in a chemical defined medium, to limit the number of possible substrates and to facilitate the analysis of excretion products (226).

Even though, these rigorous conditions can hardly be applied when growing pathogenic bacteria especially in a host-pathogen situation, the introduction of a labelled tracer for metabolic analysis of pathogenic organisms and their host has been yielding valuable insights into infection biology over the last 15 years. These results will be discussed in detail in section 1.5.2. Beforehand the terminology as well as basic assumptions for labelling experiments in general will be clarified.

Basic assumptions for isotopologue profiling in bacteria

In general, to perform isotopologue profiling, an organism is cultivated in the presence of a tracer molecule – meaning a compound that is artificially enriched for a certain isotope, like ^{13}C, ^{2}H, ^{15}N, ^{18}O or ^{33}S, beyond its natural abundance. This work focuses on experiments with tracers enriched for ^{13}C, therefore the following examples are also based on the carbon composition of metabolites. Utilisation of this tracer by the organism leads to enrichment of the respective isotope in a metabolite producing different isotopologues of this metabolite. Isotopologues have the same chemical structure and bond connectivity but differ only in their isotopic composition e. g. in the case of acetic acid CH_3COOH vs. $^{13}CH_3COOH$. Herein, the molecule containing only ^{12}C is referred to as M, while the respective isotopologues carrying ^{13}C-atoms are indicated by M+1, M+2, . . . M+n. A molecule with n carbon atoms can produce n+1 carbon isotopologues. Isotopologues can be further differentiated into isotopomers. Isotopomers have the same chemical structure, same bond connectivitiy and the same number of isotopes, but the isotopic atoms differ in terms of their position within the molecule e. g. $^{13}CH_3COOH$ and $CH_3{}^{13}COOH$. In theory, a compound with n C-atoms can produce 2^n carbon isotopomers. Analysis of the isotopomer and isotopologue composition of a metabolite allows to calculate the overall excess of the respective isotope within the molecule. Excess means the percentage of the overall enrichment of the respective isotope in a molecule, so for ^{13}C the overall percentage of ^{13}C in a molecule minus the natural abundance. Following the nomenclature for isotopologues introduced above, the excess is calculated with the following formula (227).

$$Excess = \frac{\sum_{i=1}^{n}(M + i) * i}{n}$$

Besides this terminology, some basic assumptions have to be made for isotopologue profiling in pathogenic bacteria as performed in this work. These will be explained in the following.

(i) Cells and their proteins do not distinguish between heavier and lighter isotopes. This also implies that the isotopic constitution of a metabolite is constant in the natural state. There are some limitations to this assumption, as organisms/enzymes tend to favour lighter isotopes due to higher reaction rates related to the kinetic isotope effect (61, 62). This effect is especially pronounced for hydrogen, leading to D_2O being toxic for many cell types in contrast to H_2O (228). The effect becomes smaller with heavier elements e. g. for carbon-12 versus carbon-13 this effect produces uncertainties of about 0.005 %. This effect can also be utilized in distinguishing the source of early carbon inclusions. Here a certain range of carbon isotope fractionation is associated with a biological origin (229, 230).

In terms of using labelled carbon in metabolic research, this is neglectable as enrichment is considered to be significant >0.5 % (231). However, in specific cases, this effect should be included in the analysis of isotopomer distributions, considering especially its variance depending on the respective enzymatic reactions (232).

(ii) Retrobiosynthetic analysis allows the deduction of labelling patterns from metabolic precursors and intermediates through analysis of stable products. As already mentioned, the metabolome comprises thousands of compounds and even restriction to central metabolic compounds still leaves hundreds of molecules. Analysis of each individual compound is practically impossible

especially talking into account the low abundance and instability of some compounds (16). Analysis in labelling studies therefore mostly focuses on highly abundant, stable compounds – protein-bound amino acids (233). As half of the cellular dry weight typically accounts for proteins (234), amino acids are easy to obtain and analyse from little cell material (225). Although more and more applications based on liquid chromatography coupled to mass spectrometry (LC-MS) are developed to analyse more metabolites simultaneously and to capture also low-abundant labile intermediates (211), analysis of protein-bound amino acids with gas-chromatography coupled to mass spectrometry (GC-MS) still remains the gold standard for reliable and robust metabolic flux analysis (220).

The retrobiosynthetic approach, borrowing principles from synthetic chemistry, now allows statements about the labelling patterns of metabolites that were not directly assessed. Therefore, the biosynthesis of the respective amino acid or in general the compound under analysis is traced back to the compound of interest with considerations of eventual rearrangements of the carbon skeleton (233, 235). "If the labelled precursor is proffered together with a large amount of unlabelled material, the resulting secondary metabolites will be mosaics assembled from labelled as well as unlabelled modules. The site of the building blocks is easily gleaned from this mosaic pattern (233)." Data interpretation initially often relies on identifying the shortest metabolic link between the tracer, the compound of interest and the molecule under analysis.

(iii) Isotopic as well as metabolic steady state has to be reached in the experiment. Metabolic and isotopic steady state should ideally be achieved in the labelling experiment to generate reliable data. Metabolic steady state means that the metabolic fluxes as well as the extracellular and intracellular metabolite concentrations are constant. Similarly, at isotopic steady state the isotopic composition of all metabolites remains constant (236).

During *in vitro* cultivation of bacteria real metabolic steady-state can be reached through chemostat cultivation (237); additionally, a quasi-steady state is generally assumed to be reached during exponential growth, as the division rate of cells is at its peak (236). At isotopic steady state fluxes are independent of the metabolite concentration; the isotopologue composition of a metabolite solely depends on the production fluxes and is independent of its consumption fluxes (238). The time-frame for metabolites to reach isotopic steady state generally depends on the growth rate of the bacterium and greatly varies for example between soluble cytosolic metabolites and amino acids bound in proteins or sugars fixated in the cell wall. While soluble metabolites equilibrate their isotopic composition within minutes after introduction of a labelled tracer, this can take several hours for bound metabolites (217, 236). Isotopic steady state can be verified by assessing the isotopic composition of a metabolite at several time-points after the introduction of the label (239). When studying microbial carbon fixation, metabolic or isotopic steady-state is usually ensured through harvest of the cells at mid-exponential phase. This can be difficult to achieve in pathogen-host situations, as labelling periods are more likely to be governed by infection periods feasible for bacterial replication, viability of the host or with regard to the timescale of an actual infection. However, comparison of isotopologue compositions under different conditions or between wild-type and mutant strains can still allow statements about the activity of metabolic pathways. The next chapter will describe several examples of isotope labelling experiments to analyse bacterial metabolism.

1.5.2 Isotopologue profiling of bacterial metabolism

With the use of stable isotope labelled metabolites, in this context of this work referred to as isotopologue profiling, significant progress has been made in the understanding of microbial metabolism. The next section will discuss the relevance of isotope labelling in discovering carbon fixation pathways as well as deciphering the metabolism of pathogenic bacteria.

Elucidation of microbial carbon fixation pathways

Section 1.5.1 already alluded to the importance of isotopically labelled precursors, especially CO_2 for the understanding of biological carbon fixation. For the discovery of the CB-cycle, and the WL-pathway in the 1950s and 1960s, experiments relied on analysing the incorporation of $^{14}CO_2$ into the metabolic end-products of the respective pathway, meaning sugars in the case of the CB-cycle or acetate for the WL-pathway (37, 38). For analysis of the rTCA label incorporation was already shown for a direct intermediate of the cycle (succinate) as well as amino acid analogues of intermediates (aspartate for OAA; glutamate for 2-OG) (39). Discovery of the 3-HP cycle involved a combination of ^{14}C- as well as ^{13}C-labelled precursors. Initial experiments with ^{13}C-labelled propionate or acetate and subsequent positional analysis of label incorporation into amino acids and nucleosides through NMR analysis hinted at a novel CO_2-fixation pathway (240), which was subsequently confirmed with enzymes assays and $H^{14}CO_3$-incorporation experiments (40). Similarly, discovery of the DC/4-HB was facilitated by using a combination of labelled precursors. In detail, selectively ^{13}C-labelled 4-hydroxybutyrate, succinate and pyruvate were used. These compounds were all intermediates of the newly proposed carbon fixation cycle. Subsequent analysis of isotopologue patterns in protein-bound amino acids through GC-MS allowed the validation of the predicted pathway (42).

In terms of the roTCA, NMR analysis from supernatants supplied with [U-$^{13}C_6$]citrate were crucial, as oxaloacetate/malate and acetyl-CoA could be unequivocally identified in the ^{13}C-spectrum thereby proving the central step of this cycle (43). Finally, activity of the reductive glycine pathway was supported by experiments using ^{13}C-labelled formate. Similar to the discovery of the DC/4-HB-pathway, GC-MS analysis of label incorporation into specific positions of proteinogenic amino acids confirmed the predicted pathway (44).

While the study of carbon fixation pathways yielded results that could be generalized to a variety of organisms, the metabolism in pathogenic bacteria is species-specific. Although general trends like a bipartite metabolic network and the connection between virulence and metabolism on different levels of regulation (see section 1.4) can be extracted, the actual metabolic phenotypes differ greatly. This is again attributed to the wide array of ecological niches within the human host that are occupied by these organisms and subsequently require metabolic adaption. The following section presents a few examples, where isotopologue profiling allowed medicinally relevant insights into the metabolism of pathogenic bacteria.

Listeria monocytogenes

Extensive work has been done on the metabolism of *L. monocytogenes*. Investigations concerned the central carbon metabolism as well as the nitrogen metabolism of *L. monocytogenes* under *in vitro* as well as *in vivo* conditions. Initial experiments, where ^{13}C-enrichment in proteinogenic amino acids was determined by NMR after growth on [U-^{13}C$_6$]glucose in broth already revealed differences in the metabolic capabilities compared to the genome based metabolic network (241). While the pathways for production of serine and isoleucine are annotated in the genome of *L. monocytogenes* (242), they were found to be inactive under experimental conditions. Further, labelling revealed the importance of pyruvate carboxylation to oxaloacetate as a compensating reaction for the incomplete TCA cycle (241).

After establishing metabolic capacities of *L. monocytogenes* grown in broth, experiments with the pathogen growing inside primary as well as transformed macrophages revealed discrepancies between *in vitro* and *in vivo* metabolism (93, 243, 244). As observed for many intracellular pathogens, *de novo* synthesis of basic metabolic building blocks like amino acids is generally avoided and compensated by the uptake of these compounds from the host (56). Still synthesis of alanine, aspartate, glutamate, threonine and valine by *L. monocytogenes* could be observed using mutants that are defective in glucose uptake (243). In depth analysis of the isotopologue profiles from the host as well as bacterial fraction further supported *de novo* synthesis of these amino acids. The incomplete TCA cycle in *L. monocytogenes* led to a pronounced M+3 isotopologue in aspartate compared to the host, when metabolising glucose (244). Further experiments revealed a bipartite metabolic network for intracellularly growing *L. monocytogenes*, where glycerol is only used for catabolic purposes but not for gluconeogenesis (93). Together these data provided insights into a metabolic network, which is highly adapted to its intracellular niche. While some metabolic capabilities are neglected during intracellular growth, the utilisation of selected pathways is tightly controlled, probably to increase the overall energy-/carbon-efficiency under nutrient-limiting conditions and to dampen the metabolic burden on the host. Additionally, labelling experiments with intracellular pathogens allowed the simultaneous analysis of the host metabolism, when host and bacterial fractions were separated. Looking at primary and transformed macrophages as host cells for *L. monocytogenes* infection, primary macrophages showed a distinct upregulation of glycolysis due to infection (244).

Mycobacteria

Mycobacteria and especially *M. tuberculosis* have also been already extensively studied using isotopologue profiling. During cultivation *in vitro*, the general metabolic capabilities of this pathogen were assessed using glucose, acetate and glycerol as potential substrates. Surprisingly *M. tuberculosis* showed co-utilisation of these substrates, which accelerated growth in comparison to the theoretical addition of growth rates on single substrates (245). Subsequently rigorous ^{13}C-MFA was performed in chemostat culture. This revealed the activity and importance of the so-called GAS-pathway (glyoxylate shunt-anaplerosis-succinyl-CoA synthetase) for *M. tuberculosis* growth. Herein, acetate is the main substrate and utilization proceeds through the glyoxylate shunt. Next, oxaloacetate is decarboxylated to allow for gluconeogenesis, while succinyl-CoA synthetase

compensates for the interrupted TCA cycle (177). ^{13}C-MFA of *M. tuberculosis* during growth in macrophages for the first time provided direct evidence for carbon substrate usage of this bacterium during infection. A mixture of labelled amino acids as well as acetate were taken up from the host and experiments with ^{13}C-bicarbonate demonstrated active carboxylation reactions during infection. Additionally, the results suggested the usage of a C3-substrate as another carbon source (239). Based on these results, infection in human macrophages revealed the critical role of lactate as carbon substrate during intracellular growth besides lipids as the main substrates (246). As lactate is produced in excess in activated macrophages, this presents an elegant exploit of the immune reaction caused by bacterial infection (247). Studies using *Mycobacterium leprae* infecting Schwann cells revealed the active usage of host glucose by the pathogen to synthesize amino acids. While *M. tuberculosis* uses the PEP carboxykinase for anaplerosis of acetate, in *M. leprae* this reaction is crucial for glucose catabolism (248).

Other intracellular pathogens

For *Chlamydia trachomatis* labelling studies revealed efficient metabolization of [U-^{13}C$_4$]malate to diaminopimelate, a component of peptidoglycan, during intracellular growth in HeLa or CaCo-2 cells. Herein, the host cells were pre-labelled before infection (183). Further studies of *C. trachomatis* infection in primary human umbilical vein endothelial cells (HUVEC) revealed the importance of host glutamine metabolism for *C. trachomatis* replication, as the infection led to up-regulation of glutamine import and metabolization *via* a glutaminase (102). Together these studies provide insight on how *C. trachomatis* infection influences the host metabolism and how this pathogen uses specific substrates to compensate for its incomplete TCA cycle to allow intracellular growth.

An elegant study by Kentner *et al.* combined proteomics, metabolomics and ^{13}C-profiling with [U-^{13}C$_6$]glucose or [U-^{13}C$_3$]pyruvate to show that *Shigella flexneri* reroutes almost all pyruvate produced through host glycolysis for its own metabolism. Pyruvate is further metabolized to acetate by the pathogen, which is then again excreted by the host cell. This nutrient scavenging by *S. flexneri* allows fast replication inside the host, with generation times comparable to cultivation in broth under ideal conditions (249).

Coxiella burnetii is another obligate intracellular pathogen that was grown in axenic medium in 2009 for the first time (250). Experiments with ^{13}C-glucose, ^{13}C-serine and ^{13}C-glycerol under these conditions showed again a bipartite metabolism, where serine mainly contributes to energy generation through the TCA cycle, while glycerol enters gluconeogenesis. Analysis of the activity of metabolic modules was facilitated by comparing the ^{13}C-enrichment in representative intermediates, e. g. alanine for glycolysis, aspartate for the TCA cycle as well as diaminopimelate and glucosamine for cell wall synthesis (95).

Experiments with *Salmonella enterica* growing inside CaCo-2 cells, revealed glucose as a nutrient source during intracellular replication. This finding was corroborated by labelling experiments with mutants deficient in glucose uptake (251).

Extracellular pathogens

Similarly, to the already discussed intracellular pathogens, isotopologue profiling is also used to characterize the central carbon metabolism of extracellular pathogens as in the case of *Streptococcus pneumoniae*. Here experiments with [U-^{13}C$_6$]glucose and [U-^{13}C$_2$]glycine revealed glycolysis as the main glycolytic pathway. Further, serine is not produced from 3-phosphoglycerate but exclusively from glycine through the addition of formate. Interestingly, mutants with defects related to virulence showed no differences in metabolism, when grown in liquid cultures (252). Similarly, metabolic capabilities were assessed in *Streptococcus suis*. Herein, the EMP pathway was again identified as the main catabolic route for glucose. Further the PEP carboxylase reaction plays a central role in the metabolism to produce oxaloacetate, as other anaplerotic reactions are absent and the TCA cycle is incomplete (253). This observation is similar to experiments in *M. leprae* and underlines the importance of this metabolic node especially, when the TCA cycle is incomplete.

For *Staphylococcus aureus*, the metabolic phenotype of the wild-type strain was compared to a small colony-variant, which is related to persistent infections. Experiments with [U-^{13}C$_6$]glucose together with transcriptome analysis showed reduced ^{13}C-excess in TCA cycle related amino acids due to a reduced aconitase activity in the small-colony variant (254).

In *Campylobacter jejuni*, isotopologue profiling was combined with a transposon insertion library to evaluate metabolic requirements for the colonization of mice. This revealed a metabolic network with limited capabilities and low redundancy as well as the importance for the uptake of serine and aromatic amino acids during infection (255).

In *Pseudomonas aeruginosa* using [1-^{13}C]glucose, the ED pathway was identified as the main route for glucose catabolism (256). Further studies during growth on labelled glycerol or acetate revealed a bipartite metabolic network, as already discussed for other pathogens. While glycerol preferentially enters gluconeogenesis, acetate is mainly metabolized in the TCA cycle (257). Another study reported metabolic differences between clinical isolates of *P. aeruginosa* suggesting adaption to the respective niche in the host. Either, TCA cycle and ED pathway activities were high, while PPP activity was low or *vice versa* pointing to different extents of biofilm formation in the isolates or adaption to different oxygen levels (258).

Another study compared usage of ^{13}C-glucose of enterohemorrhagic *E. coli* in different media, that imitate growth in the ileum or the colon, respectively. Both conditions produced different metabolic phenotypes as well as different expression of virulence factors, suggesting a close connection between virulence and metabolism that is governed by the respective ecological niche (259). Together these experiments show the valuable insights into the metabolism of various bacteria that can be gained by isotopologue profiling. The next sections will introduce the organisms studied in this work together with the respective objective.

1.6 *Hippea maritima* – **carbon fixation in environments similar to early earth**

H. maritima is a Gram-negative bacterium that grows at elevated temperatures (40-75 °C) with an optimum at 53 °C in anoxic conditions, while tolerating pH 6-7.5 but requiring the presence of 0.1 % yeast extract when grown in broth. Sulfur reduction producing H_2S serves as the energy source for growth (260). This reaction is carried out by a membrane-bound polysulphide:quinone oxidoreductase as well as a cytoplasmic sulphide:NADPH oxidoreductase (261). *H. maritima* is motile using one flagellum and its genome (~1.7 mbp) was sequenced in 2011 (262).

Initial assessment of the 16S rRNA led to classification of *H. maritima* as a deltaproteobacterium, but more recent analysis suggests the family of Hippeaceae to be a subspecies within the Desulfurellacaea, which represents a monophylogenetic class within the epsilonproteobacteria (263, 264). This is also underlined by the 87 % sequence similarity between the 16S rRNA gene of *H. maritima* and members of the genus of *Desulfurella* (265).

Initially, *H. maritima* was isolated from shallow-water hot vents of the Bay of Plenty in the southwestern Pacific Ocean (260) but its presence has also been recognized in meta-genomes from the sister peak hydrothermal chimney (266), the sungai khan hot spring (267) and upper-sediments from lake Baikal (268). Isolates from hydrothermal fields at the mid-atlantic ridge as well as the east pacific rise yielded *Hippea jasoniae* and *Hippea alviniae* as additional members of the genus *Hippea* (265). All these environments are characterized by elevated temperatures, absence of oxygen as well as increased CO_2-concentrations. Hence, *H. maritima* is suited as a surrogate organism for the metabolism at the origin of cellular life. In terms of carbon fixation pathways, the genome does not feature any pathway-specific enzymes. This absence of pathway-specific enzymes together with the close genetic relationship to the family of Desulfurellacae suggests activity of the roTCA cycle in *H. maritima*.

1.7 *Helicobacter pylori* – metabolic adaptions after prolonged evolution in the human stomach

H. pylori is a Gram-negative, spiral-shaped bacterium hence the name from greek "helix" meaning anything assuming a spiral shape. It was first isolated in 1982 from gastric biopsy samples taken from the pylorus of patients with gastritis and ulcers (269). After the realisation that the highly acidic gastric environment does not prevent colonization of the stomach by microorganisms, *H. pylori* infection was quickly identified as the biggest risk-factor for the development of gastric cancer (270). In 2018, gastric cancer accounted for more than one million cases with 783.000 deaths making it the 6th most common type of cancer (271).

H. pylori can withstand the acidic conditions in the gastric juice only for several minutes, but long enough to reach the pH-neutral gastric mucosa – the actual ecological niche of this bacterium (272). The pathogen has a rather intimate relation with humans, who are its only natural host and colonization has been found to prevail for at least 88.000 years already (273). Today, infection affects about half of the global population and usually persists throughout life (274). *H. pylori* treatment suffers from antibiotic resistance and therefore was listed on the WHO priority list for new antibiotics in 2017 (275).

Studies on the metabolism of *H. pylori* were mostly performed in the 1990s relying on photometric enzyme assays, NMR-analysis of cell extracts and genome-based reconstruction of the metabolic capacities (276, 277). These studies will be explained in more detail in section 2.2. The pathogens life style suggests extensive connections between metabolism and virulence, as discussed in general for bacterial pathogens in section 1.4.

Vacuolating toxin A (VacA) is a protein-toxin that is secreted by *H. pylori* during gastric colonization. Amongst a variety of deleterious effects for the host cell it leads to increased autophagy through inhibition of mTORC1 signalling (278) and can induce apoptosis in epithelial cells as well as macrophages (279). Together, these could be mechanisms to enhance the concentration of free amino acids in the host cell, which are then released upon apoptosis and can subsequently be used by *H. pylori*.

The cytotoxin associated gene A protein (CagA) is directly injected into cells that *H. pylori* has adhered to *via* a type 4 secretion system. Similar to VacA, the CagA protein interferes with a variety of cellular functions in the host, but instead of apoptosis leads to increased cell proliferation in host cells (280, 281), which could be one reason why the presence of CagA is closely related to gastric cancer development after *H. pylori* infection (282). Highly proliferating cells and especially cancer cells generally adopt a Warburg-type metabolism, where energy is generated mainly through glycolysis and lactate is excreted as the end-product (283). Lactate, produced by gastric epithelial cells, was already reported to be used by *H. pylori* under *in vitro* conditions (284) and the presence of the lactate-responsive chemoreceptor TlpC suggests lactate as a chemotactic signal for *H. pylori* (285). Additionally, both VacA and CagA interfere with the structural integrity of the gastric epithelium thereby potentially facilitating access to nutrients for *H. pylori* (279, 286).

γ-Glutamyl-transpeptidase, another virulence factor secreted by *H. pylori* during infection, catalyzes the conversion of glutamine into glutamate and ammonia as well as the production of glutamate from glutathione (287). On the one side this deprives host cells of glutamine, an important metabolite especially for immune cells; on the other side glutamate can be utilized by *H. pylori* e. g. through incorporation in the TCA cycle (288).

H. pylori lives in close association with gastric epithelial cells and has a variety of adhesins (289) that anchor the pathogen to the epithelial host cell to avoid mucosal shedding (290). As the mucosa itself does not provide nutrients for bacterial replication (291), the host cells are the most likely source for nutrients during infection (292). Indeed, experiments, using co-cultivation of *H. pylori* together with gastric epithelial cell lines *in vitro* showed that metabolites secreted by the putative host cells allowed growth of *H. pylori* in an otherwise unfavourable medium. Namely, hypoxanthine, *L*-alanine, *L*-proline and lactate were identified as crucial for *H. pylori* replication under these conditions (284, 293). In this work, the central carbon metabolism of *H. pylori* is investigated using isotopologue profiling. To mimic the ecological niche of *H. pylori* during infection, a nutrient rich, complex medium is chosen, as gastric epithelial cells potentially yield a diverse mixture of abundant nutrients.

1.8 *Legionella pneumophila* – growth in amoeba resembles human infection

L. pneumophila was first recognized during the annual convention of the American legion in 1976, were among 221 attendees 34 fatal cases of pneumonia were reported (294). Since then, *L. pneumophila* is known as one of the major environmental causes of community acquired pneumonias (295), and although overall case numbers are low (0.3-56.4 per 1.000.000 inhabitants) they show a constant increase (296). Additionally, due to under-diagnosis and variations in awareness levels the actual extent of Legionellosis is difficult to estimate (297). Yet, *L. pneumophila* is only an accidental human pathogen and normally lives in fresh-water and soil environments within bio-films or protozoa as its natural hosts (298).

The pathogen has a biphasic life-style: after entry into a suitable host cell, bacteria start replicating in a *Legionella* containing vacuole (LCV) until nutrients, especially amino acids, become limited (299). Subsequently, virulent traits are expressed to initiate the transmissive phase, wherein *L. pneumophila* leaves the LCV and initial host cell to look for a new replication site (300). The expression of virulence factors due to nutrient shortage clearly establishes the connection between metabolism and virulence in *L. pneumophila* (301). The overall mechanisms for host colonization are thought to be highly similar in amoeba and macrophages (302, 303), proposing amoeba as a suitable surrogate system to study human infection. Additionally, the association of *L. pneumophila* with amoeba in fresh-water reservoirs affects eradication efficiency by standard treatment like heat or low-concentration chlorine-solution (304). Therefore, understanding the relation between *L. pneumophila* and its amoebal host could help to boost eradication efficacy in fresh-water reservoirs.

During its intracellular life-phase, *L. pneumophila* secretes over 300 effector proteins into the host cell, which is the largest arsenal known so far by any pathogen (305). As described in section 1.4, these proteins contribute to virulence as well as the metabolic demands of the pathogen during infection. Many effector proteins interfere with the host metabolism to provide nutrients for *L. pneumophila*. LamA, an amylase leads to glycogen degradation in the host, potentially providing sugars for the pathogen (306). Among other proteins interfering with protein degradation in the host, the effector AnkB recruits polyubiquitinated proteins to the LCV surface, where they are subjected to proteasomal degradation and thereby providing amino acids for *L. pneumophila* (153, 307). Another strategy is the T4SS-dependent induction of mitochondrial fragmentation, leading to a Warburg-like metabolism in the host cell that favours bacterial replication (308). The metabolism of *L. pneumophila* and other factors of its interaction with host cells will be further discussed in section 2.3.

The metabolism of *L. pneumophila* has already been under investigations using isotopologue profiling. To understand biosynthetic capabilities, *L. pneumophila* was grown under standard culture conditions with [U-^{13}C$_6$]glucose, [1,2-^{13}C$_2$]glucose and [U-^{13}C$_3$]serine in the medium. Both glucose and serine were efficiently metabolized by *L. pneumophila*. Using [1,2-^{13}C$_2$]glucose as a precursor, it was possible to differentiate between glycolysis and the ED pathway as the preferred sugar catabolism. Herein, glucose was almost exclusively metabolized *via* the ED pathway, even though both pathways are completely annotated in the genome. Additionally, analysis of polyhydroxybutyrate (PHB) revealed efficient transfer of carbon from glucose into this macromolecular storage compound that is formed from acetyl-CoA units (309).

Further experiments expanded the substrate palette used by *L. pneumophila*, as [U-^{13}C$_3$]glycerol was used *in vitro* as well as *in vivo*. Metabolisation of glycerol mainly proceeded through glycolysis, supporting a bipartite metabolism already observed in other pathogens (55, 94). Experiments with a CsrA-mutant of *L. pneumophila* showed the role of this global regulator in mediating the switch from amino acid metabolism during exponential growth to glycerolipid metabolism, when amino acids became limited. Further, using [1,2,3,4-^{13}C$_4$]palmitate as a precursors, the role of lipids as carbon substrates was corroborated using isotopologue profiling (123).

To get more insights into the metabolism of *L. pneumophila* with a special regard to its biphasic life-cycle, the growth-phase dependent metabolism was investigated during cultivation in broth. Using [U-^{13}C$_6$]glucose and [U-^{13}C$_3$]serine, which were added at the beginning of the early exponential, post-exponential or stationary phase, respectively, a growth-phase dependent metabolization of these compounds was indeed observed (310). While serine is predominantly used during early phases of exponential growth *via* the TCA cycle, glucose mainly serves for PHB synthesis during the later stages (310, 311). Building on these experiments, in this work the analysis of the growth-phase dependent metabolism is transferred into a scenario more closely related to infection, namely the intracellular growth of *L. pneumophila* in an amoebal host cell.

1.9 Objective

This work aims to characterize the interrelation between environment and metabolism in bacteria to gain insights into metabolic phenotypes that are not directly accessible but highly important. As explained in section 1.5, incorporation of stable isotopes into metabolic intermediates provides the most direct imprint of cellular metabolism. For this purpose, metabolites are extracted from cellular material after bacterial cultivation in the presence of an isotopically enriched tracer molecule; subsequent enrichment-analysis of central metabolic intermediates provides insight into the presence and activity of metabolic pathways. This analysis is performed using gas-chromatography coupled to mass spectrometry (GC-MS) and focuses on protein-bound amino acid, which are derived from intermediates of the central carbon metabolism, as well as cytosolic metabolites like fatty acids and dicarboxylates.

As explained in section 1.3, one of the most important but inaccessible bacterial metabolic phenotypes is the metabolism of the earliest cellular organism. Understanding the metabolism of this organism bridges the gap between abiotic reactions producing initial biomolecules and the emergence of cellular life. Regarding the metabolism of this earliest cellular organism, *H. maritima* is used as a model that lives under potentially similar conditions. As introduced earlier autotrophic carbon fixation is the foundation of any cellular metabolism on the early earth. *H. maritima* potentially operates the roTCA cycle for carbon fixation, which is among the possible candidates for the earliest carbon fixation pathway to have emerged. To understand the activity and driving force of this cycle, initial experiments with $^{13}CO_2$ as a tracer allow to check for the activity of this pathway in *H. maritima*. As explained earlier, metabolism is dictated by the environmental niche of the respective organism. To test the pathways relevance for the earliest cellular organism, activity of the roTCA cycle will also be analysed under elevated CO_2-concentrations that were present on the early earth. Further, experiments with $[1-^{13}C_1]$glutamate allow in depth characterisation of the cycle by yielding isotopologue patterns that are specific for the roTCA cycle.

To extend and thereby generalize the connection between environment and bacterial metabolism, two heterotrophic bacteria will further be studied in this work; despite both being heterotrophs, these organisms still show great disparities in their life style. While *L. pneumophila* is found ubiquitously in soil and fresh-water with replication occurring only inside host cells like amoeba, *H. pylori* solely colonizes the human stomach. To mimic these niches, different experimental setups are used.

The metabolism of *H. pylori* is investigated during growth in nutrient-rich *Brucella broth* medium with 10% fetal calve serum. This complex medium provides a diverse mixture of possible substrates thereby reflecting conditions during *H. pylori* colonization of the gastric epithelium, where the bacterium obtains a potentially equally complex mixture of nutrients from gastric epithelial cells (312-314). In terms of *L. pneumophila* labelling experiments will be performed during intracellular growth in *A. castellanii*, a natural host of this bacterium. In contrast to earlier studies, this work will focus on the growth-phase dependent metabolism of *L. pneumophila* during replication inside the amoebal host. Despite the knowledge about the biphasic life cycle of this organism, the underlying metabolic changes during replication inside a host are poorly understood.

Besides extending the relation between environment and metabolism to heterotrophic organisms living in different ecological niches, studying *H. pylori* and *L. pneumophila* additionally provides

new insights into treating bacterial infections, as both of these organisms are human pathogens. Due to rising antibiotic resistance, new treatment strategies are desperately needed. Herein, the central carbon metabolism offers a promising target but is often poorly characterised regarding the actual infection. Further the metabolic capabilities of human bacterial pathogen are highly diverse due to variety of niches they colonize. This requires individual characterisation of pathogens in terms of their metabolic capabilities. Therefore, this work also aims to contribute a deeper understanding to the actual metabolism of *H. pylori* and *L. pneumophila* during infection to open new avenues for potential treatment strategies.

2 Results

2.1 High CO$_2$ levels drive the TCA cycle towards autotrophy

Steffens L.*, Pettinato E., Steiner T. M.*, Mall A., König S., Eisenreich W., Berg I. A. Nature 592, 748-788 (2021), 10.1038/s41586-021-03456-9.

*These authors contributed equally as first authors.

Summary A study in 2018 identified the reversed oxidative TCA cycle (roTCA cycle) as a new pathway for CO$_2$-fixation. Herein, the ATP-dependent citrate lyase, which was thought to be necessary for a CO$_2$-fixating TCA cycle, is replaced by a reversible citrate synthase, thereby saving one molecule of ATP per acetyl-CoA produced from CO$_2$. This makes the roTCA cycle the most energy-efficient CO$_2$-fixation pathway known today but its driving force and prevalence in nature were unclear.

The cycle is difficult to identify through bioinformatics, as it lacks pathway-specific enzymes but it requires high expression levels of citrate synthase to work. Therefore, codon usage analysis allowed to search for other organisms that potentially operate the roTCA cycle. Analysis yielded *H. maritima*, which showed high citrate synthase expression but no genes related to other CO$_2$-fixation pathways. The bacterium was grown with ^{13}CO$_2$ at different concentrations (4 %, 10 %, 20 %) to monitor ^{13}C-incorporation into protein-bound amino acids. Comparative analysis of isotopologue distributions in alanine, aspartate and glutamate revealed a correlation between CO$_2$-partial pressure and activity of the roTCA cycle. Operation of the roTCA cycle at low CO$_2$-concentrations could still be undoubtedly shown by supplementing [1-^{13}C]glutamate to the growth medium. Subsequently, analysis of ^{13}C-incorporation in different parts of the carbon skeleton of aspartate and glutamate showed low but significant ^{13}C-excess in Asp(C2-4) and Glu(C2-5) as expected from an active roTCA cycle.

Besides roTCA cycle activity, overall growth of the bacterium was also enhanced with increasing CO$_2$-concentrations. This behaviour was corroborated for other organisms that operate the roTCA cycle. In depth analysis of amino acid fragments from the experiments with ^{13}CO$_2$ revealed the connection between CO$_2$-partial pressure and roTCA cycle activity. The carboxylation of acetyl-CoA to pyruvate was shown to be highly dependent on the CO$_2$-concentration. Citrate cleavage by the citrate synthase requires a high CoA:acetyl-CoA ratio to operate under physiological conditions. This imbalance puts an energetic burden on the pyruvate carboxylase reaction but can be compensated by increased CO$_2$-concentrations.

These observations suggest that the roTCA cycle might by highly prevalent among organism living under conditions with high CO$_2$-levels. Additionally, early earth's atmosphere contained high levels of CO$_2$ suggesting the roTCA cycle as the most probable ancient CO$_2$-fixation pathway.

Author contribution I was involved in the design of the labelling experiments with ^{13}CO$_2$ and [1-^{13}C]glutamate to track the activity of the roTCA cycle and performed the subsequent isotopologue analysis. Additionally, I carried out analysis of amino acid distribution in *Hippea maritima* proteins as well as analysis of the growth medium to quantify amino acid consumption as well as potential fermentation products. I was involved in all steps of preparing the final manuscript.

Article

High CO$_2$ levels drive the TCA cycle backwards towards autotrophy

Lydia Steffens[1,6], Eugenio Pettinato[1,6], Thomas M. Steiner[2,6], Achim Mall[3,4], Simone König[5], Wolfgang Eisenreich[2✉] & Ivan A. Berg[1✉]

It has recently been shown that in anaerobic microorganisms the tricarboxylic acid (TCA) cycle, including the seemingly irreversible citrate synthase reaction, can be reversed and used for autotrophic fixation of carbon[1,2]. This reversed oxidative TCA cycle requires ferredoxin-dependent 2-oxoglutarate synthase instead of the NAD-dependent dehydrogenase as well as extremely high levels of citrate synthase (more than 7% of the proteins in the cell). In this pathway, citrate synthase replaces ATP-citrate lyase of the reductive TCA cycle, which leads to the spending of one ATP-equivalent less per one turn of the cycle. Here we show, using the thermophilic sulfur-reducing deltaproteobacterium *Hippea maritima*, that this route is driven by high partial pressures of CO$_2$. These high partial pressures are especially important for the removal of the product acetyl coenzyme A (acetyl-CoA) through reductive carboxylation to pyruvate, which is catalysed by pyruvate synthase. The reversed oxidative TCA cycle may have been functioning in autotrophic CO$_2$ fixation in a primordial atmosphere that is assumed to have been rich in CO$_2$.

Various natural autotrophic CO$_2$ fixation pathways have been identified to date[3–5]. These pathways are adapted to organisms that live in specific ecological niches. In addition to the variety in autotrophic CO$_2$ fixation mechanisms, variants of these pathways exist that strongly differ from each other in their properties[4,6]. A recently identified reversed oxidative tricarboxylic acid (roTCA) cycle[1,2] is a version of the autotrophic reductive tricarboxylic acid (rTCA) cycle. The rTCA cycle differs from the oxidative TCA cycle mainly by replacing reactions that are irreversible under physiological conditions with reversible ones—that is, using ferredoxin-dependent 2-oxoglutarate synthase instead of the NAD-dependent dehydrogenase and using ATP-citrate lyase (ACL) (citrate + ATP + CoA → oxaloacetate + acetyl-CoA + ADP + P$_i$) instead of citrate synthase (acetyl-CoA + oxaloacetate + H$_2$O → citrate + CoA). By contrast, the roTCA cycle uses citrate synthase rather than ACL[1,2] (Fig. 1a). The usage of citrate synthase for citrate cleavage is thermodynamically unfavourable (free-energy change $\Delta G'$ of more than 35 kJ mol^{-1})[7] but enables the spending of one ATP molecule less per acetyl-CoA synthesized from two molecules of CO$_2$, making the roTCA cycle a highly efficient autotrophic carbon fixation pathway. This pathway was shown in two obligatory anaerobic bacteria that exhibit hydrogen oxidation coupled with sulfur reduction, the deltaproteobacterium *Desulfurella acetivorans*[2] and *Thermosulfidibacter takaii*[1], a representative of the Aquificae phylum[1]. These bacteria grow equally well under autotrophic and heterotrophic conditions and have generation times of 5–7 h[1,2], which suggests that they are not affected kinetically by the use of this pathway. Therefore, the question arises which factors limit the distribution of the roTCA cycle—or, in other words, why the roTCA cycle did not outcompete the apparently less efficient ACL-containing rTCA cycle, considering the almost universal distribution of citrate synthase in autotrophic bacteria.

An important feature of the roTCA cycle is that it lacks unique enzymes, making it cryptic for bioinformatics analyses and possibly leading to the underestimation of its occurrence in the microbial world. The only characteristic feature is an extremely high activity of the citrate synthase reaction in cell extracts (more than 10 μmoles min^{-1} mg^{-1} protein)[1,2]. Therefore, we decided to study the enzyme that catalyses this reaction in *D. acetivorans* in more detail. The genome contains three citrate synthase homologues, *desace_08345*, *desace_09325* and *desace_06860* (Extended Data Fig. 1). In order to determine which of the corresponding proteins is responsible for the citrate synthase reaction in vivo, we heterologously produced all three proteins in *Escherichia coli* (Extended Data Fig. 2) and used them as standards for protein quantification with target high-resolution mass spectrometry. Desace_08345 was shown to be the main citrate synthase in *D. acetivorans* and one of the most abundant proteins in the lysates of autotrophically grown cells, contributing 7.2% to the total protein content, whereas Desace_09325 and Desace_06860 were much less abundant (0.2 and 0.1%, respectively) (Extended Data Fig. 3). Furthermore, comparison of expression in the proteomes of the autotrophically and heterotrophically grown cells hardly revealed any regulation in the synthesis of the enzymes of the roTCA cycle (Supplementary Tables 1, 2). Thus, Desace_08345 is responsible for both the cleavage and synthesis of citrate, depending on the growth conditions.

Desace_08345 had the kinetic properties of a typical citrate synthase from heterotrophic organisms, being highly active in the direction of citrate synthesis but having only low activity in the reaction of citrate cleavage (V_{max} of 157 and 1 μmoles min^{-1} mg^{-1} protein for acetyl-CoA and citrate, respectively) (Extended Data Table 1). This is in line with the Haldane equation[8], which relates the catalytic efficiencies (V_{max}/K_m) of the backward and forward reactions to the equilibrium constant

[1]Institute for Molecular Microbiology and Biotechnology, University of Münster, Münster, Germany. [2]Bavarian NMR Center–Structural Membrane Biochemistry, Department of Chemistry, Technische Universität München, Garching, Germany. [3]K. G. Jebsen Centre for Deep Sea Research, University of Bergen, Bergen, Norway. [4]Department of Biological Sciences, University of Bergen, Bergen, Norway. [5]Core Unit Proteomics, Interdisciplinary Center for Clinical Research, Medical Faculty, University of Münster, Münster, Germany. [6]These authors contributed equally: Lydia Steffens, Eugenio Pettinato, Thomas M. Steiner. ✉e-mail: wolfgang.eisenreich@mytum.de; ivan.berg@uni-muenster.de
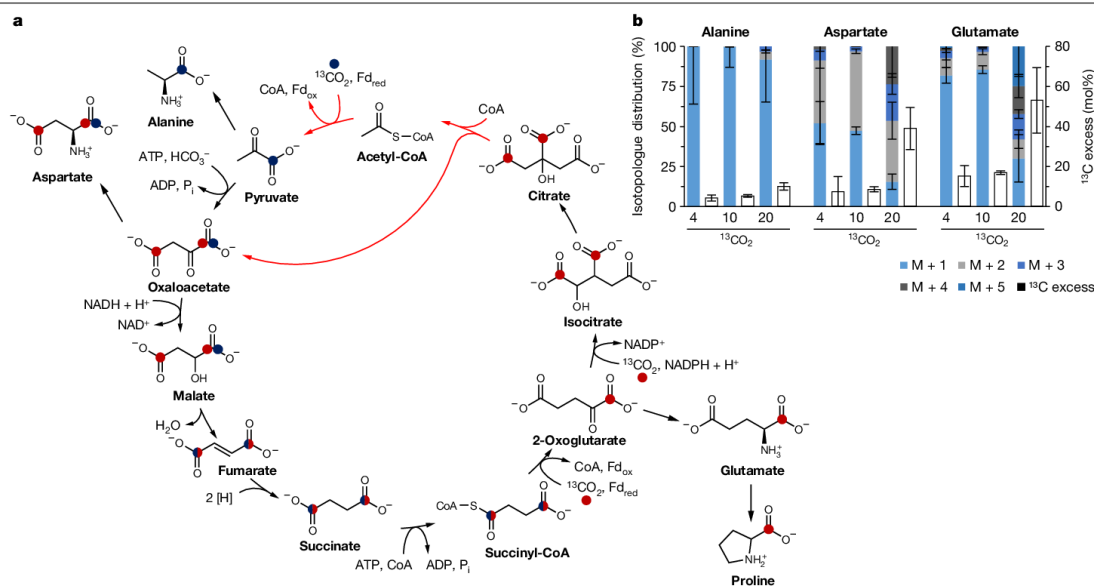
Fig. 1 | The roTCA cycle in *H. maritima*. a, The cycle and incorporation of $^{13}CO_2$ through pyruvate synthase and pyruvate carboxylase (blue) or 2-oxoglutarate synthase and isocitrate dehydrogenase (red). Half-circles indicate a statistical distribution of the ^{13}C label between both positions. **b**, ^{13}C-isotopologue fractions (normalized to 100%) and ^{13}C excess in Ala, Asp and Glu after growth with H_2, S^0, 0.2 g l^{-1} yeast extract, and 4%, 10% or 20% $^{13}CO_2$ (Supplementary Tables 4–6). M + X refers to isotopologues carrying X ^{13}C atoms, where X is 1–5. Data are mean ± s.e.m. of six biological replicates for 4% $^{13}CO_2$ and of three biological replicates for 10% and 20% $^{13}CO_2$.

$(2.24 \times 10^6$ at pH 7)[7]. Indeed, the Haldane equation predicts low V_{max} and high K_m for an enzyme that catalyses the reversal of a reaction with a high equilibrium constant. Therefore, large amounts of the enzyme are required to maintain the required flux for citrate cleavage. This was indeed observed in *D. acetivorans* cells and may again indicate that the high abundance of citrate synthase is a characteristic feature of the roTCA cycle, due to the high expression of the corresponding genes. Notably, the kinetic properties of *D. acetivorans* citrate synthase differ from the properties of the enzyme from *T. takaii* (K_m values of 0.24 and 11 mM (Extended Data Table 1) versus 0.017 and 0.009 mM for CoA and citrate[1], respectively). The driving force for the evolution of the high specificity of the citrate synthase of *T. takaii* to its substrates is not clear, as high intracellular concentrations of citrate and CoA are necessary to enable the citrate cleavage reaction (1.4 and 1.1 mM in *D. acetivorans*, respectively)[2]. The *T. takaii* enzyme is closely related to the citrate synthase of Deltaproteobacteria and eukaryotes (Extended Data Fig. 1), which do not share its high affinities for CoA and citrate[2].

Codon usage pattern of the genes can be used for the prediction of highly expressed genes[9]. We performed a codon usage analysis for various autotrophic bacteria using the software Interactive Codon Analysis (INCA)[10] to evaluate whether this method can be used to predict the presence of the roTCA cycle based on the exceptionally high expression of the gene that encodes citrate synthase. In this analysis, the codon usage of ribosomal genes (which are supposed to be highly expressed) was compared to the codon usage of the remaining genes in the genome, and those genes that belonged to the top 400 expressed genes were regarded as highly expressed. The analysis was done for *D. acetivorans* and other Desulfurellaceae with fully sequenced genomes as well as for *T. takaii* and other sequenced Aquificae. As a control, a corresponding analysis was performed using 11 genomes of bacteria that belonged to different phylogenetic groups (Chlorobi, Nitrospirae, Alphaproteobacteria, Gammaproteobacteria

and Deltaproteobacteria) that use the ACL version of the cycle for autotrophic growth but nevertheless also possess a citrate synthase gene in their genomes. As expected, their citrate synthase genes were predicted to be only modestly expressed (Supplementary Table 3).

Among 13 studied Aquificae genomes, three possessed a citrate synthase gene: *T. takaii*, *Persephonella marina* and *Sulfurihydrogenibium azorense*. The genomes of *P. marina* and *S. azorense* also had a gene that encodes ACL. As expected, the citrate synthase gene of *T. takaii* was predicted to be highly expressed (Supplementary Table 3). Low expression of the citrate synthase gene and high expression of the ACL gene were predicted for *P. marina*. Indeed, this bacterium uses the classical rTCA cycle[1]. However, genes encoding both ACL and citrate synthase are predicted to be highly expressed in *S. azorense* (Supplementary Table 3), and only biochemical analysis could confirm the functioning of the ACL variant of the rTCA cycle in this bacterium (Extended Data Table 2). Therefore, although in silico analysis could predict the roTCA cycle in Aquificae, controversial cases need to be validated by biochemical assays.

Citrate synthase was predicted to be highly expressed in all sequenced Desulfurellaceae (7 genomes), with *D. amilsii* being the only exception (Supplementary Table 3). Notably, a high level of expression of the citrate synthase gene was predicted for *H. maritima*, which is not capable of autotrophic growth and requires yeast extract for growth[11]. In our study, *H. maritima* grew not only with H_2 and CO_2 up to around 1.2×10^8 cells per ml by means of sulfur reduction (Extended Data Fig. 4a), but also only in the presence of yeast extract (Extended Data Fig. 5a) – that is, under mixotrophic conditions. A slight decrease in amino acid concentrations in the medium after growth and the absence of fermentation products suggest that yeast extract is used for anabolism (Extended Data Fig. 4b). Similar to *D. acetivorans*[2], *H. maritima* could grow under heterotrophic conditions with acetate in the presence of CO_2 and yeast extract, both with and without H_2 (Extended

Article

Table 1 | Enzymes of carbon metabolism in *H. maritima*

Enzyme	Specific activity (μmol min^{-1} mg^{-1} protein)		Candidate gene(s)
	Acetate + H$_2$ + CO$_2$	CO$_2$ + H$_2$	
Citrate synthase (F)[a]	15.9 ± 0.7 (n = 3)	16.2 ± 3.3 (n = 3)	AEA33516.1
Citrate synthase (R) (NADH oxidation)[b]	0.71 ± 0.11 (n = 3)	0.50 ± 0.04 (n = 3)	AEA33516.1
Citrate synthase (R) (acetyl-CoA formation)[c]	0.53 ± 0.04 (n = 2)	0.81 ± 0.05 (n = 3)	AEA33516.1
ATP-citrate lyase (F)	<0.001 (n = 2)	<0.001 (n = 3)	–
Citrate lyase (F)	<0.003 (n = 2)	<0.003 (n = 3)	–
Aconitase (F)	0.44 ± 0.20 (n = 3)	0.78 ± 0.20 (n = 2)	AEA33195.1
Isocitrate dehydrogenase (NADP) (F)	19.5 ± 1.7 (n = 3)	19.4 ± 1.4 (n = 3)	AEA34490.1
2-Oxoglutarate synthase (BV) (R)	2.07 ± 0.36 (n = 3)	1.83 ± 0.09 (n = 2)	AEA34486.1, AEA34487.1 and AEA34488.1
Succinyl-CoA synthetase (F)	0.23 ± 0.01 (n = 3)	0.14 ± 0.04 (n = 3)	AEA34365.1 and AEA34366.1
Fumarase (F)	3.93 ± 0.01 (n = 2)	3.46 ± 0.71 (n = 3)	AEA33115.1 and AEA33116.1
Malate dehydrogenase (NADH) (R)	38.9 ± 4.4 (n = 3)	57.5 ± 5.0 (n = 3)	AEA33114.1
Pyruvate synthase (MV) (R)	0.25 ± 0.06 (n = 3)	0.19 ± 0.04 (n = 3)	AEA33766.1, AEA33767.1 and AEA33768.1AEA33558.1, AEA33559.1 and AEA33560.1
Pyruvate carboxylase (F)	0.06 ± 0.01 (n = 2)	0.05 ± 0.01 (n = 3)	AEA33111.1
PEP carboxylase (F)	<0.003 (n = 3)	<0.003 (n = 3)	–
PEP carboxykinase (F)	<0.003 (n = 3)	<0.003 (n = 3)	–
Malate dehydrogenase (decarboxylating) (NADP) (F)	0.1 ± 0.03 (n = 3)	0.19 ± 0.01 (n = 3)	AEA33079.1
PEP synthase (R)	0.11 ± 0.02 (n = 3)	0.10 ± 0.01 (n = 3)	AEA33056.1

Specific activities were measured at 55 °C; data are mean ± s.d. and the number of biological repetitions (n) is shown. For each biological replication, at least two technical replications were carried out. Forward (F) and reverse (R) indicate in which direction the enzyme was measured (with respect to enzyme name). GenBank accession for candidate genes are included. –, no gene in the genome; BV, benzyl viologen; MV, methyl viologen.
[a]Citrate synthase was measured here as oxaloacetate-dependent CoA formation from acetyl-CoA.
[b]Citrate synthase was measured here after oxaloacetate formation from citrate in the presence of CoA (with malate dehydrogenase).
[c]Acetyl-CoA formation from citrate and CoA was measured with ultrahigh-performance liquid chromatography.

Data Fig. 5b). Nevertheless, *H. maritima* cell extracts possessed high activities of citrate synthase and other enzymes of the roTCA cycle, while ACL activity was absent (Table 1), and genes for the characteristic enzymes of other autotrophic pathways were missing. Experiments of ^{13}C incorporation with *H. maritima* during growth on 0.2 g l^{-1} yeast extract in the presence of 4%, 10% or 20% of ^{13}CO$_2$ showed that only a minor part of the carbon in proteins was derived from ^{13}CO$_2$, decreasing from 16.1% to 4.4% with a decrease in the CO$_2$ concentration from 20% to 4%, respectively (Fig. 1b and Supplementary Tables 4–7). Moreover, heavier isotopologues that carried multiple ^{13}C labels of, for example, Asp, Glu and related amino acids were formed in particular at higher ^{13}CO$_2$ concentrations. This suggests that the amount of CO$_2$ fixed into cell material was determined by the concentration of CO$_2$ (Fig. 1b and Supplementary Tables 4–6).

We therefore wondered whether the roTCA cycle is involved in mixotrophic metabolism of *H. maritima*. The high amount of fully labelled (M + 5) glutamate (22%) (Fig. 1b and Supplementary Table 6) in the cells grown at 20% ^{13}CO$_2$ proves the operation of the roTCA cycle in this bacterium. This isotopologue arises through multiple rounds of the roTCA cycle with continuous ^{13}CO$_2$ incorporation. Although ^{13}C incorporation was low when the bacteria grew with 4% ^{13}CO$_2$ (Fig. 1b and Supplementary Table 4), the roTCA cycle also functioned under these growth conditions, as was revealed by the labelling patterns in amino acids after growth with 14 mg l^{-1} of [1-^{13}C]glutamate, unlabelled 4% CO$_2$ and 0.2 g l^{-1} yeast extract. In general, [1-^{13}C]glutamate can either be oxidized in the oxidative TCA cycle with the irrevocable loss of the label from the C1 of glutamate, or be converted into [1-^{13}C] citrate and further into acetyl-CoA and [4-^{13}C]oxaloacetate (and thus [4-^{13}C]aspartate) through the reactions of the roTCA cycle (Fig. 2a). In *H. maritima*, the observed ^{13}C excess in multiple amino acids (Fig. 2b) strongly supports the latter hypothesis (Fig. 2b and Supplementary Table 8). As a signature for the *Si*-specific citrate synthase that is forming the (pro-*S*)-carboxymethyl moiety in citrate from acetyl-CoA, the

^{13}C contents in the mass fragments carrying C1–C4 (Asp418) and C2–C4 (Asp390) were identical, which suggests that mainly the C4 but not the C1 of aspartate carried the ^{13}C label (Fig. 2c). The fact that glutamate also acquired a ^{13}C label at positions 2–5, as indicated by the labelling of Glu404 (which carries C2–C5), further supported the functionality of the roTCA cycle.

The strong dependence of the metabolism of *H. maritima* on the concentration of CO$_2$ was further confirmed in growth experiments under mixotrophic conditions with 0.2 g l^{-1} yeast extract. Whereas the culture grew well at 20% and 40% CO$_2$ in the gas mixture (generation time of 17 ± 1.1 h and 17.2 ± 1.4 h, respectively) and moderately at 5% CO$_2$ (generation time of 29.3 ± 1.9 h), no growth was detected with 1% or 2% CO$_2$ (Fig. 3a). The same dependence (under strictly autotrophic conditions) was observed for the other studied Desulfurellaceae species (*D. acetivorans*, *Desulfurella multipotens* and *Desulfurella propionica*) (Fig. 3b–d). By contrast, the sulfate-reducing autotrophic deltaproteobacterium *Desulfobacter hydrogenophilus*, which reportedly uses the ACL variant of the rTCA cycle[12], grew equally well with 1%, 2%, 5%, 20% and 40% CO$_2$ in the gas phase (Fig. 3e). Note that all studied CO$_2$ concentrations are much higher than the atmospheric concentration of CO$_2$ (0.04%, around 40 Pa).

We next investigated how the dependence of the roTCA cycle on the CO$_2$ concentration could be explained. Isotopologue profiling at different ^{13}CO$_2$ concentrations (Fig. 1) revealed a sharp difference in the ^{13}C enrichments of amino acids of, for example, Ala (which is derived from pyruvate) and Glu (which is derived from 2-oxoglutarate) (Fig. 1b). These differences became especially evident in the carboxylic atoms (Fig. 1a) that originate from CO$_2$ in very similar ferredoxin-dependent carboxylation reactions, which are catalysed by pyruvate and 2-oxoglutarate synthases. More specifically, the ^{13}C incorporation into C1 of Ala decreased with the decrease in CO$_2$ concentration faster than the incorporation into C1 of Glu (Extended Data Fig. 6) despite the fact that further metabolism of 2-oxoglutarate in isocitrate dehydrogenase
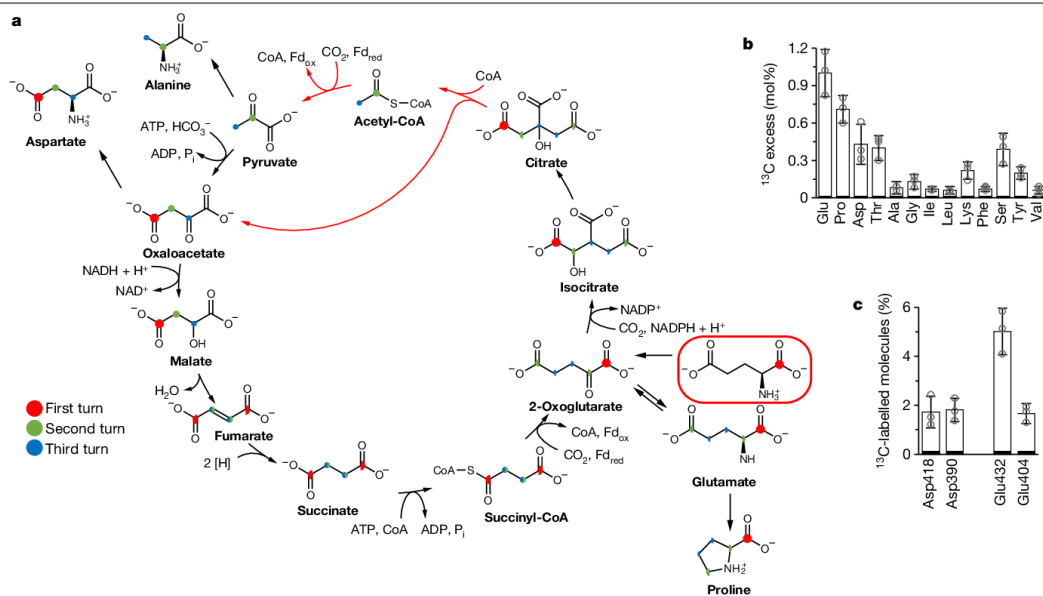
Fig. 2 | Incorporation of the [1-¹³C]glutamate in *H. maritima* via the roTCA cycle. a, Incorporation of exogenous [1-¹³C]glutamate (red box) after growth with 4% CO_2, H_2, S^0, 0.2 g l⁻¹ yeast extract and 14 mg l⁻¹ [1-¹³C]glutamate via the roTCA cycle. Half-circles indicate a statistical distribution of the ¹³C label between both positions. **b**, Detected ¹³C excess in amino acids. **c**, Percentage of ¹³C-labelled molecules in different fragments of Asp (Asp418 = C1–4, Asp390 = C2–4) and Glu (Glu432 = C1–5, Glu404 = C2–5). Data are mean ± s.e.m. of three biological replicates.

reaction is endergonic, whereas pyruvate conversion in either pyruvate carboxylase or phosphoenolpyruvate (PEP) synthase reactions is exergonic, accelerating pyruvate formation[3]. It can be concluded that *H. maritima* preferentially uses Ala from yeast extract, whereas Glu is preferentially synthesized from CO_2, even though it is the most abundant amino acid in yeast extract (Extended Data Fig. 4). High consumption of Glu from the medium can probably account for the channelling of exogenous Glu into nitrogen metabolism. This observation suggests that pyruvate synthase is not functioning efficiently at low CO_2 concentrations. Indeed, the backward reaction of citrate synthase requires a high CoA:acetyl-CoA ratio (90 for *D. acetivorans* compared with around 2 for *E. coli*, in which the TCA cycle functions in the oxidative direction)[2,13]. Acetyl-CoA carboxylation to pyruvate, with a standard

redox potential of −500 mV, is thermodynamically challenging[3], and an unfavourable CoA:acetyl-CoA ratio places a further burden on this reaction. We propose that this is compensated for by an increased CO_2 concentration, enabling the assimilation of acetyl-CoA, the product of the roTCA cycle. In fact, the unfavourable CoA:acetyl-CoA ratio could be compensated for by an increase of around two orders of magnitude in inorganic carbon concentration, as predicted by our calculation of the bioenergetic efficiency of the 2-oxoglutarate synthase and pyruvate synthase reactions (Extended Data Fig. 7), whereas a 10⁴-fold increase in the concentration of inorganic carbon is necessary to compensate for the difference in free energy between the ACL and citrate synthase variants of the rTCA cycle (Extended Data Fig. 7). Notably, the *H. maritima* genome does not contain genes responsible for the synthesis of proteins involved in the active transport of inorganic carbon. Their usage would dissipate the energy rescued in the citrate cleavage reaction. A gene encoding a carbonic anhydrase is also missing from the genome.

In this study, we show that an increase in the CO_2 partial pressure allows bacteria to use the roTCA cycle. As citrate synthase in *D. acetivorans* does not have any specific adaptations to work backwards (Extended Data Table 1), this cycle can evolve easily and may be widespread among organisms that live in anoxic conditions at high CO_2 concentrations such as submarine hot vents and hydrothermal springs and sediments, where Desulfurellaceae are abundant[14,15]. The concentration of CO_2 in the gas from the hot vents where *D. acetivorans* and *H. maritima* come from can be 90% and even higher[16,17]. The roTCA cycle has recently been shown in *Geobacter sulfurreducens* (Deltaproteobacteria) during the growth on formate with Fe(III)citrate as the electron acceptor[18]. This species was previously considered to be strictly heterotrophic. In addition, genomic analyses suggested that the cycle is functional in '*Candidatus* Nitrotheca patiens' (Chloroflexi)[19] and *Deferribacter autotrophicus* (Deferribacteres)[20]. In all of these cases, bacteria grew autotrophically in medium with elevated concentrations of inorganic carbon. Our codon usage analysis predicted that
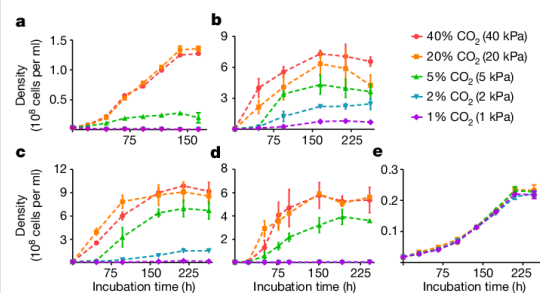

Fig. 3 | Growth of different bacteria depending on the concentration of CO₂. a–e, Growth of *H. maritima* (**a**), *D. acetivorans* (**b**), *D. multipotens* (**c**), *D. propionica* (**d**) and *D. hydrogenophilus* (**e**) in H_2 (80 kPa) at 1% (1 kPa) CO_2, 2% (2 kPa) CO_2, 5% (5 kPa) CO_2, 20% (20 kPa) CO_2 and 40% (40 kPa) CO_2. For *H. maritima*, yeast extract (0.2 g l⁻¹) was added to the medium. Data are mean ± s.e.m. of three biological replicates.

Article

the citrate synthase gene of *G. sulfurreducens* and *D. autotrophicus* is highly expressed (Supplementary Table 3). This is in line with the proposed functioning of the roTCA cycle in these bacteria. The potential functioning of the roTCA cycle in uncultivated, hyperthermophilic members of the Aigarchaeota has also been discussed[21], however a codon bias analysis for the closely related '*Candidatus* Caldiarchaeum subterraneum' did not show a strong expression of citrate synthase (Supplementary Table 3), and it is uncertain whether these organisms can grow autotrophically. Nevertheless, the roTCA cycle could also contribute to mixotrophic growth, as we have shown for *H. maritima*. In fact, autotrophic growth using the rTCA (or roTCA) cycle has not been demonstrated in Archaea yet. The early proposals that the cycle functions in some Crenarchaeota were later rejected[22].

The direction of the roTCA cycle is probably determined by the CO$_2$ concentration and/or the presence of acetate in the medium. Although some of the enzymes of the roTCA cycle were slightly more abundant in *D. acetivorans* under heterotrophic growth conditions (Supplementary Tables 1, 2), the regulation was not marked and reflected higher activities of the corresponding enzymes in cell extracts under these conditions[2]. These unusually high activities of citrate synthase and malate dehydrogenase are necessary for citrate cleavage in the roTCA cycle but not for citrate synthesis during acetate oxidation. Thus, their high activity under both growth conditions[2] (Table 1) suggests that the cells are always prepared for autotrophic (or mixotrophic) CO$_2$ fixation through the roTCA cycle once environmental conditions enable its operation. The comparison of proteomes of *H. maritima* cells grown at 4% and 20% CO$_2$ hardly revealed any regulation in the synthesis of the roTCA cycle enzymes (Supplementary Tables 2, 9), which suggests that the roTCA cycle may be directly controlled by environmental conditions that permit its functioning (or do not permit it, which results in growth arrest).

The early atmosphere of Earth probably contained high amounts[23] of CO$_2$, creating ideal conditions for establishing the roTCA cycle as an ancient CO$_2$ fixation pathway. Previously, the ancestry of the roTCA cycle has been proposed based on phylometabolic evaluations[1]. High concentrations of CO$_2$ still prevail in many contemporary ecological niches. Hydrothermal vent fluids are highly enriched in CO$_2$, with concentrations that are often between tens and hundreds of millimolars[24,25], and even a deep-sea hydrothermal vent that emits almost pure liquid CO$_2$ (2.7 moles CO$_2$ kg^{-1} in hot vent fluid) has been described[26]. In natural CO$_2$ reservoirs at moderate depths, the pressure of CO$_2$ can reach 40–50 MPa, compared with 40 Pa at ambient pressure in air[27]. The eruption of the aquifers to the surface results in CO$_2$-driven cold-water geysers that bring to the surface groundwater that contains a complex microbial community, including autotrophic microorganisms, which use the reductive acetyl-CoA pathway and the rTCA (and possibly the roTCA) cycle, as revealed by coupled analyses using lipidomics and metagenomics[28].

An increased energetic efficiency at high CO$_2$ concentrations can also be envisaged for the reductive acetyl-CoA pathway (Wood–Ljungdahl pathway), arguably the most ancient metabolic pathway[29] that functions in acetogenic bacteria and methanogenic archaea. Although acetogenesis and methanogenesis are usually associated with a change in free energy ($\Delta G'$) that is insufficient to drive the synthesis of 1 mol ATP per mol of product under physiological conditions[30,31], the Gibbs free energy difference in this pathway may become sufficient for substrate phosphorylation at high partial pressures of CO$_2$ (50 kJ mol^{-1} at 1 MPa CO$_2$, 10 mM acetate and 100 Pa H$_2$ partial pressure) (Extended Data Fig. 8 and Supplementary Discussion).

Biotechnological use of autotrophic organisms with high-CO$_2$-dependent, energetically efficient pathways can be advantageous in, for example, bioreactors under increased pressure, which results in a more efficient conversion of the substrate to a product. Even the existence of previously unknown pathways that are thermodynamically impossible under normal conditions could be envisaged,

thus offering a new perspective on the study and design of autotrophic CO$_2$ fixation pathways.

Online content

Any methods, additional references, Nature Research reporting summaries, source data, extended data, supplementary information, acknowledgements, peer review information; details of author contributions and competing interests; and statements of data and code availability are available at https://doi.org/10.1038/s41586-021-03456-9.

1. Nunoura, T. et al. A primordial and reversible TCA cycle in a facultatively chemolithoautotrophic thermophile. *Science* **359**, 559–563 (2018).
2. Mall, A. et al. Reversibility of citrate synthase allows autotrophic growth of a thermophilic bacterium. *Science* **359**, 563–567 (2018).
3. Fuchs, G. Alternative pathways of carbon dioxide fixation: insights into the early evolution of life? *Annu. Rev. Microbiol.* **65**, 631–658 (2011).
4. Berg, I. A. Ecological aspects of the distribution of different autotrophic CO$_2$ fixation pathways. *Appl. Environ. Microbiol.* **77**, 1925–1936 (2011).
5. Song, Y. et al. Functional cooperation of the glycine synthase-reductase and Wood–Ljungdahl pathways for autotrophic growth of *Clostridium drakei*. *Proc. Natl Acad. Sci. USA* **117**, 7516–7523 (2020).
6. Könneke, M. et al. Ammonia-oxidizing archaea use the most energy-efficient aerobic pathway for CO$_2$ fixation. *Proc. Natl Acad. Sci. USA* **111**, 8239–8244 (2014).
7. Guynn, R. W., Gelberg, H. J. & Veech, R. L. Equilibrium constants of the malate dehydrogenase, citrate synthase, citrate lyase, and acetyl coenzyme A hydrolysis reactions under physiological conditions. *J. Biol. Chem.* **248**, 6957–6965 (1973).
8. Bisswanger, H. *Enzyme Kinetics: Principles and Methods* (Wiley, 2008).
9. Supek, F. & Vlahovicek, K. Comparison of codon usage measures and their applicability in prediction of microbial gene expressivity. *BMC Bioinformatics* **6**, 182 (2005).
10. Supek, F. & Vlahovicek, K. INCA: synonymous codon usage analysis and clustering by means of self-organizing map. *Bioinformatics* **20**, 2329–2330 (2004).
11. Miroshnichenko, M. L., Rainey, F. A., Rhode, M. & Bonch-Osmolovskaya, E. A. *Hippea maritima* gen. nov., sp. nov., a new genus of thermophilic, sulfur-reducing bacterium from submarine hot vents. *Int. J. Syst. Bacteriol.* **49**, 1033–1038 (1999).
12. Schauder, R., Widdel, F. & Fuchs, G. Carbon assimilation pathways in sulfate-reducing bacteria. II. Enzymes of a reductive citric acid cycle in the autotrophic *Desulfobacter hydrogenophilus*. *Arch. Microbiol.* **148**, 218–225 (1987).
13. Bennett, B. D. et al. Absolute metabolite concentrations and implied enzyme active site occupancy in *Escherichia coli*. *Nat. Chem. Biol.* **5**, 593–599 (2009).
14. Greene, A. C. in *The Prokaryotes* (eds Rosenberg, E. et al.) 135–142 (Springer, 2014).
15. Dahle, H. et al. Energy landscapes in hydrothermal chimneys shape distributions of primary producers. *Front. Microbiol.* **9**, 1570 (2018).
16. Zhao, W. *Diversity and Potential Geochemical Functions of Prokaryotes in Hot Springs of the Uzon Caldera, Kamchatka*. PhD thesis, Univ. Georgia, Athens (2008).
17. Obzhirov, A. I. Chemistry of free and dissolved gases of Matupit Bay, Rabaul Caldera, Papua New Guinea. *Geo-Mar. Lett.* **12**, 54–59 (1992).
18. Zhang, T., Shi, X.-C., Ding, R., Xu, K. & Tremblay, P.-L. The hidden chemolithoautotrophic metabolism of *Geobacter sulfurreducens* uncovered by adaptation to formate. *ISME J.* **14**, 2078–2089 (2020).
19. Spieck, E. et al. Extremophilic nitrite-oxidizing *Chloroflexi* from Yellowstone hot springs. *ISME J.* **14**, 364–379 (2020).
20. Slobodkin, A. et al. Genomic insights into the carbon and energy metabolism of a thermophilic deep-sea bacterium *Deferribacter autotrophicus* revealed new metabolic traits in the phylum Deferribacteres. *Genes* **10**, 849 (2019).
21. Hua, Z. S. et al. Genomic inference of the metabolism and evolution of the archaeal phylum Aigarchaeota. *Nat. Commun.* **9**, 2832 (2018).
22. Berg, I. A. Autotrophic carbon fixation in archaea. *Nat. Rev. Microbiol.* **8**, 447–460 (2010).
23. Zahnle, K. et al. Emergence of a habitable planet. *Space Sci. Rev.* **129**, 35–78 (2007).
24. German, C. R. & Von Damm, K. L. in *Treatise on Geochemistry* (eds Turekian, K. K. & Holland, H. D.) 18–222 (Elsevier, 2006).
25. Pedersen, R. B. et al. Discovery of a black smoker vent field and vent fauna at the Arctic Mid-Ocean Ridge. *Nat. Commun.* **1**, 126 (2010).
26. Lupton, J. et al. Submarine venting of liquid carbon dioxide on a Mariana Arc volcano. *Geochem. Geophys. Geosyst.* **7**, Q08007 (2006).
27. Ajo-Franklin, J., Voltolini, M., Molins, S. & Yang, L. in *Geological Carbon Storage: Subsurface Seals and Caprock Integrity* (eds Vialle, S. et al.) 187–206 (Wiley, 2019).
28. Probst, A. J. et al. Lipid analysis of CO$_2$-rich subsurface aquifers suggests an autotrophy-based deep biosphere with lysolipids enriched in CPR bacteria. *ISME J.* **14**, 1547–1560 (2020).
29. Martin, W. F. Older than genes: the acetyl CoA pathway and origins. *Front. Microbiol.* **11**, 817 (2020).
30. Thauer, R. K., Kaster, A. K., Seedorf, H., Buckel, W. & Hedderich, R. Methanogenic archaea: ecologically relevant differences in energy conservation. *Nat. Rev. Microbiol.* **6**, 579–591 (2008).
31. Schuchmann, K. & Müller, V. Autotrophy at the thermodynamic limit of life: a model for energy conservation in acetogenic bacteria. *Nat. Rev. Microbiol.* **12**, 809–821 (2014).

Methods

Data reporting

No statistical methods were used to predetermine sample size. The experiments were not randomized and the investigators were not blinded to allocation during experiments and outcome assessment.

Materials

Chemicals and gases were obtained from Sigma-Aldrich, Merck, Serva, Roth or VWR. Biochemicals were from Roche Diagnostics and Appli-Chem. ^{13}C-labelled chemicals were obtained from Sigma-Aldrich and 99.0 atom% [13]CO_2 gas was from Eurisotop. Materials for molecular biology were purchased from New England BioLabs, Qiagen, Merck and Sartorius. Materials and equipment for protein purification were obtained from GE Healthcare, Macherey-Nagel or Millipore. Lead acetate paper was obtained from Macherey-Nagel. Primers were synthesized by Sigma-Aldrich.

Synthesis of CoA esters

Acetyl-CoA was synthesized from the corresponding anhydrides and CoA according to a previously described method[32].

Strains and growth conditions

All bacterial strains with the exception of *E. coli* were obtained from the Deutsche Sammlung von Mikroorganismen und Zellkulturen (DSMZ). Their growth was determined using Neubauer counting chambers. In addition, the growth of sulfur and sulfate reducers was monitored through H_2S production using lead acetate paper.

H. maritima MH$_2^T$ (DSM 10411) was grown mixotrophically in medium (DSMZ medium 854) containing 6.2 mM NH_4Cl, 2.2 mM $CaCl_2 \cdot 2H_2O$, 1.6 mM $MgCl_2 \cdot 6H_2O$, 4.4 mM KCl, 2.4 mM KH_2PO_4, 427.8 mM NaCl, 14.3 mM MOPS buffer, 200 mg l^{-1} yeast extract, 1 mg l^{-1} resazurin, 10 g l^{-1} sulfur powder, 10 ml l^{-1} trace element solution out of DSMZ medium 141 and 1 ml l^{-1} Wolfe's vitamin solution (20 mg l^{-1} biotin, 20 mg l^{-1} folic acid, 100 mg l^{-1} pyridoxamine dihydrochloride, 50 mg l^{-1} thiamine dihydrochloride, 50 mg l^{-1} riboflavin, 50 mg l^{-1} nicotinic acid, 50 mg l^{-1} DL-Ca-pantothenate, 1 mg l^{-1} cyanocobalamin, 50 mg l^{-1} 4-aminobenzoic acid and 50 mg l^{-1} lipoic acid). The medium was prepared without sulfur and vitamin solution, made anaerobic by bubbling with N_2 (100%) and reduced by the addition of $Na_2S \cdot 9H_2O$ to a final concentration of 0.05% (w/v). The pH of the medium was adjusted to 5.5–6.0. The medium was dispensed anaerobically into serum bottles containing sulfur powder; the bottles were sealed with butyl-rubber stoppers and aluminium caps and autoclaved for 40 min at 110 °C. Before inoculation, the vitamin solution was added and the gas phase was replaced with the required quantities of H_2:CO_2 (60:40, 80:20, 95:5, 98:2 or 99:1) at 1 bar overpressure. For heterotrophic cultures, the medium was additionally supplemented with 5 g l^{-1} sodium acetate and the gas phase was replaced with N_2:CO_2 (80:20) at 1 bar overpressure. In some cases, the cells were cultured without yeast extract or with N_2, H_2:N_2 (80:20) or N_2:CO_2 (80:20) as a gas phase. Cultures were incubated at 55 °C while shaking at 130 rpm. For labelling experiments, either 14 mg l^{-1} [1-^{13}C]glutamate or 99.0 atom% [13]CO_2 gas (4, 10 or 20%) was added to the medium before inoculation. Cells were collected during mid-exponential growth for activity measurements and during late-exponential growth for gas chromatography–mass spectrometry (GC–MS) analysis.

D. acetivorans A63 (DSM 5264), *D. multipotens* RH-8 (DSM 8415) and *D. propionica* U-8 (DSM 10410) were grown autotrophically in medium containing 6.2 mM NH_4Cl, 2.2 mM $CaCl_2 \cdot 2H_2O$, 1.6 mM $MgCl_2 \cdot 6H_2O$, 4.4 mM KCl, 2.4 mM KH_2PO_4, 14.3 mM MOPS, 10 g l^{-1} sulfur powder, 1 mg l^{-1} resazurin, 1 ml l^{-1} SL-10 trace element solution (3 g l^{-1} $FeCl_2 \cdot 4H_2O$, 70 mg l^{-1} $ZnCl_2$, 100 mg l^{-1} $MnCl_2 \cdot 4H_2O$, 4 mg l^{-1} $CuCl_2 \cdot 2H_2O$, 24 mg l^{-1} $NiCl_2 \cdot 6H_2O$, 36 mg l^{-1} $Na_2MoO_4 \cdot 2H_2O$, 30 mg l^{-1} H_3BO_3, 224 mg l^{-1} $CoCl_2 \cdot 6H_2O$) and 1 ml l^{-1} Wolfe's vitamin solution. The medium was prepared without sulfur and vitamin solution, made anaerobic by

bubbling with N_2 (100%) and reduced by the addition of $Na_2S \cdot 9H_2O$ to a final concentration of 0.05% (w/v). The pH of the medium was adjusted to 7.3. The medium was dispensed anaerobically into serum bottles containing sulfur powder; the bottles were sealed with butyl rubber stoppers and aluminium caps and autoclaved for 40 min at 110 °C. Before inoculation, the vitamin solution was added and the gas phase was replaced with the required quantities of H_2:CO_2 (60:40, 80:20, 95:5, 98:2 or 99:1) at 1 bar overpressure. After the gas phase exchange, the pH was adjusted according to the optimum of each strain: pH 6.5–7.0 for *D. acetivorans*; pH 6.4–6.8 for *D. multipotens*; and pH 6.9–7.2 for *D. propionica*. Cultures were incubated at 55 °C while shaking at 130 rpm.

D. hydrogenophilus AcRS1 (DSM 3380) was grown autotrophically in DSMZ medium 195 containing 21.1 mM Na_2SO_4, 1.4 mM KH_2PO_4, 5.6 mM NH_4Cl, 359.3 mM NaCl, 15.3 mM $MgCl_2 \cdot 6H_2O$, 6.7 mM KCl, 1.0 mM $CaCl_2 \cdot 2H_2O$, 1 ml l^{-1} selenite-tungstate solution out of DSMZ medium 385, 1 mg l^{-1} resazurin, 1 ml l^{-1} trace element solution SL-10 and 1 ml l^{-1} Wolfe's vitamin solution. The medium was prepared without vitamin solution and made anaerobic by bubbling with N_2:CO_2 (80:20) to reach a pH below 6.0. The medium was dispensed anaerobically into serum bottles; the bottles were sealed with butyl-rubber stoppers and aluminium caps and autoclaved for 20 min at 121 °C. Before inoculation, the medium was reduced by the addition of $Na_2S \cdot 9H_2O$ to a final concentration of 0.05% (w/v) and the vitamin solution was supplemented, resulting in a final pH of 7.1–7.4. The gas phase was replaced with the required quantities of H_2:CO_2 (60:40, 80:20, 95:5, 98:2 or 99:1) at 1 bar overpressure. After the gas phase exchange, the pH was adjusted to 7.1–7.4. Cultures were incubated at 30 °C while shaking at 130 rpm.

S. azorense AZ-Fu1 (DSM 15241) was grown autotrophically in DSMZ medium 1003 of the following composition: 28.4 mM $MgSO_4 \cdot 7H_2O$, 12.6 mM NaS_2O_3, 2.7 mM $CaCl_2 \cdot 2H_2O$, 6.4 mM KCl, 8.2 mM $MgCl_2$, 10 mM MES, 2 ml l^{-1} solution A (1.6 M NH_4Cl, 0.9 M $MgCl_2 \cdot 6H_2O$ and 0.3 M $CaCl_2 \cdot 2H_2O$), 1.5 ml l^{-1} solution B (0.4 M K_2HPO_4), 10 ml l^{-1} trace element solution (1.5 mM Na-EDTA·$2H_2O$, 0.6 mM $CoCl_2 \cdot 6H_2O$, 0.5 mM $MnCl_2 \cdot 4H_2O$, 0.4 mM $FeSO_4 \cdot 7H_2O$, 0.7 mM $ZnCl_2$, 0.2 mM $AlCl_3 \cdot 6H_2O$, 0.1 mM Na_2WO_4, 0.2 mM $CuCl_2 \cdot 2H_2O$, 0.05 mM $Ni_2SO_4 \cdot 6H_2O$, 0.07 mM Na_2SeO_3, 0.17 mM H_3BO_3 and 0.05 mM $Na_2MoO_4 \cdot 2H_2O$). The pH was adjusted to 6.0. The medium was dispensed aerobically into serum bottles; the bottles were sealed with butyl-rubber stoppers and aluminium caps and sparged with CO_2 (100%) for 20 min, then autoclaved for 20 min at 121 °C. For the microaerophilic growth condition, before inoculation, the gas phase was replaced with 0.25 ml of O_2 per ml medium and H_2 at 1.38 bar overpressure. Cultures were incubated at 68 °C while shaking at 130 rpm.

E. coli strains (Top10, DH5α, Rosetta 2 (DE3) and C41) were grown at 37 °C in lysogeny broth medium. Antibiotics were added to the cultures to a final concentration of 100 μg ml^{-1} ampicillin and 34 μg ml^{-1} chloramphenicol.

Analysis of medium from *H. maritima*

To quantify the concentrations of amino acids in the medium during *H. maritima* growth, 250 μl of the medium at the respective time point was centrifuged (14,000 rpm, 4 °C, 15 min) and the supernatant was transferred to remove the elemental sulfur and bacterial cells. Samples were lyophilized after addition of 25 μl Norvaline solution (5 mM, aqueous) as an internal standard. The residue was hydrolysed in 6 M HCl (105 °C, 15 h) to account for free as well as peptide- and protein-bound amino acids. After hydrolysis, the sample was dried under a stream of nitrogen at 70 °C. The dried residue was derivatized with 50 μl anhydrous acetonitrile (ACN; Sigma-Aldrich) and 50 μl *N*-(*tert*-butyldimethylsilyl)-*N*-methyltrifluoroacetamide (MTBSTFA) with 1% *N*-*tert*-butyldimethylsilylchloride (TBDMS; Sigma-Aldrich) at 70 °C for 1 h. The TBDMS derivatives of amino acids were then analysed by GC–MS.

To quantify formate, acetate, lactate and succinate in the medium, 750 μl of the centrifuged medium at the respective time point was

Article

lyophilized after addition of 25 µl Norvaline solution (5 mM, aqueous) as an internal standard. Then, 1 ml of methanol (VWR, HPLC-grade) was added to the dried residue and the mixture was treated for 15 min in an ultrasonic bath. After centrifugation (2 min, 7,000 rpm), the supernatant was dried under a stream of nitrogen at room temperature. The residue was derivatized with 50 µl anhydrous ACN (Sigma-Aldrich) and 50 µl MTBSTFA (Sigma-Aldrich) at 70 °C for 1 h. The TBDMS derivatives of acids were then analysed by GC–MS.

Preparation of cell extracts from *H. maritima*
H. maritima cultures (200 ml) were filtrated (Whatman Schleicher & Schuell, diameter 240 mm) under aerobic conditions to remove the elemental sulfur before centrifugation. The cells were collected during mid-exponential growth by centrifugation (8,000 rpm, 4 °C, 30 min). The supernatant was carefully transferred, and the cell pellet was resuspended in 20 ml of fresh medium. The resuspended cell suspension was centrifuged again (4,000 rpm, 4 °C, 30 min) and the supernatant was removed gently with the pipette. The cell pellet was washed with 0.9% saline and the cell solution was centrifuged again (4,000 rpm, 4 °C, 30 min). The cells were frozen in liquid nitrogen and stored at −80 °C. The cells were resuspended in 20 mM Tris-HCl pH 8, 5 mM dithioerythritol (DTE) and lysed by sonification aerobically with SONOPULS mini20 or anaerobically in the glove box with UW2070 (Bandelin Electronic) on ice (60% amplitude, 4 min, 1-s pulse, 2-s breaks; total energy input 2,000 kJ). Insoluble material was removed by centrifugation (14,000 rpm, 30 min, 4 °C). The protein concentration was determined using the Bradford method[33] with bovine serum albumin as a standard.

Protein hydrolysis
Isolation of protein bound amino acids was done as described previously[34]. About 2 mg of bacterial sample (lyophilized cell pellet) was suspended in 500 µl of 6 M hydrochloric acid and hydrolysed overnight at 105 °C. The reaction mixture was dried under a stream of nitrogen. The residue was suspended in 200 µl of 50% acetic acid. Amino acids were isolated using a small column of Dowex 50W X8 (7 × 10 mm; 200–400 mesh, 34–74 µm, H⁺-form). The column was first washed with 2 ml H₂O, then amino acids were eluted with 1 ml 4 M aqueous ammonia solution. The ammonia eluate was dried under a stream of nitrogen at 70 °C. The dried residue was treated with 50 µl of MTBSTFA containing 1% TBDMS and 50 µl of anhydrous ACN at 70 °C for 30 min. The TBDMS derivatives of amino acids were then analysed by GC–MS. Furthermore, acid hydrolysis leads to the conversion of glutamine and asparagine to glutamate and aspartate, respectively. Therefore, results given for aspartate and glutamate correspond to asparagine or aspartate and glutamine or glutamate, respectively.

For the analysis of the composition of the amino acids, samples were treated as described above. To account for different derivatization and ionization efficiency of each amino acid, an equimolar amino acid mixture (2.5 µM in 0.1 M HCl, Sigma Aldrich) was used to determine the response factor for each amino acid. Therefore, 200 µl of the amino acid mixture was dried under a stream of nitrogen at 70 °C. The dried residue was treated with 50 µl MTBSTFA containing 1% TBDMS and 50 µl anhydrous ACN at 70 °C for 30 min.

GC–MS analysis
GC–MS analysis was performed with a QP2010 Plus gas chromatograph–mass spectrometer (Shimadzu) equipped with a fused silica capillary column (Equity TM-5; 30 m × 0.25 mm, 0.25-µm film thickness; SUPELCO) and a quadrupole detector working with electron impact ionization at 70 eV. An aliquot (0.1–6 µl) of the TBDMS-derivatized samples was injected in 1:5 split mode at an interface temperature of 260 °C and a helium inlet pressure of 70 kPa. For the analysis of ¹³C excess and isotopologue composition of bacterial amino acids, selected ion monitoring was used with a sampling rate of 0.5 s and

LABSOLUTION software (Shimadzu) was used for data collection and analysis. Isotopologue calculations were performed for m/z [M − 57]⁺ or m/z [M − 85]⁺. For analysis of the relative amino acid composition in *H. maritima* protein as well as the medium composition, measurements were performed in scan mode in a mass range from 45 m/z to 700 m/z with an injection volume of 0.1 µl.

For amino acids, the column was heated to 150 °C and kept at 150 °C for 3 min, after which was heated to 280 °C (7 °C per min) and held at that temperature for 3 min. For analysis of the TBDMS derivatives of formate, acetate, lactate and succinate, the column was heated to 60 °C and kept at 60 °C for 6 min. Then, the column was heated to 280 °C with a gradient of 10 °C min⁻¹ and kept at that temperature for another 3 min. The injector temperature was 260 °C. Measurements were performed in SCAN mode with a scan interval of 0.5 s and a mass range of 50–600 m/z. All samples were measured three times for technical replicates.

The calculation of ¹³C excess was done as described previously[34] and comprises (1) the detection of GC–MS spectra of unlabelled derivatized metabolites; (2) the determination of the absolute mass of isotopologue enrichments and distributions of labelled metabolites of the experiment; and (3) the correction of the absolute ¹³C incorporation by subtracting the contributions of the heavy isotopologues due to the natural abundances in the derivatized metabolites to calculate the enrichments and distributions of the isotopologues. For the ¹³C-labelling data analysis, Isotopo-4 software was used[35].

Cloning of *D. acetivorans* citrate synthase genes in *E. coli*
Standard protocols were used for the purification, cloning, transformation and amplification of DNA[36].

The gene encoding Desace_08345 was amplified by Gibson assembly[37] with Q5 High-Fidelity DNA Polymerase, using a forward primer (5′-GCCATCATCATCATCATCACAGCAGCG GCATGTCCTTT TTAAAGGAAAAATTAG-3′) and a reverse primer (5′GCTTTGTTAG CAGCCGGATCTTACTTAATTCCTGCCCATTTC-3′). PCR conditions for the amplification of the gene of interest were as follows: 35 cycles of 10 s denaturation at 98 °C, 30 s primer annealing at 57.5 °C and 3 min elongation at 72 °C. The expression vector pET28b was amplified by PCR with Q5 High-Fidelity DNA Polymerase using a forward primer (5′-GATCCGGCTGCTAACAAAG-3′) and a reverse primer (5′-GCCGCTGCTGTGATGATG-3′). PCR conditions were as follows: 35 cycles of 10 s denaturation at 98 °C, 30 s primer annealing at 64 °C and 3 min elongation at 72 °C. The reaction mixture contained 100 ng of the insert and 50 ng of the vector and it was incubated in a thermocycler at 50 °C for 15 min. The resulting pET28b vector containing the gene of interest with a N-terminal His₆-tag was transformed into *E. coli* Top10 for amplification, followed by purification and sequencing.

The gene encoding Desace_09325 was amplified by PCR with Q5 High-Fidelity DNA Polymerase using a forward primer (5′-GCGTA**GAATTC**CA TGAAGCTTAAAGAAAAAC-3′) introducing an EcoRI site (bold) and a reverse primer (5′-ATTATA**GTCGAC**TTAAAACCACACTTTAGCT-3′) introducing a SalI site (bold). PCR conditions were as follows: 35 cycles of 10 s denaturation at 98 °C, 30 s primer annealing at 66 °C and 3 min elongation at 72 °C. The PCR product was isolated and ligated into the expression vector pET28b containing a N-terminal His₆-Tag and transformed into *E. coli* TOP10 for amplification, followed by purification and sequencing.

The gene encoding Desace_06860 was amplified by PCR with Q5 High-Fidelity DNA Polymerase using a forward primer (5′-CGTAG**CATATG**TCAAGATTTTTTG-3′) introducing a NdeI site (bold) and a reverse primer (5′-CAGA**AAGCTT**AATCCTAGTTTTGTTTAG-3′) introducing a HindIII site (bold). PCR conditions were as follows: 30 cycles of 10 s denaturation at 98 °C, 30 s primer annealing at 61 °C and 40 s elongation at 72 °C. The PCR product was isolated and cloned into pJET1.2 and transformed into *E. coli* Top10. After plasmid amplification, purification and sequencing, the PCR product was digested

and ligated into the expression vector pET23b containing a C-terminal His$_6$-tag.

Heterologous expression of *D. acetivorans* citrate synthase genes in *E. coli*

The recombinant enzymes (Desace_08345, Desace_09325 and Desace_06860) were produced in *E. coli* Rosetta 2 (DE3) or *E. coli* C41 that had been transformed with the corresponding plasmids. The cells were grown at 37 °C in lysogeny broth medium supplemented with ampicillin and chloramphenicol. Expression was induced at an optical density ($OD_{600 nm}$) of 0.6–0.8 with 1 mM isopropyl-β-D-thiogalactopyranoside (IPTG) and the temperature was lowered to 20 °C. The cells were collected after overnight growth and stored at −20 °C until use.

Preparation of cell extracts

Frozen cells were suspended in triple volume of 20 mM Tris-HCl (pH 7.8), containing 500 mM NaCl, 20 mM imidazole and 0.1 mg ml^{-1} DNase I. The cell suspensions were lysed by a threefold passage through a chilled French pressure cell (137 MPa), and the cell lysates were centrifuged for 1 h (100,000g; 4 °C). The supernatant (cell extract) was immediately used for protein purification or enzyme assays.

Purification of recombinant proteins

The heterologously produced His-tagged citrate synthase Desace_08345, Desace_09325, Desace_06860 enzymes were purified using affinity chromatography. The corresponding cell extracts were applied at a flow rate of 0.5 ml min^{-1} to a 1-ml Protino Ni-NTA column (Macherey-Nagel) that had been equilibrated with 20 mM Tris-HCl (pH 7.8) containing 500 mM NaCl and 20 mM imidazole. The column was washed at a flow rate of 0.5 ml min^{-1} to elute unwanted protein with the same buffer containing 50 mM imidazole for Desace_08345; in two steps with the same buffer containing 35 mM and 70 mM imidazole for Desace_09325 and 50 mM and 70 mM imidazole for Desace_06860. The recombinant enzymes were eluted with the same buffer containing 500 mM imidazole. The enzymes were concentrated and the imidazole washed out using 10K Vivaspin Turbo 4 and stored at −20 °C with 50% glycerol. The identity of the purified recombinant proteins was confirmed using in-gel digestion by trypsin followed by liquid chromatography (LC)−MS/MS on a Synapt G2 Si instrument coupled to M-Class reversed-phase nanoUPLC (Waters).

Enzyme assays

Spectrophotometric enzyme assays (0.3 ml assay mixture) were performed in a glass (for visible light) cuvette at 55 °C for *H. maritima* cell extracts and *D. acetivorans* citrate synthase (Desace_08345) and at 42 °C or 55 °C for *S. azorense* cell extracts, depending on the stability of the helping enzymes and substrates used in an assay. For anaerobic assays, cuvettes were sealed with rubber plugs, made anaerobic by gassing with N$_2$, and the anaerobic reaction mixture and substrates were added with Hamilton syringes. For LC analysis, reactions were stopped in an equal amount of stop solution (1 M HCl, 10% ACN). Proteins and insoluble particles were removed with three centrifugation steps (16,000g, 15 min, 4 °C). Samples were analysed with the Agilent 1290 Infinity II UHPLC system using a reversed-phase C18 column (Agilent InfinityLab Poroshell 120 EC-C18, 1.9 μm, 2.1 mm × 50 mm column). An ACN gradient from 2% to 8% in 10 mM potassium phosphate buffer (pH 7) with a flow rate of 0.55 ml min^{-1} was used. The retention times of succinyl-CoA, CoA and acetyl-CoA were 0.7, 0.8 and 1.6 min, respectively. The identification of the CoA esters was based on co-chromatography with standards and analysis of the ultraviolet-light spectra of the products.

Citrate synthase was measured spectrophotometrically at 412 nm as the oxaloacetate-dependent formation of free CoA from acetyl-CoA. The reaction mixture contained 100 mM Tris-HCl (pH 7.5), 5 mM oxaloacetate, 0.5 mM acetyl-CoA, 1 mM DTNB (ε_{412} = 14.2 mM^{-1} cm^{-1})[38] and cell extract. For citrate synthase characterization in *D. acetivorans*

(Desace_08345), Tris-HCl (pH 7.5) was substituted with MOPS (pH 7). The backward reaction was measured spectrophotometrically at 365 nm in combination with malate dehydrogenase as the citrate- and CoA-dependent oxidation of NADH (ε_{365} = 3.4 mM^{-1} cm^{-1})[39] and via UHPLC as the citrate-, CoA- and NADH-dependent formation of acetyl-CoA. For spectrophotometric assays, the assay mixture contained 100 mM Tris-HCl (pH 7.8), 5 mM DTE, 5 mM MgCl$_2$, 0.5 mM CoA, 20 mM citrate, 0.5 mM NADH and cell extract. For the characterization of Desace_08345, 20 U ml^{-1} porcine malate dehydrogenase (Sigma M1567) was added. For UHPLC assays, 1 mM CoA and 5 mM of NADH were used instead and 20 U ml^{-1} porcine malate dehydrogenase (Sigma M1567) was added. To stop the reaction, samples were mixed at each time point with an equal amount of 1 M HCl and 10% ACN. Proteins and insoluble particles were removed with three centrifugation steps (16,000g, 15 min, 4 °C).

ATP-citrate lyase and citrate lyase were measured at 42 °C spectrophotometrically at 365 nm by coupling to malate dehydrogenase, which reduces the produced oxaloacetate with NADH. The reaction mixture for ATP-citrate lyase was based on a previously published study[40] and contained 100 mM Tris-HCl (pH 7.5), 5 mM MgCl$_2$, 0.5 mM ATP, 0.5 mM CoA, 0.4 mM NADH, 20 U ml^{-1} porcine malate dehydrogenase (Sigma M1567) and 20 mM citrate. The reaction was started by the addition of ATP. The reaction mixture for citrate lyase contained 100 mM Tris-HCl (pH 7.5), 5 mM dithiothreitol (DTT), 5 mM MgCl$_2$, 0.5 mM NADH, 20 U ml^{-1} porcine malate dehydrogenase (Sigma M1567) and 20 mM citrate.

Isocitrate dehydrogenase was measured spectrophotometrically at 365 nm as the isocitrate-dependent reduction of NADP (ε_{365} = 3.5 mM^{-1} cm^{-1})[39]. The assay mixture contained 100 mM Tris-HCl (pH 7.5), 5 mM DTE, 5 mM MgCl$_2$, 1 mM NADP, 10 mM DL-isocitrate and cell extract.

Aconitase was measured spectrophotometrically at 365 nm under anaerobic conditions in combination with endogenous isocitrate dehydrogenase as the citrate-dependent reduction of NADP. The reaction mixture contained 100 mM Tris-HCl (pH 8), 5 mM DTE, 5 mM MgCl$_2$, 1 mM NADP, 5 mM citrate and cell extract.

Malate dehydrogenase was measured spectrophotometrically at 365 nm as the oxaloacetate-dependent oxidation of NADH. The assay mixtures contained 100 mM Tris-HCl (pH 8), 5 mM DTE, 5 mM MgCl$_2$, 0.5 mM NADH, 2.5 mM oxaloacetate and cell extract.

Malic enzyme (malate dehydrogenase, decarboxylating) was measured spectrophotometrically through the malate-dependent reduction of NADP. The reaction mixture contained 100 mM Tris-HCl (pH 7.5), 5 mM MgCl$_2$, 5 mM DTE, 1 mM NADP, 30 mM malate and cell extract.

Fumarase was measured spectrophotometrically under anaerobic conditions at 240 nm as the cell-extract-dependent formation of malate from fumarate (ε_{240} = 2.4 mM^{-1} cm^{-1})[41]. The assay mixture contained 100 mM Tris-HCl (pH 7.5), 5 mM MgCl$_2$, 5 mM DTT, 0.4 mM fumarate and cell extract.

Pyruvate synthase and 2-oxoglutarate synthase activities were measured spectrophotometrically at 578 nm by following the pyruvate- or 2-oxoglutarate-dependent reduction of methyl viologen (ε_{578} = 9.7 mM^{-1} cm^{-1})[42] in the case of pyruvate synthase and of benzyl viologen (ε_{578} = 8.65 mM^{-1} cm^{-1})[42] in the case of 2-oxoglutarate synthase. The assay mixture contained 50 mM Tris-HCl (pH 7.5), 5 mM MgCl$_2$, 2.5 mM DTE, 0.5 mM CoA, 1 mM methyl or benzyl viologen and 10 mM pyruvate or 2-oxoglutarate. Anaerobic cuvettes and reaction mixture were flushed with N$_2$ gas before the measurement. The reactions were started by the addition of the substrates.

PEP carboxylase activity was measured spectrophotometrically in a coupled assay with endogenous malate dehydrogenase as the PEP-dependent oxidation of NADH. The reaction mixture contained 100 mM MOPS-KOH (pH 7.2), 4 mM MnCl$_2$, 5 mM DTE, 40 mM NaHCO$_3$, 0.5 mM NADH, 5 mM PEP and cell extract.

PEP carboxykinase activity was measured spectrophotometrically, as described above for PEP carboxylase, but the reaction was started with 0.5 mM ADP.

Article

Pyruvate carboxylase activity was measured spectrophotometrically in a coupled assay with endogenous malate dehydrogenase as the pyruvate- and ATP-dependent oxidation of NADH. The reaction mixture contained 100 mM Tris-HCl (pH 7.5), 20 mM MgCl₂, 5 mM DTE, 15 mM NaHCO₃, 0.5 mM NADH, 0.2 mM acetyl-CoA, 40 mM pyruvate, 5 mM ATP (pH 7.0) and cell extract.

PEP synthase activity was measured spectrophotometrically backwards as phosphate-dependent formation of pyruvate from PEP and AMP by coupling it to the lactate dehydrogenase reaction. The reaction mixture (55 °C) contained 100 mM Na-K phosphate buffer (pH 7.0), 100 mM MgCl₂, 50 mM AMP (pH 6.8), 2 mM PEP, 0.5 mM NADH, 10 U lactate dehydrogenase (Sigma L2500) and cell extract. The reaction was started by adding the PEP and was AMP-dependent.

Succinyl-CoA synthetase was measured using UHPLC as the ATP-dependent formation of succinyl-CoA from succinate and CoA. The assay mixture contained 100 mM Tris-HCl (pH 7.5), 5 mM DTE, 5 mM MgCl₂, 10 mM succinate, 5 mM ATP, 1 mM CoA and cell extract.

Protein quantification using MS

Recombinantly expressed isoforms of citrate synthase (Desace_08345, Desace_09325, Desace_06860) were heterologously produced, characterized and used as standards for quantification and MS method development. To that end, gel bands were destained in 25 mM ammonium bicarbonate containing 50% methanol, washed with water and desolvated by adding ACN. The gel bands were dried in a speedvac before adding 100 mM DTT in 50 mM ammonium bicarbonate for 1 h reduction at room temperature. After removal of the solution, the gel piece was dried again and alkylated for 30 min in the dark by adding iodoacetamide. After the removal of the solution and drying of the gel piece, a DTT solution was added for quenching (15 min). The solution was removed, ACN added and the band was dried. For digestion, 30 μl trypsin (20 ng μl⁻¹) in 50 mM ammonium bicarbonate containing 10% ACN was added. Once the solution was taken up by the gel, the band was covered with the ammonium bicarbonate solution to prevent drying out. Digestion was performed at 37 °C overnight. Peptides were extracted with 1% formic acid solution containing 10%, 50% and 80% ACN. Extracts were pooled, dried and redissolved in 20 μl 0.1% formic acid containing 5% ACN. Pseudo-multiple reaction monitoring (MRM) experiments were set up for the isoforms individually on a Synapt G2 Si instrument coupled to a M-Class reversed-phase nanoUPLC (Waters; column 1.8 μm HSS T3: 75 μm × 150 mm; trap column M-class Trap Symmetry C18: 5 μm; 180 μm × 20 mm, 100 Å; 300 nl min⁻¹; solvents: A, 0.1% aqueous formic acid; B, 0.1% formic acid in ACN) using the most abundant unique tryptic peptides (as chosen by Skyline (Extended Data Fig. 3a)). Calibration curves were generated by injecting 0.1, 0.2, 0.3, 0.4 and 0.5 μl (Extended Data Fig. 3b).

To quantify the corresponding proteins in *D. acetivorans* cells, the proteins were separated using one-dimensional polyacrylamide gel electrophoresis (PAGE). Analyses were subsequently performed on the isoform bands that had been separated using gel electrophoresis in triplicate. In addition, the relative quantification of the cell lysate proteomes of *D. acetivorans* and *H. maritima* was achieved with data-independent label-free high-definition (HD)MS protein expression analysis on Synapt G2 Si[43] following filter-based tryptic digestion (1 μg on-column) using the UniProt *D. acetivorans* and *H. maritima* databases as previously described[44]. In brief, cell lysates were reduced, alkylated and tryptically digested on 10 kDa centrifugal filter devices and prepared for LC–MS at 250 ng μl⁻¹ in 0.1% formic acid and 5% ACN. This method measures the entire proteomes of replicate samples in single experiments. It is not as accurate as the MRM method, but it still verifies the concentration range of the three isoforms (Supplementary Table 10). For statistical analyses, Progenesis QIP software was used (nonlinear diagnostics/Waters, fixed modification carbamidomethylation, variable modification methionine oxidation, 1 missed cleavage allowed).

Bioinformatics

Query sequences for the database searches were obtained from the National Center for Biotechnology Information (NCBI) database. The BLAST searches were performed using the NCBI BLAST server (http://www.ncbi.nlm.nih.gov/BLAST/).

INCA[10] was used for codon usage analysis for various bacteria using each ribosomal proteins as a reference set. On the basis of a previously published study[9], the method Measure Independent of Length and Composition (MILC) was chosen for the *x* (to the reference set) and *y* axes (to all genes) and its derivative method MILC-based Expression Level Predictor (MELP) was used as a filter to quantitatively predict gene expression levels from genomic data. The genes were listed from the highest MELP value to the lowest and genes shorter than 100 codons were excluded from the analysis.

Other methods

The concentration of hydrogen sulfide in *H. maritima* cultures was measured by a previously published colorimetric method[45]. Samples were taken after inoculation and every 24 h until the stationary phase was reached. SDS–PAGE (12.5%) was performed as described by previously[46]. An unstained protein marker (Pierce Unstained Protein MW Marker, 14.4–116 kDa, Thermo Scientific) was used as a molecular mass standard. Apparent K_m and V_{max} values and growth curves were calculated using GraphPad Prism5 software. Circles were drawn with ChemDraw Professional. DNA sequence determination was performed by Eurofins. Standard deviations and standard errors of mean were calculated using Microsoft Excel.

Reporting summary

Further information on research design is available in the Nature Research Reporting Summary linked to this paper.

Data availability

All data generated in this manuscript are included within the paper (and its Supplementary Information). The raw data are presented in the manuscript and/or available from the corresponding authors upon reasonable request. For any further inquiries about our work please contact the corresponding authors. Source data are provided with this paper.

32. Simon, E. J. & Shemin, D. The preparation of S-succinyl coenzyme A. *J. Am. Chem. Soc.* **75**, 2520 (1953).
33. Bradford, M. M. A rapid and sensitive method for the quantitation of microgram quantities of protein utilizing the principle of protein-dye binding. *Anal. Biochem.* **72**, 248–254 (1976).
34. Eylert, E. et al. Carbon metabolism of *Listeria monocytogenes* growing inside macrophages. *Mol. Microbiol.* **69**, 1008–1017 (2008).
35. Ahmed, Z. et al. 'Isotopo' a database application for facile analysis and management of mass isotopomer data. *Database* **2014**, bau077 (2014).
36. Ausubel, F. M. et al. *Current Protocols in Molecular Biology* (Wiley, 1987).
37. Gibson, D. G. et al. Enzymatic assembly of DNA molecules up to several hundred kilobases. *Nat. Methods* **6**, 343–345 (2009).
38. Riddles, P. W., Blakeley, R. L. & Zerner, B. Ellman's reagent: 5,5'-dithiobis(2-nitrobenzoic acid)—a reexamination. *Anal. Biochem.* **94**, 75–81 (1979).
39. Bergmeyer, H. U. Neue Werte für die molaren Extinktions-Koeffizienten von NADH und NADPH zum Gebrauch im Routine-Laboratorium. *Z. Klin. Chem. Klin. Biochem.* **13**, 507–508 (1975).
40. Hügler, M., Huber, H., Molyneaux, S. J., Vetriani, C. & Sievert, S. M. Autotrophic CO₂ fixation via the reductive tricarboxylic acid cycle in different lineages within the phylum Aquificae: evidence for two ways of citrate cleavage. *Environ. Microbiol.* **9**, 81–92 (2007).
41. Flint, D. H. Initial kinetic and mechanistic characterization of *Escherichia coli* fumarase A. *Arch. Biochem. Biophys.* **311**, 509–516 (1994).
42. Dawson, R. M. C., Elliott, D. C., Elliott, W. H. & Jones, K. M. *Data for Biochemical Research* (Clarendon, 1986).
43. Distler, U., Kuharev, J., Navarro, P. & Tenzer, S. Label-free quantification in ion mobility-enhanced data-independent acquisition proteomics. *Nat. Protoc.* **11**, 795–812 (2016).
44. Wildschütz, L. et al. Transcriptomic and proteomic analysis of iris tissue and aqueous humor in juvenile idiopathic arthritis-associated uveitis. *J. Autoimmun.* **100**, 75–83 (2019).

45. Trüper, H. G. & Schlegel, H. G. Sulphur metabolism in Thiorhodaceae. I. Quantitative measurements on growing cells of *Chromatium okenii*. *Antonie van Leeuwenhoek* **30**, 225–238 (1964).
46. Laemmli, U. Cleavage of structural proteins during the assembly of the head of bacteriophage T4. *Nature* **227**, 680–685 (1970).
47. Edgar, R. C. MUSCLE: multiple sequence alignment with high accuracy and high throughput. *Nucleic Acids Res.* **32**, 1792–1797 (2004).
48. Minh, B. Q. et al. IQ-TREE 2: new models and efficient methods for phylogenetic inference in the genomic era. *Mol. Biol. Evol.* **37**, 1530–1534 (2020).
49. Noor, E. et al. Pathway thermodynamics highlights kinetic obstacles in central metabolism. *PLOS Comput. Biol.* **10**, e1003483 (2014).
50. Witt, A., Pozzi, R., Diesch, S., Hädicke, O. & Grammel, H. New light on ancient enzymes – in vitro CO₂ fixation by pyruvate synthase of *Desulfovibrio africanus* and *Sulfolobus acidocaldarius*. *FEBS J.* **286**, 4494–4508 (2019).
51. Furdui, C. & Ragsdale, S. W. The role of pyruvate ferredoxin oxidoreductase in pyruvate synthesis during autotrophic growth by the Wood–Ljungdahl pathway. *J. Biol. Chem.* **275**, 28494–28499 (2000).
52. Flamholz, A., Noor, E., Bar-Even, A. & Milo, R. eQuilibrator—the biochemical thermodynamics calculator. *Nucleic Acids Res.* **40**, D770–D775 (2012).

Author contributions L.S. and E.P. performed growth experiments, cloning, purification and characterization of enzymes and enzyme assays. L.S performed codon usage analysis and sulfide determination. T.M.S. performed isotopologue profiling experiments and GC–MS analysis of *H. maritima* medium. S.K. conducted proteomics analyses. A.M. performed phylogenetic analysis and bioenergetics calculations. I.A.B. and W.E. wrote the manuscript with input from other authors. L.S., E.P., T.M.S., A.M., S.K. and W.E. prepared figures. The manuscript was reviewed and approved by all coauthors.

2.2 Substrate usage determines carbon flux *via* the citrate cycle in *Helicobacter pylori*

Steiner T. M.*, Lettl C.*, Schindele F., Goebel W., Haas R., Fischer W., Eisenreich W. Molecular Microbiology, 116, 841-860 (2021), 10.1111/mmi.14775.

*These authors contributed equally as first authors.

Summary *H. pylori* is a pathogen, colonizing the human gastric mucosa, with a world-wide infection rate of about 50 %. Despite the infection mostly proceeding asymptomatically, it can also lead to gastritis and gastric cancer, which accounted for ~810.000 deaths in 2018. As eradication efficacies of established treatments are declining, new targets are desperately needed. The central carbon metabolism of *H. pylori* so far was only characterised through genome annotation and enzyme assays with cell supernatants. This produced ambiguities, especially regarding the structure of the TCA cycle, which was either reported to operate as a full cycle in the oxidative direction or in a bifurcate fashion with succinate as the product of the reductive branch and 2-oxoglutarate as the product in the oxidative branch.

To characterise the actual architecture of the central carbon metabolism in *H. pylori*, this study used a comprehensive set of ^{13}C-labelled tracers to characterise the central carbon metabolism of *H. pylori* during growth in *Brucella* broth with 10 % FCS (BB/FCS). After cultivation in the presence of a labelled substrate, cells were harvested and ^{13}C-excess as well as isotopologue compositions were determined for 24 metabolites isolated from the cytosol as well as for 14 protein-bound amino acids. BB/FCS represents a nutrient-rich medium that ensures optimal, reproducible growth of *H. pylori* and reflects medicinally relevant conditions. During infection *H. pylori* is associated with gastric epithelial cells, which also provide a diverse set of nutrients for bacterial growth.

While [U-^{13}C$_6$]glucose was efficiently utilised in the ED pathway and for fatty acid synthesis, incorporation into the TCA cycle occurred at a much lower level. In contrast [U-^{13}C$_4$]aspartate, [U-^{13}C$_5$]glutamate and [U-^{13}C$_4$]succinate produced high enrichments in the TCA cycle but were barely utilised for gluconeogenesis. This pattern alluded to a bipartite metabolic network already observed for other pathogenic bacteria. Analysis of the incorporation pathways revealed a TCA cycle generally operating in a closed oxidation fashion in contrast to earlier reports. Additional fluxes in the reverse direction from oxaloacetate to succinate or from 2-oxoglutarate to citrate were observed when supplying [U-^{13}C$_4$]aspartate or [U-^{13}C$_5$]glutamate, respectively. Further, isotopologue compositions especially of malate indicated the activity of the glyoxylate bypass, which was thought to be absent in *H. pylori*. Activity of an isocitrate lyase was further demonstrated through an *in vitro* assay. The glyoxylate bypass could fulfil anaplerotic functions in *H. pylori* as classical carboxylation reactions to build up TCA cycle intermediates are missing in this bacterium. This was also corroborated through experiments with H^{13}CO$_3$ in this study. Hence the glyoxylate bypass, which is absent in humans, could be essential for *H. pylori* and thereby present a target for further drug development,

Author contribution I was involved in the design of the labelling experiments and performed the subsequent isotopologue analysis of polar metabolites and protein-bound amino acids. Additionally, I carried out analysis of the composition of BB/FCS-medium as well as quantification of metabolic products from *H. pylori*. I wrote the first draft of the manuscript and was involved in all steps of preparing the final manuscript.

RESEARCH ARTICLE

WILEY

Substrate usage determines carbon flux *via* the citrate cycle in *Helicobacter pylori*

Thomas M. Steiner[1] | Clara Lettl[2,3] | Franziska Schindele[2] | Werner Goebel [2] |
Rainer Haas[2,3] | Wolfgang Fischer [2,3] | Wolfgang Eisenreich [1]

[1]Bavarian NMR Center—Structural Membrane Biochemistry, Department of Chemistry, Technische Universität München, Garching, Germany

[2]Chair of Medical Microbiology and Hospital Epidemiology, Max von Pettenkofer Institute of Hygiene and Medical Microbiology, Faculty of Medicine, LMU Munich, München, Germany

[3]German Center for Infection Research (DZIF), Partner Site Munich, München, Germany

Correspondence
Wolfgang Fischer, Chair of Medical Microbiology and Hospital Epidemiology, Max von Pettenkofer Institute of Hygiene and Medical Microbiology, Faculty of Medicine, LMU Munich, München, Germany.
Email: Fischer@mvp.lmu.de

Wolfgang Eisenreich, Bavarian NMR Center—Structural Membrane Biochemistry, Department of Chemistry, Technische Universität München, Garching, Germany.
Email: wolfgang.eisenreich@mytum.de

Funding information
German Center for Infection Research (DZIF), Grant/Award Number: 8025806810; Deutsche Forschungsgemeinschaft, Grant/Award Number: 364653263

Abstract

Helicobacter pylori displays a worldwide infection rate of about 50%. The Gram-negative bacterium is the main reason for gastric cancer and other severe diseases. Despite considerable knowledge about the metabolic inventory of *H. pylori*, carbon fluxes through the citrate cycle (TCA cycle) remained enigmatic. In this study, different ^{13}C-labeled substrates were supplied as carbon sources to *H. pylori* during microaerophilic growth in a complex medium. After growth, ^{13}C-excess and ^{13}C-distribution were determined in multiple metabolites using GC–MS analysis. [U-^{13}C$_6$] Glucose was efficiently converted into glyceraldehyde but only less into TCA cycle-related metabolites. In contrast, [U-^{13}C$_5$]glutamate, [U-^{13}C$_4$]succinate, and [U-^{13}C$_4$] aspartate were incorporated at high levels into intermediates of the TCA cycle. The comparative analysis of the ^{13}C-distributions indicated an adaptive TCA cycle fully operating in the closed oxidative direction with rapid equilibrium fluxes between oxaloacetate—succinate and α-ketoglutarate—citrate. ^{13}C-Profiles of the four-carbon intermediates in the TCA cycle, especially of malate, together with the observation of an isocitrate lyase activity by in vitro assays, suggested carbon fluxes *via* a glyoxylate bypass. In conjunction with the lack of enzymes for anaplerotic CO_2 fixation, the glyoxylate bypass could be relevant to fill up the TCA cycle with carbon atoms derived from acetyl-CoA.

KEYWORDS

Helicobacter pylori, isocitrate lyase, isotopologue profiling, metabolic adaption, metabolism, TCA cycle

1 | INTRODUCTION

Helicobacter pylori (*H. pylori*) was first described in 1983 and since then it has been a subject of intense research (Warren & Marshall, 1983). The human pathogen colonizes the stomach of about 50% of the world's population (Hooi et al., 2017). While most infected individuals remain asymptomatic during their lifetime, *H. pylori* is considered to be the main cause of gastric cancer, which accounted for about 810,000 deaths worldwide in 2018 (de Martel et al., 2020). Additionally, the pathogen is responsible for a number of other diseases *e.g.* peptic ulcer disease, which is declining in prevalence, although to a regionally different extent (Lanas & Chan, 2017).

Thomas M. Steiner and Clara Lettl are contributed equally to this work as first authors.

43

2.2 Substrate usage determines carbon flux *via* the citrate cycle in *Helicobacter pylori*

Even though there is an established treatment of either first-line triple-therapy or second-line quadruple-therapy (Malfertheiner et al., 2017), the efficiency of the first-line therapy has declined below 80% in many countries (Fock et al., 2009; Megraud et al., 2013). There are still alternatives and additives for the current treatment, *e. g.* susceptibility-guided treatment, bismuth-therapy, or the usage of the potassium-competitive acid blocker vonoprazan as an alternative to proton pump inhibitors (O'Connor et al., 2019). Nevertheless, new means to fight resistant *H. pylori* are needed. The central bacterial metabolism is a promising target for novel antibiotics (Bhargava & Collins, 2015; Bishai, 2017; Murima et al., 2014). However, as a prerequisite for metabolism-guided drug development, full knowledge about the functional metabolic pathways of bacterial pathogens is required (Bhargava & Collins, 2015). To this aim, the unbiased, observation driven analysis of bacterial metabolism is timely as many species differ from the established metabolic pathways determined for model species. There are even metabolic differences within a species that can allow for resistance (Zampieri et al., 2017). Moreover, genome sequences alone hardly provide a complete view upon functional metabolism, especially under medicinally relevant conditions.

H. pylori is known to metabolize different carbon sources, especially glucose and amino acids. Metabolic usage of alanine, proline, arginine, aspartate, glutamate and serine was reported during growth in continuous culture (Stark et al., 1997). Arginine, histidine, isoleucine, leucine, methionine, phenylalanine and valine were shown to be essential for *H. pylori* (Reynolds et al., 1994). Glucose utilization was demonstrated (Hazell et al., 1997) either *via* the Entner-Doudoroff-pathway (ED-pathway) or the pentose phosphate pathway (PPP) (Mendz et al., 1994a). These pathways depend on a species-specific glucokinase in difference to the more general hexokinase found in many other organisms (Mendz et al., 1993a). NMR analysis of *H. pylori* cell extracts grown in medium supplemented with [U-^{13}C$_6$] glucose identified ^{13}C-labeled lactate as the main product, suggesting an active lactate fermentation pathway (Mendz et al., 1993b). Subsequently, experiments with ^{13}C-labeled pyruvate yielded labeled lactate, acetate, formate, and succinate, which were secreted into the medium. This metabolism is generally referred to as mixed acid fermentation, wherein pyruvate is metabolized to different organic acids without participation of oxygen. On this basis, it can be assumed that reduction of pyruvate into lactate serves to regenerate NAD$^+$, while transformation of pyruvate to acetyl-phosphate and further to acetate produces ATP (Mendz et al., 1994b). Formate is most likely produced through the pyruvate formate lyase reaction (Mendz et al., 1994b). Additionally, secretion of succinate suggests active fumarate reduction to regenerate reducing equivalents under microaerophilic conditions (also cf. Figure 1). Pyruvate was reported to enter the TCA cycle either by anaplerotic reactions, i.e., by carboxylation to oxaloacetate or malate, or *via* oxidation to acetyl-CoA, although genes encoding a potential pyruvate dehydrogenase complex are missing in the genome of *H. pylori* (Inamoto et al., 1995). H^{14}CO$_3^-$ was used as a tracer to detect potential carboxylation reactions in *H. pylori* (Hughes et al., 1995; St Maurice et al., 2007). These

experiments excluded anaplerotic activities in general, such as reactions catalyzed by pyruvate carboxylase or PEP carboxykinase. However, the data indicated action of a novel four-subunit pyruvate flavodoxin oxidoreductase (PFOR, enzyme 1 in Figure 1) and a pyruvate formate lyase converting pyruvate to a mixture of acetyl-CoA and formate in a reversible reaction (Hughes et al., 1998). These enzymes replace pyruvate dehydrogenase, which is typically observed in organisms operating an oxidative metabolism.

The architecture of the TCA cycle in *H. pylori* is still puzzling. There was experimental evidence for a closed and fully functioning TCA cycle (Ge, 2002; Hoffman et al., 1996). Notably, however, no activity for succinate dehydrogenase could be detected in the earlier studies, leaving the cycle incomplete (Pitson et al., 1999). In an alternative scenario, an incomplete, bifurcate topology of the TCA cycle was proposed (Han et al., 2018; Lee et al., 2017; Pitson et al., 1999) in which the cycle is split into two branches. Here, the putative oxidative branch produces succinyl-CoA from citrate *via* 2-oxoglutarate, while the reductive branch forms succinate from oxaloacetate through malate and fumarate. Indeed, carbon fluxes *via* an active succinate dehydrogenase or a reversibly acting fumarate reductase could be shown (Chen et al., 1999; Ge, 2002; Kather et al., 2000).

Similar experimental ambiguity was reported for a potential glyoxylate shunt where the TCA cycle intermediate isocitrate is transformed into succinate and glyoxylate. The latter product could then assemble with acetyl-CoA to form malate. Indeed, activity for malate synthase converting acetyl-CoA and glyoxylate into malate was detected on the basis of NMR assays, but there were no indications for an active isocitrate lyase (Pitson et al., 1999). On the other hand, earlier photometric assays suggested an active isocitrate lyase (Hoffman et al., 1996), leaving the question about a glyoxylate bypass in *H. pylori* unanswered.

Analysis of the *H. pylori* genome using the COG and KEGG databases (Galperin et al., 2015; Kanehisa et al., 2016) as well as recent annotations (Karlsson et al., 2016; Resende et al., 2013), suggests a fully functional TCA cycle with some alterations to the canonical enzymes (enzymes 2, 3, and 4 in Figure 1). Activity of these alternative enzymes has been observed experimentally. The reaction from 2-oxoglutarate to succinyl-CoA (enzyme 2) uses ferredoxin as an oxidizing agent instead of NAD$^+$ (Hughes et al., 1998); succinyl-CoA is transformed to succinate through a CoA-transferase (enzyme 3) using acetoacetate as the CoA-acceptor (Corthesy-Theulaz et al., 1997). Finally, malate oxidation to oxaloacetate uses quinone as the electron-acceptor (enzyme 4) (Kather et al., 2000). Although no designated succinate dehydrogenase is found in the genome, this reaction could be carried out by the respective fumarate reductase, whose bidirectionality was already observed, although with a strong preference for fumarate reduction (Lancaster et al., 2002). It is also noteworthy that genes encoding malate synthase or isocitrate lyase have not been annotated in the genome of *H. pylori*.

To investigate the carbon fluxes in the overall central metabolism of bacteria, labeling experiments starting from stable ^{13}C-enriched substrates (such as glucose, acetate, amino acids) and in-depth isotopologue profiling of the resulting metabolic products are now
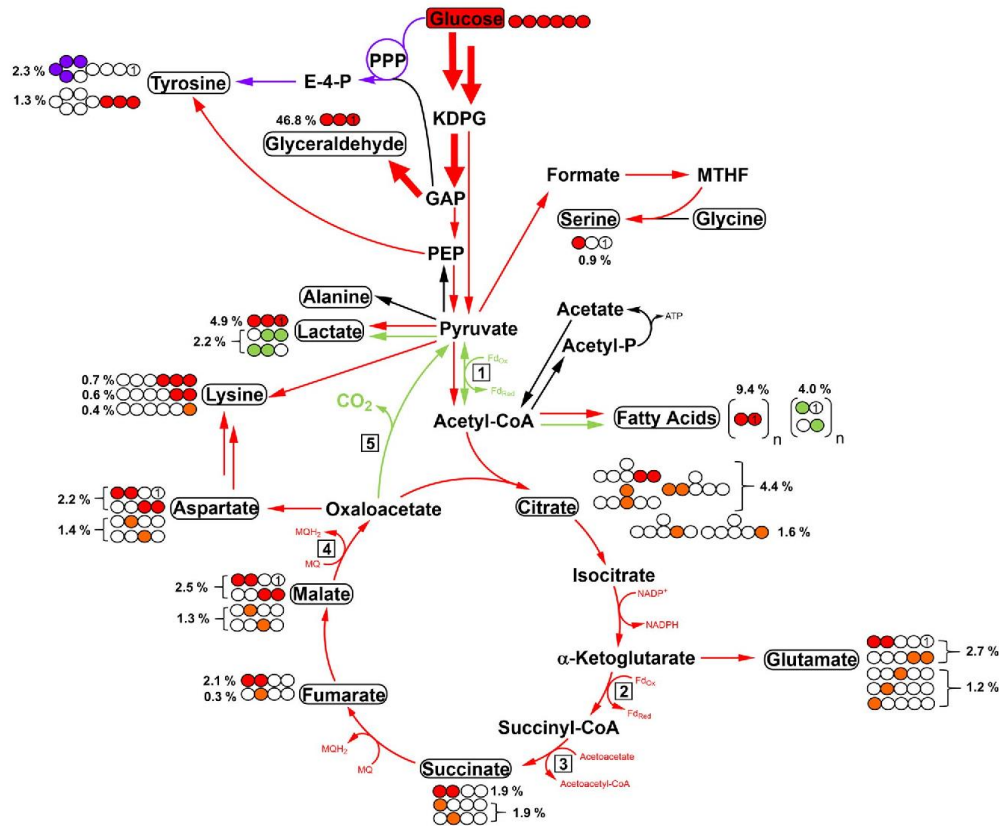
FIGURE 1 ^{13}C-Profiles in a model for the central carbon metabolism of *H. pylori* starting from [U-^{13}C$_6$]glucose. Red arrows indicate ^{13}C-incorporation *via* direct transformation of the substrate. Green arrows indicate carbon flux following the decarboxylation of oxaloacetate to pyruvate. Purple arrows indicate flux *via* the PPP. Colored circles signifiy the theoretical labeling positions for the respective isotopologue, while orange circles show isotopologues arising through propagation of labeled molecules through the TCA cycle. Percentages represent the observed ^{13}C-excess for the respective isotopologue. Metabolites in boxes were directly analysed *via* GC–MS. Numbers in boxes indicate unusual enzymes in the metabolism of *H. pylori*. 1: pyruvate-ferredoxin oxidoreductase; 2: 2-oxoglutarate-ferredoxin oxidoreductase; 3: succinyl-CoA:acetoacetate-CoA transferase; 4: malate:quinone oxidoreductase; 5: (4*S*)-4-hydroxy-2-oxoglutarate aldolase. PPP: pentose phosphate pathway; KDPG: 2-keto-3-desoxy-phosphogluconate; GAP: glyceraldehyde-3-phosphate; PEP: phosphoenolpyruvate; MTHF: methyltetrahydrofolate; Acetyl-P: acetyl-phosphate; MQ: menaquinone; Fd: ferredoxin

proven technologies (Buescher et al., 2015; Eisenreich et al., 2006; Long & Antoniewicz, 2019). In a typical setting, bacteria are grown in the presence of the labeled precursors for an appropriate period. After that, metabolic products are isolated from the cells and analyzed by mass spectrometry and/or NMR spectroscopy. Based on these analytical data, the ^{13}C-enrichments and their positional distribution can be determined in considerable detail. For example, the relative fractions of specific isotopologues (molecular species containing a given number of ^{13}C-atoms) assign the efficacies and pathways of substrate usages in the functional metabolic networks under study. As examples, this approach helped to elucidate metabolic pathways and fluxes in a variety of bacterial pathogens, including *Campylobacter jejuni*, a close relative to *H. pylori* (Gao et al., 2017).

Especially, ^{13}C-labeling experiments with intracellular pathogens served to elucidate carbon usage and fluxes in bipartite metabolic networks (Grubmüller et al., 2014; Häuslein et al., 2016). In these bipartite topologies, two or more carbon substrates are utilized, with each substrate fulfilling a distinct metabolic role. In a simplified view, one class of substrates is used to produce sugars for cell wall synthesis and another class of substrates serves to produce energy. This co-utilization of multiple substrates allows for more metabolic flexibility during changes in the nutritional environment throughout infection and additionally reduces the metabolic burden on the host, as no selective deprivation of a single substrate occurs due to infection (Best & Abu Kwaik, 2019; Eisenreich et al., 2015, 2017, 2019). We now have exploited the ^{13}C-technology for a comprehensive

2.2 Substrate usage determines carbon flux *via* the citrate cycle in *Helicobacter pylori*

analysis of substrate usages in the core carbon metabolism of *H. pylori* with a special focus on carbon fluxes *via* the TCA cycle.

2 | RESULTS AND DISCUSSION

2.1 | Glucose and amino acids serve as main carbon substrates for growth of *H. pylori* in *Brucella* broth medium

To assess the metabolic capabilities of *H. pylori*, we grew the pathogen in the complex *Brucella* broth medium containing 10% fetal calf serum (BB/FCS). Growth in minimal medium could provoke stress response and lead to a degenerate metabolic phenotype, which is not representative for the actual metabolic capabilities of the pathogen. Additionally, *H. pylori* resides in the mucus layer in close proximity to human gastric epithelial cells (Dunne et al., 2014; Schreiber et al., 2004). In this environment, various carbon substrates provided by the epithelial cells most probably serve as nutrients for bacterial survival and replication during infection (Hirayama et al., 2009; Tan et al., 2009). In conclusion, an in vitro setting where the bacteria are grown in the presence of several potential carbon sources appeared superior to a setting where the bacteria are replicating under precarious conditions such as in a minimal medium with a limited supply of potential carbon substrates. Moreover, there are no reports about carbon catabolite repression being active in *H. pylori* (Windham et al., 2018) again suggesting the parallel usage of multiple carbon substrates, as already observed for other pathogens (Eisenreich et al., 2017).

To assess the amounts of potential substrates in BB/FCS, especially of those compounds, which were added as ^{13}C-tracers in the labeling experiments described below, we analyzed the dried medium by GC–MS (Table 1). To account for protein/peptide-bound amino acids, the medium was also hydrolyzed using hydrochloric acid and the resulting hydrolysate was again analyzed by GC–MS. Free amino acids were found at amounts of 0.4–4.1 mM only. Notably, the concentrations of those amino acids, which were supplied as ^{13}C-tracers in the labeling experiments, did not significantly exceed 1 mM. As expected, these levels increased to 2.8–20.1 mM when the proteins/peptides in the medium were hydrolyzed under harsh acidic conditions. Glycerol was present at a low concentration of 0.5 mM, while succinate was found at minor amounts of 0.1 mM. Citrate as well as acetate were virtually absent (<0.01 mM). According to the manufacturer's specifications, glucose was present at a concentration of 4.5 mM in BB/FCS medium. On this basis, glucose and peptides/amino acids can be considered as the main carbon substrates for *H. pylori* grown in BB/FCS medium. In the labeling experiments, ^{13}C-tracers were added at concentrations of 5 or 10 mM. Thus, these concentrations largely exceeded the amounts of the respective compounds in fresh BB/FCS medium except for glucose (see above). Under the respective conditions of the labeling experiments, a potential reprogramming of the carbon metabolism of *H. pylori* can therefore be envisaged due to the changing substrate availabilities.

TABLE 1 Concentration of potential carbon substrates in BB/FCS. To account for protein- and peptide-bound amino acids, the medium was also hydrolyzed in 6 M HCl

Metabolite	Concentration [mM]	Concentration after hydrolysis [mM]
Alanine	1.4 ± 0.3	8.2 ± 0.3
Glycine	0.5 ± 0.1	8.1 ± 0.2
Valine	1.3 ± 0.3	7.3 ± 0.2
Leucine	4.1 ± 0.8	11.1 ± 0.1
Isoleucine	1.2 ± 0.2	4.8 ± 0.1
Proline	0.4 ± 0.1	10.6 ± 0.1
Serine	1.1 ± 0.3	6.5 ± 1.8
Phenylalanine	1.5 ± 0.3	4.6 ± 0.1
Aspartate	0.4 ± 0.1	13.4 ± 0.2
Glutamate	1.1 ± 0.2	20.1 ± 0.2
Lysine	1.2 ± 0.1	7.1 ± 0.4
Tyrosine	0.5 ± 0.1	2.8 ± 0.1
Glycerol	0.5 ± 0.3	n.d.
Succinate	0.1 ± 0.1	n.d.
Citrate	0.0 ± 0.0	n.d.

Note: Standard deviations are based on six values (2 × biological replicates and 3 × technical replicates each).
Abbreviation: n.d. = not determined.

2.2 | [U-^{13}C$_6$]Glucose is efficiently metabolized via the ED-pathway providing labeled glyceraldehyde, pyruvate and acetyl-CoA for fatty acid biosynthesis

Glucose was already reported as a main nutrient used by *H. pylori* growing on horse blood agar plates (Mendz et al., 1993a). To test this finding for *H. pylori* growing in BB/FCS, we added [U-^{13}C$_6$]glucose to this medium at a final concentration of 10 mM and grew *H. pylori* for 15 hr until the mid-exponential growth phase. A representative growth curve is shown in the supplementary information (Figure S1). Bacteria were harvested and GC–MS analysis of multiple metabolites served to elucidate the uptake and metabolic pathways for glucose usage. From cytosolic metabolites obtained *via* mechanical disruption of the cells in methanol, ^{13}C-excess and isotopologue profiles for 24 metabolites were determined (for numerical values, see Table S1). The most important results are summarized in Figure 1, integrating the detected ^{13}C-incorporation of key metabolites into a best possible model for the central carbon metabolism of *H. pylori*. This model was designed on the basis of enzyme activities as expected from the reported genome of *H. pylori* P12 in the KEGG database (Fischer et al., 2010) and recent genome annotations (Kanehisa et al., 2016; Karlsson et al., 2016; Resende et al., 2013).

Efficient uptake and degradation of glucose *via* the ED-pathway and/or the PPP was reflected by the ^{13}C-excess of 47% in the predominant M + 3 species in glyceraldehyde, i.e., the isotopologue carrying three ^{13}C-atoms obtained by conversion of [U-^{13}C$_6$]glucose into [U-^{13}C$_3$]glyceraldehyde phosphate (GAP) and further to [U-^{13}C$_3$]

glyceraldehyde (i.e., M + 3) either by a phosphatase or chemical hydrolysis during sample processing.

Tyrosine is constructed in the shikimate pathway from erythrose 4-phosphate (E-4-P) originating from the PPP, as well as phosphoenolpyruvate (PEP), which is produced from GAP. ^{13}C-Excess in tyrosine is therefore another indication of active glucose metabolization *via* the ED-pathway and the PPP. Indeed, tyrosine displayed significant ^{13}C-excess in form of the M + 3 isotopologue (1.3%) and the M + 4 isotopologue (2.3%). This pattern was in line with an active shikimate pathway using M + 3 ^{13}C-labeled PEP derived from [U-^{13}C$_3$]GAP and M + 4 E-4-P, produced in the PPP from [U-^{13}C$_6$] glucose.

Phenylalanine biosynthesis also proceeds *via* the shikimate pathway. In contrast to tyrosine, phenylalanine did not acquire significant ^{13}C-excess >0.5% (Table S1). Similarly, valine, leucine, isoleucine and methionine were also unlabeled from [U-^{13}C$_6$]glucose. This was expected as these amino acids are essential for *H. pylori* growth and their respective biosynthetic pathways are not or only partially annotated in the genome of *H. pylori* (Nedenskov, 1994; Reynolds et al., 1994). Also, alanine, proline and glycine did not display significant ^{13}C-excess, even though *H. pylori* would have been capable of synthesizing them based on the genome annotations. However, as shown above, these amino acids were abundant in free as well as in bound form in the BB/FCS medium and were presumably taken up (in unlabeled form) from the environment. Looking at the physiological environment of *H. pylori*, the gastric juice of *H. pylori*-infected individuals also contains high amounts of proline and alanine (Nagata et al., 2003). Additionally, proline and glycine are the main components of the amino acid backbone in the collagen structure (Shoulders & Raines, 2009), and *H. pylori* has been shown to secrete a collagenase upon infection, which is essential for colonization in vivo (Kavermann et al., 2003). The abundance of these substrates in the ecological niche of *H. pylori* might therefore explain the reduced preference for their synthesis as an adaption to this niche.

In serine, only the M + 1 isotopologue was observed with a ^{13}C-excess of 0.9%, but not the M + 3-isotopologue that would have indicated serine biosynthesis *via* [U-^{13}C$_3$]3-phosphoglycerate and phosphohydroxypyruvate. This was also expected from genomic data where a gene for phosphohydroxypyruvate transaminase is not annotated. The observed M + 1 isotopologue in serine rather arose through a C$_1$-fixation pathway starting from unlabeled glycine and a ^{13}C$_1$-source. Most likely, ^{13}C$_1$-formate is generated as a product from [U-^{13}C$_3$]pyruvate by mixed acid fermentation affording formate and acetate (Mendz et al., 1994b). ^{13}C-Formate could then be converted by a 10-formyltetrahydrofolate amidohydrolase into ^{13}C$_1$-10-formyltetrahydrofolate, which can further be reduced to ^{13}C$_1$-5,10-methylene-5,6-7,8-tetrahydrofolate (MTHF) serving as the precursor for serine catalyzed by serine hydroxymethyltransferase.

The production of labeled lactate from [U-^{13}C$_6$]glucose corroborated an active lactate dehydrogenase (Mendz et al., 1993b). Indeed, the dominant isotopologue was the M + 3 species (4.9%) which can be explained by the lactate dehydrogenase reaction, i.e., it is derived from [U-^{13}C$_3$]pyruvate. Interestingly, there was also a significant fraction of M + 2 present in lactate (2.2%). Analysis of the fragmentation patterns in the mass spectrum of silylated lactate, i.e., by comparison of the mass fractions in fragments comprising C1–C3 or C2–C3 of lactate, revealed similar amounts of [1,2-^{13}C$_2$]- and [2,3-^{13}C$_2$]lactate. The formation of [1,2-^{13}C$_2$]lactate suggested an oxaloacetate decarboxylating enzyme that converts [1,2-^{13}C$_2$]oxaloacetate into [1,2-^{13}C$_2$]pyruvate (cf. Figure 1, enzyme 5). However, PEP carboxykinase or oxaloacetate decarboxylase are not annotated in the genome of *H. pylori*. Therefore, an alternative non-classical oxaloacetate decarboxylating enzyme must be active. Most probably, this reaction is catalyzed by a (4S)-4-hydroxy-2-oxoglutarate aldolase annotated in the genome (enzyme 5 in Figure 1). Indeed, this enzyme is known to produce pyruvate from oxaloacetate (Nishihara & Dekker, 1972), thereby explaining the formation of [1,2-^{13}C$_2$]pyruvate from [1,2-^{13}C$_2$]oxaloacetate. [1,2-^{13}C$_2$]Pyruvate could then be reduced to [1,2-^{13}C$_2$]lactate (cf. Figure 1). The formation of [2,3-^{13}C$_2$]lactate suggested additional carbon fluxes *via* the reversible PFOR (enzyme 1, Figure 1) (St Maurice et al., 2007) starting from [U-^{13}C$_2$]acetyl-CoA. This reaction yields [2,3-^{13}C$_2$]pyruvate, which is reduced to [2,3-^{13}C$_2$]lactate.

However, the main role of formed acetyl-CoA *via* PFOR (enzyme 1 in Figure 1) (St Maurice et al., 2007) seemed to be its function as the substrate for fatty acid synthesis as reflected by significant ^{13}C-excess in evenly (9.4%) and unevenly (4.0%) labeled isotopologues of myristate (see Figure 1), which represents the major component in lipid extracts from *H. pylori* (Inamoto et al., 1995). The isotopologue profiles of all detected fatty acids displayed mostly even-numbered labeled isotopologues using ^{13}C$_2$-acetyl-CoA as the precursor, but also a significant portion of odd label, indicating the usage of M + 1-labeled acetyl-CoA for fatty acid synthesis as well. The formation of this isotopologue can be explained by fluxes involving the citrate cycle and action of enzymes 5 and 1, respectively (cf. Figure 1; green colored). For example, following this route, [1,2-^{13}C$_2$] oxaloacetate could be converted into [1,2-^{13}C$_2$]pyruvate and further into [1-^{13}C$_1$]acetyl-CoA.

To further examine the architecture of the TCA cycle, we analyzed citrate, fumarate, malate and succinate as direct intermediates as well as aspartate and glutamate (Figure 1, Table S1). These amino acids can be used as approximations for oxaloacetate and α-ketoglutarate, respectively (Eisenreich et al., 2006). The ^{13}C-incorporation into these compounds was much lower in comparison to glyceraldehyde (see Table S1 and Figure S1). This immediately suggests that the TCA cycle was mainly fueled by unlabeled substrates rather than from the labeled glucose (see also below).

Nevertheless, the observed low ^{13}C-enrichments and profiles still allowed some insights into the fluxes through the TCA cycle (cf. Figure 1). Citrate and free glutamate mainly displayed the M + 1 and M + 2 isotopologues, reflecting the usage of ^{13}C$_2$- and ^{13}C$_1$-acetyl-CoA for the formation of citrate in the TCA-cycle and its conversion into α-ketoglutarate/glutamate. The presence of the M + 3 and M + 4 isotopologues at lower abundances indicated that oxaloacetate, the other precursor for citrate, also carried ^{13}C-atoms (Table S1). The labeling pattern of glutamate generally corresponded

2.2 Substrate usage determines carbon flux *via* the citrate cycle in *Helicobacter pylori*

well to succinate and the other TCA cycle intermediates, leading to significant fractions of the M + 2 and M + 1 isotopologues in succinate, fumarate, malate, and oxaloacetate/aspartate, respectively. Interestingly, all C_4-compounds also showed minor amounts of the M + 3 isotopologues (Table S1). Since *H. pylori* appears to lack enzymes converting M + 3 pyruvate or PEP into oxaloacetate or malate, this was indicative of an alternative anaplerotic route and will be further discussed below with the experiment using ^{13}C-bicarbonate. As the M + 3 isotopologue was most prominent in malate, it was tempting to speculate that ^{13}C$_3$-malate could arise in a reaction catalyzed by malate synthase combining M + 2 or M + 1 labeled acetyl-CoA with labeled glyoxylate. Notably, earlier in vitro enzyme assays reported the presence of a malate synthase reaction in cell extracts of *H. pylori* (Pitson et al., 1999) (see also below).

We also analyzed the ^{13}C-excess and isotopologue distribution of 13 different proteinogenic amino acids, which were obtained after acidic hydrolysis (Table S11). Here, the values mostly matched the ones of free amino acids in the cytosolic fraction of *H. pylori* underlining the expected metabolic and isotopic steady state conditions in our experimental setting. The similarity in terms of isotopologue composition between protein-bound and free amino acids validated the experimental protocol as it excludes metabolic alterations due to sample processing. Such alterations would translate within minutes into the isotopologue composition of cytosolic amino acids (Buescher et al., 2015), leading to differences compared to their bound equivalents, which were not observed. The labeling pattern of lysine could only be observed after protein hydrolysis. Here, the observed M + 3, M + 2 and M + 1 isotopologues indicated the well-known biosynthetic pathway using the detected ^{13}C-specimens in aspartate and pyruvate as precursors.

2.3 | [U-^{13}C$_3$]Glycerol is not metabolized by *H. pylori*

To eventually gain more insight into the downstream reactions of carbohydrate degradation, [U-^{13}C$_3$]glycerol was supplied to *H. pylori* (Table S5). Glycerol could have entered the PPP *via* its transformation to glyceraldehyde 3-phosphate. However, besides efficient uptake of the substrate resulting in 54% ^{13}C-excess in glycerol re-isolated from the cytosolic fraction, no significant incorporation into other metabolites was detected. Therefore, glycerol did not serve as a major carbon substrate under the experimental conditions. However, we could not rule out that exogenous glycerol was used as a building block for the glycerol moiety in glycerolipids, which were not among the metabolites under study.

2.4 | [U-^{13}C$_3$]Serine is efficiently utilized and the labeling data support the metabolic model derived from the glucose experiment

Serine, a major component of gastric juice, was reported, next to glucose, as another main carbon source for *H. pylori* (Nagata

et al., 2007). In line with this hypothesis, addition of serine increased the respiratory activity of *H. pylori* under in vitro conditions (Nagata et al., 2003). Two possible uptake systems for serine exist in *H. pylori*, SdaC specifically for *L*-serine, and DagA for *D*-serine as well as for *D*-alanine and glycine (Tomb et al., 1997). Indeed, the high ^{13}C-excess of ~63% in free serine from the polar fraction (Figure S2, Table S2) indicated efficient uptake of the [U-^{13}C$_3$]serine supplement in our experimental setting. The label distribution in other metabolites showed similarities to the experiment with [U-^{13}C$_6$]glucose (Figure 1, Table S1) since both precursors afford [U-^{13}C$_3$]pyruvate as a common intermediate. This was not unexpected, since [U-^{13}C$_3$]serine is directly converted to M + 3 pyruvate *via* serine dehydratase, and the detection of the M + 3 isotopologues in lactate (3.5%) and alanine (0.5%) derived from pyruvate confirmed this route. Here, lactate showed significant ^{13}C-excess of 8.6%, but the isotopologue profile differed significantly from the one in serine, although the carbon skeleton should remain unchanged through the transformation from serine to lactate *via* pyruvate. The M + 1 (2.6%) and M + 2 (4.2%) isotopologues in lactate were much more prevalent than in serine. This indicated that a higher fraction of lactate was produced from pyruvate arising through decarboxylation of oxaloacetate (enzyme 5, Figure S2), and not *via* deamination of serine. At the level of M + 3 pyruvate, the downstream reactions followed the pathways described above for the labeling experiments with [U-^{13}C$_6$]glucose. Indeed, transformation of M + 3-labeled pyruvate yielded M + 2 acetyl-CoA, fatty acids and TCA cycle-related metabolites at low but significant ^{13}C-excess (Figure S2). Additionally, and in contrast to the glucose experiment, significant ^{13}C-excess was found in M + 2 glycine (17.6%), providing evidence for an active serine hydroxymethyltransferase (see also above) forming ^{13}C$_2$-glycine from ^{13}C$_3$-serine (Figure S2).

Compared to the glucose labeling experiment, with no detectable ^{13}C-enrichment in free alanine, there was now a low but significant ^{13}C-excess in form of the M + 3 isotopologue (0.5%). This could be due to the action of amino acid uptake by DagA, which is capable of the uptake of serine, alanine and glycine. In contrast to the glucose experiment, the addition of large amounts of ^{13}C-serine to the medium might raise the need for de novo alanine synthesis, as the DagA uptake system (also capable of alanine uptake) could be saturated by the abundant serine supply and the uptake of alanine was therefore hampered. The proteinogenic amino acids (Table S12) showed again similar excess values and isotopologue distribution as the ones from the cytosolic fraction.

2.5 | Use of ^{13}C-bicarbonate shows only minor carboxylating activities in *H. pylori* and excludes classical anaplerotic reactions

To investigate the usage of bicarbonate in anaplerotic reactions and, generally, to get more insights into the capnophilic nature of *H. pylori* (Bury-Mone et al., 2006), we grew *H. pylori* in BB/FCS medium containing 50 mM ^{13}C-bicarbonate. In a similar setting, the efficient

usage of ^{13}C-bicarbonate was shown for *C. jejuni*, a close relative to *H. pylori* (Gao et al., 2017). Notably, gastric extracts contain 25 mM bicarbonate, thus providing a potential (additional) carbon source for *H. pylori* (Feldman, 1983).

In our labeling experiment, ^{13}C-bicarbonate did not produce ^{13}C-excess in the metabolites under study, except for minor enrichments (<2%) in citrate, glycerol and serine as M + 1 isotopologues (Table S6). The data suggested that a minor fraction of M + 1 ^{13}C-pyruvate was generated through carboxylation of acetyl-CoA *via* PFOR as reported earlier (enzyme 1, as indicated in Figure 1) and using ^{13}C-bicarbonate as a substrate (Hughes et al., 1995; St Maurice et al., 2007). M + 1 ^{13}C-pyruvate could then be converted into M + 1 glycerol and M + 1 serine following the routes shown in Figure 1. No evidence was obtained for other CO_2 or bicarbonate utilizing pathways, in particular producing labeled acetyl-CoA, which would have been detected in labeled fatty acids or TCA cycle intermediates. Notably, fatty acids and TCA cycle intermediates (except for a minor fraction of ^{13}C-citrate, see below) were devoid of ^{13}C-label in this experiment.

This finding also indicated that *H. pylori* did not use reactions indicative for the reductive TCA cycle *via* citrate lyase or its variant *via* citrate synthase (Mall et al., 2018), the 3-hydroxypropionate/4-hydroxybutyrate cycle or the dicarboxylate/4-hydroxybutyrate cycle (Hügler et al., 2011), thus confirming the metabolic model shown in Figure 1. The small amount of M + 1 label present in citrate (0.8%) could be explained by a reversible isocitrate dehydrogenase in line with the results of the [U-^{13}C$_5$]glutamate experiment (see below).

Looking at the genomes of the 61 *H. pylori* strains in the KEGG database (Kanehisa et al., 2016), including *H. pylori* P12 used in this study, all of them lack any form of phosphoenolpyruvate carboxylase or pyruvate carboxylase. In contrast, all other members of the family of *Helicobacteriaceae*, of which the genomes are sequenced, including other *Helicobacter* species, *Sulfurimonas denitrificans* (Sievert et al., 2008), *Wolinella succinogenes* (Baar et al., 2003), *Sulfuricurvum kujiense* (Han et al., 2012), and *Sulfurovum lithotrophicum* (Jeon et al., 2017), show the genomic sequence for at least one of these carboxylating enzymes. *Helicobacter acinonychis* is the only exception, but was shown to be the closest relative to *H. pylori* when analyzing the 16S and 23S rRNA genes of 55 *Helicobacter* species (Dewhirst et al., 2005), and is supposed to have originated from *H. pylori* after a host jump (Eppinger et al., 2006). Looking further into the order of *Campylobacterales*, anaplerotic enzymes also appear as a common feature. Moreover, other extracellular pathogens like enterohemorrhagic *Escherichia coli* (Perna et al., 2001), *Pseudomonas aeruginosa* (Stover et al., 2000) or *Staphylococcus aureus* (Kuroda et al., 2001) show the ability to replenish the TCA cycle *via* carboxylation reactions. Therefore, the lack of "classical" anaplerosis seems to be a specific feature of *H. pylori* metabolism probably resulting from the coevolution with its human host for at least 88,000 years (Moodley et al., 2012). This coevolution led to a high level of adaption of *H. pylori* to its ecological niche (Ailloud et al., 2019; Atherton & Blaser, 2009). This is also apparent by the reduced genome size of *H. pylori* (~ 1.68 Mbp) compared to *W. succinogenes* (~ 2.1 Mbp).

More specifically, *H. pylori* probably adapted to utilize a variety of substrates from its environment without the need for an efficient C1-anaplerosis using either bicarbonate or CO_2—metabolic traits that probably go back to the early evolution and origin of life (Fuchs, 2011; Weiss et al., 2016). Rather, the finding that CO_2 or bicarbonate are not relevant in the metabolic network of *H. pylori* supported the hypothesis that the capnophilic nature of *H. pylori* is related to non-metabolic cellular functions like the control of acetyl-CoA carboxylase (Burns et al., 1995), buffering of the periplasmic pH through carbonic anhydrase (Marcus et al., 2005), or suppressing the stringent response (Park et al., 2011).

2.6 | [U-^{13}C$_5$]Glutamate or [U-^{13}C$_4$]succinate is efficiently metabolized *via* a closed TCA cycle, with rapid equilibrium fluxes between α-ketoglutarate and citrate

As discussed above, ^{13}C-glucose was efficiently used in the ED-pathway but yielded comparably low ^{13}C-incorporation into TCA cycle related metabolites. This suggested that the cycle had to be fueled by additional carbon sources without the involvement of C1-anaplerosis (see above). To identify these carbon sources and to further elucidate the carbon fluxes in the TCA cycle, we used [U-^{13}C$_5$] glutamate or [U-^{13}C$_4$]succinate as supplements to *H. pylori* growing in BB/FCS.

The high excess in free glutamate (46%) isolated from the polar fraction of bacteria supplemented with [U-^{13}C$_5$]glutamate suggested its efficient uptake. Quite obviously, [U-^{13}C$_5$]glutamate entered the TCA cycle *via* transamination to [U-^{13}C$_5$]α-ketoglutarate (Figure 2). Consequently, succinate and citrate displayed high ^{13}C-excess values in terms of the M + 4 (17.3%) or M + 5 isotopologues (10.9%), respectively. A typical α-ketoglutarate dehydrogenase is absent in *H. pylori* (Pitson et al., 1999). However, the production of M + 4 succinate from [U-^{13}C$_5$]α-ketoglutarate/glutamate can be explained by an α-ketoglutarate oxidoreductase producing ^{13}C$_4$-succinyl-CoA (enzyme 2 in Figure 2) (Hughes et al., 1998). ^{13}C$_4$-Succinyl-CoA is then converted to [U-^{13}C$_4$]succinate *via* a known CoA-transferase of *H. pylori* (enzyme 3 in Figure 2), which uses acetoacetate as the CoA-acceptor (Corthesy-Theulaz et al., 1997). Further propagation of M + 4 succinate through the TCA cycle produced the predominant M + 4 isotopologues in fumarate, malate and aspartate.

Formation of M + 5 labeled citrate suggested a rapid equilibrium between citrate and glutamate through the action of a reversible isocitrate dehydrogenase leading to [U-^{13}C$_5$]aconitate by reaction of [U-^{13}C$_5$]α-ketoglutarate with unlabeled bicarbonate/CO_2 (Buchanan et al., 2017; Kanao et al., 2002). Aconitase was already shown to act reversibly in *H. pylori* (Pitson et al., 1999), thus affording the detected M + 5 ^{13}C-citrate from [U-^{13}C$_5$]aconitate. Further reaction *via* an active citrate lyase or reverse citrate synthase reaction producing acetyl-CoA and oxaloacetate can be excluded as utilization of M + 5 citrate would produce M + 3 labeled aspartate, malate and fumarate, but not the observed predominant M + 4 labeled specimens

2.2 Substrate usage determines carbon flux *via* the citrate cycle in *Helicobacter pylori*
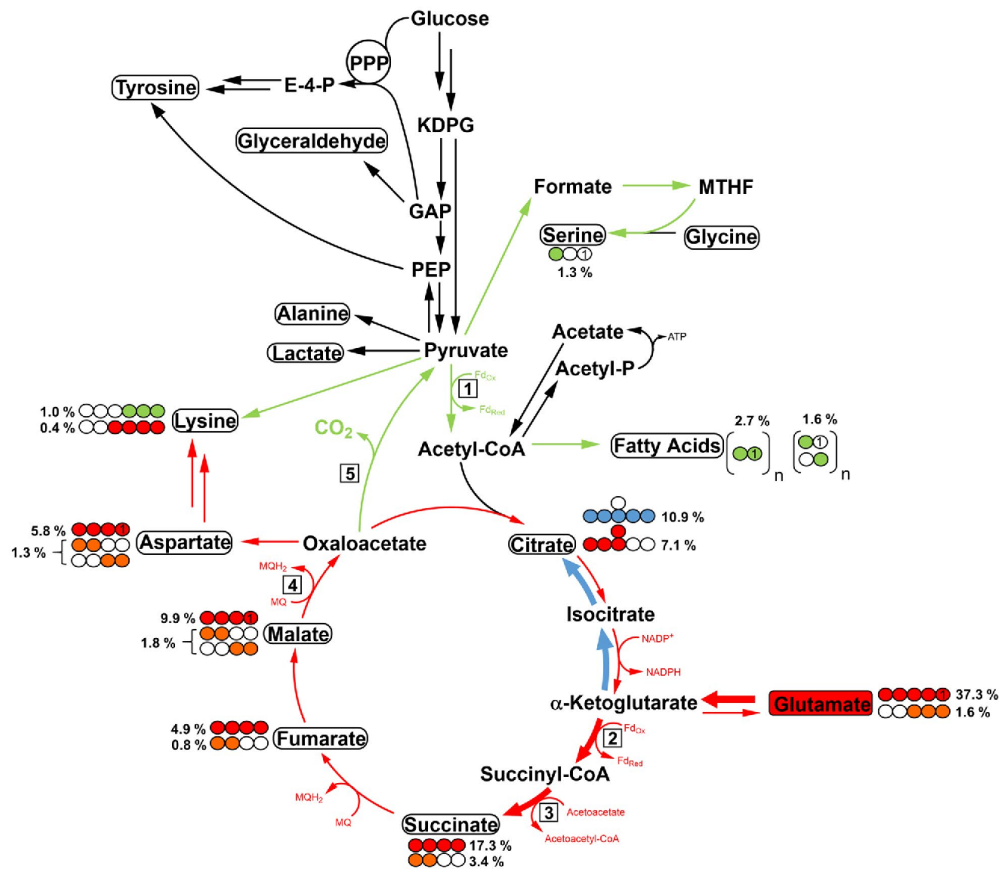
FIGURE 2 ^{13}C-Profiles in a model for the central carbon metabolism of *H. pylori* starting from [U-^{13}C$_5$]glutamate in the central carbon metabolism of *H. pylori*. Red arrows indicate ^{13}C-incorporation *via* direct transformation of the substrate, while blue arrows signify metabolisation *via* the TCA cycle in the reverse direction. Green arrows indicate carbon flux following the decarboxylation of oxaloacetate to pyruvate. Colored circles signifiy the theoretical labeling positions for the respective isotopologue, while orange circles show isotopologues arising through propargation of labeled molecules through the TCA cycle. Percentages represent the observed ^{13}C-excess for the respective isotopologue. Metabolites in boxes were directly analysed *via* GC–MS. Numbers in boxes indicate unusual enzymes in the metabolism of *H. pylori*. 1: pyruvate-ferredoxin oxidoreductase; 2: 2-oxoglutarate-ferredoxin oxidoreductase; 3: succinyl-CoA:acetoacetate-CoA transferase; 4: malate:quinone oxidoreductase; 5: (4S)-4-hydroxy-2-oxoglutarate aldolase. PPP: pentose phosphate pathway; KDPG: 2-keto-3-desoxy-phosphogluconate; GAP: glyceraldehyde-3-phosphate; PEP: phosphoenolpyruvate; MTHF: methyltetrahydrofolate; Acetyl-P: acetyl-phosphate; MQ: menaquinone; Fd: ferredoxin

of these metabolites. The apparent equilibrium between labeled α-ketoglutarate and labeled citrate supported carbon fluxes from α-ketoglutarate in the reverse direction of the TCA cycle potentially filling up the pools for isocitrate (required as a substrate for the isocitrate lyase reaction, see below) or the generation of NADP$^+$ in the reverse isocitrate dehydrogenase reaction (required *e.g.* as the oxidant in the glucose 6-phosphate dehydrogenase reaction of the ED-pathway). Alternatively, it is also tempting to speculate that citrate is the desired product *via* this route, which might then be secreted and used as a signal for host cells. To further check this hypothesis, we analyzed the amount of citrate in the medium by GC–MS from the

growth experiment with [U-^{13}C$_5$]glutamate as well as with [U-^{13}C$_2$] glycine, [U-^{13}C$_3$]serine, or [U-^{13}C$_4$]aspartate for comparison (Table S23). However, the detected reverse flux caused by ^{13}C-glutamate in the TCA cycle did not lead to increased levels of citrate or isocitrate in the supernatant as compared to the other experiments. Nevertheless, it cannot be excluded that secretion of citrate could be relevant when *H. pylori* thrives in the human host environment.

[U-^{13}C$_4$]Succinate was also efficiently taken up and metabolized, thereby producing similar labeling patterns in aspartate, fumarate and malate as in the experiment with [U-^{13}C$_5$]glutamate (Figure S3). Besides succinate from the cytosolic fraction, malate had the highest

^{13}C-excess (31.6%) followed by fumarate (23.4%) and aspartate (11.8%) (Table S8). The data did not support a reverse α-ketoglutarate oxidoreductase since the fraction of the M + 4 isotopologue in glutamate was very low (1.2%). Citrate showed a diverse labeling pattern with M + 4 as the main isotopologue. The formation of this isotopologue starting from either [U-^{13}C$_5$]glutamate or [U-^{13}C$_4$]succinate provided strong evidence for fluxes *via* a closed oxidative TCA cycle as the complete ^{13}C-backbone of the respective tracers remained intact throughout the cycle. Photometric measurements in *H. pylori* cell extracts also support the activity of a succinate oxidizing enzyme (Chen, 1999; Lancaster & Simon, 2002). However, it is still unclear whether the fumarate reductase in *H. pylori* can act in a reversible fashion, as proposed earlier (Ge et al., 2000), or whether another unidentified enzyme is capable of succinate oxidation.

2.7 | Labeling profiles produced from [U-^{13}C$_4$] aspartate support the closed TCA cycle topology

In earlier experiments, it was shown that the addition of aspartate increases the growth rate of *H. pylori* during co-incubation with gastric epithelial cells (van Amsterdam & Ende, 2004). On the other hand, aspartate did not increase the respiratory activity when added during in vitro cultivation (Nagata et al., 2003). However, in our labeling experiment with [U-^{13}C$_4$]aspartate, we observed very high ^{13}C-excess especially in TCA cycle related metabolites, which are indirectly connected to respiratory activity (Table S3, Figure S3). More specifically, malate, succinate and fumarate reflected efficient incorporation of [U-^{13}C$_4$]aspartate by M + 4 isotopologues above 26% (Figure 3). Besides transamination of aspartate to oxaloacetate, aspartate can be converted into fumarate by the catalytic action of aspartate ammonia lyase, a well-known reaction in *H. pylori* (Mendz & Hazell, 1995). Minor amounts of the M + 3 species (about 3%, Table S3) in these metabolites could be due to an active malate synthase reaction combining M + 1 or M + 2 labeled acetyl-CoA and glyoxylate (see below).

Additionally, citrate and glutamate were also significantly labeled, as well as fatty acids (Table S3). The predominant M + 4 (citrate) or M + 3 (glutamate) isotopologues in these metabolites arose through the conversion of ^{13}C$_4$-aspartate to M + 4 oxaloacetate, which was subsequently used by the citrate synthase affording M + 4 citrate. Subsequently, M + 4 citrate was transformed into M + 3 α-ketoglutarate and the detected M + 3 glutamate. Accordingly, the heavier isotopologues resulted from combinations of M + 4 oxaloacetate and M + 1/M + 2 acetyl-CoA. The production of M + 3 pyruvate/alanine as well as M + 2 acetyl-CoA/fatty acids again corroborated the activity of an oxaloacetate decarboxylating enzyme, most likely of the (4*S*)-4-hydroxy-2-oxoglutarate aldolase (see above; enzyme 5 in Figure 3).

The proteinogenic amino acid fraction (Table S13) also showed significant ^{13}C-excess in aspartate, glutamate and threonine. Additionally, alanine, lysine and tyrosine displayed ^{13}C-excess values ranging from 1.5% to around 10%. These profiles matched the data of

free amino acids from the polar fraction. The isotopologue composition of lysine was dominated by M + 3 (3.7%) and M + 4 (4.0%) species, while tyrosine mostly consisted of M + 1-, M + 2- and M + 3-labeled molecules (0.8%). In terms of lysine, this indicated the usage of fully labeled aspartate (M + 4) or pyruvate (M + 3) as precursors, while tyrosine was synthesized with differently labeled PEP as a building block. The absence of significant amounts of heavier isotopologues (>M + 3) in tyrosine reflected that labeled E-4-P was not produced *via* gluconeogenesis and the PPP at significant rates (cf. Figure 3).

2.8 | [U-^{13}C$_4$]Aspartate leads to rapid equilibrium fluxes between oxaloacetate and succinate and subsequent succinate secretion

When supplementing [U-^{13}C$_4$]aspartate, succinate displayed an anomaly in terms of ^{13}C-excess and isotopologue pattern. Its overall ^{13}C-excess was higher (32%) than in glutamate (8%) and the labeling pattern of succinate only partially resembled the one of glutamate. On this basis, it can be assumed that succinate was not only formed from aspartate/oxaloacetate *via* the oxidative TCA cycle and α-ketoglutarate/glutamate as its direct precursor. Rather, the high ^{13}C-enrichment in succinate could be caused by the reaction of the aspartate ammonia lyase producing M + 4 fumarate (see also above) and further M + 4 succinate by the fumarate reductase. This reaction path together with aspartate assimilation through transamination to oxaloacetate is depicted in blue in Figure 3.

To account for eventual succinate excretion due to this reverse carbon flux in the TCA cycle, we analyzed the amount of succinate in the medium after growth with [U-^{13}C$_4$]aspartate and [U-^{13}C$_5$] glutamate/[U-^{13}C$_2$]glycine/[U-^{13}C$_3$]serine/[1,5-^{13}C$_2$]citrate for comparison. Indeed, GC–MS-quantification revealed a 4–9-fold increase in the concentration of medium succinate after growth with ^{13}C-aspartate as compared to other ^{13}C-substrates, while the isotopologue profile of secreted succinate was similar to cellular succinate (Table S23).

This reverse flow in the TCA cycle probably allows for an active fumarate respiration (Ge et al., 2000), which is energetically less efficient than using O$_2$ as the terminal electron acceptor. Similarly, aspartate uptake also leads to increased fumarate respiration in *Salmonella typhimurium* (Nguyen et al., 2020). Active fumarate respiration upon aspartate usage could also explain the discrepancy between efficient aspartate metabolization observed in this work and the lack of oxygen consumption after addition of aspartate to *H. pylori* growing in broth as observed earlier (Nagata et al., 2003).

To verify that the apparent active fumarate reduction upon excess of exogenous aspartate was not due to decreasing levels of oxygen during the cultivation, we performed the same experiment with a shortened labeling period of only two hours. After this short period of growth, it can be assumed that the oxygen concentration is still relatively high. The labeling patterns of the TCA cycle intermediates (Table S21) resembled the ones of the 8-hr labeling experiment, although the ^{13}C-excess values were generally lower. Thus, there is no indication of
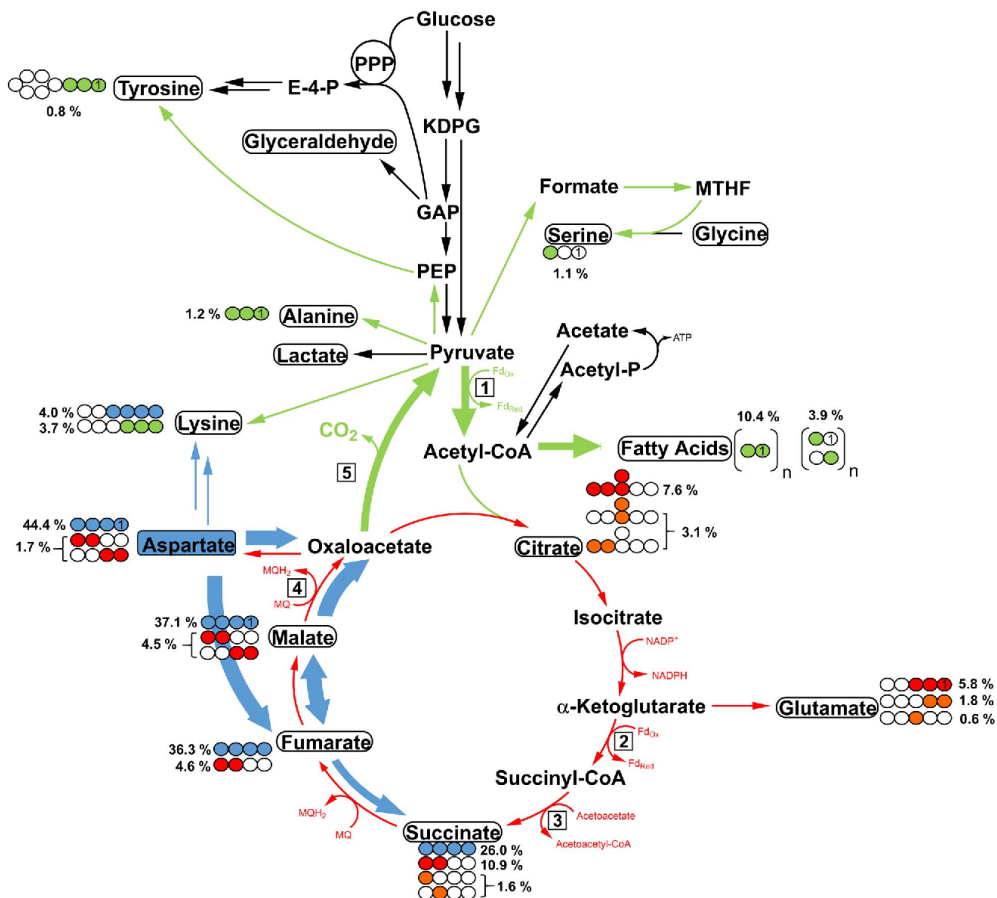
FIGURE 3 ^{13}C-Profiles in a model for the central carbon metabolism of *H. pylori* starting from [U-[13]C$_4$]aspartate in the central carbon metabolism of *H. pylori*. Red arrows indicate ^{13}C-incorporation *via* direct transformation of the substrate, while blue arrows signify metabolisation *via* the TCA cycle in the reverse direction. Green arrows indicate carbon flux following the decarboxylation of oxaloacetate to pyruvate. Colored circles signifiy the theoretical labeling positions for the respective isotopologue, while orange circles show isotopologues arising through propargation of labeled molecules through the TCA cycle. Percentages represent the observed ^{13}C-excess for the respective isotopologue. Metabolites in boxes were directly analysed *via* GC–MS. Numbers in boxes indicate unusual enzymes in the metabolism of *H. pylori*. 1: pyruvate-ferredoxin oxidoreductase; 2: 2-oxoglutarate-ferredoxin oxidoreductase; 3: succinyl-CoA:acetoacetate-CoA transferase; 4: malate:quinone oxidoreductase; 5: (4S)-4-hydroxy-2-oxoglutarate aldolase. PPP: pentose phosphate pathway; KDPG: 2-keto-3-desoxy-phosphogluconate; GAP: glyceraldehyde-3-phosphate; PEP: phosphoenolpyruvate; MTHF: methyltetrahydrofolate; Acetyl-P: acetyl-phosphate; MQ: menaquinone; Fd: ferredoxin

a biphasic growth behavior with a general reversal of carbon flux in the TCA cycle during growth of *H. pylori* under these conditions.

2.9 | Evidence for reactions *via* a full or partial glyoxylate bypass, and possible pathways for the generation of glyoxylate

The labeling experiments with ^{13}C-aspartate and ^{13}C-glutamate demonstrated that both amino acids efficiently serve to fill up the

TCA cycle of *H. pylori*. However, the lack of classical anaplerotic reactions raised the question of alternative metabolic pathways to replenish TCA cycle intermediates under conditions where aspartate or glutamate are not available from the environment in sufficient amounts. The need for the presence of such a metabolic pathway also becomes apparent since aspartate, asparagine, glutamate and glutamine are non-essential for *H. pylori* (Reynolds & Penn, 1994).

In the following, we provide some evidence for the malate synthase reaction as a possible alternative for filling up intermediates in the TCA cycle. This reaction could allow the formation of malate

solely from acetyl-CoA, a metabolite that can be produced from various sources *e. g.* by degradation of glucose or amino acids. One molecule of acetyl-CoA is directly utilized in the malate synthase reaction, while the carbon skeleton of glyoxylate could also potentially come from acetyl-CoA *via* the citrate synthase and subsequent isocitrate lyase reaction. A corresponding gene for a malate synthase is not assigned in the *H. pylori* genome so far, but its activity was observed in *H. pylori* supernatants *via* ^{1}H-NMR as well as in photometric assays (Hoffman et al., 1996; Pitson et al., 1999).

To experimentally substantiate an active malate synthase in a potential glyoxylate bypass, leading to the specific ^{13}C-incorporations described above, we tested different possible origins of glyoxylate in experiments using [U-^{13}C$_2$]acetate, [1,5-^{13}C$_2$]citrate, [U-^{13}C$_5$] proline, or [U-^{13}C$_2$]glycine as precursors. In case of an active isocitrate lyase, [1-^{13}C]glyoxylate would be generated from [1,5-^{13}C$_2$] citrate (Dolan & Welch, 2018). [U-^{13}C$_5$]Proline could be converted to ^{13}C$_3$-pyruvate and ^{13}C$_2$-glyoxylate *via* a pathway that is only partially annotated in *H. pylori* (Nishihara & Dekker, 1972; Watanabe et al., 2012). [U-^{13}C$_2$]Glycine could lead to [U-^{13}C$_2$]glyoxylate *via* an aminotransferase that has not been described in *H. pylori* so far (Nishiya & Imanaka, 1998). Additionally, glycine could also be used *via* the β-hydroxyaspartate cycle, recently found in some marine proteobacteria. Herein, the combination of glycine and glyoxylate would lead to aspartate/oxaloacetate and subsequently to malate as an alternative to the malate synthase reaction (Schada von Borzyskowski et al., 2019). Finally, [U-^{13}C$_2$]acetate could be transformed to acetyl-CoA, which, amongst other pathways, could serve as a starting substrate for the glyoxylate bypass or, alternatively for the ethylmalonyl-CoA pathway (Erb et al., 2009). *Via* this pathway, ^{13}C$_2$-glyoxylate would be generated retaining the carbon skeleton of the acetyl-moiety in acetyl-CoA (Peyraud et al., 2009). All these potential pathways for the generation of glyoxylate are summarized in Figure 4.

2.10 | [U-^{13}C$_5$]Proline, [U-^{13}C$_2$]glycine, and [U-^{13}C$_2$] acetate are excluded as potential precursors for glyoxylate formation

[U-^{13}C$_2$]Glycine uptake was high as gleaned from the detected ^{13}C-excess (57%) in re-isolated glycine from the polar fraction, but its metabolization only yielded significant ^{13}C-excess in serine with the M + 2-isotopologue being the most prominent species (Table S9). No labeling was found in aspartate or other TCA cycle related metabolites. On this basis, an active β-hydroxyaspartate cycle as well as the formation of glyoxylate from glycine can be ruled out for *H. pylori*. [U-^{13}C$_5$]Proline was mainly converted to [U-^{13}C$_5$]glutamate and to downstream products as described above. However, there was no indication for production of labeled pyruvate since lactate and alanine did not show significant ^{13}C-incorporation (Table S10). Accordingly, no labeled glyoxylate was produced from [U-^{13}C$_5$]proline. [U-^{13}C$_2$] Acetate only led to small ^{13}C-excess values in fatty acids and citrate (Figure S4). Exogenous acetate can therefore also be excluded as

origin of a potential glyoxylate bypass. The ethylmalonyl-CoA pathway can also be excluded on this basis (Table S22).

2.11 | The labeling patterns from [1,5-^{13}C$_2$]citrate as well as a photometric assay support an active isocitrate lyase as the source of glyoxylate

Metabolization of [1,5-^{13}C$_2$]citrate led to M + 2 glutamate (5.0%) and M + 1 succinate (5.1%, Figure S5). Further propagation through the TCA cycle led to M + 1 malate (2.7%) and aspartate (1.8%). GC–MS-analysis of the mass distributions in the fragments of aspartate indicated an equal distribution of the ^{13}C-label between the C1- and C4-positions. This suggests that aspartate/oxaloacetate is formed from citrate through symmetrical intermediates, such as succinate (Table S7). Although this pattern could generally be well explained by a cyclic TCA cycle structure, it is notable that the ^{13}C-excess in malate was significantly higher than in fumarate. It is therefore tempting to speculate that [1,5-^{13}C$_2$]citrate was converted into [1,5-^{13}C$_2$]isocitrate, and subsequently into [1-^{13}C$_1$]succinate and [1-^{13}C]glyoxylate *via* the isocitrate lyase reaction, followed by the malate synthase reaction to yield ^{13}C$_1$-malate from [1-^{13}C]glyoxylate (Figure 4 D). Formation of [1-^{13}C]succinate leads to randomization of the label through the terminal positions (i.e., C-1 and C-4) in the downstream products fumarate, malate, oxaloacetate/aspartate, as detected in aspartate. On the other hand, starting from [1-^{13}C]glyoxylate the malate synthase reaction yields [1-^{13}C]malate, which could be directly converted to [1-^{13}C]oxaloacetate/aspartate and not into the observed 1:1 mixture of [1-^{13}C]- and [4-^{13}C]aspartate. However, the finding of equal ^{13}C-incorporation into C-1 and C-4 of aspartate in the experiment with [1,5-^{13}C$_2$]citrate does not exclude the glyoxylate hypothesis since label randomization could also have occurred by the highly active fumarase in *H. pylori* establishing a rapid equilibrium between the malate and fumarate pools with loss of the positional ^{13}C-labeling information in malate and its downstream products (Pitson et al., 1999).

As already mentioned above, the glyoxylate bypass hypothesis is challenged by the fact that a gene for isocitrate lyase is not assigned in the genome of *H. pylori*. To provide direct experimental evidence for a non-conventional isocitrate lyase in *H. pylori*, we performed photometric assays using crude cell extracts of *H. pylori*. Non-conventional here means that the enzyme was so far not detectable by genome annotations or BLAST search despite indications for its activity. Herein, *H. pylori* P12 cells were disrupted by ultra-sonification and the supernatants were used in enzyme assays containing isocitrate as a potential substrate. Here, the formation of glyoxylate is monitored photometrically *via* the formation of the phenylhydrazone of glyoxylate. As a positive control, we used cell extracts of *E. coli* possessing the enzymes of a glyoxylate pathway including isocitrate lyase (Chung et al., 1988). As shown in Figure 5, the photometric test with cell extracts of *H. pylori* was positive with a similar signal intensity for glyoxylate formation as observed for the *E. coli* extract. This activity was dependent on isocitrate and magnesium ions in the assay. Together, this provided substantial evidence

2.2 Substrate usage determines carbon flux *via* the citrate cycle in *Helicobacter pylori*
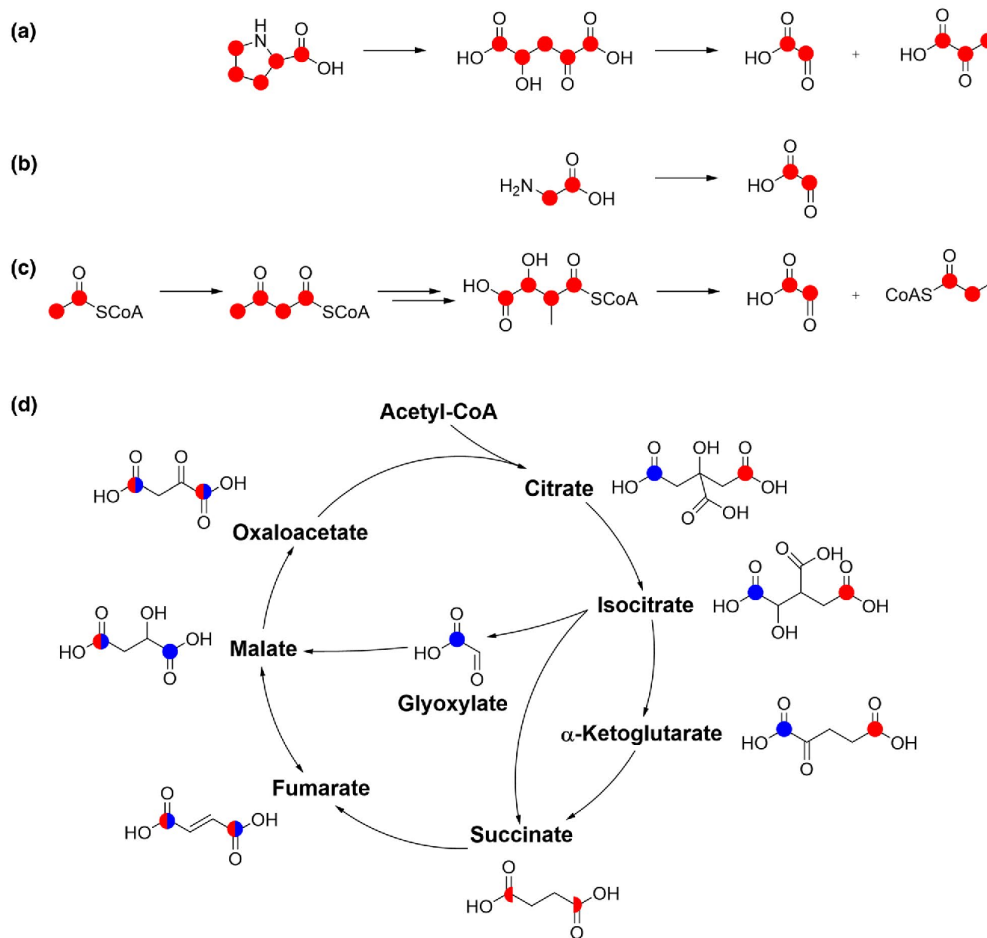
FIGURE 4 Potential origins of glyoxylate, which are examined by labeling experiments. Red dots indicate ^{13}C-label in the substrates as well as potential ^{13}C-incorporation in the expected products. (A) Production *via* proline degradation was tested with [U-^{13}C$_5$]proline. (B) Transamination of glycine was tested with [U-^{13}C$_2$]glycine. (C) The ethylmalonyl-CoA-pathway was tested with [U-^{13}C$_2$]acetate. (D) Production *via* isocitrate lyase was tested with [1,5-^{13}C$_2$]citrate. Blue dots indicate ^{13}C-incorporation *via* the glyoxylate bypass. Mixed colored dots indicate ^{13}C-incorporation *via* the oxidative TCA cycle and/or the glyoxylate bypass. The detected labeling patterns were only in agreement with the predictions *via* (D)

for a Mg^{2+}-dependent activity of isocitrate lyase or an isocitrate lyase like enzyme in cell extracts of *H. pylori*. Several other *H. pylori* strains were tested and showed the same isocitrate-dependent activities. As another control, an *E. coli* Δ*aceA* mutant lacking the gene for isocitrate lyase did not show the same activity in this assay, excluding potential unspecific reactions in the supernatant leading to a false positive result (Figure 5). Together with earlier reports for malate synthase activity in *H. pylori* (Hoffman et al., 1996; Pitson et al., 1999), the labeling experiments using [1,5-^{13}C$_2$]citrate as well as the detected activity of a non-conventional isocitrate lyase supported a functional glyoxylate bypass in *H. pylori*.

It is currently unknown which enzymes catalyze the reaction of a putative glyoxylate bypass in *H. pylori*. As mentioned above, there are no indications for either malate synthase or isocitrate lyase in the genome of *H. pylori*. More specifically, BLAST searches using various sequences of isocitrate lyase or malate synthase from other organisms (*e. g. E. coli, P. aeruginosa*, other ε-proteobacteria) did not retrieve any weak orthologs in the *H. pylori* genome. This suggests that these reactions are carried out in *H. pylori* by enzymes that developed substrate promiscuity or changed their substrate specificity during adaption of *H. pylori* to the human host, similar to (*4S*)-4-hydroxy-2-oxoglutarate aldolase catalyzing oxaloacetate decarboxylation in *H. pylori*.
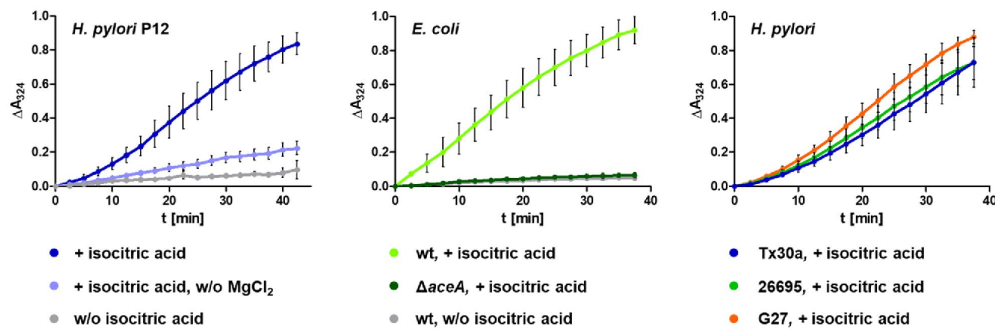
FIGURE 5   Isocitrate lyase activity is detectable in lysates of different *H. pylori* strains. Bacterial lysates were incubated with (+) or without (w/o) isocitric acid and the formation of glyoxylate-phenylhydrazone was spectrophotometrically assessed at 324 nm. The isocitrate lyase activity of *H. pylori* P12 cell extracts was strongly dependent on the presence of the cofactor Mg^{2+} (left). As expected, no glyoxylate-phenylhydrazone formation was observed in an *E. coli* Δ*aceA* mutant (middle). Further *H. pylori* strains were tested and showed comparable isocitrate lyase activities (right). Data show means and standard deviations of three independent experiments

3 | CONCLUSION

In this work, the central carbon metabolism of *H. pylori* was elucidated using a comprehensive ^{13}C-labeling strategy starting from various substrates. On one hand, the data showed that exogenous glucose was efficiently utilized *via* the ED-pathway and the PPP, leading to triose phosphates, but less efficiently downstream of pyruvate/acetyl-CoA *via* the TCA cycle for ATP generation. On the other hand, substrates entering the metabolism *via* the TCA cycle yielded high ^{13}C-enrichments in the intermediates of the TCA cycle and related products, but not in metabolites upstream of pyruvate/ PEP (Figure 6). This was a clear indication for multiple substrate usage in a bipartite metabolic network in which glucose serves an efficient source to build up bacterial cell walls and lipids, whereas multiple substrates serve to feed the citrate cycle with fluxes determined by the nutrient available from the environment (Figure 6). The dampened TCA cycle activity in response to *e. g.* glucose could reflect means to support chronic colonization—a hallmark of *H. pylori* infection (Lina et al., 2014)—as it produces less energy but still allows respiration in the absence of oxygen *via* fumarate as a terminal electron acceptor (Ge, 2002). Further, a connection between a reduced activity of the closed oxidative TCA cycle and persistence becomes more and more apparent in other pathogens (Jung et al., 2019; Trastoy et al., 2018). In *E. coli*, upregulation of fumarate reductase, possibly allowing for more efficient fumarate respiration, led to increased persister formation (Kim et al., 2016), while in *S. aureus* inactivation of α-ketoglutarate dehydrogenase subunits resulted in an interrupted TCA cycle and increased persister formation during stationary growth (Wang et al., 2018). In *Burkholderia cepacia* biofilms, downregulation of TCA cycle-related genes led to reduced ROS (reactive oxygen species) production (Van Acker et al., 2013). The balance of carbon usages *via* an adaptive TCA cycle could therefore reflect a smart toolbox for *H. pylori* to rapidly react to its changing environment and to allow the formation of persister cells.

With all substrates under study, we observed a closed TCA cycle topology, standing in contrast to earlier reports about a bifurcate TCA cycle structure (Han et al., 2018; Pitson et al., 1999). However, the adaptive fluxes through the TCA cycle observed in our study might produce a bifurcate-like metabolic phenotype under different cultivation conditions thereby explaining the discrepancy. We could show that *H. pylori* reacts to environmental succinate and glutamate with an apparent shift of carbon fluxes. This adaption could have been acquired by *H. pylori* to rapidly respond to immune reactions of its host. Glutamine is the main carbon substrate for immune cells especially during proliferation and, in part, it also acts as a signaling molecule for immune cell activation (Cruzat et al., 2018). *H. pylori* could utilize this extracellular glutamine by secretion of a γ-glutamyltranspeptidase, which converts glutamine to glutamate and thereby makes it accessible to *H. pylori* as a carbon substrate (Shibayama et al., 2007). Similarly, succinate accumulates upon infection in M1 macrophages (O'Neill & Pearce, 2016) and also works as a signaling molecule. Extracellular succinate binds to GPR91 leading to proinflammatory IL-1β expression *via* HIF-1α (de Castro Fonseca et al., 2016; Fernandez-Veledo & Vendrell, 2019; Tannahill et al., 2013) and increases cytokine production in dendritic cells (Rubic et al., 2008). These functions of succinate and glutamine in the context of immunometabolism also make them abundant and welcome substrates for *H. pylori* when being challenged by immune cells. Scavenging extracellular succinate as well as glutamine could therefore be advantageous for *H. pylori* to deal with immunological reactions of the human host cell. Decreasing the concentrations of these metabolites could reduce proinflammatory responses due to *H. pylori* infection as well as macrophage proliferation, thereby allowing persistent *H. pylori* infection. Additionally, the surplus in energy produced by TCA cycle activation due to glutamate and succinate usage could be beneficial for defense mechanisms, like energy intensive shedding of outer membrane vesicles (OMVs), which protect *H. pylori* against oxidative burst (Kulp & Kuehn, 2010; Lekmeechai et al., 2018).

2.2 Substrate usage determines carbon flux *via* the citrate cycle in *Helicobacter pylori*
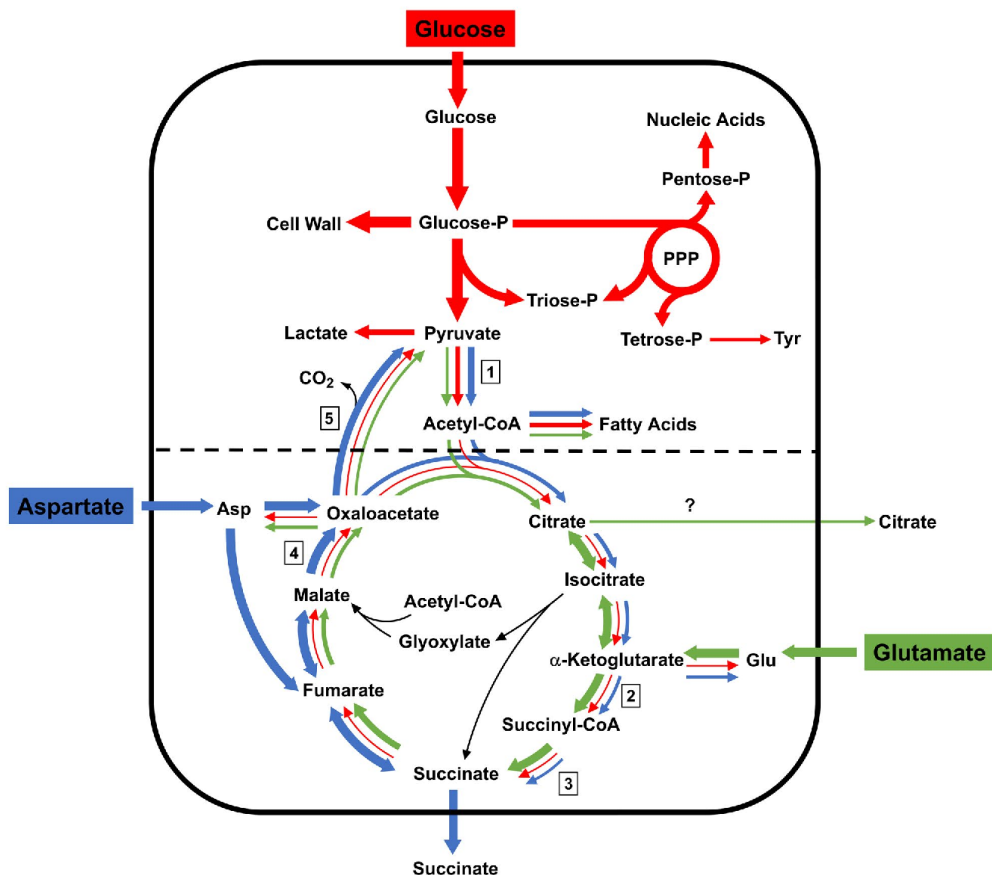
FIGURE 6 Metabolic scheme of *H. pylori*. Glucose (red) is metabolized *via* the ED pathway as well as the PPP. Metabolization in the TCA cycle happens *via* the closed oxidative cycle. Glutamate (green) leads to a closed cyclic structure with an additional equilibrium flux in the reverse direction leading to citrate. Aspartate (blue) leads to a closed cyclic structure with an additional equilibrium flux in the reverse direction leading to succinate, which is excreted into the medium. The dashed line alludes to a possible bipartite metabolism. Black arrows indicate a putatively full glyoxylate bypass. Numbers in boxes indicate unusual enzymes in the metabolism of *H. pylori*. 1: pyruvate-ferredoxin oxidoreductase; 2:2-oxoglutarate-ferredoxin oxidoreductase; 3: succinyl-CoA:acetoacetate-CoA transferase; 4: malate:quinone oxidoreductase; 5: (*4S*)-4-hydroxy-2-oxoglutarate aldolase. P indicates a phosphate-group

The observed lack of classical anaplerosis, some anomalies observed in our labeling experiments, and the detected enzymatic activities of malate synthase (Hoffman et al., 1996; Pitson et al., 1999) and isocitrate lyase in cell extracts of *H. pylori* (Hoffman et al., 1996 and this study) suggest the dependency of the citrate cycle on a putative glyoxylate bypass (Figure 6), although there are no homologies for malate synthase and isocitrate lyase in the genome sequences of *H. pylori*. These still uncharacterized enzymes may provide new opportunities for antimicrobial targets especially given the metabolic orthogonality to the human host (Dolan & Welch, 2018), besides other TCA cycle related enzymes such as α-ketoglutarate oxidase and fumarate reductase shown to be essential for *H. pylori* survival (Chen et al., 2012; Tsugawa et al., 2008). Noteworthy, there has

already been a considerable amount of research about the glyoxylate shunt and its inhibition in *Mycobacterium tuberculosis* yielding promising drug candidates against either isocitrate lyase or malate synthase (Krieger et al., 2012; Pham et al., 2017).

4 | EXPERIMENTAL PROCEDURES

4.1 | *H. pylori* growth conditions and labeling experiments

H. pylori strains P12, G27, 26,695 and Tx30a were cultured on GC agar plates (Oxoid) supplemented with 8% horse serum (Life

Technologies) and 1% vitamin mix under microaerobic atmosphere (85% N_2, 10% CO_2, 5% O_2) at 37°C. For ^{13}C-labeling experiments, *H. pylori* P12 grown on plates were diluted to an OD_{550} of 0.1 in *Brucella* broth (Becton Dickinson)/10% fetal calf serum (FCS, heat inactivated, Life Technologies) and precultured for 8 hr under a microaerobic atmosphere (85% N_2, 10% CO_2, 5% O_2) at 37°C and shaking at 100 rpm. Next, main cultures (50 ml) were inoculated to a final OD_{550} of 0.05 in *Brucella* broth/10% FCS and supplemented with either 5 mM [U-$^{13}C_3$]*L*-serine, 5 mM [U-$^{13}C_4$]*L*-aspartate, 5 mM [U-$^{13}C_5$]*L*-glutamate, 5 mM [U-$^{13}C_4$]succinate, 5 mM [U-$^{13}C_5$]*L*-proline, 5 mM [1,5-$^{13}C_2$]citrate, 10 mM [U-$^{13}C_6$]*D*-glucose, 10 mM [U-$^{13}C_3$] glycerol, 15 mM [U-$^{13}C_2$]acetate or 50 mM sodium [^{13}C]bicarbonate, respectively (all tracers with 99% ^{13}C-content, purchased from Sigma-Aldrich). Cultures were again shaken for 14–16 hr under a microaerobic atmosphere (85% N_2, 10% CO_2, 5% O_2) at 37°C and 100 rpm until the exponential growth phase. Bacteria were harvested by centrifugation at 4,000 rpm and 4°C for 20 min. Pellets were inactivated by freezing (30 min, dry ice) and subsequent boiling for 20 min. The samples were stored at −80°C and freeze-dried before further analysis. All experiments were done in duplicates. Similarly, main cultures (50 ml) were again inoculated to a final OD_{550} of 0.1 and supplemented with 5 mM [U-$^{13}C_4$]*L*-aspartic acid, but growth was only allowed for 2 hr. Harvest and further processing of the pellets was done as described above.

4.2 | Metabolite extraction procedure

An amount of 5 mg of the freeze-dried cell pellet was mixed with 1 ml of cold (4°C) methanol (VWR). After the addition of 800 mg of glass beads (ø 0.25–0.5 mm), mechanical cell lysis was performed using a ribolyser system (Hybaid) for 1×20 s at 4.0 ms^{-1} and for 4×20 s at 6.5 ms^{-1}. Afterwards, the sample was centrifuged at 3,200 *g* for 10 min and the supernatant was dried under a stream of nitrogen. For silylation, 50 μl of anhydrous acetonitrile as well as 50 μl of *N*-(*tert*-butyldimethylsilyl)-*N*-methyl-trifluoroacetamide (Sigma) were added and the mixture was incubated at 70°C for 1 hr. The resulting *tert*-butyldimethylsilyl-derivatives (TBDMS) were analyzed *via* GC–MS as described below.

4.3 | Analysis of the growth medium

A volume of 1 ml of fresh BB/FCS medium was lyophilized and the residue was extracted with 1 ml of methanol (VWR). After centrifugation (5 min, 3,200 *g*), 500 μl of the supernatant were mixed with 50 μl of a solution of 5 mM norvaline in methanol (internal standard). The mixture was dried under a stream of nitrogen and the residue was incubated with 50 μl of anhydrous acetonitrile as well as 50 μl of *N*-(*tert*-butyldimethylsilyl)-*N*-methyl-trifluoroacetamide (Sigma) at 70°C for 1 hr. The resulting *tert*-butyldimethylsilyl-derivatives (TBDMS) were again analyzed *via* GC–MS. The same procedure was

used for the analysis of succinate and citrate in the medium after *H. pylori* growth.

4.4 | Protein hydrolysis

For analysis of protein-bound amino acids, 2 mg of the bacterial sample (lyophilized cell pellet) were suspended in 1 ml of 6 M hydrochloric acid and hydrolyzed for 15 hr at 105°C. The reaction mixture was dried under a stream of nitrogen at 70°C. The residue was suspended in 200 μL of 50% aqueous acetic acid using an ultrasonic bath for 3 min. The solution was applied onto a small column of Dowex 50WX8 (7×10 mm; 200–400 mesh, 34–74 μm, H$^+$-form, Alfa Aesar). The column was first washed with 2 ml of H_2O, then eluted with 1 ml of 4 M aqueous ammonia. The ammonia eluate was dried under a stream of nitrogen at 70°C. The residue was treated with 50 μL of *N*-(*tert*-butyldimethylsilyl)-*N*-methyltrifluoroacetamide and 50 μL of anhydrous acetonitrile at 70°C for 30 min. The TBDMS-derivatives of amino acids were again analyzed by GC–MS. Due to degradation of tryptophan, methionine and cysteine during acid hydrolysis, these amino acids could not be analyzed. Due to inefficient derivatization, TBDMS-arginine could also not be detected in sufficient amounts. Furthermore, acid hydrolysis led to conversion of glutamine and asparagine to glutamate and aspartate, respectively. Therefore, results given for aspartate and glutamate correspond to asparagine/aspartate and glutamine/glutamate, respectively.

4.5 | Gas chromatography-mass spectrometry (GC–MS) analysis

GC–MS analysis was performed with a QP2010 Plus gas chromatograph/mass spectrometer (Shimadzu) equipped with a fused silica capillary column (Equity TM-5; 30 m, 0.25 mm, 0.25 μm film thickness; SUPELCO) and a quadrupole detector working with electron impact ionization at 70 eV. An aliquot (0.1 to 6 μl) of the derivatized samples were injected in 1:5 split mode at an interface temperature of 260°C and a helium inlet pressure of 70 kPa. Selected ion monitoring (SIM) was used with a sampling rate of 0.5 s. LABSOLUTION software (Shimadzu) was used for data collection and analysis. For the measurement of polar metabolites, the column was kept at 100°C for 2 min after sample injection. Following, the column was developed with a first gradient of 3°C min^{-1} until a final temperature of 234°C. Subsequently, a second temperature gradient of 1°C min^{-1} until a final temperature of 237°C, and a third temperature gradient of 3°C min^{-1} to a final temperature of 260°C was performed.

For the measurement of proteinogenic amino acids, the column was held at 150°C for 3 min followed by a temperature gradient of 10°C min^{-1} to a final temperature of 280°C. Isotopologue calculations were typically performed with molecular fragments at m/z of [M-57]$^+$, where M is the molecular mass of the respective TBDMS-derivative. For analysis of the growth medium, analysis was done in

the SCAN mode using the temperature program from the analysis of polar metabolites with a mass range of 50–700 m/z.

All samples were measured three times to obtain technical replicates. ^{13}C-Excess values and isotopologue compositions were calculated as previously described (Eylert et al., 2008). This comprises (i) the detection of GC–MS spectra of unlabeled derivatized metabolites, (ii) determination of the absolute mass of isotopologue enrichments and distributions of labeled metabolites of the experiment, and (iii) correction of the absolute ^{13}C-incorporation by subtracting the heavy isotopologue contributions due to the natural abundances in the derivatized metabolites (Eylert et al., 2008; Lee et al., 1991).

4.6 | Generation of an *E. coli* aceA mutant

An *E. coli aceA* deletion mutant was generated according to the protocol established by Datsenko and Wanner (Datsenko & Wanner, 2000). The DNA fragments used for targeted gene replacement were amplified by PCR using primers with 70-nt extensions that are homologous to *aceA* and the resistance cassette-encoding template plasmid pKD4 (CL77: TACCGCCTGTTAGCGTAAACCACCAC ATAACTATGGAGCATCTGCACATGGTGTAGGCTGGAGCTGCTTC, CL78: GGCCTACAGTCAGCAACGGTTGTTGTTGCTTAGAACTGCGA TTCTTCAGTCATATGAATATCCTCCTTAG). Chemically competent *E. coli* BW25113 carrying the pKD46 plasmid (λ Red system) were transformed with the PCR products, and knockouts obtained by recombination were selected via kanamycin resistance. The gene deletion was confirmed by PCR (CL79: AGGAATCGACCATACTGAGCA, CL80: CAGTACATCGAAGCGTGGATC).

4.7 | Photometric assay of isocitrate lyase activity

Bacteria were harvested from agar plates and diluted to a final OD_{550} of 10 in D-PBS (w/o $MgCl_2$, life technologies). After lysis *via* sonication, unbroken cells and cell debris were removed by centrifugation (10,000 g, 30 min, 4°C). Isocitrate lyase activity was measured using a protocol adapted from Reeves et al. (1971). Briefly, 25 µl bacterial lysate were mixed with 120 µl reaction buffer (10 µl 500 mM Tris-HCl, pH 7.5, 5 µl 100 mM $MgCl_2$, 5 µl 1 mM *L*-cysteine; 10 µl 100 mM phenylhydrazine-HCl (Sigma), 90 µl ddH_2O) in a 96-well plate (clear, flat-bottom, falcon). A volume of 5 µl 20 mM *DL*-isocitric acid trisodium salt hydrate (Acros organics) was added and measurement was immediately started in a pre-warmed plate reader (30°C, Clariostar BMG Labtech). The formation of glyoxylate-phenylhydrazone was recorded by measuring the absorbance at 324 nm every 2.5 min for 30 min. Before each measurement, plates were automatically mixed for 2 s at 500 rpm double orbital shaking. As a blank control, 5 µl ddH_2O instead of *DL*-isocitric acid was added to the respective samples.

4.8 | *H. pylori* growth curves

Bacteria grown on plates were diluted to an OD_{550} of 0.075 in BB/FCS and subcultured in 96-well plates (clear, flat-bottom). Plates were sealed with a gas permeable membrane (Breathe-Easy® sealing membrane, Diversified Biotech) and incubated at 37°C, 200 rpm in a plate reader (Clariostar, BMG Labtech). CO_2 levels were adjusted to 10% using an atmospheric control unit (BMG Labtech). OD_{550} was automatically measured every 5 min until the stationary phase was reached. Alternatively, bacteria were inoculated to an initial OD_{550} of 0.05 in BB/FCS and incubated under microaerobic atmosphere under gentle agitation. At the indicated time points, the OD_{550} was measured manually.

CONFLICT OF INTEREST

The authors declare that the research was conducted in the absence of any commercial or financial relationships that could be construed as a potential conflict of interest.

AUTHOR CONTRIBUTIONS

TS, WE, CL, RH, WG and WF designed the study. TS, CL, WE and WF wrote the manuscript. TS, CL and FS performed the experiments. WE, WF and RH provided the laboratory space and equipment.

ORCID

Werner Goebel https://orcid.org/0000-0003-4851-2083
Wolfgang Fischer https://orcid.org/0000-0002-8683-5089
Wolfgang Eisenreich https://orcid.org/0000-0002-9832-8279

REFERENCES

Ailloud, F., Didelot, X., Woltemate, S., Pfaffinger, G., Overmann, J., Bader, R.C. et al (2019) Within-host evolution of *Helicobacter pylori* shaped by niche-specific adaptation, intragastric migrations and selective sweeps. *Nature Communications*, *10*(1), 2273. https://doi.org/10.1038/s41467-019-10050-1

Atherton, J.C. & Blaser, M.J. (2009) Coadaptation of *Helicobacter pylori* and humans: Ancient history, modern implications. *Journal of Clinical Investigation*, *119*(9), 2475–2487. https://doi.org/10.1172/JCI38605

Baar, C., Eppinger, M., Raddatz, G., Simon, J., Lanz, C., Klimmek, O. et al (2003) Complete genome sequence and analysis of *Wolinella succinogenes*. *Proceedings of the National Academy of Sciences*, *100*(20), 11690–11695. https://doi.org/10.1073/pnas.1932838100

Best, A. & Abu Kwaik, Y. (2019) Nutrition and bipartite metabolism of intracellular pathogens. *Trends in Microbiology*, *27*(6), 550–561. https://doi.org/10.1016/j.tim.2018.12.012

Bhargava, P. & Collins, J.J. (2015) Boosting bacterial metabolism to combat antibiotic resistance. *Cell Metabolism*, *21*(2), 154–155. https://doi.org/10.1016/j.cmet.2015.01.012

Bishai, W.R. (2017) Drug development: Locking down metabolism. *Nature Chemical Biology*, 13(9), 925–926. https://doi.org/10.1038/nchembio.2452

Buchanan, B.B., Sirevåg, R., Fuchs, G., Ivanovsky, R.N., Igarashi, Y., Ishii, M. et al (2017) The Arnon-Buchanan cycle: A retrospective, 1966–2016. *Photosynthesis Research*, 134(2), 117–131. https://doi.org/10.1007/s11120-017-0429-0

Buescher, J.M., Antoniewicz, M.R., Boros, L.G., Burgess, S.C., Brunengraber, H., Clish, C.B. et al (2015) A roadmap for interpreting ^{13}C metabolite labeling patterns from cells. *Current Opinion in Biotechnology*, 34, 189–201. https://doi.org/10.1016/j.copbio.2015.02.003

Burns, B.P., Hazell, S.L. & Mendz, G.L. (1995) Acetyl-CoA carboxylase activity in *Helicobacter pylori* and the requirement of increased CO_2 for growth. *Microbiology*, 141(Pt 12), 3113–3118. https://doi.org/10.1099/13500872-141-12-3113

Bury-Mone, S., Kaakoush, N.O., Asencio, C., Megraud, F., Thibonnier, M., De Reuse, H. et al (2006) Is *Helicobacter pylori* a true microaerophile? *Helicobacter*, 11(4), 296–303. https://doi.org/10.1111/j.1523-5378.2006.00413.x

Chen, M., Andersen, L.P., Zhai, L. & Kharazmi, A. (1999) Characterization of the respiratory chain of *Helicobacter pylori*. *FEMS Immunology and Medical Microbiology*, 24(2), 169–174. https://doi.org/10.1111/j.1574-695X.1999.tb01278.x

Chen, Z., Zhou, Q. & Ge, R. (2012) Inhibition of fumarase by bismuth(III): Implications for the tricarboxylic acid cycle as a potential target of bismuth drugs in *Helicobacter pylori*. *BioMetals*, 25(1), 95–102. https://doi.org/10.1007/s10534-011-9485-7

Chung, T., Klumpp, D.J. & LaPorte, D.C. (1988) Glyoxylate bypass operon of *Escherichia coli*: Cloning and determination of the functional map. *Journal of Bacteriology*, 170(1), 386–392. https://doi.org/10.1128/jb.170.1.386-392.1988

Corthesy-Theulaz, I.E., Bergonzelli, G.E., Henry, H., Bachmann, D., Schorderet, D.F., Blum, A.L. et al (1997) Cloning and characterization of *Helicobacter pylori* succinyl CoA: Acetoacetate CoA-transferase, a novel prokaryotic member of the CoA-transferase family. *Journal of Biological Chemistry*, 272(41), 25659–25667. https://doi.org/10.1074/jbc.272.41.25659

Cruzat, V., Macedo Rogero, M., Noel Keane, K., Curi, R. & Newsholme, P. (2018) Glutamine: Metabolism and immune function, supplementation and clinical translation. *Nutrients*, 10(11), https://doi.org/10.3390/nu10111564

Datsenko, K.A. & Wanner, B.L. (2000) One-step inactivation of chromosomal genes in *Escherichia coli* K-12 using PCR products. *Proceedings of the National Academy of Sciences*, 97(12), 6640–6645. https://doi.org/10.1073/pnas.120163297

de Castro Fonseca, M., Aguiar, C.J., da Rocha Franco, J.A., Gingold, R.N. & Leite, M.F. (2016) GPR91: Expanding the frontiers of Krebs cycle intermediates. *Cell Communication and Signaling*, 14, 3. https://doi.org/10.1186/s12964-016-0126-1

de Martel, C., Georges, D., Bray, F., Ferlay, J. & Clifford, G.M. (2020) Global burden of cancer attributable to infections in 2018: A worldwide incidence analysis. *Lancet Glob Health.*, 8(2), e180–e190. https://doi.org/10.1016/s2214-109x(19)30488-7

Dewhirst, F.E., Shen, Z., Scimeca, M.S., Stokes, L.N., Boumenna, T., Chen, T. et al (2005) Discordant 16S and 23S rRNA gene phylogenies for the genus *Helicobacter*: Implications for phylogenetic inference and systematics. *Journal of Bacteriology*, 187(17), 6106–6118. https://doi.org/10.1128/JB.187.17.6106-6118.2005

Dolan, S.K. & Welch, M. (2018) The glyoxylate shunt, 60 years on. *Annual Review of Microbiology*, 72, 309–330. https://doi.org/10.1146/annurev-micro-090817-062257

Dunne, C., Dolan, B. & Clyne, M. (2014) Factors that mediate colonization of the human stomach by *Helicobacter pylori*. *World Journal of Gastroenterology*, 20(19), 5610–5624. https://doi.org/10.3748/wjg.v20.i19.5610

Eisenreich, W., Heesemann, J., Rudel, T. & Goebel, W. (2015) Metabolic adaptations of intracellullar bacterial pathogens and their mammalian host cells during Infection ("Pathometabolism"). *Microbiology Spectrum*, 3(3), https://doi.org/10.1128/microbiolspec.MBP-0002-2014

Eisenreich, W., Rudel, T., Heesemann, J. & Goebel, W. (2017) To eat and to be eaten: Mutual metabolic adaptations of immune vells and intracellular bacterial pathogens upon Infection. *Frontiers in Cellular and Infection Microbiology*, 7, 316. https://doi.org/10.3389/fcimb.2017.00316

Eisenreich, W., Rudel, T., Heesemann, J. & Goebel, W. (2019) How viral and intracellular bacterial pathogens reprogram the metabolism of host cells to allow their intracellular replication. *Frontiers in Cellular and Infection Microbiology*, 9. https://doi.org/10.3389/fcimb.2019.00042

Eisenreich, W., Slaghuis, J., Laupitz, R., Bussemer, J., Stritzker, J., Schwarz, C. et al (2006) ^{13}C isotopologue perturbation studies of *Listeria monocytogenes* carbon metabolism and its modulation by the virulence regulator PrfA. *Proceedings of the National Academy of Sciences of the USA*, 103(7), 2040–2045. https://doi.org/10.1073/pnas.0507580103

Eppinger, M., Baar, C., Linz, B., Raddatz, G., Lanz, C., Keller, H. et al (2006) Who ate whom? Adaptive *Helicobacter* genomic changes that accompanied a host jump from early humans to large felines. *PLoS Genetics*, 2(7), e120. https://doi.org/10.1371/journal.pgen.0020120

Erb, T.J., Brecht, V., Fuchs, G., Müller, M. & Alber, B.E. (2009) Carboxylation mechanism and stereochemistry of crotonyl-CoA carboxylase/reductase, a carboxylating enoyl-thioester reductase. *Proceedings of the National Academy of Sciences*, 106(22), 8871–8876. https://doi.org/10.1073/pnas.0903939106

Eylert, E., Schär, J., Mertins, S., Stoll, R., Bacher, A., Goebel, W. et al (2008) Carbon metabolism of *Listeria monocytogenes* growing inside macrophages. *Molecular Microbiology*, 69(4), 1008–1017. https://doi.org/10.1111/j.1365-2958.2008.06337.x

Feldman, M. (1983) Gastric bicarbonate secretion in humans. Effect of pentagastrin, bethanechol, and 11,16,16-trimethyl prostaglandin E2. *J Clin Invest.*, 72(1), 295–303. https://doi.org/10.1172/jci110969

Fernandez-Veledo, S. & Vendrell, J. (2019) Gut microbiota-derived succinate: Friend or foe in human metabolic diseases? *Reviews in Endocrine & Metabolic Disorders*, 20(4), 439–447. https://doi.org/10.1007/s11154-019-09513-z

Fischer, W., Windhager, L., Rohrer, S., Zeiller, M., Karnholz, A., Hoffmann, R. et al (2010) Strain-specific genes of *Helicobacter pylori*: Genome evolution driven by a novel type IV secretion system and genomic island transfer. *Nucleic Acids Research*, 38(18), 6089–6101. https://doi.org/10.1093/nar/gkq378

Fock, K.M., Katelaris, P., Sugano, K., Ang, T.L., Hunt, R., Talley, N.J. et al (2009) Second Asia-pacific consensus guidelines for *Helicobacter pylori* infection. *Journal of Gastroenterology and Hepatology*, 24(10), 1587–1600. https://doi.org/10.1111/j.1440-1746.2009.05982.x

Fuchs, G. (2011) Alternative pathways of carbon dioxide fixation: Insights into the early evolution of life? *Annual Review of Microbiology*, 65, 631–658. https://doi.org/10.1146/annurev-micro-090110-102801

Galperin, M.Y., Makarova, K.S., Wolf, Y.I. & Koonin, E.V. (2015) Expanded microbial genome coverage and improved protein family annotation in the COG database. *Nucleic Acids Research*, 43(Database issue), D261–269. https://doi.org/10.1093/nar/gku1223

Gao, B., Vorwerk, H., Huber, C., Lara-Tejero, M., Mohr, J., Goodman, A.L. et al (2017) Metabolic and fitness determinants for in vitro growth and intestinal colonization of the bacterial pathogen *Campylobacter jejuni*. *PLoS Biology*, 15(5), e2001390. https://doi.org/10.1371/journal.pbio.2001390

Ge, Z. (2002) Potential of fumarate reductase as a novel therapeutic target in *Helicobacter pylori* infection. *Expert Opin Ther Targets.*, *6*(2), 135–146. https://doi.org/10.1517/14728222.6.2.135

Ge, Z., Feng, Y., Dangler, C.A., Xu, S., Taylor, N.S. & Fox, J.G. (2000) Fumarate reductase is essential for *Helicobacter pylori* colonization of the mouse stomach. *Microbial Pathogenesis*, *29*(5), 279–287. https://doi.org/10.1006/mpat.2000.0391

Grubmüller, S., Schauer, K., Goebel, W., Fuchs, T.M. & Eisenreich, W. (2014) Analysis of carbon substrates used by *Listeria monocytogenes* during growth in J774A.1 macrophages suggests a bipartite intracellular metabolism. *Frontiers in Cellular and Infection Microbiology*, *4*, 156. https://doi.org/10.3389/fcimb.2014.00156

Han, B., Zhang, Z., Xie, Y., Hu, X., Wang, H., Xia, W. et al (2018) Multiomics and temporal dynamics profiling reveal disruption of central metabolism in *Helicobacter pylori* on bismuth treatment. *Chem Sci.*, *9*(38), 7488–7497. https://doi.org/10.1039/c8sc01668b

Han, C., Kotsyurbenko, O., Chertkov, O., Held, B., Lapidus, A., Nolan, M. et al (2012) Complete genome sequence of the sulfur compounds oxidizing chemolithoautotroph *Sulfuricurvum kujiense* type strain (YK-1(T)). *Stand Genomic Sci.*, *6*(1), 94–103. https://doi.org/10.4056/sigs.2456004

Häuslein, I., Manske, C., Goebel, W., Eisenreich, W. & Hilbi, H. (2016) Pathway analysis using ^{13}C-glycerol and other carbon tracers reveals a bipartite metabolism of *Legionella pneumophila*. *Molecular Microbiology*, *100*(2), 229–246. https://doi.org/10.1111/mmi.13313

Hazell, S.L. & Mendz, G.L. (1997) How *Helicobacter pylori* works: An overview of the metabolism of *Helicobacter pylori*. *Helicobacter.*, *2*(1), 1–12. https://doi.org/10.1111/j.1523-5378.1997.tb00050.x

Hirayama, A., Kami, K., Sugimoto, M., Sugawara, M., Toki, N., Onozuka, H. et al (2009) Quantitative metabolome profiling of colon and stomach cancer microenvironment by capillary electrophoresis time-of-flight mass spectrometry. *Cancer Research*, *69*(11), 4918–4925. https://doi.org/10.1158/0008-5472.CAN-08-4806

Hoffman, P.S., Goodwin, A., Johnsen, J., Magee, K. & Veldhuyzen van Zanten, S.J.O. (1996) Metabolic activities of metronidazole-sensitive and -resistant strains of *Helicobacter pylori*: Repression of pyruvate oxidoreductase and expression of isocitrate lyase activity correlate with resistance. *Journal of Bacteriology*, *178*(16), 4822–4829. https://doi.org/10.1128/jb.178.16.4822-4829.1996

Hooi, J.K.Y., Lai, W.Y., Ng, W.K., Suen, M.M.Y., Underwood, F.E., Tanyingoh, D. et al (2017) Global prevalence of *Helicobacter pylori* infection: Systematic review and meta-Analysis. *Gastroenterology*, *153*(2), 420–429. https://doi.org/10.1053/j.gastro.2017.04.022

Hughes, N.J., Chalk, P.A., Clayton, C.L. & Kelly, D.J. (1995) Identification of carboxylation enzymes and characterization of a novel foursubunit pyruvate:flavodoxin oxidoreductase from *Helicobacter pylori*. *Journal of Bacteriology*, *177*(14), 3953–3959. https://doi.org/10.1128/jb.177.14.3953-3959.1995

Hughes, N.J., Clayton, C.L., Chalk, P.A. & Kelly, D.J. (1998) *Helicobacter pylori* porCDAB and oorDABC genes encode distinct pyruvate:flavodoxin and 2-oxoglutarate:acceptor oxidoreductases which mediate electron transport to NADP. *Journal of Bacteriology*, *180*(5), 1119–1128.

Hügler, M. & Sievert, S.M. (2011) Beyond the Calvin cycle: Autotrophic carbon fixation in the ocean. *Annual Review of Marine Science*, *3*, 261–289. https://doi.org/10.1146/annurev-marine-120709-142712

Inamoto, Y., Hamanaka, S., Hamanaka, Y., Nagate, T., Kondo, I., Takemoto, T. & et al (1995) Lipid composition and fatty acid analysis of *Helicobacter pylori*. *Journal of Gastroenterology*, *30*(3), 315–318. https://doi.org/10.1007/bf02347505

Jeon, W., Priscilla, L., Park, G., Lee, H., Lee, N., Lee, D. et al (2017) Complete genome sequence of the sulfur-oxidizing chemolithoautotrophic *Sulfurovum lithotrophicum* 42BKT(T). *Standards in Genomic Sciences*, *12*, 54. https://doi.org/10.1186/s40793-017-0265-z

Jung, S.H., Ryu, C.M. & Kim, J.S. (2019) Bacterial persistence: Fundamentals and clinical importance. *Journal of Microbiology*, *57*(10), 829–835. https://doi.org/10.1007/s12275-019-9218-0

Kanao, T., Kawamura, M., Fukui, T., Atomi, H. & Imanaka, T. (2002) Characterization of isocitrate dehydrogenase from the green sulfur bacterium *Chlorobium limicola*. A carbon dioxide-fixing enzyme in the reductive tricarboxylic acid cycle. *European Journal of Biochemistry*, *269*(7), 1926–1931. https://doi.org/10.1046/j.1432-1033.2002.02849.x

Kanehisa, M., Sato, Y., Kawashima, M., Furumichi, M. & Tanabe, M. (2016) KEGG as a reference resource for gene and protein annotation. *Nucleic Acids Research*, *44*(D1), D457–462. https://doi.org/10.1093/nar/gkv1070

Karlsson, R., Thorell, K., Hosseini, S., Kenny, D., Sihlbom, C., Sjöling, Å. et al (2016) Comparative analysis of two *Helicobacter pylori* strains using genomics and mass spectrometry-based proteomics. *Frontiers in Microbiology*, *7*, 1757. https://doi.org/10.3389/fmicb.2016.01757

Kather, B., Stingl, K., Van der Rest, M.E., Altendorf, K. & Molenaar, D. (2000) Another unusual type of citric acid cycle enzyme in *Helicobacter pylori*: The malate:Quinone oxidoreductase. *Journal of Bacteriology*, *182*(11), 3204–3209. https://doi.org/10.1128/Jb.182.11.3204-3209.2000

Kavermann, H., Burns, B.P., Angermüller, K., Odenbreit, S., Fischer, W., Melchers, K. et al (2003) Identification and characterization of *Helicobacter pylori* genes essential for gastric colonization. *Journal of Experimental Medicine*, *197*(7), 813–822. https://doi.org/10.1084/jem.20021531

Kim, J.-S., Cho, D.-H., Heo, P., Jung, S.-C., Park, M., Oh, E.-J. et al (2016) Fumarate-mediated persistence of *Escherichia coli* against antibiotics. *Antimicrobial Agents and Chemotherapy*, *60*(4), 2232–2240. https://doi.org/10.1128/AAC.01794-15

Krieger, I.V., Freundlich, J.S., Gawandi, V.B., Roberts, J.P., Gawandi, V.B., Sun, Q. et al (2012) Structure-guided discovery of phenyldiketo acids as potent inhibitors of *M. tuberculosis* malate synthase. *Chemistry & Biology*, *19*(12), 1556–1567. https://doi.org/10.1016/j.chembiol.2012.09.018

Kulp, A. & Kuehn, M.J. (2010) Biological functions and biogenesis of secreted bacterial outer membrane vesicles. *Annual Review of Microbiology*, *64*, 163–184. https://doi.org/10.1146/annurev.micro.091208.073413

Kuroda, M., Ohta, T., Uchiyama, I., Baba, T., Yuzawa, H., Kobayashi, I. et al (2001) Whole genome sequencing of meticillin-resistant *Staphylococcus aureus*. *Lancet*, *357*(9264), 1225–1240. https://doi.org/10.1016/s0140-6736(00)04403-2

Lanas, A. & Chan, F.K.L. (2017) Peptic ulcer disease. *Lancet*, *390*(10094), 613–624. https://doi.org/10.1016/s0140-6736(16)32404-7

Lancaster, C.R.D. & Simon, J. (2002) Succinate:Quinone oxidoreductases from ε-proteobacteria. *Biochem Biophys Acta Bioenerg.*, *1553*(1–2), 84–101. https://doi.org/10.1016/s0005-2728(01)00230-4

Lee, W.N., Byerley, L.O., Bergner, E.A. & Edmond, J. (1991) Mass isotopomer analysis: Theoretical and practical considerations. *Biological Mass Spectrometry*, *20*(8), 451–458. https://doi.org/10.1002/bms.1200200804

Lee, W.C., Goh, K.L., Loke, M.F. & Vadivelu, J. (2017) Elucidation of the metabolic network of *Helicobacter pylori* J99 and malaysian clinical strains by phenotype microarray. *Helicobacter*, *22*(1), https://doi.org/10.1111/hel.12321

Lekmeechai, S., Su, Y.-C., Brant, M., Alvarado-Kristensson, M., Vallström, A., Obi, I. et al (2018) *Helicobacter pylori* outer membrane vesicles protect the pathogen from reactive oxygen species of the respiratory burst. *Frontiers in Microbiology*, *9*, 1837. https://doi.org/10.3389/fmicb.2018.01837

Lina, T.T., Alzahrani, S., Gonzalez, J., Pinchuk, I.V., Beswick, E.J. & Reyes, V.E. (2014) Immune evasion strategies used by *Helicobacter pylori*.

chemolithoautotroph *Sulfurimonas denitrificans*. *Applied and Environment Microbiology*, *74*(4), 1145–1156. https://doi.org/10.1128/AEM.01844-07

St Maurice, M., Cremades, N., Croxen, M.A., Sisson, G., Sancho, J. & Hoffman, P.S. (2007) Flavodoxin:quinone reductase (FqrB): A redox partner of pyruvate:ferredoxin oxidoreductase that reversibly couples pyruvate oxidation to NADPH production in *Helicobacter pylori* and *Campylobacter jejuni*. *Journal of Bacteriology*, *189*(13), 4764–4773. https://doi.org/10.1128/JB.00287-07

Stark, R.M., Suleiman, M.S., Hassan, I.J., Greenman, J. & Millar, M.R. (1997) Amino acid utilisation and deamination of glutamine and asparagine by *Helicobacter pylori*. *Journal of Medical Microbiology*, *46*(9), 793–800. https://doi.org/10.1099/00222615-46-9-793

Stover, C.K., Pham, X.Q., Erwin, A.L., Mizoguchi, S.D., Warrener, P., Hickey, M.J. et al (2000) Complete genome sequence of *Pseudomonas aeruginosa* PAO1, an opportunistic pathogen. *Nature*, *406*(6799), 959–964. https://doi.org/10.1038/35023079

Tan, S., Tompkins, L.S. & Amieva, M.R. (2009) *Helicobacter pylori* usurps cell polarity to turn the cell surface into a replicative niche. *PLoS Path*, *5*(5), e1000407. https://doi.org/10.1371/journal.ppat.1000407

Tannahill, G.M., Curtis, A.M., Adamik, J., Palsson-McDermott, E.M., McGettrick, A.F., Goel, G. et al (2013) Succinate is an inflammatory signal that induces IL-1beta through HIF-1alpha. *Nature*, *496*(7444), 238–242. https://doi.org/10.1038/nature11986

Tomb, J.-F., White, O., Kerlavage, A.R., Clayton, R.A., Sutton, G.G., Fleischmann, R.D. et al (1997) The complete genome sequence of the gastric pathogen *Helicobacter pylori*. *Nature*, *388*(6642), 539–547. https://doi.org/10.1038/41483

Trastoy, R., Manso, T., Fernández-García, L., Blasco, L., Ambroa, A., Pérez del Molino, M.L. et al (2018) Mechanisms of bacterial tolerance and persistence in the gastrointestinal and respiratory environments. *Clinical Microbiology Reviews*, *31*(4), https://doi.org/10.1128/CMR.00023-18

Tsugawa, H., Suzuki, H., Nakagawa, I., Nishizawa, T., Saito, Y., Suematsu, M. et al (2008) Alpha-ketoglutarate oxidoreductase, an essential salvage enzyme of energy metabolism, in coccoid form of *Helicobacter pylori*. *Biochemical and Biophysical Research Communications*, *376*(1), 46–51. https://doi.org/10.1016/j.bbrc.2008.08.078

Van Acker, H., Sass, A., Bazzini, S., De Roy, K., Udine, C., Messiaen, T. et al (2013) Biofilm-grown *Burkholderia cepacia* complex cells survive antibiotic treatment by avoiding production of reactive oxygen species. *PLoS One*, *8*(3), e58943. https://doi.org/10.1371/journal.pone.0058943

van Amsterdam, K. & van der Ende, A. (2004) Nutrients released by gastric epithelial cells enhance *Helicobacter pylori* growth. *Helicobacter.*, *9*(6), 614–621. https://doi.org/10.1111/j.1083-4389.2004.00272.x

Wang, Y., Bojer, M.S., George, S.E., Wang, Z., Jensen, P.R., Wolz, C. et al (2018) Inactivation of TCA cycle enhances *Staphylococcus aureus* persister cell formation in stationary phase. *Scientific Reports*, *8*(1), 10849. https://doi.org/10.1038/s41598-018-29123-0

Warren, J.R. & Marshall, B. (1983) Unidentified curved bacilli on gastric epithelium in active chronic gastritis. *Lancet*, *1*(8336), 1273–1275.

Watanabe, S., Morimoto, D., Fukumori, F., Shinomiya, H., Nishiwaki, H., Kawano-Kawada, M. et al (2012) Identification and characterization of *D*-hydroxyproline dehydrogenase and delta1-pyrroline-4-hydroxy-2-carboxylate deaminase involved in novel *L*-hydroxyproline metabolism of bacteria: Metabolic convergent evolution. *Journal of Biological Chemistry*, *287*(39), 32674–32688. https://doi.org/10.1074/jbc.M112.374272

Weiss, M.C., Sousa, F.L., Mrnjavac, N., Neukirchen, S., Roettger, M., Nelson-Sathi, S. et al (2016) The physiology and habitat of the last universal common ancestor. *Nature Microbiology*, *1*(9), 16116. https://doi.org/10.1038/nmicrobiol.2016.116

Windham, I.H., Servetas, S.L., Whitmire, J.M., Pletzer, D., Hancock, R.E.W. & Merrell, D.S. (2018) *Helicobacter pylori* biofilm formation is differentially affected by common culture conditions, and proteins play a central role in the biofilm matrix. *Applied and Environment Microbiology*, *84*(14), https://doi.org/10.1128/AEM.00391-18

Zampieri, M., Zimmermann, M., Claassen, M. & Sauer, U. (2017) Nontargeted metabolomics reveals the multilevel response to antibiotic perturbations. *Cell Reports*, *19*(6), 1214–1228. https://doi.org/10.1016/j.celrep.2017.04.002

SUPPORTING INFORMATION

Additional supporting information may be found online in the Supporting Information section.

2.3 Metabolic adaption of *Legionella pneumophila* during intracellular growth in *Acanthamoeba castellanii*

Kunze M.*, Steiner T.*, Chen F., Huber C., Rydzewski K., Stämmler M., Heuner K., Eisenreich W. International Journal of Medical Microbiology 311, 151504 (2021), 10.1016/j.ijmm.2021.151504.

*These authors contributed equally as first authors.

Summary *L. pneumophila* is an accidental human pathogen that typically resides in fresh-water and soil either in biofilms or inside of amoeba. The mechanisms of replication in amoeba are considered to be highly similar to growth in human macrophages, making amoeba an ideal model system to study human infections. Within these host cells, *L. pneumophila* resides inside the so-called *Legionella* containing vacuole (LCV), wherein the bacterium replicates until nutrients become limiting. Following this replicative phase, *L. pneumophila* enters its transmissive phase and leaves the initial host cell. The two phases of the *L. pneumophila* life cycle are highly different in terms of morphology, gene transcription, virulence and metabolism. There have already been investigations on the growth-phase dependent metabolism of *L. pneumophila* yet only during cultivation in broth.

Hence, this work investigated the metabolism of *L. pneumophila* during three different phases (lag phase, early exponential phase; post-exponential phase) of intracellular growth in *Acanthamoeba castellanii*, while amoeba were supplemented with $[U-^{13}C_6]$glucose or $[U-^{13}C_3]$serine during the respective time-period. After harvest the bacterial and amoebal fraction were separated followed by analysis of ^{13}C-excess and isotopologue analysis in protein-bound amino acids in the bacterial (F2) as well as in the amoebal fraction (F3). Additionally, for F2 3-hydroxybutyrate was analysed as a substitute for polyhydroxybutyrate, a macromolecular storage compound produced by *L. pneumophila*. Experiments were performed analogously with *L. pneumophila* Δzwf; this strain is deficient of the first step of the ED pathway thereby contributing to understand the role of glucose for *L. pneumophila* during intracellular growth.

Analysis of the host fraction revealed up-regulation of glycolysis upon infection, while the TCA cycle was not affected. While *L. pneumophila* mostly imported labelled amino acids from the host, there were also clear signs of glucose and serine metabolization by the pathogen, when comparing isotopologue distributions in alanine and glutamate between host and pathogen as well as between *L. pneumophila* WT and Δzwf. Serine utilisation was increased during later growth phases especially for production of 3-hydroxybutyrate/PHB. FT-IR measurements also showed that the total amount of PHB increased towards later growth phases, suggesting PHB as an important carbon storage for *L. pneumophila* during the transmissive phase. Glucose usage was most pronounced during the first growth phase (lag phase/early exponential phase) but observable during all growth phases; still, the overall contribution in terms of carbon excess was very low. This suggests a potential role for glucose as a trigger for *L. pneumophila* replication upon entry into the host cell.

Author contribution I performed the isotopologue analysis of protein-bound amino acids and 3-hydroxybutyrate in the F2- as well as the F3-fraction from all experiments with $[U-^{13}C_3]$serine and part of the experiments involving $[U-^{13}C_6]$glucose. I wrote the first draft of the manuscript and was involved all steps of preparing the final manuscript.

Contents lists available at ScienceDirect

International Journal of Medical Microbiology

journal homepage: www.elsevier.com/locate/ijmm

Metabolic adaption of *Legionella pneumophila* during intracellular growth in *Acanthamoeba castellanii*

Mareike Kunze [a,1], Thomas Steiner [b,1], Fan Chen [b], Claudia Huber [b], Kerstin Rydzewski [a], Maren Stämmler [c], Klaus Heuner [a,*], Wolfgang Eisenreich [b,*]

[a] Working Group: Cellular Interactions of Bacterial Pathogens, Centre for Biological Threats and Special Pathogens, ZBS 2, Robert Koch Institute, Berlin, Germany
[b] Bavarian NMR Center – Structural Membrane Biochemistry, Department of Chemistry, Technische Universität München, Garching, Germany
[c] Proteomics and Spectroscopy, ZBS 6, Robert Koch Institute, Berlin, Germany

A B S T R A C T

The metabolism of *Legionella pneumophila* strain Paris was elucidated during different time intervals of growth within its natural host *Acanthamoeba castellanii*. For this purpose, the amoebae were supplied after bacterial infection (t =0 h) with 11 mM [U-^{13}C$_6$]glucose or 3 mM [U-^{13}C$_3$]serine, respectively, during 0−17 h, 17−25 h, or 25−27 h of incubation. At the end of these time intervals, bacterial and amoebal fractions were separated. Each of these fractions was hydrolyzed under acidic conditions. ^{13}C-Enrichments and isotopologue distributions of resulting amino acids and 3-hydroxybutyrate were determined by gas chromatography – mass spectrometry. Comparative analysis of the labelling patterns revealed the substrate preferences, metabolic pathways, and relative carbon fluxes of the intracellular bacteria and their amoebal host during the time course of the infection cycle. Generally, the bacterial infection increased the usage of exogenous glucose *via* glycolysis by *A. castellanii*. In contrast, carbon fluxes *via* the amoebal citrate cycle were not affected. During the whole infection cycle, intracellular *L. pneumophila* incorporated amino acids from their host into the bacterial proteins. However, partial bacterial *de novo* biosynthesis from exogenous ^{13}C-Ser and, at minor rates, from ^{13}C-glucose could be shown for bacterial Ala, Asp, Glu, and Gly. More specifically, the catabolic usage of Ser increased during the post-exponential phase of intracellular growth, whereas glucose was utilized by the bacteria throughout the infection cycle and not only late during infection as assumed on the basis of earlier *in vitro* experiments. The early usage of ^{13}C-glucose by the intracellular bacteria suggests that glucose availability could serve as a trigger for replication of *L. pneumophila* inside the vacuoles of host cells.

1. Introduction

Legionella pneumophila (*Lp*) is ubiquitously found in aquatic systems where it resides either in biofilms resistant to environmental stress or inside protozoa (amoebae), such as *Acanthamoeba castellanii* (*Ac*) (Rowbotham, 1980, 1986; Taylor et al., 2009; Lau et al., 2013). Infection of human alveolar macrophages can also occur mainly *via* inhalation of *Lp* containing aerosols from aquatic reservoirs (Fraser et al., 1977; Mondino et al., 2020) causing Legionnaires' disease, an atypical pneumonia accounting for 2–9 % of community acquired pneumonias (Cunha et al., 2016; Cunha and Cunha, 2017). The mechanisms of replication inside amoebae and human macrophages are thought to be highly similar. Therefore, infected amoebae are considered as a valid model for the human infection (Swart et al., 2018). Upon entry into the host cell, *Lp* builds up a compartment for replication – the *Legionella* containing vacuole (LCV) (Steiner et al., 2018). Inside this vacuole, *Lp* replicates until nutrients become limited. After this replicative phase, *Lp* leaves the LCV and changes to a mature intracellular transmissive form (MIF). These phases significantly differ in terms of morphology, gene transcription, virulence and metabolism (Byrne and Swanson, 1998; Heuner et al., 1999; Faulkner and Garduno, 2002; Brüggemann et al., 2006; Faucher et al., 2011; Price et al., 2014; Heuner and Eisenreich, 2016; Oliva et al., 2018). Generally, intracellular bacterial pathogens are characterized by a sophisticated control of their specific substrate preferences and metabolic pathways during their life cycles (Eisenreich and Heuner, 2016; Eisenreich et al., 2017; Oliva et al., 2018; Eisenreich

2.3 Metabolic adaption of *L. pneumophila* during intracellular growth in *A. castellanii*
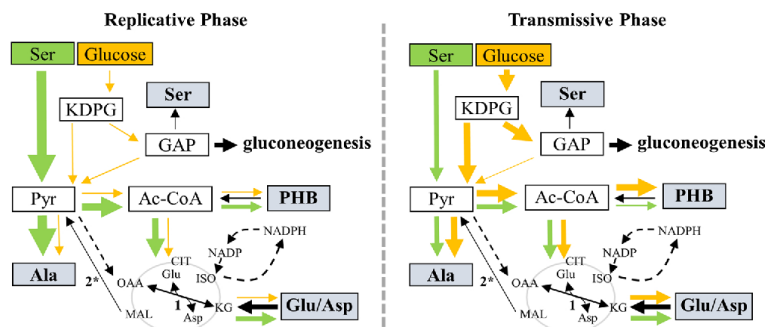
Fig. 1. Model of substrate preferences and metabolic pathways for different growth phases of *Lp* growing in AYE medium (Gillmaier et al., 2016; **modified**). Relative carbon fluxes are indicated by the thickness of the arrows using glucose (orange) or serine (green) as substrates. Analysed metabolites are indicated by grey boxes. The citrate cycle is indicated in grey. 1, Glu/Asp transaminase; 2*, malic enzyme (MEZ, *lpp3043* and *lpp0705*, respectively). Ac-CoA, acetyl-CoA; CIT, citrate; GAP, glyceraldehyde-3-phosphate; ISO, isocitrate; KG, α-ketoglutarate; KDPG, 2-keto-3-desoxy-6--phosphogluconate; MAL, malate; OAA, oxaloacetate; PHB, polyhydroxybutyrate; Pyr, pyruvate.

et al., 2019; Richardson, 2019; Russell et al., 2019). There is also emerging evidence that intracellular bacteria use multiple substrates orchestrated in bipartite metabolic networks (Grubmüller et al., 2014; Eisenreich and Heuner, 2016; Häuslein et al., 2016, 2017; Mehlitz et al., 2017; Best et al., 2018a, 2018b). This flexibility could enable these bacteria to rapidly adapt to the different and changing supplies of their host cells.

In line with this metabolic flexibility, substrate preferences during the respective growth phases of *Lp* growing in liquid medium were observed. During the early phase, Ser was identified as a preferred carbon substrate, whereas fatty acids, glucose and/or glycerol served as additional carbon sources during the late exponential growth phase, mainly for biosynthesis of poly-hydroxybutyrate (PHB) (Gillmaier et al., 2016; Häuslein et al., 2016) (Fig. 1).

However, the substrate usages and carbon fluxes during the infection cycle of intracellular *Lp* are only partially understood. It is established knowledge that host amino acids are among the major nutrients and are also crucial for the survival of the intracellular bacteria. Thus, a neutral amino acid transporter of the host cell (SLC1A5 in MM6 monocyte cells) as well as a bacterial threonine transporter (PhtA) were shown to be necessary for successful replication of *Lp* inside monocytes (Sauer et al., 2005; Wieland et al., 2005). In addition, some effector proteins, *i.e.* proteins which are transferred into the host cytosol using the type IV secretion system (T4SS) of *Lp* such as AnkB, catalyze poly-ubiquitinylation of host proteins. This leads to their proteasomal degradation into amino acids as welcome nutrients for intracellular *Lp* (Price et al., 2009; Lomma et al., 2010; Price et al., 2011, 2014). Moreover, the ubiquitinating enzyme SidE and the glucosyltransferase Lgt work synergistically to inhibit host translation through regulation of the mechanistic target of rapamycin complex 1 (mTORC1) (Belyi et al., 2008; De Leon et al., 2017). The upregulation of genes encoding various ABC transporters, proteases, phospholipases and amino acid permeases of intracellular *Lp* further supports the role of amino acids as nutrients (Brüggemann et al., 2006). In earlier labelling studies with *Lp* growing in amoebae, we could also confirm that host derived amino acids are directly incorporated into the bacterial proteins (Schunder et al., 2014; Eisenreich and Heuner, 2016; Häuslein et al., 2016).

The role of glucose as a potential nutrient for intracellular *Lp* is still obscure, although several earlier findings already pointed towards the importance of the carbohydrate during intracellular survival (Eylert et al., 2010; Harada et al., 2010; Herrmann et al., 2011; Gillmaier et al., 2016). Indeed, the ability of glucose uptake by *Legionella* was shown to be necessary for intracellular replication, although it did not affect bacterial growth *in vitro* (Best et al., 2018a, 2018b). Amylases and enzymes of the Entner Doudoroff pathway (ED pathway) catalyzing glucose degradation were also reported to be important for intracellular replication (Eylert et al., 2010; Harada et al., 2010; Häuslein et al., 2016; Manske et al., 2016; Häuslein et al., 2017; Best et al., 2018a, 2018b;

Levanova et al., 2019). More specifically, the Δ*lamB* amylase mutant was severely attenuated in intra-pulmonary proliferation in mice (Best et al., 2018a, 2018b) and the *zwf* gene encoding glucose-6-phosphate dehydrogenase in the ED pathway for glucose usage was induced during growth in amoebae, but not in human macrophages (Brüggemann et al., 2006; Faucher et al., 2011). The Δ*zwf* mutant showed reduced growth in both amoebae and macrophages (Eylert et al., 2010; Harada et al., 2010). In line with these findings, myo-inositol derived from glucose metabolism accumulated inside the LCV and enhanced intracellular growth (Manske et al., 2016).

The effect of bacterial infections upon the metabolism of their host organisms has also hardly been investigated. Before infection by bacterial pathogens, the typical metabolic state of most host cells does not meet the extensive need for nutrients and energy by the invasive bacteria. To increase the supply of nutrients, energy, and metabolites for replication inside their host cells, most intracellular bacteria have therefore developed smart mechanisms to reprogram the metabolism of their hosts (Price et al., 2014; Best and Abu Kwaik, 2019; Eisenreich et al., 2019). For example, the uptake and metabolism of glucose is strongly increased in primary murine or human cells as a response upon infection by intracellular *Listeria monocytogenes* (Krawczyk et al., 2010; Gillmaier et al., 2012). In *Dictyostelium discoideum*, another amoebal host for *Lp*, infection with *Lp* downregulated genes involved in defense reactions against the infection, but upregulated many genes encoding enzymes for general metabolic functions (*e.g.* protein biosynthesis and carbohydrate metabolism) and the stress response (Farbrother et al., 2006). Experiments with *Acanthamoeba polyphaga* as a host revealed increased lactate secretion and higher levels of glucose-6-phosphate in the amoebal cytosol during infection dependent on the T4SS of *Lp*, which could point at a stimulation of glycolysis triggered by effector proteins (Price et al., 2020).

To reveal the substrate usages and the core energy metabolism of *Lp* for different time periods of the infection and to elucidate impacts of the infection upon the host metabolism, we here took advantage of ^{13}C-labelling experiments. Specifically, [U-^{13}C$_6$]glucose or [U-^{13}C$_3$]serine were supplied to infected *Ac* during various intervals of the infection cycle. This technique provided direct insights into the relative carbon fluxes and was therefore qualified to determine differential substrate usages and metabolic pathways in the infection cycle. Using the same setting, we also analysed the Δ*zwf* mutant of *Lp* to better understand the role of glucose during intracellular growth. Since the protein encoded by the *zwf* gene catalyzes the entry reaction of the ED pathway, the main route for glucose usage in *Lp* (Eylert et al., 2010; Harada et al., 2010), the Δ*zwf* mutant strain was especially useful to clarify the importance of glucose metabolism by intracellular *Lp*.

2

2. Materials and methods

2.1. Strains, growth conditions, media, and buffer

L. pneumophila Paris wild type (in the following *Lp*) was used in this study (Cazalet et al., 2004). For comparison, the following mutant strains were studied by *in vivo* infection assays: *L. pneumophila* Paris *zwf* (*lpp0483*, glucose-6-phosphate-dehydrogenase) (Eylert et al., 2010) and *L. pneumophila* Corby *fliA* (Heuner et al., 2002). *Lp* was grown in yeast extract broth buffered with *N*-(2-acetoamido)-2-aminoethanesulfonic acid (AYE) consisting of 10 g of *N*-(2-acetoamido)-2-aminoethane-sulfonic acid, 10 g of yeast extract, 0.4 g of *L*-Cys, and 0.25 g of ferric pyrophosphate per L (adjusted to pH 6.8 with 3 M KOH and sterile fil-trated) at 37 °C with agitation at 250 rpm or on buffered charcoal-yeast extract (BCYE) agar for 3 days at 37 °C. Bacterial growth in broth was monitored by determining the A_{600} with a Thermo Scientific GENESYS 10 Bio spectrophotometer (VWR, Darmstadt, Germany). When appro-priate, media were supplemented with kanamycin at final concentra-tions of 8 or 40 µg/mL, respectively. For cultivation of *Lp* on agar plates, kanamycin was used at a final concentration of 12.5 µg/mL.

A. castellanii ATCC 30010 (in the following *Ac*) was cultured in PYG712 medium (2 % proteose peptone, 0.1 % yeast extract, 0.1 M glucose, 4 mM $MgSO_4$ x 7 H_2O, 0.4 M $CaCl_2$ x 2 H_2O, 0.1 % sodium citrate dihydrate, 0.05 mM $Fe(NH_4)_2(SO_4)_2$ x 6 H_2O, 2.5 mM NaH_2PO_4, and 2.5 mM K_2HPO_4) at 20 °C. The so-called *Acanthamoeba* (Ac) buffer was PYG712 medium without peptone, yeast extract, and glucose.

2.2. Intracellular replication and determination of time points

Intracellular replication was monitored by lysing infected amoebae at different time points followed by plating the supernatant onto BCYE agar plates and determination of the CFUs. Infection was also observed microscopically by counting intact amoebae and "rotating vacuoles" (Rowbotham, 1986) as a result from motile *Lp* inside vacuoles due to the formation of flagellae.

2.3. ^{13}C-Labelling experiments of Lp growing in Ac

Ac was cultivated in 12 cell culture flasks (175 cm²) (Heuner et al., 2019). A volume of 50 mL PYG712 medium was inoculated (1:10) and incubated for 3 days at room temperature. The adhered amoebae were washed two times by gently shaking the flask with 10 mL of Ac buffer and then incubated for 2 h at 37 °C in 50 ml of fresh Ac buffer. *Lp* grown on a BCYE agar plate for 3 days was diluted in Ac buffer. The suspension was adjusted to an A_{600} of 1, and 1 mL of the suspension (about 10^9 bacteria) per flask was used for infection resulting in a MOI of about 100. After 2 h at 37 °C, all extracellular bacteria were removed by washing with 10 mL Ac buffer and by adding 50 µg/mL gentamicin for 1 h at 37 °C. Gentamicin was removed by washing with 10 mL Ac buffer. Infected amoebae were incubated in 50 mL fresh Ac buffer for given time periods. For ^{13}C-labelling, the infected amoebae were incubated in Ac buffer supplemented with 11 mM [U-$^{13}C_6$]glucose or 3 mM [U-$^{13}C_3$]serine during time periods of 0−17 h, 17−25 h and 25−27 h after infection (t = 0) at 37 °C, respectively. Additionally, infected amoeba were incubated in Ac buffer supplemented with 55 mM [U-$^{13}C_6$]glucose during the time intervals 17−25 h and 25−27 h after infection. Cells were harvested at the end of the given time interval and an aliquot was plated out on LB agar plates. The plates were incubated for 24 h to exclude the possibility of contaminations. The infected amoebae were frozen for at least 2 h at −80 °C, thawed in a 37 °C water bath and vortexed for 20 s. Successful lysis was monitored microscopically. Differential centrifugation allowed separation of unlysed amoebae and high-density cellular components (fraction 1, F1), *Lp* (fraction 2, F2), and the cytosolic proteins of *Ac* (fraction 3, F3) using the protocol as follows. The suspension was first centrifuged at 600*g* and 4 °C for 15 min. The pellet containing F1 was washed three times with Ac buffer. The supernatant was then transferred

to a new tube and centrifuged at 3600*g* and 4 °C for 15 min. The resulting pellet (F2) was washed two times in distilled water, and the supernatant F3 was filtrated through a 0.22 µm pore filter to exclude contaminating bacteria. All three fractions were autoclaved at 120 °C for 20 min and stored at −20 °C until work-up for GC–MS analysis.

2.4. SDS PAGE and immunoblotting

SDS-PAGE and Western blotting were done as described elsewhere (Laemmli, 1970; Towbin et al., 1979). Fractions F1–F3 obtained from four flasks of infected *Ac* were dissolved in 200 µL of distilled water. For SDS-PAGE, 10 µL of each fraction were resuspended with 4 µL of Roti-Load denaturating sample buffer, boiled for 10 min, and loaded on a 12 % SDS-polyacrylamide gel. Synthesis of the flagella was detected using polyclonal anti-FlaA antiserum diluted in 1 % milk and tris-buffered saline (1:1000). The horseradish peroxidase-conjugated goat α-rabbit IgG antibody was used as the secondary antibody (1:1000) (Dianova, Hamburg, Germany). Lysates of stationary *Lp* WT and the mutant Δ*fliA*, unable to express flagella, served as a control. FlaA was visualized using commercially available Pierce enhanced luminol-based chemiluminescent (ECL) Western blotting substrate and ECL detection solution (Thermo Fisher Scientific), which was exposed to X-ray films.

2.5. Fourier-transform infrared absorption spectroscopy of whole Lp cells to quantify poly-hydroxybutyrate (PHB)

F2 was diluted in 1 µL distilled water. Fourier-transform infrared (FT-IR) absorption spectra were obtained using a FT-IR microscope IR Scope II, coupled to an IFS28/B spectrometer (Bruker Optics, Ettlingen, Germany) and equipped with a broadband mercury–cadmium–telluride (MCT)-detector, and a motorized x,y stage. The measurements were performed in transmission/absorbance mode and the parameters used were: 6 cm^{-1} nominal spectral resolution, zero-filling-factor of 4, and a Blackman–Harris-Three-Term apodization function prior to Fourier transformation. All spectra were collected with a 15× Cassegrain-objective and were acquired under stable measurement and nearly free of water vapour conditions in the spectral region between 600 cm^{-1} and 4000 cm^{-1}. The measurements of samples were performed selecting aperture diameters of 50 µm and averaging 64 interferograms. Spectral data processing was performed using the software OPUS 5.5 for Win-dows XP Professional (Bruker Optics, Ettlingen, Germany).

2.6. Measurement of glycogen in Ac by FT-IR spectroscopy

Ac cells were cultivated in 175 cm² flasks in PYG medium for 8 days. Co-cultivation with *Lp* was carried out as described above or cells were left uninfected. About 10^7 cells were harvested 17, 25 or 27 h after infection and frozen for at least 2 h at −80 °C and thawed afterwards followed by centrifugation at 3600*g* for 15 min at 4 °C. Cells were washed with 0.9 % NaCl. The pellet was resuspended in 100 µL H_2O_{dd} and applied onto a ZnSe sample holder and dried to a film in a desiccator under moderate vacuum (0.9 bar) over P_4O_{10} (Sicapent, Merck) for 30 min. The sample holder was sealed with a KBr cover plate. FT-IR spectra for glycogen were measured as described before for PHB (Gillmaier et al., 2016). Background spectra were collected from an empty position of the ZnSe sample holder. Spectral data processing was performed using the software OPUS 5.5 for Windows XP Professional (Bruker Optics, Ettlingen, Germany).

2.7. Sample preparation for ^{13}C-isotopologue analysis of proteinogenic amino acids and 3-hydroxybutyrate

Each of F2- and F3-fractions was dried by lyophilization. Analysis of protein bound amino acids and PHB in the form of 3-hydroxybutyrate was basically done as described earlier (Eylert et al., 2008; Schunder
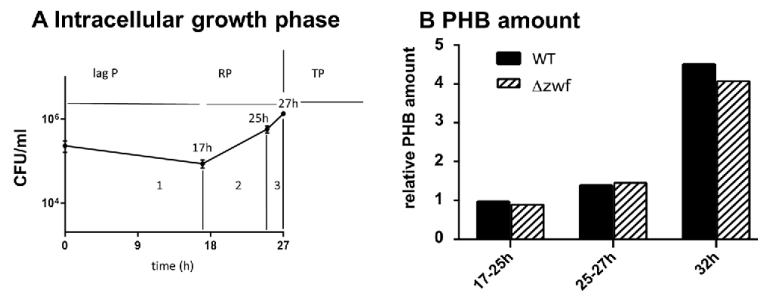
Fig. 2. Growth phase dependent analysis of PHB amounts during intracellular growth of *Lp*. A. Analysis of CFU during intracellular replication in *Ac* (n = 2). Lag P, lag-phase; RP, replicative phase; TP, transmissive phase. B. Relative amounts of PHB in *Lp* WT and the Δzwf mutant as measured by FT-IR analysis.

et al., 2014). In brief, about 2 mg of the dried fractions were subjected to acidic hydrolysis (0.5 mL of 6 M HCl, 15 h, 105 °C). Afterwards, cation exchange chromatography using Dowex 50 W X8 (7 × 10 mm; 200–400 mesh, 34–74 μm, H+-form, Alfa Aesar) yielded an aqueous eluate containing 3-hydroxybutyrate and an alkaline eluate containing amino acids. For derivatization of the amino acid-fraction, the alkaline eluate was dried under a stream of nitrogen at 70 °C and the residue was mixed with 50 μL of anhydrous acetonitrile and 50 μL of *N*-methyl--*N-tert*-butyldimethylsilyltrifluoroacetamide (Sigma Aldrich). The mixture was incubated at 70 °C for 30 min. For derivatization of 3-hydroxybutyrate, the water eluate was dried under a stream of nitrogen at 70 °C and the residue was mixed with 100 μL of *N*-methyl--*N*-trimethylsilyl-trifluoroacetamide (Sigma Aldrich). This mixture was incubated at 40 °C for 90 min while shaking with 110 rpm.

2.8. GC–MS parameters for ^{13}C-isotopologue analysis

In general, the silylated derivatives were analysed using a Shimadzu GC–MS (GCMS-QP 2010 Plus spectrometer, Shimadzu, Duisburg, Germany) as described earlier (Häuslein et al., 2016). For GC–MS analysis of silylated amino acids, the column was heated to 150 °C and kept for 3 min. A gradient of 7 °C/min was then applied until a final temperature of 280 °C, which was held for 3 min. For GC–MS analysis of silylated 3-hydroxybutyrate, the column was developed at 70 °C for 3 min and then with a temperature gradient of 10 °C/min to a final temperature of 150 °C. This was followed by a temperature gradient of 50 °C/min to a final temperature of 280 °C, which was held for 3 min.

2.9. Data evaluation and statistics

GC–MS data evaluation was performed using Shimadzu LabSolution software V4.20. ^{13}C-Excess values were calculated using an Excel-based in-house software based on an earlier procedure (Lee et al., 1991). Labelling experiments were typically performed twice to afford two biological replicates. GC–MS measurements were performed in triplicates for each sample to demonstrate the robustness of the measurements.

3. Results and discussion

3.1. Establishing a growth-phase dependent infection model of Lp in Ac

The major object of this study was to determine the dynamics of substrate usages and metabolic pathways during the full growth cycle of *Lp* in amoebae. In earlier studies of intracellular *Lp*, we supplied [U-^{13}C$_6$]glucose to *Ac* before infection (t =0 h), which gave some insights into *Lp* metabolism during the whole infection cycle (Heuner et al., 2019). To achieve time resolution during the infection cycle, we now selected three different time intervals 1–3 (see Fig. 2A), where we

Table 1
Growth phase dependent characterisation of intracellularly growing *Lp*. Replication of *Lp* was determined by CFU. Flagellin expression was determined in a Western blot using an α-flagellin-antiserum (data not shown). Rotating vacuoles, which are a result of flagellated *Lp* moving inside the vacuole, and lysed amoeba were monitored and counted microscopically. PHB was determined by FT-IR analysis. Data are based on two biological replicates.

	17 h after infection	25 h after infection	27 h after infection	32 h after infection
Lp replication	+	++	++	n.d.
Lp flagellation[*]	–	+	++	n.d.
"Rotating vacuoles"		1.3 %	2.5 %	0.8 %
Lysed amoeba	–	4.2 %	15 %	50.2 %
Relative PHB amount	–	+	+	+++

n.d., not determined.
[*] Indirectly determined by the detection of flagellin protein.

added ^{13}C-glucose or alternatively ^{13}C-Ser to the infected amoebae. Western blot analysis using an anti-flagellin antiserum and microscopic analysis of the fraction of "rotating vacuoles" as an indication of flagellated *Lp* moving inside the vacuoles (Table 1) (Rowbotham, 1986) were used to assess intracellular motility of *Lp*. These results suggested that the time interval 1 (0−17 h after the infection of the amoebae) represented the lag phase of *Lp* and the beginning of intracellular replication. During this phase, the bacteria were non-flagellated and accordingly "rotating vacuoles" were not detected. The time interval 2 (17−25 h) represented the main peak of the replicative phase (RP), where *Lp* started to express the flagellum towards the 25 h-time point. However, still only a small fraction of amoebae (< 2 %, Table 1) contained "rotating vacuoles" at this time. During time interval 3 (25−27 h), the bacteria rapidly reached the post-exponential phase (PE), in which most *Lp* became flagellated and motile. A minor fraction of amoebae (about 15 %, Table 1) had already been lysed at the 27 h-time point. During this late interval, the bacteria synthesized high amounts of PHB (Fig. 2B). The subsequent transmissive phase (TP) (stationary phase, 27−32 h, Table 1) showed the presence of huge amounts of extracellular bacteria (> 50 % at 32 h). Although the synthesis of PHB reached its maximum during this phase (Fig. 2B), this time interval was not further studied by ^{13}C-profiling since the respective labelling data would largely reflect the fraction of extracellular *Lp*.

After harvest at the end of the indicated time intervals, the bacteria (highly enriched in the F2 fraction) were separated from the cytosolic amoebal proteins (F3), hydrolysed, converted into volatile silyl derivatives, and subjected to GC–MS analysis following established protocols (Schunder et al., 2014; Heuner et al., 2019). In both fractions, the ^{13}C-labelling patterns of 14 amino acids could be determined (Supplemental Tables 1–24). The differential ^{13}C-excess values of these amino
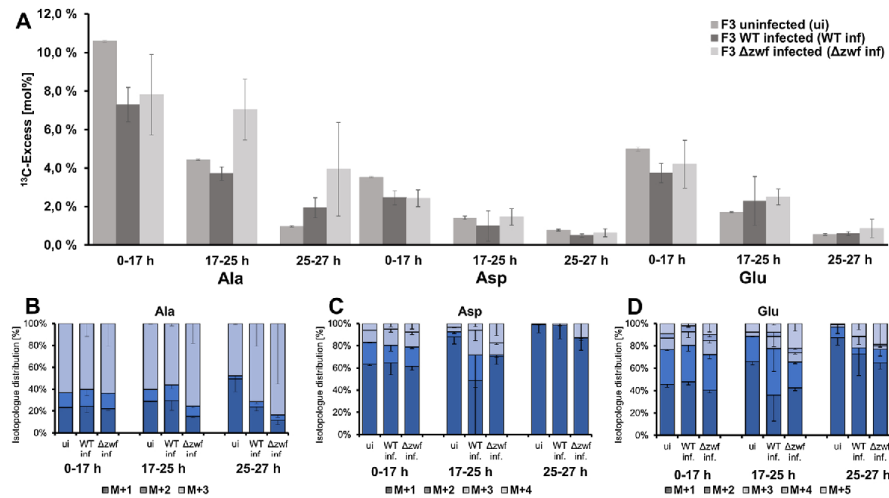
4

Fig. 3. Effects of the *Lp*-infection upon amoebal metabolism. (A) ^{13}C-Enrichments in mol% of amino acids from amoebal proteins, *i.e.* from the F3 fraction, in uninfected *Ac* and after infection with *Lp* WT or the Δ*zwf* mutant in the experiment with [U-[13]C$_6$]glucose. (B–D) Relative isotopologue compositions of labelled Ala, Asp and Glu in the experiment with [U-[13]C$_6$]glucose. M + X indicates an isotopologue containing X ^{13}C-atoms. Error bars indicate standard deviations based on two biological replicates (n = 2) with three technical replicates each, except for the experiment with uninfected amoeba, which are based on one biological replicate (n = 1) with three technical replicates.

acids with their relative fractions of specific isotopologues (*i.e.* molecules containing a certain number of ^{13}C-atoms were now taken as the basis to derive key metabolic pathways of the intracellular bacteria and their host cells. Moreover, the labelling patterns of silylated 3-hydroxybutyrate resulting from hydrolysis of bacterial PHB in F2 allowed to specifically analyse the metabolism of the storage compound (Supplemental Tables 25–33).

3.2. Amoebal glycolysis is stimulated by the bacterial infection

By comparing the labelling patterns of amino acids from *Lp*-infected amoebae (F3) with the corresponding ones from uninfected *Ac*, we could study the impact of the *Legionella* infection upon the amoebal metabolism (Fig. 3). Here, we focused on the ^{13}C-patterns of Ala, since this amino acid directly derives from pyruvate, the product of glycolysis (Fig. 3B). Similarly, Asp was a useful reporter since it is the amination product of the TCA cycle-intermediate oxaloacetate, and is therefore a valid reporter for fluxes *via* the TCA cycle as well as for pyruvate carboxylation forming oxaloacetate (Fig. 3C). Following the same methodology, Glu was taken as the reporter for the TCA cycle-intermediate α-ketoglutarate, and thus also reflects fluxes *via* the TCA cycle (Fig. 3D).

In the experiment with [U-[13]C$_6$]glucose, Ala, Asp, and Glu from the amoebal fraction (F3) displayed significant ^{13}C-excess values (1–10 %) for uninfected as well as for infected amoebae during the three time periods in our experiments (Fig. 3A, Supplemental Tables 1, 3, 5, 7, 9, 11, 34). Generally, these values decreased towards the latter time periods, probably influenced by the shorter time spans. As another reason, the observed degradation of glycogen in amoebae over time (see FT-IR analysis, SI Fig. 1) led to the release of unlabelled glucose, which may have caused dilution of ^{13}C-excess in free (available) glucose, thus also resulting in lower ^{13}C-enrichments of amino acids during the late time periods. Importantly, however, this decrease was less pronounced for Ala (reporter for glycolytic flux) from the infected cells and, as a noticeable exception, even reversed during the third period, when comparing infected with uninfected cells (Fig. 3A). This could be taken as clear evidence that amoebal glycolysis was stimulated by the bacterial

infection with increasing rates towards the replicative phase of intracellular *Lp*.

In line with this conclusion, ^{13}C-excess values of Ala in F3 were higher in amoebae infected by the Δ*zwf* mutant strain as compared with amoebae infected with *Lp* WT (Fig. 3A). Obviously, more ^{13}C-glucose was available for amoebal glycolysis in the experiment with the mutant, since the Δ*zwf* strain was unable to retrieve ^{13}C-glucose from the host for bacterial metabolism (see below). Thus, all these observations indicated that the bacterial infection stimulated the formation of ^{13}C-Ala *via* conversion of ^{13}C-glucose into ^{13}C-pyruvate followed by transamination to ^{13}C-Ala. Differences in the relative isotopologue fractions became also evident in the labelling patterns of Ala from F3 (Fig. 3B, Supplemental Tables 2, 4, 6, 8, 10, 12, 35). As expected, the ^{13}C-profile of amoebal Ala was indicative for [U-[13]C$_6$]glucose degradation *via* glycolysis mainly resulting in the [13]C$_3$-isotopologue (*i.e.* Ala carrying three ^{13}C-atoms, also denoted as M + 3). The M + 3 fraction was highest in Ala from the infected amoebae of the late time interval, which again corroborated that amoebal glycolysis was stimulated during the bacterial infection. This effect was stronger when the amoebae were infected with the Δ*zwf* mutant of *Lp* (Fig. 3B). Interestingly, the detected increase of glycolytic flux of *Lp*-infected *Ac* was in line with the previously reported upregulation of genes involved in glucose homeostasis and cell wall catabolism of *Lp*-infected *Dictyostelium* (Farbrother et al., 2006) and upregulation of glycolysis in the amoeba *A. polyphaga* due to the T4SS of *Lp* (Price et al., 2020).

From the unchanged labelling data for Asp and Glu from F3 of infected *vs.* uninfected *Ac*, it could be concluded that the amoebal TCA cycle and glutaminolysis were less or not affected by the bacterial infection (Fig. 3A, C, D; Supplemental Tables 2, 4, 6, 8, 10, 12, 35). Not surprisingly, the isotopologue compositions of Asp and Glu reflected their origin *via* the TCA cycle and related anaplerotic reactions but these patterns were almost identical for uninfected and infected *Ac* (Fig. 3C, D).

3.3. The dynamics of PHB metabolism in intracellular Lp

The polymerisation and depolymerisation of PHB by intracellular *Lp*
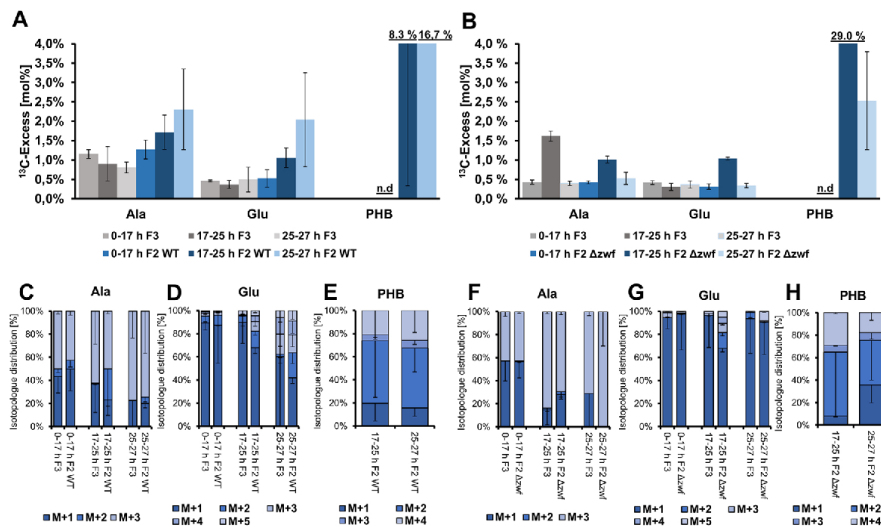
Fig. 4. Key data from the labelling experiment with [U-^{13}C$_3$]serine. Analysis of the ^{13}C-patterns in amino acids in comparison of the different growth phases of intracellular *Lp* WT and its Δ*zwf* mutant. ^{13}C-Excess in mol% of amino acids in *Ac* (from the F3 fractions) and amino acids and 3-hydroxybutyrate (from the respective F2 fractions) in *Lp* WT (A) and its Δ*zwf* mutant (B). Isotopologue profiles of the respective compounds from *Lp* WT (C–E) and its Δ*zwf* mutant (F–H). M + X indicates the isotopologue with X ^{13}C-atoms incorporated into the respective compound. Error bars indicate standard deviations based on two biological replicates (n = 2) with three technical replicates each, except for the data with ^{13}C-serine and *Lp* Δ*zwf*, which is based on one biological experiment (n = 1) with three technical replicates. n. d., not determined.
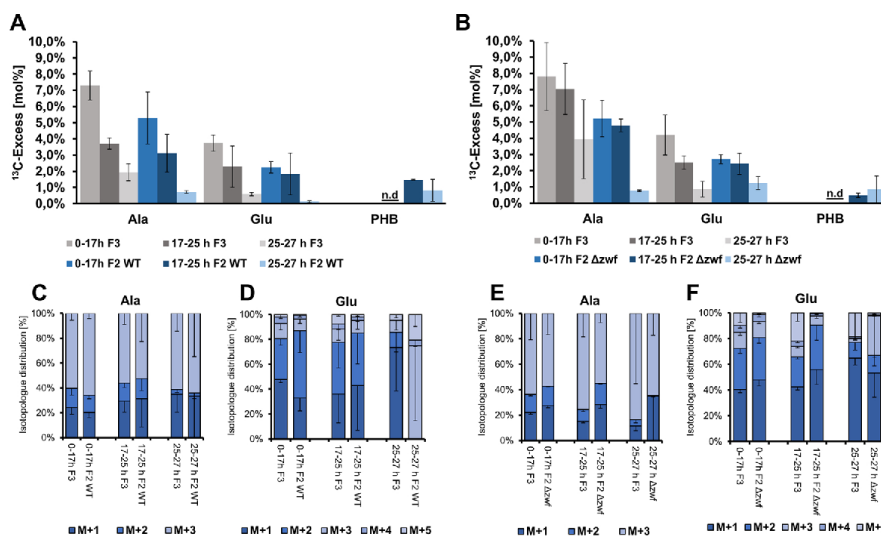

Fig. 5. Key data from the labelling experiment with [U-^{13}C$_6$]glucose. Analysis of the ^{13}C-patterns in amino acids in comparison of the different growth phases of intracellular *Lp* WT and its Δ*zwf* mutant. ^{13}C-Excess in mol% of amino acids in *Ac* (from the F3 fractions) and amino acids and 3-hydroxybutyrate (from the respective F2 fractions) in *Lp* WT (A) and its Δ*zwf* mutant (B). Isotopologue profiles of the respective compounds from *Lp* WT (C, D) and its Δ*zwf* mutant (E, F). M + X indicates the isotopologue with X ^{13}C-atoms incorporated into the respective compound. Error bars indicate standard deviations based on two biological replicates (n = 2) with three technical replicates each. n.d., not determined.

has not yet been investigated in detail. It seemed as if PHB synthesis by intracellular *Lp* is higher than by bacteria grown in medium, and that PHB, generated in the MIF inside amoebae, is important for subsequent

extracellular survival of *Lp* (Rowbotham, 1986; James et al., 1999; Garduno et al., 2002; Robertson et al., 2014).

Based on the observed ^{13}C values and patterns of 3-hydroxybutyrate

isolated from the hydrolysed F2 fraction (as the proxy for bacterial PHB) either starting from ^{13}C-glucose or ^{13}C-serine in our setting, it was obvious that 3-hydroxybutyrate formation not only occurs late in the life cycle of intracellular *Lp*, but already during the first growth phase (Figs. 4A, 5 A). Then, polymerisation of 3-hydroxybutyrate into PHB increased during the late replicative phase, as reflected by the higher amounts of cellular PHB detected by FT-IR spectrometry (Fig. 2B). During the late growth phase, incorporation from ^{13}C-serine into 3-hydroxybutyrate further increased (Fig. 4A). In the transmissive phase, PHB amounts also increased (Fig. 2B, 32 h). ^{13}C-Flux from glucose into PHB slightly decreased during the transmissive phase (Fig. 5A, B, SI Fig. 2). Thus, PHB synthesis seemed to peak very shortly before lysis of the host cell. The previously reported negative effect of the Δ*zwf* mutant strain on ^{13}C-flux from glucose into PHB synthesis under *in vitro* conditions (Gillmaier et al., 2016) was also detected during intracellular growth in *Ac* (SI Fig. 2, Supplemental Table 36). However, the amount of PHB was nearly similar in *Lp* WT and the Δ*zwf* mutant (Fig. 2B), which was partly at odds to our earlier finding under *in vitro* conditions, where the *zwf* mutant strain synthesized less PHB (51–68 %) (Gillmaier et al., 2016). Other substrates such as fatty acids (Häuslein et al., 2017), leucine (Heuner, unpublished results; Tesh et al., 1983), as well as further genes, like those encoding for ketothiolase (*lpp1788*), the PHB polymerase (*lpp650*), the alternative fatty acid degradation pathway (*lpp0931-33*) (Gillmaier et al., 2016), and the *bdhA* (PHB dehydrogenase) (Aurass et al., 2009) have been shown to be involved in the metabolism of PHB at different efficiencies when comparing intracellular *Lp* with *Lp* grown in medium. The complex interplay of these factors under intracellular conditions could explain the apparent discrepancies between the *in vivo* and *in vitro* results.

3.4. Differential usage of Ser during the infection cycle of Lp

In the experiment with [U-^{13}C$_3$]serine, the ^{13}C-enrichments of Ala, Glu and 3-hydroxybutyrate from *Lp* (F2 fraction) increased with the duration of the experiment (Fig. 4A, B, Supplemental Tables 13, 15, 17, 19, 21, 23, 29, 31). Labelled Ala mostly consisted of the M + 3-isotopologue (Fig. 4C, F, Supplemental Tables 14, 16, 18, 20, 22, 24, 30, 32), while the isotopologue profile of Glu comprised a diverse pattern of isotopologues arising through multiple rounds of the TCA cycle (Fig. 4D, G). The labelling pattern of 3-hydroxybutyrate reflected the incorporation of one or two evenly or unevenly labelled acetyl-CoA precursor molecules (Fig. 4E, H, Supplemental Tables 30, 33). These findings could be taken as evidence that ^{13}C-Ser or a closely related compound was transferred from the host into the LCV and converted by the bacterial metabolism into pyruvate, acetyl-CoA, and α-ketoglutarate. These metabolites were then used at increasing rates during the experiment as precursors for Ala, 3-hydroxybutyrate (PHB), and Glu biosynthesis, respectively. This conclusion was especially underlined by the ^{13}C-data of 3-hydroxybutyrate. Its ^{13}C-excess increased from 8.3 % during the second time interval up to 16.7 % towards the post-exponential phase in *Lp* WT (Fig. 4A).

Notably, the finding that Ser serves as a carbon source for intracellular *Lp* at increasing rates during the late growth phase was partially in contrast to data from earlier *in vitro* experiments where Ser was the preferred carbon substrate during the early phase of growth (Gillmaier et al., 2016). However, this apparent discrepancy could be explained by the induction of a serine transport protein (Lpp2269) during the transmissive phase of intracellular growth (Brüggemann et al., 2006) resulting in the increased usage of ^{13}C-Ser during the late phase of the intracellular life cycle.

3.5. Differential usage of glucose during the infection cycle of Lp

In the experiment with [U-^{13}C$_6$]glucose, the detected ^{13}C-excess in 3-hydroxybutyrate from the F2 fraction (as the proxy for *Lp*-specific PHB) again indicated that the external ^{13}C-glucose was transported into the

LCV where it was used as a carbon source for bacterial metabolism (Fig. 5A, B, Supplemental Tables 1, 3, 5, 7, 9, 11, 25, 27). To get more insight into the pathways for glucose usage by intracellular *Lp*, we again focussed on the labelling patterns of Ala from F2 (reporter for the bacterial ED pathway), Glu, Asp (reporters for the bacterial TCA cycle) (Fig. 5C–F, Supplemental Tables 2, 4, 6, 8, 10, 12, 26, 28) and, additionally Gly, because its biosynthesis depends on NADPH, which is produced *via* the oxidative branch of the bacterial pentose phosphate pathway (PPP). However, the interpretation of the ^{13}C-patterns in Ala, Asp, Glu and Gly was complicated by the fact that these amino acids were also efficiently formed by the host metabolism from the glucose supply (Schunder et al., 2014) and partly taken up by *Lp* already in ^{13}C-labelled form from their host. As a general prerequisite for proper data interpretation, it was therefore important to compare the ^{13}C-patterns of bacterial amino acids (F2 fraction) with the ^{13}C-patterns of the respective host amino acids (F3 fraction). Moreover, data interpretation was facilitated by control experiments using the Δ*zwf* mutant of *Lp* hampered in glucose metabolism (Eylert et al., 2010).

3.5.1. Glucose usage during the early phase of intracellular growth

During the first time interval (0–17 h) of the experiment with [U-^{13}C$_6$]glucose, when the bacteria established the LCV and began to replicate, the relative fractions of M + 3 and M + 2 isotopologues in Ala and Glu, respectively, were significantly higher in the bacterial fraction F2 as compared to the host fraction F3 (Fig. 5C, D). Notably, the overall ^{13}C-excess values of Ala and Glu from the intracellular bacteria were also highest during this period (Fig. 5A). These findings indicated that, already during the early period, ^{13}C-glucose contributed to the *de novo* biosynthesis of the bacterial amino acids, which was again partly in contrast to the earlier findings for *Lp* grown under *in vitro* conditions, where glucose was barely among the carbon substrates during the early replicative phase of *Lp* (Eylert et al., 2010).

However, the early usage of glucose by intracellular *Lp* was also clearly confirmed by the corresponding *in vivo* labelling experiment with the Δ*zwf* mutant of *Lp*. In sharp contrast to the corresponding ^{13}C-data from intracellular *Lp* WT, the fractions of M + 3 and M + 2 in Ala and Glu, respectively, were significantly lower during this first time interval (0–17 h) for the mutant (Fig. 5E, F). Indeed, this provided firm evidence that external [U-^{13}C$_6$]glucose could not be utilized by the mutant and that mainly (or only) labelled Ala und Glu from the host were incorporated into bacterial protein as already seen in our earlier experiments with ^{13}C-prelabelled amoebae (Schunder et al., 2014).

Importantly, the finding that host glucose was utilized during the early infection period may indicate that the carbohydrate could serve as a signal that – besides other factors – triggers the transition from the lag-phase to the replicative phase, similar to amino acid starvation controlling the shift from the replicative phase to the transmissive phase in *Lp* (Hammer and Swanson, 1999; Sauer et al., 2005). In support of this hypothesis, *Lp* exhibits a homolog of GidA (*lpp2948*), which in *Escherichia coli* encodes for a glucose-sensitive division protein, and which is also involved in the pathogenicity of various pathogens (Sha et al., 2004; Cho and Caparon, 2008; Gupta et al., 2009; Rehl et al., 2013). Further studies are required to unravel the potentially regulatory role of glucose and GidA during intracellular growth of *Lp*.

3.5.2. Glucose usage during the later phases of intracellular growth

During the later periods of the experiment (17–25 h, 25–27 h), the isotopologue profiles of host and bacterial amino acids in *Lp* WT as well as in the Δ*zwf* mutant became more and more similar, indicating that other substrates may have competed as efficient precursors for the reporter amino acids (Fig. 5C–F). However, the experiment with the Δ*zwf* mutant strain of *Lp* suggested that the bacteria replicating inside the vacuole still had access to the externally supplied glucose also during the late phase. This conclusion was especially underlined by comparing the ratios of ^{13}C-excess values (ratios F2:F3) for Ala, Asp and Gly (SI Fig. 3). In the late phase, these ratios were significantly higher for the *Lp* WT in
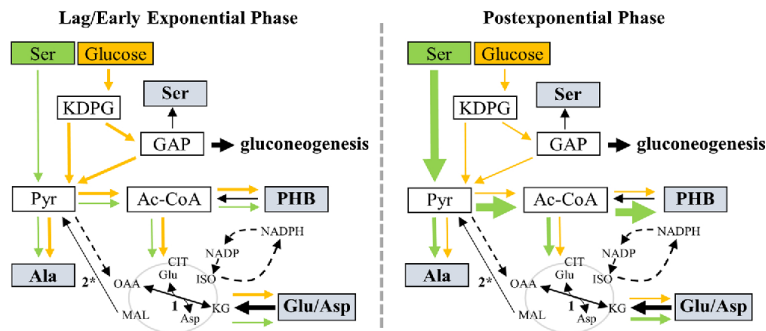
7

Fig. 6. Model of substrate preferences and metabolic pathways for different growth phases of *Lp* growing inside *Ac* (Gillmaier et al., 2016; **modified**). Relative carbon fluxes are indicated by the thickness of the arrows starting from glucose (orange) or serine (green) as substrates. Analysed metabolites are indicated by grey boxes. The citrate cycle is indicated in grey. 1, Glu/Asp transaminase; 2*, malic enzyme (MEZ, *lpp3043* and *lpp0705*, respectively). Ac-CoA, acetyl-CoA; CIT, citrate; GAP, glyceraldehyde-3-phosphate; ISO, isocitrate; KG, α-ketoglutarate; KDPG, 2-keto-3-desoxy-6-phosphogluconate MAL, malate; OAA, oxaloacetate; PHB, polyhydroxybutyrate; Pyr, pyruvate.

comparison to the ratios for the Δ*zwf* mutant. Indeed, higher ratios for *Lp* WT indicated their metabolic usage of ^{13}C-glucose in contrast to the mutant strain, which was unable to utilize glucose *via* the ED pathway. In conclusion, ^{13}C-glucose was metabolized/cycled during the late phase at higher efficiencies in the WT (thus increasing the values for F2 for the WT) than in the Δ*zwf* mutant. In addition, using ^{13}C-glucose as a substrate for *Lp* WT, the M + 1 fraction in Gly (F2) was higher than the M + 2 fraction with an increasing trend over time, which is in contrast to the host (F3), but which is in accordance with in-medium grown *Lp*. This indicated that Gly was synthesized from the ^{13}C-supply by intracellular *Lp* itself leading to the observed differences in the isotopologue profiles between F2 and F3 with only less Gly taken up from the host cell. Notably, the ^{13}C-excess ratio of F2:F3 in Gly increased over time in the WT bacteria, but decreased in the Δ*zwf* mutant strain (SI Fig. 3), again indicating that the synthesis of Gly from glucose is *zwf*-dependent in *Lp*. Together, all these observations are in line with the conclusion that glucose is used throughout the intracellular growth.

3.5.3. Glucose is only a minor carbon source for the energy metabolism of intracellular Lp, but could serve a more prominent role in biosynthesis and as a growth regulator

The ^{13}C-experiments demonstrated for the first time that glucose from the host cell is utilized by intracellular *Lp* for its core metabolism *via* the ED pathway and TCA cycle. Hereby, glucose is metabolized already during the lag and early exponential phase of the bacterial growth cycle (Fig. 6). However, the absolute contributions of glucose as a source to drive the overall energy metabolism of *Lp* seemed to be small, when comparing the differences of ^{13}C-incorporation by *Lp* WT and the Δ*zwf* strain into PHB and amino acids derived from acetyl-CoA, pyruvate, and intermediates of the TCA cycle, respectively. In line with this, glucose also does not enhance bacterial growth or enhance oxygen consumption rates in broth cultivation, further contradicting its role as a main energy source (Weiss et al., 1980; Tesh and Miller, 1981; Tesh et al., 1983; Eylert et al. 2008; Häuslein et al., 2017). Nevertheless, exogenous glucose could serve as a more efficient precursor for anabolic processes such as providing the building units for peptidoglycan biosynthesis under intracellular conditions. Further studies are required to elucidate these upstream metabolic fluxes in a putatively bipartite metabolic network where amino acids serve as main substrates for energy generation and glucose or its phosphate as a source for cell wall and nucleic acid biosynthesis.

The importance of glucose especially for intracellular *Lp* is underlined by the finding that *Lp* strains with defects of the ED pathway were hampered for replication inside amoebae, but were not hindered when growing in broth (Eylert et al., 2010; Harada et al., 2010). The same behaviour holds true for mutants defective in inositol usage when comparing growth in amoebae with growth in broth (Manske et al., 2016).

Besides reduced rates of glucose utilization, the *Lp* Δ*zwf* strain used in this study also showed some differences in terms of Ser metabolization. This could add evidence for a regulatory role of intracellular glucose and related downstream metabolites in *Lp*, as already mentioned above. Interestingly, in *Francisella tularensis*, the "moonlight-protein" fructose-1,6-bisphosphate aldolase was shown to act as a global transcriptional regulator (Ziveri et al., 2017) and several enzymes of the ED pathway were shown to play multiple roles in Archaea (Lamble et al., 2003, 2004; Angelov et al., 2005). Indeed, the role of glucose as a nutrient and a signalling compound for intracellular *Lp* is underlined by the diverse environmental conditions for the bacterium. Before encountering a suitable host, *Lp* reside in fresh water as planktonic bacteria and biofilms without replicating (Steinert et al., 2002; Hilbi et al., 2011). Since fresh water only contains glucose in neglectable amounts in contrast to the cytosol of amoebae, glucose or carbohydrate levels could constitute a key signal for *Lp*, in addition to Cys and Thr (Sauer et al., 2005; Ewann and Hoffman, 2006), to identify the new intracellular environment suitable for replication. This role of glucose for intracellularly replicating *Lp* still needs to be further investigated as well as potential metabolic processes during the lag phase in general, which are only rudimentarily understood (Bertrand, 2019).

Declaration of Competing Interest

None.

Appendix A. Supplementary data

Supplementary material related to this article can be found, in the online version, at doi:https://doi.org/10.1016/j.ijnm.2021.151504.

References

Angelov, A., Futterer, O., Valerius, O., Braus, G.H., Liebl, W., 2005. Properties of the recombinant glucose/galactose dehydrogenase from the extreme thermoacidophile, *Picrophilus torridus*. FEBS J. 272 (4), 1054–1062. https://doi.org/10.1111/j.1742-4658.2004.04539.x.

Aurass, P., Pless, B., Rydzewski, K., Holland, G., Bannert, N., Flieger, A., 2009. bdhA-patD operon as a virulence determinant, revealed by a novel large-scale approach for identification of *Legionella pneumophila* mutants defective for amoeba infection. Appl. Environ. Microbiol. 75 (13), 4506–4515. https://doi.org/10.1128/AEM.00187-09.

8

Belyi, Y., Tabakova, I., Stahl, M., Aktories, K., 2008. Lgt: a family of cytotoxic glucosyltransferases produced by *Legionella pneumophila*. J. Bacteriol. 190 (8), 3026–3035. https://doi.org/10.1128/JB.01798-07.

Bertrand, R.L., 2019. Lag phase is a dynamic, organized, adaptive, and evolvable period that prepares bacteria for cell division. J. Bacteriol. 201 (7) https://doi.org/10.1128/JB.00697-18.

Best, A., Abu Kwaik, Y., 2019. Nutrition and bipartite metabolism of intracellular pathogens. Trends Microbiol. 27 (6), 550–561. https://doi.org/10.1016/j.tim.2018.12.012.

Best, A., Jones, S., Abu Kwaik, Y., 2018a. Mammalian solute carrier (SLC)-like transporters of *Legionella pneumophila*. Sci. Rep. 8 (1), 8352. https://doi.org/10.1038/s41598-018-26782-x.

Best, A., Price, C., Ozanic, M., Santic, M., Jones, S., Abu Kwaik, Y., 2018b. A *Legionella pneumophila* amylase is essential for intracellular replication in human macrophages and amoebae. Sci. Rep. 8 (1), 6340. https://doi.org/10.1038/s41598-018-24724-1.

Brüggemann, H., Cazalet, C., Buchrieser, C., 2006. Adaptation of *Legionella pneumophila* to the host environment: role of protein secretion, effectors and eukaryotic-like proteins. Curr. Opin. Microbiol. 9 (1), 86–94. https://doi.org/10.1016/j.mib.2005.12.009.

Byrne, B., Swanson, M.S., 1998. Expression of *Legionella pneumophila* virulence traits in response to growth conditions. Infect. Immun. 66 (8), 3029–3034.

Cazalet, C., Rusniok, C., Brüggemann, H., Zidane, N., Magnier, A., Ma, L., Tichit, M., Jarraud, S., Bouchier, C., Vandenesch, F., Kunst, F., Etienne, J., Glaser, P., Buchrieser, C., 2004. Evidence in the *Legionella pneumophila* genome for exploitation of host cell functions and high genome plasticity. Nat. Genet. 36 (11), 1165–1173. https://doi.org/10.1038/ng1447.

Cho, K.H., Caparon, M.G., 2008. tRNA modification by GidA/MnmE is necessary for *Streptococcus pyogenes* virulence: a new strategy to make live attenuated strains. Infect. Immun. 76 (7), 3176–3186. https://doi.org/10.1128/IAI.01721-07.

Cunha, C.B., Cunha, B.A., 2017. Legionnaire's disease since philadelphia: lessons learned and continued progress. Infect. Dis. Clin. North Am. 31 (1), 1–5. https://doi.org/10.1016/j.idc.2016.10.001.

Cunha, B.A., Burillo, A., Bouza, E., 2016. Legionnaires' disease. Lancet 387 (10016), 376–385. https://doi.org/10.1016/S0140-6736(15)60078-2.

De Leon, J.A., Qiu, J., Nicolai, C.J., Counihan, J.L., Barry, K.C., Xu, L., Lawrence, R.E., Castellano, B.M., Zoncu, R., Nomura, D.K., Luo, Z.Q., Vance, R.E., 2017. Positive and negative regulation of the master metabolic regulator mTORC1 by two families of *Legionella pneumophila* effectors. Cell Rep. 21 (8), 2031–2038. https://doi.org/10.1016/j.celrep.2017.10.088.

Eisenreich, W., Heuner, K., 2016. The life stage-specific pathometabolism of *Legionella pneumophila*. FEBS Lett. 590 (21), 3868–3886. https://doi.org/10.1002/1873-3468.12326.

Eisenreich, W., Rudel, T., Heesemann, J., Goebel, W., 2017. To eat and to be eaten: mutual metabolic adaptations of immune vells and intracellular bacterial pathogens upon Infection. Front. Cell. Infect. Microbiol. 7, 316. https://doi.org/10.3389/fcimb.2017.00316.

Eisenreich, W., Rudel, T., Heesemann, J., Goebel, W., 2019. How viral and intracellular bacterial pathogens reprogram the metabolism of host cells to allow their intracellular replication. Front. Cell. Infect. Microbiol. 9 https://doi.org/10.3389/fcimb.2019.00042.

Ewann, F., Hoffman, P.S., 2006. Cysteine metabolism in *Legionella pneumophila*: characterization of an *L*-cystine-utilizing mutant. Appl. Environ. Microbiol. 72 (6), 3993–4000. https://doi.org/10.1128/AEM.00684-06.

Eylert, E., Schär, J., Mertins, S., Stoll, R., Bacher, A., Goebel, W., Eisenreich, W., 2008. Carbon metabolism of *Listeria monocytogenes* growing inside macrophages. Mol. Microbiol. 69 (4), 1008–1017. https://doi.org/10.1111/j.1365-2958.2008.06337.x.

Eylert, E., Herrmann, V., Jules, M., Gillmaier, N., Lautner, M., Buchrieser, C., Eisenreich, W., Heuner, K., 2010. Isotopologue profiling of *Legionella pneumophila*: role of serine and glucose as carbon substrates. J. Biol. Chem. 285 (29), 22232–22243. https://doi.org/10.1074/jbc.M110.128678.

Farbrother, P., Wagner, C., Na, J., Tunggal, B., Morio, T., Urushihara, H., Tanaka, Y., Schleicher, M., Steinert, M., Eichinger, L., 2006. *Dictyostelium* transcriptional host cell response upon infection with *Legionella*. Cell. Microbiol. 8 (3), 438–456. https://doi.org/10.1111/j.1462-5822.2005.00633.x.

Faucher, S.P., Mueller, C.A., Shuman, H.A., 2011. *Legionella pneumophila* transcriptome during intracellular multiplication in human macrophages. Front. Microbiol. 2, 60. https://doi.org/10.3389/fmicb.2011.00060.

Faulkner, G., Garduno, R.A., 2002. Ultrastructural analysis of differentiation in *Legionella pneumophila*. J. Bacteriol. 184 (24), 7025–7041. https://doi.org/10.1128/jb.184.24.7025-7041.2002.

Fraser, D.W., Tsai, T.R., Orenstein, W., Parkin, W.E., Beecham, H.J., Sharrar, R.G., Harris, J., Mallison, G.F., Martin, S.M., McDade, J.E., Shepard, C.C., Brachman, P.S., 1977. Legionnaires' disease: description of an epidemic of pneumonia. N. Engl. J. Med. 297 (22), 1189–1197. https://doi.org/10.1056/NEJM197712012972201.

Garduno, R.A., Garduno, E., Hiltz, M., Hoffman, P.S., 2002. Intracellular growth of *Legionella pneumophila* gives rise to a differentiated form dissimilar to stationary-phase forms. Infect. Immun. 70 (11), 6273–6283. https://doi.org/10.1128/iai.70.11.6273-6283.2002.

Gillmaier, N., Götz, A., Schulz, A., Eisenreich, W., Goebel, W., 2012. Metabolic responses of primary and transformed cells to intracellular *Listeria monocytogenes*. PLoS One 7 (12), e52378. https://doi.org/10.1371/journal.pone.0052378.

Gillmaier, N., Schunder, E., Kutzner, E., Tlapak, H., Rydzewski, K., Herrmann, V., Stämmler, M., Lasch, P., Eisenreich, W., Heuner, K., 2016. Growth-related metabolism of the carbon storage poly-3-hydroxybutyrate in *Legionella pneumophila*. J. Biol. Chem. 291 (12), 6471–6482. https://doi.org/10.1074/jbc.M115.693481.

Grubmüller, S., Schauer, K., Goebel, W., Fuchs, T.M., Eisenreich, W., 2014. Analysis of carbon substrates used by *Listeria monocytogenes* during growth in J774A.1 macrophages suggests a bipartite intracellular metabolism. Front. Cell. Infect. Microbiol. 4, 156. https://doi.org/10.3389/fcimb.2014.00156.

Gupta, R., Gobble, T.R., Schuster, M., 2009. GidA posttranscriptionally regulates rhl quorum sensing in *Pseudomonas aeruginosa*. J. Bacteriol. 191 (18), 5785–5792. https://doi.org/10.1128/JB.00335-09.

Hammer, B.K., Swanson, M.S., 1999. Co-ordination of *Legionella pneumophila* virulence with entry into stationary phase by ppGpp. Mol. Microbiol. 33 (4), 721–731. https://doi.org/10.1046/j.1365-2958.1999.01519.x.

Harada, E., Iida, K., Shiota, S., Nakayama, H., Yoshida, S., 2010. Glucose metabolism in *Legionella pneumophila*: dependence on the Entner-Doudoroff pathway and connection with intracellular bacterial growth. J. Bacteriol. 192 (11), 2892–2899. https://doi.org/10.1128/JB.01535-09.

Häuslein, I., Manske, C., Goebel, W., Eisenreich, W., Hilbi, H., 2016. Pathway analysis using ^{13}C-glycerol and other carbon tracers reveals a bipartite metabolism of *Legionella pneumophila*. Mol. Microbiol. 100 (2), 229–246. https://doi.org/10.1111/mmi.13313.

Häuslein, I., Sahr, T., Escoll, P., Klausner, N., Eisenreich, W., Buchrieser, C., 2017. *Legionella pneumophila* CsrA regulates a metabolic switch from amino acid to glycerolipid metabolism. Open Biol. 7 (11) https://doi.org/10.1098/rsob.170149.

Herrmann, V., Eidner, A., Rydzewski, K., Bladel, I., Jules, M., Buchrieser, C., Eisenreich, W., Heuner, K., 2011. GamA is a eukaryotic-like glucoamylase responsible for glycogen- and starch-degrading activity of *Legionella pneumophila*. Int. J. Med. Microbiol. 301 (2), 133–139. https://doi.org/10.1016/j.ijmm.2010.08.016.

Heuner, K., Eisenreich, W., 2016. In: Unden, G., Thines, E., Schüffler, A. (Eds.), Crosstalk between Metabolism and Virulence of *Legionella pneumophila*. Host - Pathogen Interaction; Microbial Metabolism, Pathogenicity and Antiinfectives. Wiley-VCH Verlag GmbH & Co. KGaA, Weinheim, Germany, pp. 19–36.

Heuner, K., Brand, B.C., Hacker, J., 1999. The expression of the flagellum of *Legionella pneumophila* is modulated by different environmental factors. FEMS Microbiol. Lett. 175 (1), 69–77.

Heuner, K., Dietrich, C., Skriwan, C., Steinert, M., Hacker, J., 2002. Influence of the alternative sigma(28) factor on virulence and flagellum expression of *Legionella pneumophila*. Infect. Immun. 70 (3), 1604–1608.

Heuner, K., Kunze, M., Chen, F., Eisenreich, W., 2019. The pathometabolism of *Legionella* studied by isotopologue profiling. Methods Mol. Biol. 1921, 21–44. https://doi.org/10.1007/978-1-4939-9048-1_2.

Hilbi, H., Hoffmann, C., Harrison, C.F., 2011. *Legionella spp.* outdoors: colonization, communication and persistence. Environ. Microbiol. Rep. 3 (3), 286–296. https://doi.org/10.1111/j.1758-2229.2011.00247.x.

James, B.W., Mauchline, W.S., Dennis, P.J., Keevil, C.W., Wait, R., 1999. Poly-3-hydroxybutyrate in *Legionella pneumophila*, an energy source for survival in low-nutrient environments. Appl. Environ. Microbiol. 65 (2), 822–827.

Krawczyk, C.M., Holowka, T., Sun, J., Blagih, J., Amiel, E., DeBerardinis, R.J., Cross, J. R., Jung, E., Thompson, C.B., Jones, R.G., Pearce, E.J., 2010. Toll-like receptor-induced changes in glycolytic metabolism regulate dendritic cell activation. Blood 115 (23), 4742–4749. https://doi.org/10.1182/blood-2009-10-249540.

Laemmli, U.K., 1970. Cleavage of structural proteins during the assembly of the head of bacteriophage T4. Nature 227 (5259), 680–685.

Lamble, H.J., Heyer, N.I., Bull, S.D., Hough, D.W., Danson, M.J., 2003. Metabolic pathway promiscuity in the archaeon *Sulfolobus solfataricus* revealed by studies on glucose dehydrogenase and 2-keto-3-deoxygluconate aldolase. J. Biol. Chem. 278 (36), 34066–34072. https://doi.org/10.1074/jbc.M305818200.

Lamble, H.J., Milburn, C.C., Taylor, G.L., Hough, D.W., Danson, M.J., 2004. Gluconate dehydratase from the promiscuous Entner-Doudoroff pathway in *Sulfolobus solfataricus*. FEBS Lett. 576 (1–2), 133–136. https://doi.org/10.1016/j.febslet.2004.08.074.

Lau, R., Maqsood, S., Harte, D., Caughley, B., Deacon, R., 2013. Prevalence of *Legionella* strains in cooling towers and legionellosis cases in New Zealand. J. Environ. Health 75 (6), 82–89.

Lee, W.N., Byerley, L.O., Bergner, E.A., Edmond, J., 1991. Mass isotopomer analysis: theoretical and practical considerations. Biol. Mass Spectrom. 20 (8), 451–458. https://doi.org/10.1002/bms.1200200804.

Levanova, N., Mattheis, C., Carson, D., To, K.N., Jank, T., Frankel, G., Aktories, K., Schroeder, G.N., 2019. The *Legionella* effector LtpM is a new type of phosphoinositide-activated glucosyltransferase. J. Biol. Chem. 294 (8), 2862–2879. https://doi.org/10.1074/jbc.RA118.005952.

Lomma, M., Dervins-Ravault, D., Rolando, M., Nora, T., Newton, H.J., Sansom, F.M., Sahr, T., Gomez-Valero, L., Jules, M., Hartland, E.L., Buchrieser, C., 2010. The *Legionella pneumophila* F-box protein Lpp2082 (AnkB) modulates ubiquitination of the host protein parvin B and promotes intracellular replication. Cell. Microbiol. 12 (9), 1272–1291. https://doi.org/10.1111/j.1462-5822.2010.01467.x.

Manske, C., Schell, U., Hilbi, H., 2016. Metabolism of myo-inositol by *Legionella pneumophila* promotes infection of amoeba and macrophages. Appl. Environ. Microbiol. 82 (15), 5000–5014. https://doi.org/10.1128/AEM.01018-16.

Mehlitz, A., Eylert, E., Huber, C., Lindner, B., Vollmuth, N., Karunakaran, K., Goebel, W., Eisenreich, W., Rudel, T., 2017. Metabolic adaptation of *Chlamydia trachomatis* to mammalian host cells. Mol. Microbiol. 103 (6), 1004–1019. https://doi.org/10.1111/mmi.13603.

Mondino, S., Schmidt, S., Rolando, M., Escoll, P., Gomez-Valero, L., Buchrieser, C., 2020. Legionnaires' disease: state of the art knowledge of pathogenesis mechanisms of *Legionella*. Annu. Rev. Pathol. 15, 439–466. https://doi.org/10.1146/annurev-pathmechdis-012419-032742.

9

Oliva, G., Sahr, T., Buchrieser, C., 2018. The life cycle of *L. pneumophila*: cellular differentiation is linked to virulence and metabolism. Front. Cell. Infect. Microbiol. 8 (3) https://doi.org/10.3389/fcimb.2018.00003.

Price, C.T., Al-Khodor, S., Al-Quadan, T., Santic, M., Habyarimana, F., Kalia, A., Kwaik, Y.A., 2009. Molecular mimicry by an F-box effector of *Legionella pneumophila* hijacks a conserved polyubiquitination machinery within macrophages and protozoa. PLoS Pathog. 5 (12), e1000704 https://doi.org/10.1371/journal.ppat.1000704.

Price, C.T., Al-Quadan, T., Santic, M., Rosenshine, I., Abu Kwaik, Y., 2011. Host proteasomal degradation generates amino acids essential for intracellular bacterial growth. Science 334 (6062), 1553–1557. https://doi.org/10.1126/science.1212868.

Price, C.T., Richards, A.M., Abu Kwaik, Y., 2014. Nutrient generation and retrieval from the host cell cytosol by intra-vacuolar *Legionella pneumophila*. Front. Cell. Infect. Microbiol. 4, 111. https://doi.org/10.3389/fcimb.2014.00111.

Price, C., Jones, S., Mihelcic, M., Santic, M., Abu Kwaik, Y., 2020. Paradoxical pro-inflammatory responses by human macrophages to an *Amoebae* host-adapted *Legionella* effector. Cell Host Microbe 27 (4), 571–584. https://doi.org/10.1016/j.chom.2020.03.003 e577.

Rehl, J.M., Shippy, D.C., Eakley, N.M., Brevik, M.D., Sand, J.M., Cook, M.E., Fadl, A.A., 2013. GidA expression in *Salmonella* is modulated under certain environmental conditions. Curr. Microbiol. 67 (3), 279–285. https://doi.org/10.1007/s00284-013-0361-2.

Richardson, A.R., 2019. Virulence and metabolism. Microbiol. Spectr. 7 (2) https://doi.org/10.1128/microbiolspec.GPP3-0011-2018.

Robertson, P., Abdelhady, H., Garduno, R.A., 2014. The many forms of a pleomorphic bacterial pathogen-the developmental network of *Legionella pneumophila*. Front. Microbiol. 5, 670. https://doi.org/10.3389/fmicb.2014.00670.

Rowbotham, T.J., 1980. Preliminary report on the pathogenicity of *Legionella pneumophila* for freshwater and soil amoebae. J. Clin. Pathol. 33 (12), 1179–1183.

Rowbotham, T.J., 1986. Current views on the relationships between amoebae, *legionellae* and man. Isr. J. Med. Sci. 22 (9), 678–689.

Russell, D.G., Huang, L., VanderVen, B.C., 2019. Immunometabolism at the interface between macrophages and pathogens. Nat. Rev. Immunol. 19 (5), 291–304. https://doi.org/10.1038/s41577-019-0124-9.

Sauer, J.D., Bachman, M.A., Swanson, M.S., 2005. The phagosomal transporter A couples threonine acquisition to differentiation and replication of *Legionella pneumophila* in macrophages. Proc. Natl. Acad. Sci. U. S. A. 102 (28), 9924–9929. https://doi.org/10.1073/pnas.0502767102.

Schunder, E., Gillmaier, N., Kutzner, E., Herrmann, V., Lautner, M., Heuner, K., Eisenreich, W., 2014. Amino acid uptake and metabolism of *Legionella pneumophila*

hosted by *Acanthamoeba castellanii*. J. Biol. Chem. 289 (30), 21040–21054. https://doi.org/10.1074/jbc.M114.570085.

Sha, J., Kozlova, E.V., Fadl, A.A., Olano, J.P., Houston, C.W., Peterson, J.W., Chopra, A. K., 2004. Molecular characterization of a glucose-inhibited division gene, gidA, that regulates cytotoxic enterotoxin of *Aeromonas hydrophila*. Infect. Immun. 72 (2), 1084–1095. https://doi.org/10.1128/iai.72.2.1084-1095.2004.

Steiner, B., Weber, S., Hilbi, H., 2018. Formation of the *Legionella*-containing vacuole: phosphoinositide conversion, GTPase modulation and ER dynamics. Int. J. Med. Microbiol. 308 (1), 49–57. https://doi.org/10.1016/j.ijmm.2017.08.004.

Steinert, M., Hentschel, U., Hacker, J., 2002. *Legionella pneumophila*: an aquatic microbe goes astray. FEMS Microbiol. Rev. 26 (2), 149–162. https://doi.org/10.1111/j.1574-6976.2002.tb00607.x.

Swart, A.L., Harrison, C.F., Eichinger, L., Steinert, M., Hilbi, H., 2018. *Acanthamoeba* and *Dictyostelium* as cellular models for *Legionella* infection. Front. Cell. Infect. Microbiol. 8, 61. https://doi.org/10.3389/fcimb.2018.00061.

Taylor, M., Ross, K., Bentham, R., 2009. *Legionella*, protozoa, and biofilms: interactions within complex microbial systems. Microb. Ecol. 58 (3), 538–547. https://doi.org/10.1007/s00248-009-9514-z.

Tesh, M.J., Miller, R.D., 1981. Amino acid requirements for *Legionella pneumophila* growth. J. Clin. Microbiol. 13 (5), 865–869. https://doi.org/10.1128/JCM.13.5.865-869.1981.

Tesh, M.J., Morse, S.A., Miller, R.D., 1983. Intermediary metabolism in *Legionella pneumophila*: utilization of amino acids and other compounds as energy sources. J. Bacteriol. 154 (3), 1104–1109.

Towbin, H., Staehelin, T., Gordon, J., 1979. Electrophoretic transfer of proteins from polyacrylamide gels to nitrocellulose sheets: procedure and some applications. Proc. Natl. Acad. Sci. U. S. A. 76 (9), 4350–4354.

Weiss, E., Peacock, M.G., Williams, J.C., 1980. Glucose and glutamate metabolism of *Legionella pneumophila*. Curr. Microbiol. 4 (1), 1–6. https://doi.org/10.1007/bf02602882.

Wieland, H., Ullrich, S., Lang, F., Neumeister, B., 2005. Intracellular multiplication of *Legionella pneumophila* depends on host cell amino acid transporter SLC1A5. Mol. Microbiol. 55 (5), 1528–1537. https://doi.org/10.1111/j.1365-2958.2005.04490.x.

Ziveri, J., Tros, F., Guerrera, I.C., Chhuon, C., Audry, M., Dupuis, M., Barel, M., Korniotis, S., Fillatreau, S., Gales, L., Cahoreau, E., Charbit, A., 2017. The metabolic enzyme fructose-1,6-bisphosphate aldolase acts as a transcriptional regulator in pathogenic *Francisella*. Nat. Commun. 8 (1), 853. https://doi.org/10.1038/s41467-017-00889-7.

3 Outlook

This work was based on the assumption that the environment shapes the metabolism of bacteria in the respective niche. This connection became apparent in the study with *H. maritima*. Herein, the ability to fixate CO_2 through the roTCA cycle only became relevant for the overall metabolism, when cultivation was performed under conditions similar to the natural environment of this bacterium (315). As discussed in section 1.6, *H. maritima* has been found at several sights associated with hydrothermal activity hence with potentially high concentrations of CO_2. Further studies will demonstrate how wide-spread this cycle is in organisms living under similar conditions.

Regarding the origin of life, the roTCA cycle at the moment seems to be the most plausible carbon fixation pathway in the earliest cellular organism. It is energetically highly efficient (43), its intermediates act as precursors for a variety of biomolecules (316) and its activity is correlated with increased CO_2-concentrations (315). Thereby, it confers selective advantages to the WL-pathway as well as the rTCA cycle that where so far considered the premier candidates for primordial carbon fixation pathways (317). While the WL-pathway is also highly energy-efficient, it only provides acetyl-CoA for further metabolisation. The rTCA cycle produces the same metabolic precursors as the roTCA cycle, but requires more energy to operate. However, the identification of carbon fixation pathways is probably far from complete. Additionally, the location for the origin of life is under constant debate. Subsequently, a different environment would necessitate another metabolic phenotype for the first cellular organism.

In terms of heterotrophic organisms, the correlation between environment and metabolism became equally apparent in this work. Labelling experiments with *L. pneumophila* growing inside *A. castellanii* showed significant differences to growth in broth regarding the growth-phase dependent metabolization of glucose and serine (318). These differences between *in vitro* and *in vivo* metabolism are frequently observed for pathogenic bacteria and illustrate the need to choose cultivation conditions as close as possible to the actual infection for metabolic analysis.

Looking at *H. pylori*, the labelling data presented in this study allowed new insights into a rather idiosyncratic metabolic network that shows a variety of adaptions due to the prolonged co-evolution with humans (319). However, this data still refers to *in vitro* cultivation. In contrast to *L. pneumophila*, which shows similar behaviour in human and amoebal hosts, performing experiments under conditions reproducing actual infections of *H. pylori* poses several problems. This pathogen interacts with a variety of different host cells. While epithelial cells are the most important interaction partners, manipulation of macrophages and dendritic cells is potentially a major factor in persistent *H. pylori* infections. Hence co-cultivation with only a single type of host cells neglects potentially important features.

Further, human host cells used for co-cultivation typically represent immortalized cancer cells of the respective cell type. These cells already have an altered metabolism in comparison to primary host cells, hence they do not yield a true picture of metabolic remodelling due to bacterial infections. A study by Gillmaier *et al.* demonstrated different metabolic reactions of bone marrow macrophages and primary human macrophages to *L. monocytogenes* infection (244). Similar results were obtained when using physiologically activated CD8$^+$ T cells (320).

Experiments in animal models to study *H. pylori* infection provide an alternative, although also not without short-comings. In addition to general differences in embryonic development between

human and animal cells (321), infections in mice generally only lead to mild diseases, while Mongolian gerbils develop gastric cancer within weeks after the initial infection. Therefore, both settings only partially resemble actual human infections (322, 323).

In recent years, new cultivation techniques for prolonged cultivation of primary human cells have been developed leading to production of organoids. Organoids generally refer to "3D cultures composed of multiple organ-specific cell types that can recapitulate the architecture and gene expression profiles as well as some key features and functions of their corresponding organs" (324). This can be done with isolates from healthy as well as cancerous tissue thereby allowing analysis of host cells that do not already display a diverted metabolic phenotype.

In terms of *H. pylori*, studies in gastric organoids already yielded quite advanced settings that produce epithelial tissue with spatial orientation and the introduction of dendritic cells as well as cytotoxic T lymphocytes into the system is possible (321, 325-327). Experiments allowed also to replicate known alterations of the host cell due to *H. pylori* infection like the "hummingbird"-phenotype as well as increased proliferation of epithelial cells after CagA-translocation (321, 326). Further studies demonstrated the interference of *H. pylori* with tight junctions within the epithelium in a cagA-dependent manner (328).

Combining a setup described recently by Chakrabarti *et al.* with isotopologue profiling offers a variety of experimental set-ups to be investigated (327). Either epithelial cells or immune cells could be prelabelled to investigate their respective role as nutrient sources for the pathogen. Comparative experiments with wild-type and ΔVacA- or ΔcagA-mutant strains could help to elucidate the role of these virulence factors in the acquisition of nutrients by *H. pylori*, which was already indicated in section 1.7. Building on the findings in section 2.2 (319), the putative interference of immune cell activation by *H. pylori* through succinate and glutamine consumption could be investigated under these conditions. Further, this approach could be expanded to other pathogens as for example studies with *S. flexneri* or *S. typhimurium* have also already been performed in organoid cultures (322). These settings should reveal actual metabolic capacities and necessities of bacterial pathogens during infection. Based on this, metabolic bottlenecks could be further investigated for antibiotic development. Additionally, therapeutic approaches could be tested where the drug acts on the host cell instead of the pathogen. Herein production of a metabolite or a signalling pathway that is crucial for the pathogens replication could be inhibited. These host-modulating antibiotics would potentially avoid many resistance mechanisms that are commonly observed in bacteria like modification of the antibiotic target, enzymatic degradation of the compound or efflux mechanisms.

4 Reprint permissions

CCC RightsLink®

| Home | Help | Live Chat | Sign in | Create Account |

SPRINGER NATURE

High CO2 levels drive the TCA cycle backwards towards autotrophy

Author: Lydia Steffens et al
Publication: Nature
Publisher: Springer Nature
Date: Apr 21, 2021

Copyright © 2021, The Author(s), under exclusive licence to Springer Nature Limited

Author Request

If you are the author of this content (or his/her designated agent) please read the following. If you are not the author of this content, please click the Back button and select no to the question "Are you the Author of this Springer Nature content?".
Ownership of copyright in original research articles remains with the Author, and provided that, when reproducing the contribution or extracts from it or from the Supplementary Information, the Author acknowledges first and reference publication in the Journal, the Author retains the following non-exclusive rights:
To reproduce the contribution in whole or in part in any printed volume (book or thesis) of which they are the author(s).
The author and any academic institution, where they work, at the time may reproduce the contribution for the purpose of course teaching.
To reuse figures or tables created by the Author and contained in the Contribution in oral presentations and other works created by them.
To post a copy of the contribution as accepted for publication after peer review (in locked Word processing file, of a PDF version thereof) on the Author's own web site, or the Author's institutional repository, or the Author's funding body's archive, six months after publication of the printed or online edition of the Journal, provided that they also link to the contribution on the publisher's website.
Authors wishing to use the published version of their article for promotional use or on a web site must request in the normal way.

If you require further assistance please read Springer Nature's online author reuse guidelines.

For full paper portion: Authors of original research papers published by Springer Nature are encouraged to submit the author's version of the accepted, peer-reviewed manuscript to their relevant funding body's archive, for release six months after publication. In addition, authors are encouraged to archive their version of the manuscript in their institution's repositories (as well as their personal Web sites), also six months after original publication.

v1.0

BACK   CLOSE WINDOW

4 Reprint permissions

CCC

RightsLink®

Substrate usage determines carbon flux via the citrate cycle in Helicobacter pylori

Author: Thomas M. Steiner, Clara Lettl, Franziska Schindele, et al

Publication: Molecular Microbiology

Publisher: John Wiley and Sons

Date: Jul 8, 2021

© 2021 The Authors. Molecular Microbiology published by John Wiley & Sons Ltd.

Copyright Clearance Center

RightsLink®

Home   Help   Live Chat   Sign in   Create Account

Metabolic adaption of Legionella pneumophila during intracellular growth in Acanthamoeba castellanii

Author:
Mareike Kunze,Thomas Steiner,Fan Chen,Claudia Huber,Kerstin Rydzewski,Maren Stämmler,Klaus Heuner,Wolfgang Eisenreich

Publication: International Journal of Medical Microbiology

Publisher: Elsevier

Date: May 2021

© 2021 The Author(s). Published by Elsevier GmbH.

Journal Author Rights

BACK   CLOSE WINDOW

5 References

1. Lauga E, Goldstein RE. Dance of the microswimmers. Phys Today. 2012;65(9):30-5.

2. Lane N. The unseen world: reflections on Leeuwenhoek (1677) 'Concerning little animals'. Philos Trans R Soc Lond B Biol Sci. 2015;370(1666).

3. Woese CR, Kandler O, Wheelis ML. Towards a natural system of organisms: proposal for the domains Archaea, Bacteria, and Eucarya. Proc Natl Acad Sci U S A. 1990;87(12):4576-9.

4. Weiss MC, Sousa FL, Mrnjavac N, Neukirchen S, Roettger M, Nelson-Sathi S, *et al.* The physiology and habitat of the last universal common ancestor. Nat Microbiol. 2016;1(9):16116.

5. Weiss MC, Preiner M, Xavier JC, Zimorski V, Martin WF. The last universal common ancestor between ancient earth chemistry and the onset of genetics. PLoS Genet. 2018;14(8):e1007518.

6. Bar-On YM, Phillips R, Milo R. The biomass distribution on earth. Proc Natl Acad Sci U S A. 2018;115(25):6506-11.

7. Sender R, Fuchs S, Milo R. Revised estimates for the number of human and bacteria cells in the body. PLoS Biol. 2016;14(8):e1002533.

8. Merino N, Aronson HS, Bojanova DP, Feyhl-Buska J, Wong ML, Zhang S, *et al.* Living at the extremes: Extremophiles and the limits of life in a planetary context. Front Microbiol. 2019;10:780.

9. Kopp RE, Kirschvink JL, Hilburn IA, Nash CZ. The paleoproterozoic snowball earth: A climate disaster triggered by the evolution of oxygenic photosynthesis. Proc Natl Acad Sci U S A. 2005;102(32):11131-6.

10. Hug LA, Baker BJ, Anantharaman K, Brown CT, Probst AJ, Castelle CJ, *et al.* A new view of the tree of life. Nat Microbiol. 2016;1:16048.

11. Locey KJ, Lennon JT. Scaling laws predict global microbial diversity. Proc Natl Acad Sci U S A. 2016;113(21):5970-5.

12. Lennon JT, Locey KJ. More support for earth's massive microbiome. Biol Direct. 2020;15(1):5.

13. Louca S, Mazel F, Doebeli M, Parfrey LW. A census-based estimate of earth's bacterial and archaeal diversity. PLoS Biol. 2019;17(2):e3000106.

14. Dobzhansky T. Nothing in biology makes sense except in the light of evolution. Am Biol Teach. 1973;35(3):125-9.

15. Berg JM, Tymoczko JL, Gatto GJ, Stryer L. Biochemistry. 9th ed. New York: Freeman/McMillan Learning; 2019.

16. Zamboni N, Saghatelian A, Patti GJ. Defining the metabolome: size, flux, and regulation. Mol Cell. 2015;58(4):699-706.

17. Zhang Z, Cheng X, Zhao Y, Yang Y. Lighting up live-cell and *in vivo* central carbon metabolism with genetically encoded fluorescent sensors. Annu Rev Anal Chem 2020;13(1):293-314.

18. Noor E, Eden E, Milo R, Alon U. Central carbon metabolism as a minimal biochemical walk between precursors for biomass and energy. Mol Cell. 2010;39(5):809-20.

19. Barnett JA. A history of research on yeasts 5: The fermentation pathway. Yeast. 2003;20(6):509-43.

20. Bar-Even A, Flamholz A, Noor E, Milo R. Rethinking glycolysis: On the biochemical logic of metabolic pathways. Nat Chem Biol. 2012;8(6):509-17.

21. Gunsalus IC, Horecker BL, Wood WA. Pathways of carbohydrate metabolism in microorganisms. Bacteriol Rev. 1955;19(2):79-128.

22. Stincone A, Prigione A, Cramer T, Wamelink MM, Campbell K, Cheung E*, et al.* The return of metabolism: Biochemistry and physiology of the pentose phosphate pathway. Biol Rev Camb Philos Soc. 2015;90(3):927-63.

23. Entner N, Doudoroff M. Glucose and gluconic acid oxidation of *Pseudomonas Saccharophila*. J Biol Chem. 1952;196(2):853-62.

24. Conway T. The Entner-Doudoroff pathway: History, physiology and molecular biology. FEMS Microbiol Lett. 1992;103(1):1-27.

25. Stettner AI, Segre D. The cost of efficiency in energy metabolism. Proc Natl Acad Sci U S A. 2013;110(24):9629-30.

26. Kresge N, Simoni RD, Hill RL. The discovery of the glyceroneogenic pathway: The work of Richard Hanson. J Biol Chem. 2007;282(8):e6-e8.

27. Krivoruchko A, Zhang Y, Siewers V, Chen Y, Nielsen J. Microbial acetyl-CoA metabolism and metabolic engineering. Metab Eng. 2015;28:28-42.

28. Pietrocola F, Galluzzi L, Bravo-San Pedro JM, Madeo F, Kroemer G. Acetyl coenzyme A: A central metabolite and second messenger. Cell Metab. 2015;21(6):805-21.

29. Krebs HA, Johnson WA. The role of citric acid in intermediate metabolism in animal tissues. FEBS Lett. 1980;117 Suppl:K1-10.

30. Krebs HA. The history of the tricarboxylic acid cycle. Perspect Biol Med. 1970;14(1):154-70.

31. Kwong WK, Zheng H, Moran NA. Convergent evolution of a modified, acetate-driven TCA cycle in bacteria. Nat Microbiol. 2017;2:17067.

32. Kornberg HL, Krebs HA. Synthesis of cell constituents from C2-units by a modified tricarboxylic acid cycle. Nature. 1957;179(4568):988-91.

33. Dolan SK, Welch M. The glyoxylate shunt, 60 years on. Annu Rev Microbiol. 2018;72:309-30.

34. Fuchs G, Berg IA. Unfamiliar metabolic links in the central carbon metabolism. J Biotechnol. 2014;192 Pt B:314-22.

35. Schada von Borzyskowski L, Bernhardsgrütter I, Erb TJ. Biochemical unity revisited: Microbial central carbon metabolism holds new discoveries, multi-tasking pathways, and redundancies with a reason. Biol Chem. 2020;401(12):1429-41.

36. Rappe MS, Giovannoni SJ. The uncultured microbial majority. Annu Rev Microbiol. 2003;57:369-94.

5 References

37.   Bassham JA, Benson AA, Kay LD, Harris AZ, Wilson AT, Calvin M. The path of carbon in photosynthesis. XXI. The cyclic regeneration of carbon dioxide acceptor1. J Am Chem Soc. 1954;76(7):1760-70.

38.   Ljungdahl L, Irion E, Wood HG. Total synthesis of acetate from CO_2. I. Co-methylcobyric acid and CO-(methyl)-5-methoxybenzimidazolylcobamide as intermediates with *Clostridium thermoaceticum*. Biochemistry. 1965;4(12):2771-80.

39.   Evans MC, Buchanan BB, Arnon DI. A new ferredoxin-dependent carbon reduction cycle in a photosynthetic bacterium. Proc Natl Acad Sci U S A. 1966;55(4):928-34.

40.   Strauss G, Fuchs G. Enzymes of a novel autotrophic CO_2 fixation pathway in the phototrophic bacterium *Chloroflexus aurantiacus*, the 3-hydroxypropionate cycle. Eur J Biochem. 1993;215(3):633-43.

41.   Berg IA, Kockelkorn D, Buckel W, Fuchs G. A 3-hydroxypropionate/4-hydroxybutyrate autotrophic carbon dioxide assimilation pathway in Archaea. Science. 2007;318(5857):1782-6.

42.   Huber H, Gallenberger M, Jahn U, Eylert E, Berg IA, Kockelkorn D*, et al.* A dicarboxylate/4-hydroxybutyrate autotrophic carbon assimilation cycle in the hyperthermophilic Archaeum *Ignicoccus hospitalis*. Proc Natl Acad Sci U S A. 2008;105(22):7851-6.

43.   Mall A, Sobotta J, Huber C, Tschirner C, Kowarschik S, Bacnik K*, et al.* Reversibility of citrate synthase allows autotrophic growth of a thermophilic bacterium. Science. 2018;359(6375):563-7.

44.   Sanchez-Andrea I, Guedes IA, Hornung B, Boeren S, Lawson CE, Sousa DZ*, et al.* The reductive glycine pathway allows autotrophic growth of *Desulfovibrio desulfuricans*. Nat Commun. 2020;11(1):5090.

45.   Mall A, Sobotta J, Huber C, Tschirner C, Kowarschik S, Bacnik K*, et al.* Reversibility of citrate synthase allows autotrophic growth of a thermophilic bacterium. Science. 2018;359(6375):563-7.

46.   Erb TJ, Berg IA, Brecht V, Muller M, Fuchs G, Alber BE. Synthesis of C5-dicarboxylic acids from C2-units involving crotonyl-CoA carboxylase/reductase: the ethylmalonyl-CoA pathway. Proc Natl Acad Sci U S A. 2007;104(25):10631-6.

47.   Khomyakova M, Bukmez O, Thomas LK, Erb TJ, Berg IA. A methylaspartate cycle in haloarchaea. Science. 2011;331(6015):334-7.

48.   Schada von Borzyskowski L, Severi F, Kruger K, Hermann L, Gilardet A, Sippel F*, et al.* Marine proteobacteria metabolize glycolate via the beta-hydroxyaspartate cycle. Nature. 2019;575(7783):500-4.

49.   Tian J, Bryk R, Itoh M, Suematsu M, Nathan C. Variant tricarboxylic acid cycle in *Mycobacterium tuberculosis*: Identification of alpha-ketoglutarate decarboxylase. Proc Natl Acad Sci U S A. 2005;102(30):10670-5.

50.   Zhang S, Bryant DA. The tricarboxylic acid cycle in cyanobacteria. Science. 2011;334(6062):1551-3.

51.   Nikel PI, Chavarria M, Fuhrer T, Sauer U, de Lorenzo V. *Pseudomonas putida* KT2440 strain metabolizes glucose through a cycle formed by enzymes of the Entner-Doudoroff, Embden-Meyerhof-Parnas, and pentose phosphate pathways. J Biol Chem. 2015;290(43):25920-32.

52.   Gerosa L, Sauer U. Regulation and control of metabolic fluxes in microbes. Curr Opin Biotechnol. 2011;22(4):566-75.

53. Eisenreich W, Dandekar T, Heesemann J, Goebel W. Carbon metabolism of intracellular bacterial pathogens and possible links to virulence. Nat Rev Microbiol. 2010;8(6):401-12.

54. Eisenreich W, Heesemann J, Rudel T, Goebel W. Metabolic host responses to infection by i ntracellular bacterial pathogens. Front Cell Infect Microbiol. 2013;3:24.

55. Eisenreich W, Heesemann J, Rudel T, Goebel W. Metabolic adaptations of intracellullar bacterial pathogens and their mammalian host cells during Infection ("Pathometabolism"). Microbiol Spectr. 2015;3(3).

56. Eisenreich W, Rudel T, Heesemann J, Goebel W. To eat and to be eaten: mutual metabolic adaptations of immune vells and intracellular bacterial pathogens upon Infection. Front Cell Infect Microbiol. 2017;7:316.

57. Russell DG, Huang L, VanderVen BC. Immunometabolism at the interface between macrophages and pathogens. Nat Rev Immunol. 2019;19(5):291-304.

58. Martin W, Baross J, Kelley D, Russell MJ. Hydrothermal vents and the origin of life. Nat Rev Microbiol. 2008;6(11):805-14.

59. Fuchs G. Alternative pathways of carbon dioxide fixation: insights into the early evolution of life? Annu Rev Microbiol. 2011;65:631-58.

60. Nunoura T, Chikaraishi Y, Izaki R, Suwa T, Sato T, Harada T, *et al.* A primordial and reversible TCA cycle in a facultatively chemolithoautotrophic thermophile. Science. 2018;359(6375):559-63.

61. Kamen MD. Use of isotopes in biochemical research; fundamental aspects. Annu Rev Biochem. 1947;16:631-54.

62. Whelan T, Sackett WM, Benedict CR. Carbon isotope discrimination in a plant possessing the C_4 dicarboxylic acid pathway. Biochem Biophys Res Commun. 1970;41(5):1205-10.

63. Garcia AK, Cavanaugh CM, Kacar B. The curious consistency of carbon biosignatures over billions of years of Earth-life coevolution. ISME J. 2021;15(8):2183-94.

64. Mojzsis SJ, Arrhenius G, McKeegan KD, Harrison TM, Nutman AP, Friend CR. Evidence for life on Earth before 3,800 million years ago. Nature. 1996;384(6604):55-9.

65. Nutman AP, Bennett VC, Friend CR, Van Kranendonk MJ, Chivas AR. Rapid emergence of life shown by discovery of 3,700-million-year-old microbial structures. Nature. 2016;537(7621):535-8.

66. Dodd MS, Papineau D, Grenne T, Slack JF, Rittner M, Pirajno F, *et al.* Evidence for early life in Earth's oldest hydrothermal vent precipitates. Nature. 2017;543(7643):60-4.

67. Cavalazzi B, Lemelle L, Simionovici A, Cady SL, Russell MJ, Bailo E, *et al.* Cellular remains in a ~3.42-billion-year-old subseafloor hydrothermal environment. Sci Adv. 2021;7(29).

68. Huber C, Wächtershäuser G. Activated acetic acid by carbon fixation on (Fe,Ni)S under primordial conditions. Science. 1997;276(5310):245-7.

69. Huber C, Wächtershäuser G. Peptides by activation of amino acids with CO on (Ni,Fe)S surfaces: Implications for the origin of life. Science. 1998;281(5377):670-2.

70. Huber C, Wächtershäuser G. alpha-Hydroxy and alpha-amino acids under possible Hadean, volcanic origin-of-life conditions. Science. 2006;314(5799):630-2.

5 References

71. Scheidler C, Sobotta J, Eisenreich W, Wächtershäuser G, Huber C. Unsaturated C3,5,7,9-monocarboxylic acids by aqueous, one-pot carbon fixation: Possible relevance for the origin of life. Sci Rep. 2016;6:27595.

72. Sadykhov EG, Serov AE, Voinova NS, Uglanova SV, Petrov AS, Alekseeva AA, *et al.* A comparative study of the thermal stability of formate dehydrogenases from microorganisms and plants. Appl Biochem Biotechnol. 2006;42(3):236-40.

73. Bonch-Osmolovskaya EA, Sokolova TG, Kostrikina NA, Zavarzin GA. *Desulfurella acetivorans* gen. nov. and sp. nov. ?a new thermophilic sulfur-reducing eubacterium. Arch Microbiol. 1990;153(2):151-5.

74. Nunoura T, Oida H, Miyazaki M, Suzuki Y. *Thermosulfidibacter takaii* gen. nov., sp. nov., a thermophilic, hydrogen-oxidizing, sulfur-reducing chemolithoautotroph isolated from a deep-sea hydrothermal field in the Southern Okinawa Trough. Int J Syst Evol Microbiol. 2008;58(Pt 3):659-65.

75. Rohmer L, Hocquet D, Miller SI. Are pathogenic bacteria just looking for food? Metabolism and microbial pathogenesis. Trends Microbiol. 2011;19(7):341-8.

76. Collaborators GDaIIaP. Global, regional, and national incidence, prevalence, and years lived with disability for 354 diseases and injuries for 195 countries and territories, 1990–2017: A systematic analysis for the Global Burden of Disease Study 2017. Lancet. 2018;392:1789-858.

77. O'Neil J. Tackling drug-resistant infections globally: Final report and recommendations. London, United Kingdom; 2016.

78. Lakemeyer M, Zhao W, Mandl FA, Hammann P, Sieber SA. Thinking outside the box - novel antibacterials to tackle the resistance crisis. Angew Chem Int Ed Engl. 2018.

79. Martinez JL. Ecology and evolution of chromosomal gene transfer between environmental microorganisms and pathogens. Microbiol Spectr. 2018;6(1).

80. Nandakumar M, Nathan C, Rhee KY. Isocitrate lyase mediates broad antibiotic tolerance in *Mycobacterium tuberculosis*. Nat Commun. 2014;5:4306.

81. Peng B, Su YB, Li H, Han Y, Guo C, Tian YM, *et al.* Exogenous alanine and/or glucose plus kanamycin kills antibiotic-resistant bacteria. Cell Metab. 2015;21(2):249-62.

82. Vestergaard M, Nohr-Meldgaard K, Bojer MS, Krogsgard Nielsen C, Meyer RL, Slavetinsky C, *et al.* Inhibition of the ATP synthase eliminates the intrinsic resistance of *Staphylococcus aureus* towards polymyxins. mBio. 2017;8(5):e01114-17.

83. Liu Y, Li R, Xiao X, Wang Z. Bacterial metabolism-inspired molecules to modulate antibiotic efficacy. J Antimicrob Chemother. 2019;74(12):3409-17.

84. Peregrin-Alvarez JM, Tsoka S, Ouzounis CA. The phylogenetic extent of metabolic enzymes and pathways. Genome Res. 2003;13(3):422-7.

85. Pruss KM, Sonnenburg JL. *C. difficile* exploits a host metabolite produced during toxin-mediated disease. Nature. 2021;593:261-5.

86. Lopatkin AJ, Bening SC, Manson AL, Stokes JM, Kohanski MA, Badran AH, *et al.* Clinically relevant mutations in core metabolic genes confer antibiotic resistance. Science. 2021;371(6531).

87. Weinert LA, Welch JJ. Why might bacterial pathogens have small genomes? Trends Ecol Evol. 2017;32(12):936-47.

88. Brown SA, Palmer KL, Whiteley M. Revisiting the host as a growth medium. Nat Rev Microbiol. 2008;6(9):657-66.

89. Boulette ML, Baynham PJ, Jorth PA, Kukavica-Ibrulj I, Longoria A, Barrera K, *et al.* Characterization of alanine catabolism in *Pseudomonas aeruginosa* and its importance for proliferation *in vivo*. J Bacteriol. 2009;191(20):6329-34.

90. Hofreuter D, Mohr J, Wensel O, Rademacher S, Schreiber K, Schomburg D, *et al.* Contribution of amino acid catabolism to the tissue specific persistence of *Campylobacter jejuni* in a murine colonization model. PLoS One. 2012;7(11):e50699.

91. Exley RM, Wu H, Shaw J, Schneider MC, Smith H, Jerse AE, *et al.* Lactate acquisition promotes successful colonization of the murine genital tract by *Neisseria gonorrhoeae*. Infect Immun. 2007;75(3):1318-24.

92. Pandey AK, Sassetti CM. Mycobacterial persistence requires the utilization of host cholesterol. Proc Natl Acad Sci U S A. 2008;105(11):4376-80.

93. Grubmüller S, Schauer K, Goebel W, Fuchs TM, Eisenreich W. Analysis of carbon substrates used by *Listeria monocytogenes* during growth in J774A.1 macrophages suggests a bipartite intracellular metabolism. Front Cell Infect Microbiol. 2014;4:156.

94. Häuslein I, Manske C, Goebel W, Eisenreich W, Hilbi H. Pathway analysis using ^{13}C-glycerol and other carbon tracers reveals a bipartite metabolism of *Legionella pneumophila*. Mol Microbiol. 2016;100(2):229-46.

95. Häuslein I, Cantet F, Reschke S, Chen F, Bonazzi M, Eisenreich W. Multiple substrate usage of *Coxiella burnetii* to feed a bipartite metabolic network. Front Cell Infect Microbiol. 2017;7:285.

96. Bowden SD, Rowley G, Hinton JC, Thompson A. Glucose and glycolysis are required for the successful infection of macrophages and mice by *Salmonella enterica* serovar typhimurium. Infect Immun. 2009;77(7):3117-26.

97. Marrero J, Trujillo C, Rhee KY, Ehrt S. Glucose phosphorylation is required for *Mycobacterium tuberculosis* persistence in mice. PLoS Pathog. 2013;9(1):e1003116.

98. Chang DE, Smalley DJ, Tucker DL, Leatham MP, Norris WE, Stevenson SJ, *et al.* Carbon nutrition of *Escherichia coli* in the mouse intestine. Proc Natl Acad Sci U S A. 2004;101(19):7427-32.

99. Patra T, Koley H, Ramamurthy T, Ghose AC, Nandy RK. The Entner-Doudoroff pathway is obligatory for gluconate utilization and contributes to the pathogenicity of *Vibrio cholerae*. J Bacteriol. 2012;194(13):3377-85.

100. Mercado-Lubo R, Gauger EJ, Leatham MP, Conway T, Cohen PS. A *Salmonella enterica* serovar typhimurium succinate dehydrogenase/fumarate reductase double mutant is avirulent and immunogenic in BALB/c mice. Infect Immun. 2008;76(3):1128-34.

101. Mercado-Lubo R, Leatham MP, Conway T, Cohen PS. *Salmonella enterica* serovar typhimurium mutants unable to convert malate to pyruvate and oxaloacetate are avirulent and immunogenic in BALB/c mice. Infect Immun. 2009;77(4):1397-405.

102. Rajeeve K, Vollmuth N, Janaki-Raman S, Wulff TF, Baluapuri A, Dejure FR, *et al.* Reprogramming of host glutamine metabolism during *Chlamydia trachomatis* infection and its key role in peptidoglycan synthesis. Nat Microbiol. 2020.

103. Stritzker J, Janda J, Schoen C, Taupp M, Pilgrim S, Gentschev I, *et al.* Growth, virulence, and immunogenicity of *Listeria monocytogenes* aro mutants. Infect Immun. 2004;72(10):5622-9.

104. Chatterjee SS, Hossain H, Otten S, Kuenne C, Kuchmina K, Machata S, *et al.* Intracellular gene expression profile of *Listeria monocytogenes*. Infect Immun. 2006;74(2):1323-38.

105. Schauer K, Geginat G, Liang C, Goebel W, Dandekar T, Fuchs TM. Deciphering the intracellular metabolism of *Listeria monocytogenes* by mutant screening and modelling. BMC Genomics. 2010;11:573.

106. Palace SG, Proulx MK, Lu S, Baker RE, Goguen JD. Genome-wide mutant fitness profiling identifies nutritional requirements for optimal growth of *Yersinia pestis* in deep tissue. mBio. 2014;5(4).

107. Olive AJ, Sassetti CM. Metabolic crosstalk between host and pathogen: sensing, adapting and competing. Nat Rev Microbiol. 2016;14(4):221-34.

108. Agata N, Ohta M, Mori M, Shibayama K. Growth conditions of and emetic toxin production by *Bacillus cereus* in a defined medium with amino acids. Microbiol Immunol. 1999;43(1):15-8.

109. Haber A, Friedman S, Lobel L, Burg-Golani T, Sigal N, Rose J, *et al.* L-glutamine induces expression of *Listeria monocytogenes* virulence genes. PLoS Pathog. 2017;13(1):e1006161.

110. Hammer BK, Swanson MS. Co-ordination of *Legionella pneumophila* virulence with entry into stationary phase by ppGpp. Mol Microbiol. 1999;33(4):721-31.

111. Pacheco AR, Curtis MM, Ritchie JM, Munera D, Waldor MK, Moreira CG, *et al.* Fucose sensing regulates bacterial intestinal colonization. Nature. 2012;492(7427):113-7.

112. Ferrando ML, van Baarlen P, Orru G, Piga R, Bongers RS, Wels M, *et al.* Carbohydrate availability regulates virulence gene expression in *Streptococcus suis*. PLoS One. 2014;9(3):e89334.

113. Hacker J, Kaper JB. Pathogenicity islands and the evolution of microbes. Annu Rev Microbiol. 2000;54:641-79.

114. Henriquez T, Salazar JC, Marvasi M, Shah A, Corsini G, Toro CS. SRL pathogenicity island contributes to the metabolism of *D*-aspartate via an aspartate racemase in *Shigella flexneri* YSH6000. PLoS One. 2020;15(1):e0228178.

115. Elder JR, Paul NC, Burin R, Guard J, Shah DH. Genomic organization and role of SPI-13 in nutritional fitness of *Salmonella*. Int J Med Microbiol. 2018;308(8):1043-52.

116. Joseph B, Mertins S, Stoll R, Schar J, Umesha KR, Luo Q, *et al.* Glycerol metabolism and PrfA activity in *Listeria monocytogenes*. J Bacteriol. 2008;190(15):5412-30.

117. de las Heras A, Cain RJ, Bielecka MK, Vazquez-Boland JA. Regulation of *Listeria* virulence: PrfA master and commander. Curr Opin Microbiol. 2011;14(2):118-27.

118. Reniere ML, Whiteley AT, Hamilton KL, John SM, Lauer P, Brennan RG, *et al.* Glutathione activates virulence gene expression of an intracellular pathogen. Nature. 2015;517(7533):170-3.

119. Lobel L, Sigal N, Borovok I, Belitsky BR, Sonenshein AL, Herskovits AA. The metabolic regulator CodY links *Listeria monocytogenes* metabolism to virulence by directly activating the virulence regulatory gene prfA. Mol Microbiol. 2015;95(4):624-44.

120. Frenzel E, Doll V, Pauthner M, Lucking G, Scherer S, Ehling-Schulz M. CodY orchestrates the expression of virulence determinants in emetic *Bacillus cereus* by impacting key regulatory circuits. Mol Microbiol. 2012;85(1):67-88.

121. Waters NR, Samuels DJ, Behera RK, Livny J, Rhee KY, Sadykov MR*, et al.* A spectrum of CodY activities drives metabolic reorganization and virulence gene expression in *Staphylococcus aureus*. Mol Microbiol. 2016;101(3):495-514.

122. Timmermans J, Van Melderen L. Post-transcriptional global regulation by CsrA in bacteria. Cell Mol Life Sci. 2010;67(17):2897-908.

123. Häuslein I, Sahr T, Escoll P, Klausner N, Eisenreich W, Buchrieser C. *Legionella pneumophila* CsrA regulates a metabolic switch from amino acid to glycerolipid metabolism. Open Biol. 2017;7(11).

124. Sahr T, Rusniok C, Impens F, Oliva G, Sismeiro O, Coppee JY*, et al.* The *Legionella pneumophila* genome evolved to accommodate multiple regulatory mechanisms controlled by the CsrA-system. PLoS Genet. 2017;13(2):e1006629.

125. Heroven AK, Bohme K, Dersch P. The Csr/Rsm system of *Yersinia* and related pathogens: A post-transcriptional strategy for managing virulence. RNA Biol. 2012;9(4):379-91.

126. Görke B, Stülke J. Carbon catabolite repression in bacteria: Many ways to make the most out of nutrients. Nat Rev Microbiol. 2008;6(8):613-24.

127. Shelburne SA, 3rd, Keith D, Horstmann N, Sumby P, Davenport MT, Graviss EA*, et al.* A direct link between carbohydrate utilization and virulence in the major human pathogen group A *Streptococcus*. Proc Natl Acad Sci U S A. 2008;105(5):1698-703.

128. Carvalho SM, Kloosterman TG, Kuipers OP, Neves AR. CcpA ensures optimal metabolic fitness of *Streptococcus pneumoniae*. PLoS One. 2011;6(10):e26707.

129. Gore AL, Payne SM. CsrA and Cra influence *Shigella flexneri* pathogenesis. Infect Immun. 2010;78(11):4674-82.

130. Njoroge JW, Nguyen Y, Curtis MM, Moreira CG, Sperandio V. Virulence meets metabolism: Cra and KdpE gene regulation in enterohemorrhagic *Escherichia coli*. mBio. 2012;3(5):e00280-12.

131. Camejo A, Buchrieser C, Couve E, Carvalho F, Reis O, Ferreira P*, et al. In vivo* transcriptional profiling of *Listeria monocytogenes* and mutagenesis identify new virulence factors involved in infection. PLoS Pathog. 2009;5(5):e1000449.

132. Van de Velde S, Delaive E, Dieu M, Carryn S, Van Bambeke F, Devreese B*, et al.* Isolation and 2-D-DIGE proteomic analysis of intracellular and extracellular forms of *Listeria monocytogenes*. Proteomics. 2009;9(24):5484-96.

133. Panayidou S, Georgiades K, Christofi T, Tamana S, Promponas VJ, Apidianakis Y. *Pseudomonas aeruginosa* core metabolism exerts a widespread growth-independent control on virulence. Sci Rep. 2020;10(1):9505.

134. Henderson B, Martin A. Bacterial virulence in the moonlight: Multitasking bacterial moonlighting proteins are virulence determinants in infectious disease. Infect Immun. 2011;79(9):3476-91.

135.   Henderson B. An overview of protein moonlighting in bacterial infection. Biochem Soc Trans. 2014;42(6):1720-7.

136.   Kim KP, Jagadeesan B, Burkholder KM, Jaradat ZW, Wampler JL, Lathrop AA, *et al.* Adhesion characteristics of Listeria adhesion protein (LAP)-expressing *Escherichia coli* to Caco-2 cells and of recombinant LAP to eukaryotic receptor Hsp60 as examined in a surface plasmon resonance sensor. FEMS Microbiol Lett. 2006;256(2):324-32.

137.   Pancholi V, Fischetti VA. alpha-enolase, a novel strong plasmin(ogen) binding protein on the surface of pathogenic *Streptococci*. J Biol Chem. 1998;273(23):14503-15.

138.   Weng Y, Chen F, Liu Y, Zhao Q, Chen R, Pan X*, et al. Pseudomonas aeruginosa* enolase influences bacterial tolerance to oxidative stresses and virulence. Front Microbiol. 2016;7:1999.

139.   Hemmadi V, Biswas M. An overview of moonlighting proteins in *Staphylococcus aureus* infection. Arch Microbiol. 2021;203(2):481-98.

140.   Maze A, Glatter T, Bumann D. The central metabolism regulator EIIAGlc switches *Salmonella* from growth arrest to acute virulence through activation of virulence factor secretion. Cell Rep. 2014;7(5):1426-33.

141.   Wang L, Wu J, Li J, Yang H, Tang T, Liang H*, et al.* Host-mediated ubiquitination of a mycobacterial protein suppresses immunity. Nature. 2020;577(7792):682-8.

142.   Madureira P, Baptista M, Vieira M, Magalhaes V, Camelo A, Oliveira L*, et al. Streptococcus agalactiae* GAPDH is a virulence-associated immunomodulatory protein. J Immunol. 2007;178(3):1379-87.

143.   Appelberg R. Macrophage nutriprive antimicrobial mechanisms. J Leukoc Biol. 2006;79(6):1117-28.

144.   Passalacqua KD, Charbonneau ME, O'Riordan MXD. Bacterial metabolism shapes the host-pathogen interface. Microbiol Spectr. 2016;4(3).

145.   Sprenger M, Kasper L, Hensel M, Hube B. Metabolic adaptation of intracellular bacteria and fungi to macrophages. Int J Med Microbiol. 2018;308(1):215-27.

146.   Escoll P, Buchrieser C. Metabolic reprogramming of host cells upon bacterial infection: Why shift to a Warburg-like metabolism? FEBS J. 2018.

147.   Hayek I, Berens C, Lührmann A. Modulation of host cell metabolism by T4SS-encoding intracellular pathogens. Curr Opin Microbiol. 2019;47:59-65.

148.   Best A, Abu Kwaik Y. Nutrition and bipartite metabolism of intracellular pathogens. Trends Microbiol. 2019;27(6):550-61.

149.   Traven A, Naderer T. Central metabolic interactions of immune cells and microbes: Prospects for defeating infections. EMBO Rep. 2019;20(7):e47995.

150.   Eisenreich W, Rudel T, Heesemann J, Goebel W. How viral and intracellular bacterial pathogens reprogram the metabolism of host cells to allow their intracellular replication. Front Cell Infect Microbiol. 2019;9.

151.   Dramé M, Buchrieser C, Escoll P. Danger-associated metabolic modifications during bacterial infection of macrophages. Int Immunol. 2020;32(7):475-83.

152.   Allen PE, Martinez JJ. Modulation of host lipid pathways by pathogenic intracellular bacteria. Pathogens. 2020;9(8).

153.   Price CTD, Abu Kwaik Y. Evolution and adaptation of *Legionella pneumophila* to manipulate the ubiquitination machinery of its amoebae and mammalian hosts. Biomolecules. 2021;11(1).

154.   Lachmandas E, Boutens L, Ratter JM, Hijmans A, Hooiveld GJ, Joosten LA, *et al.* Microbial stimulation of different Toll-like receptor signalling pathways induces diverse metabolic programmes in human monocytes. Nat Microbiol. 2016;2:16246.

155.   Zhou R, Yazdi AS, Menu P, Tschopp J. A role for mitochondria in NLRP3 inflammasome activation. Nature. 2011;469(7329):221-5.

156.   Wolf AJ, Reyes CN, Liang W, Becker C, Shimada K, Wheeler ML, *et al.* Hexokinase is an innate immune receptor for the detection of bacterial peptidoglycan. Cell. 2016;166(3):624-36.

157.   Wu H, Gong J, Liu Y. Indoleamine 2, 3-dioxygenase regulation of immune response Mol Med Rep. 2018;17(4):4867-73.

158.   Michelucci A, Cordes T, Ghelfi J, Pailot A, Reiling N, Goldmann O, *et al.* Immune-responsive gene 1 protein links metabolism to immunity by catalyzing itaconic acid production. Proc Natl Acad Sci U S A. 2013;110(19):7820-5.

159.   Li R, Zhang P, Wang Y, Tao K. Itaconate: A metabolite regulates inflammation response and oxidative stress. Oxid Med Cell Longev. 2020;2020:5404780.

160.   Abu Kwaik Y, Bumann D. Microbial quest for food in vivo: 'Nutritional virulence' as an emerging paradigm. Cell Microbiol. 2013;15(6):882-90.

161.   Abu Kwaik Y, Bumann D. Host delivery of favorite meals for intracellular pathogens. PLoS Pathog. 2015;11(6):e1004866.

162.   Wieland H, Ullrich S, Lang F, Neumeister B. Intracellular multiplication of *Legionella pneumophila* depends on host cell amino acid transporter SLC1A5. Mol Microbiol. 2005;55(5):1528-37.

163.   Barel M, Meibom K, Dubail I, Botella J, Charbit A. *Francisella tularensis* regulates the expression of the amino acid transporter SLC1A5 in infected THP-1 human monocytes. Cell Microbiol. 2012;14(11):1769-83.

164.   Das P, Lahiri A, Lahiri A, Sen M, Iyer N, Kapoor N, *et al.* Cationic amino acid transporters and *Salmonella Typhimurium* ArgT collectively regulate arginine availability towards intracellular Salmonella growth. PLoS One. 2010;5(12):e15466.

165.   Gouzy A, Larrouy-Maumus G, Wu TD, Peixoto A, Levillain F, Lugo-Villarino G, *et al.* *Mycobacterium tuberculosis* nitrogen assimilation and host colonization require aspartate. Nat Chem Biol. 2013;9(11):674-6.

166.   Sauer JD, Bachman MA, Swanson MS. The phagosomal transporter A couples threonine acquisition to differentiation and replication of *Legionella pneumophila* in macrophages. Proc Natl Acad Sci U S A. 2005;102(28):9924-9.

167.   Almagro-Moreno S, Boyd EF. Insights into the evolution of sialic acid catabolism among bacteria. BMC Evol Biol. 2009;9:118.

168.   Ali MM, Newsom DL, Gonzalez JF, Sabag-Daigle A, Stahl C, Steidley B, *et al.* Fructose-asparagine is a primary nutrient during growth of *Salmonella* in the inflamed intestine. PLoS Pathog. 2014;10(6):e1004209.

169.   Rosenberg G, Yehezkel D, Hoffman D, Mattioli CC, Fremder M, Ben-Arosh H, *et al.* Host succinate is an activation signal for *Salmonella* virulence during intracellular infection. Science. 2021;371(6527):400-5.

170.   Kavermann H, Burns BP, Angermüller K, Odenbreit S, Fischer W, Melchers K, *et al.* Identification and characterization of *Helicobacter pylori* genes essential for gastric colonization. J Exp Med. 2003;197(7):813-22.

171.   Speer A, Sun J, Danilchanka O, Meikle V, Rowland JL, Walter K, *et al.* Surface hydrolysis of sphingomyelin by the outer membrane protein Rv0888 supports replication of *Mycobacterium tuberculosis* in macrophages. Mol Microbiol. 2015;97(5):881-97.

172.   Herker E, Ott M. Emerging role of lipid droplets in host/pathogen interactions. J Biol Chem. 2012;287(4):2280-7.

173.   Bah A, Vergne I. Macrophage autophagy and bacterial infections. Front Immunol. 2017;8:1483.

174.   Niu H, Xiong Q, Yamamoto A, Hayashi-Nishino M, Rikihisa Y. Autophagosomes induced by a bacterial Beclin 1 binding protein facilitate obligatory intracellular infection. Proc Natl Acad Sci U S A. 2012;109(51):20800-7.

175.   Tattoli I, Sorbara MT, Vuckovic D, Ling A, Soares F, Carneiro LA, *et al.* Amino acid starvation induced by invasive bacterial pathogens triggers an innate host defense program. Cell Host Microbe. 2012;11(6):563-75.

176.   Hackett EE, Charles-Messance H, O'Leary SM, Gleeson LE, Munoz-Wolf N, Case S, *et al.* *Mycobacterium tuberculosis* limits host glycolysis and IL-1beta by restriction of PFK-M *via* microRNA-21. Cell Rep. 2020;30(1):124-36 e4.

177.   Beste DJ, Bonde B, Hawkins N, Ward JL, Beale MH, Noack S, *et al.* [13]C metabolic flux analysis identifies an unusual route for pyruvate dissimilation in *Mycobacteria* which requires isocitrate lyase and carbon dioxide fixation. PLoS Pathog. 2011;7(7):e1002091.

178.   Singh V, Jamwal S, Jain R, Verma P, Gokhale R, Rao KV. *Mycobacterium tuberculosis*-driven targeted recalibration of macrophage lipid homeostasis promotes the foamy phenotype. Cell Host Microbe. 2012;12(5):669-81.

179.   Cumming BM, Addicott KW, Adamson JH, Steyn AJ. *Mycobacterium tuberculosis* induces decelerated bioenergetic metabolism in human macrophages. Elife. 2018;7.

180.   Eisele NA, Ruby T, Jacobson A, Manzanillo PS, Cox JS, Lam L, *et al.* *Salmonella* require the fatty acid regulator PPARdelta for the establishment of a metabolic environment essential for long-term persistence. Cell Host Microbe. 2013;14(2):171-82.

181.   Czyz DM, Willett JW, Crosson S. *Brucella abortus* induces a Warburg shift in host metabolism that is linked to enhanced intracellular survival of the pathogen. J Bacteriol. 2017;199(15).

182.   Xu C, Liu X, Zha H, Fan S, Zhang D, Li S, *et al.* A pathogen-derived effector modulates host glucose metabolism by arginine GlcNAcylation of HIF-1alpha protein. PLoS Pathog. 2018;14(8):e1007259.

183.   Mehlitz A, Eylert E, Huber C, Lindner B, Vollmuth N, Karunakaran K, *et al.* Metabolic adaptation of *Chlamydia trachomatis* to mammalian host cells. Mol Microbiol. 2017;103(6):1004-19.

184.   da Silva RR, Dorrestein PC, Quinn RA. Illuminating the dark matter in metabolomics. Proc Natl Acad Sci U S A. 2015;112(41):12549-50.

185.   Schoenheimer R, Rittenberg D. Deuterium as an Indicator in the study of intermediary metabolism. Science. 1935;82(2120):156-7.

186.   Hevesy G. The absorption and translocation of lead by plants: A contribution to the application of the method of radioactive indicators in the investigation of the change of substance in plants. Biochem J. 1923;17(4-5):439-45.

187.   Knoop F. Der Abbau aromatischer Fettsäuren im Tierkörper: Kuttruff; 1904.

188.   Kennedy EP. Hitler's gift and the era of biosynthesis. J Biol Chem. 2001;276(46):42619-31.

189.   King AS, Birge RT. An isotope of carbon, mass 13. Nature. 1929;124(3117):127.

190.   Giauque WF, Johnston HL. An isotope of oxygen, mass 18. Nature. 1929;123(3096):318.

191.   Naudé SM. An isotope of nitrogen, mass 15. Phys Rev. 1929;34(11):1498-9.

192.   Urey HC, Brickwedde FG, Murphy GM. A hydrogen isotope of mass 2 and its concentration. Phys Rev. 1932;40(1):1-15.

193.   Chiewitz O, Hevesy G. Radioactive indicators in the study of phosphorus metabolism in rats. Nature. 1935;136(3445):754-5.

194.   Ruben S, Kamen MD. Radioactive carbon of long half-life. Phys Rev. 1940;57(6):549-.

195.   Kamen MD. Production and isotopic assignment of long-lived radioactive sulfur Phys Rev. 1941;60(8):537-41.

196.   Erb TJ, Zarzycki J. A short history of RubisCO: The rise and fall (?) of Nature's predominant CO_2 fixing enzyme. Curr Opin Biotechnol. 2018;49:100-7.

197.   Wood HG, Werkman CH. The utilisation of CO_2 in the dissimilation of glycerol by the propionic acid bacteria. Biochem J. 1936;30(1):48-53.

198.   Wood HG, Werkman CH, Hemingway A, Nier AO. Heavy carbon as a tracer in heterotrophic carbon dioxide assimilation. J Biol Chem. 1941;139(1):365-76.

199.   Krebs HA. Carbon dioxide assimilaton in heterotrophic organisms. Annu Rev Biochem. 1943;12(1):529-50.

200.   Barker HA, Ruben S, Kamen MD. The reduction of radioactive carbon dioxide by methane-producing bacteria. Proc Natl Acad Sci U S A. 1940;26(6):426-30.

201.   Wood HG. The fixation of carbon dioxide and the inter-relationships of the tricarboxylic acid cycle. Physiol Rev. 1946;26:198-246.

202.   Klein ER, Klein PD. A selected bibliography of biomedical and environmental applications of stable isotopes. V-^{2}H, ^{13}C, ^{15}N, ^{18}O and ^{34}S, 1977-1978. Biomed Mass Spectrom. 1979;6(12):515-45.

5 References

203. Modak AS. Stable isotope breath tests in clinical medicine: A review. J Breath Res. 2007;1(1):014003.

204. Lehmann WD. A timeline of stable isotopes and mass spectrometry in the life sciences. Mass Spectrom Rev. 2017;36(1):58-85.

205. Collins BC, Hunter CL, Liu Y, Schilling B, Rosenberger G, Bader SL, *et al.* Multi-laboratory assessment of reproducibility, qualitative and quantitative performance of SWATH-mass spectrometry. Nat Commun. 2017;8(1):291.

206. Giraldez MD, Spengler RM, Etheridge A, Godoy PM, Barczak AJ, Srinivasan S, *et al.* Comprehensive multi-center assessment of small RNA-seq methods for quantitative miRNA profiling. Nat Biotechnol. 2018;36(8):746-57.

207. Noor E, Cherkaoui S, Sauer U. Biological insights through omics data integration. Curr Opin Syst Biol. 2019;15:39-47.

208. Chokkathukalam A, Kim DH, Barrett MP, Breitling R, Creek DJ. Stable isotope-labeling studies in metabolomics: New insights into structure and dynamics of metabolic networks. Bioanalysis. 2014;6(4):511-24.

209. McKnight SL. On getting there from here. Science. 2010;330(6009):1338-9.

210. Audano M, Pedretti S, Ligorio S, Giavarini F, Caruso D, Mitro N. Investigating metabolism by mass spectrometry: From steady state to dynamic view. J Mass Spectrom. 2020:e4658.

211. Shi X, Xi B, Jasbi P, Turner C, Jin Y, Gu H. Comprehensive isotopic targeted mass spectrometry: Reliable metabolic flux analysis with broad coverage. Anal Chem. 2020;92(17):11728-38.

212. Adrian L, Marco-Urrea E. Isotopes in geobiochemistry: Tracing metabolic pathways in microorganisms of environmental relevance with stable isotopes. Curr Opin Biotechnol. 2016;41:19-25.

213. Fernandez-Garcia J, Altea-Manzano P, Pranzini E, Fendt SM. Stable isotopes for tracing mammalian-cell metabolism *in vivo*. Trends Biochem Sci. 2020;45(3):185-201.

214. Dong W, Keibler MA, Stephanopoulos G. Review of metabolic pathways activated in cancer cells as determined through isotopic labeling and network analysis. Metab Eng. 2017;43(Pt B):113-24.

215. Davies PSW. Stable isotopes: Their use and safety in human nutrition studies. Eur J Clin Nutr. 2020;74(3):362-5.

216. Berg IA. Ecological aspects of the distribution of different autotrophic CO_2 fixation pathways. Appl Environ Microbiol. 2011;77(6):1925-36.

217. Wiechert W. [13]C metabolic flux analysis. Metab Eng. 2001;3(3):195-206.

218. Tang YJ, Martin HG, Myers S, Rodriguez S, Baidoo EE, Keasling JD. Advances in analysis of microbial metabolic fluxes via ^{13}C isotopic labeling. Mass Spectrom Rev. 2009;28(2):362-75.

219. Crown SB, Antoniewicz MR. Publishing ^{13}C metabolic flux analysis studies: A review and future perspectives. Metab Eng. 2013;20:42-8.

220. Long CP, Antoniewicz MR. High-resolution ^{13}C metabolic flux analysis. Nat Protoc. 2019;14(10):2856-77.

221. Sauer U. Metabolic networks in motion: ^{13}C-based flux analysis. Mol Syst Biol. 2006;2:62.

222. Jang C, Chen L, Rabinowitz JD. Metabolomics and isotope tracing. Cell. 2018;173(4):822-37.

223. Fischer E, Zamboni N, Sauer U. High-throughput metabolic flux analysis based on gas chromatography-mass spectrometry derived ^{13}C constraints. Anal Biochem. 2004;325(2):308-16.

224. Amador-Noguez D, Feng XJ, Fan J, Roquet N, Rabitz H, Rabinowitz JD. Systems-level metabolic flux profiling elucidates a complete, bifurcated tricarboxylic acid cycle in *Clostridium acetobutylicum*. J Bacteriol. 2010;192(17):4452-61.

225. Wittmann C. Fluxome analysis using GC-MS. Microb Cell Fact. 2007;6:6.

226. Schwechheimer SK, Becker J, Wittmann C. Towards better understanding of industrial cell factories: Novel approaches for ^{13}C metabolic flux analysis in complex nutrient environments. Curr Opin Biotechnol. 2018;54:128-37.

227. Lee WN, Byerley LO, Bergner EA, Edmond J. Mass isotopomer analysis: Theoretical and practical considerations. Biol Mass Spectrom. 1991;20(8):451-8.

228. Takeda H, Nio Y, Omori H, Uegaki K, Hirahara N, Sasaki S, *et al.* Mechanisms of cytotoxic effects of heavy water (deuterium oxide: D_2O) on cancer cells. Anticancer Drugs. 1998;9(8):715-25.

229. Ueno Y, Yamada K, Yoshida N, Maruyama S, Isozaki Y. Evidence from fluid inclusions for microbial methanogenesis in the early Archaean era. Nature. 2006;440(7083):516-9.

230. Bell EA, Boehnke P, Harrison TM, Mao WL. Potentially biogenic carbon preserved in a 4.1 billion-year-old zircon. Proc Natl Acad Sci U S A. 2015;112(47):14518-21.

231. Antoniewicz MR, Kelleher JK, Stephanopoulos G. Accurate assessment of amino acid mass isotopomer distributions for metabolic flux analysis. Anal Chem. 2007;79(19):7554-9.

232. Wasylenko TM, Stephanopoulos G. Kinetic isotope effects significantly influence intracellular metabolite ^{13}C labeling patterns and flux determination. Biotechnol J. 2013;8(9):1080-9.

233. Bacher A, Rieder C, Eichinger D, Arigoni D, Fuchs G, Eisenreich W. Elucidation of novel biosynthetic pathways and metabolite flux patterns by retrobiosynthetic NMR analysis. FEMS Microbiol Rev. 1998;22(5):567-98.

234. Phillips R, Milo R. A feeling for the numbers in biology. Proc Natl Acad Sci U S A. 2009;106(51):21465-71.

235. Bacher A, Eisenreich W. Metabolic studies using the retrobiosynthesis concept – theory, technology, and examples. 2010:675-94.

236. Buescher JM, Antoniewicz MR, Boros LG, Burgess SC, Brunengraber H, Clish CB, *et al.* A roadmap for interpreting ^{13}C metabolite labeling patterns from cells. Curr Opin Biotechnol. 2015;34:189-201.

237. Sauer U, Lasko DR, Fiaux J, Hochuli M, Glaser R, Szyperski T, *et al.* Metabolic flux ratio analysis of genetic and environmental modulations of *Escherichia coli* central carbon metabolism. J Bacteriol. 1999;181(21):6679-88.

238. Wang Y, Wondisford FE, Song C, Zhang T, Su X. Metabolic flux analysis-linking isotope labeling and metabolic fluxes. Metabolites. 2020;10(11).

239.   Beste DJ, Noh K, Niedenführ S, Mendum TA, Hawkins ND, Ward JL, *et al.* ^{13}C-flux spectral analysis of host-pathogen metabolism reveals a mixed diet for intracellular *Mycobacterium tuberculosis*. Chem Biol. 2013;20(8):1012-21.

240.   Eisenreich W, Strauss G, Werz U, Fuchs G, Bacher A. Retrobiosynthetic analysis of carbon fixation in the phototrophic eubacterium *Chloroflexus aurantiacus*. Eur J Biochem. 1993;215(3):619-32.

241.   Eisenreich W, Slaghuis J, Laupitz R, Bussemer J, Stritzker J, Schwarz C, *et al.* [13]C isotopologue perturbation studies of *Listeria monocytogenes* carbon metabolism and its modulation by the virulence regulator PrfA. Proc Natl Acad Sci U S A. 2006;103(7):2040-5.

242.   Buchrieser C, Rusniok C, Kunst F, Cossart P, Glaser P. Comparison of the genome sequences of *Listeria monocytogenes* and *Listeria innocua:* Clues for evolution and pathogenicity. FEMS Immun Med Microbiol. 2003;35(3):207-13.

243.   Eylert E, Schär J, Mertins S, Stoll R, Bacher A, Goebel W, *et al.* Carbon metabolism of *Listeria monocytogenes* growing inside macrophages. Mol Microbiol. 2008;69(4):1008-17.

244.   Gillmaier N, Götz A, Schulz A, Eisenreich W, Goebel W. Metabolic responses of primary and transformed cells to intracellular *Listeria monocytogenes*. PLoS One. 2012;7(12):e52378.

245.   de Carvalho LP, Fischer SM, Marrero J, Nathan C, Ehrt S, Rhee KY. Metabolomics of *Mycobacterium tuberculosis* reveals compartmentalized co-catabolism of carbon substrates. Chem Biol. 2010;17(10):1122-31.

246.   Schnappinger D, Ehrt S, Voskuil MI, Liu Y, Mangan JA, Monahan IM, *et al.* Transcriptional adaptation of *Mycobacterium tuberculosis* within macrophages: Insights into the phagosomal environment. J Exp Med. 2003;198(5):693-704.

247.   Billig S, Schneefeld M, Huber C, Grassl GA, Eisenreich W, Bange FC. Lactate oxidation facilitates growth of *Mycobacterium tuberculosis* in human macrophages. Sci Rep. 2017;7(1):6484.

248.   Borah K, Girardi K, Mendum TA, Lery LMS, Beste DJV, Lara FA, *et al.* Intracellular *Mycobacterium leprae* utilizes host glucose as a carbon source in schwann cells. mBio. 2019;10(6).

249.   Kentner D, Martano G, Callon M, Chiquet P, Brodmann M, Burton O, *et al. Shigella* reroutes host cell central metabolism to obtain high-flux nutrient supply for vigorous intracellular growth. Proc Natl Acad Sci U S A. 2014;111(27):9929-34.

250.   Omsland A, Cockrell DC, Howe D, Fischer ER, Virtaneva K, Sturdevant DE, *et al.* Host cell-free growth of the Q fever bacterium *Coxiella burnetii*. Proc Natl Acad Sci U S A. 2009;106(11):4430-4.

251.   Götz A, Eylert E, Eisenreich W, Goebel W. Carbon metabolism of enterobacterial human pathogens growing in epithelial colorectal adenocarcinoma (Caco-2) cells. PLoS One. 2010;5(5):e10586.

252.   Härtel T, Eylert E, Schulz C, Petruschka L, Gierok P, Grubmüller S, *et al.* Characterization of central carbon metabolism of *Streptococcus pneumoniae* by isotopologue profiling. J Biol Chem. 2012;287(6):4260-74.

253.   Willenborg J, Huber C, Koczula A, Lange B, Eisenreich W, Valentin-Weigand P, *et al.* Characterization of the pivotal carbon metabolism of *Streptococcus suis* serotype 2 under ex vivo and chemically defined *in vitro* conditions by isotopologue profiling. J Biol Chem. 2015;290(9):5840-54.

254. Kriegeskorte A, Grubmüller S, Huber C, Kahl BC, von Eiff C, Proctor RA*, et al. Staphylococcus aureus* small colony variants show common metabolic features in central metabolism irrespective of the underlying auxotrophism. Front Cell Infect Microbiol. 2014;4:141.

255. Gao B, Vorwerk H, Huber C, Lara-Tejero M, Mohr J, Goodman AL*, et al.* Metabolic and fitness determinants for in vitro growth and intestinal colonization of the bacterial pathogen *Campylobacter jejuni*. PLoS Biol. 2017;15(5):e2001390.

256. Lassek C, Berger A, Zuhlke D, Wittmann C, Riedel K. Proteome and carbon flux analysis of *Pseudomonas aeruginosa* clinical isolates from different infection sites. Proteomics. 2016;16(9):1381-5.

257. Dolan SK, Kohlstedt M, Trigg S, Vallejo Ramirez P, Kaminski CF, Wittmann C*, et al.* Contextual flexibility in *Pseudomonas aeruginosa* central carbon metabolism during growth in single carbon sources. mBio. 2020;11(2).

258. Opperman MJ, Shachar-Hill Y. Metabolic flux analyses of *Pseudomonas aeruginosa* cystic fibrosis isolates. Metab Eng. 2016;38:251-63.

259. Polzin S, Huber C, Eylert E, Elsenhans I, Eisenreich W, Schmidt H. Growth media simulating ileal and colonic environments affect the intracellular proteome and carbon fluxes of enterohemorrhagic *Escherichia coli* O157:H7 strain EDL933. Appl Environ Microbiol. 2013;79(12):3703-15.

260. Miroshnichenko ML, Rainey FA, Rhode M, Bonch-Osmolovskaya EA. *Hippea maritima* gen. nov., sp. nov., a new genus of thermophilic, sulfur-reducing bacterium from submarine hot vents. Int J Syst Bacteriol. 1999;49 (3):1033-8.

261. Florentino AP, Stams AJ, Sanchez-Andrea I. Genome sequence of *Desulfurella amilsii* strain TR1 and comparative genomics of Desulfurellaceae family. Front Microbiol. 2017;8:222.

262. Huntemann M, Lu M, Nolan M, Lapidus A, Lucas S, Hammon N*, et al.* Complete genome sequence of the thermophilic sulfur-reducer *Hippea maritima* type strain (MH(2)). Stand Genomic Sci. 2011;4(3):303-11.

263. Lang JM, Darling AE, Eisen JA. Phylogeny of bacterial and archaeal genomes using conserved genes: Supertrees and supermatrices. PLoS One. 2013;8(4):e62510.

264. Waite DW, Vanwonterghem I, Rinke C, Parks DH, Zhang Y, Takai K*, et al.* Comparative genomic analysis of the class Epsilonproteobacteria and proposed reclassification to Epsilonbacteraeota (phyl. nov.). Front Microbiol. 2017;8:682.

265. Flores GE, Hunter RC, Liu Y, Mets A, Schouten S, Reysenbach AL. *Hippea jasoniae* sp. nov. and *Hippea alviniae* sp. nov., thermoacidophilic members of the class Deltaproteobacteria isolated from deep-sea hydrothermal vent deposits. Int J Syst Evol Microbiol. 2012;62(Pt 6):1252-8.

266. Perner M, Gonnella G, Kurtz S, LaRoche J. Handling temperature bursts reaching 464 degrees C: Different microbial strategies in the sisters peak hydrothermal chimney. Appl Environ Microbiol. 2014;80(15):4585-98.

267. Chan CS, Chan KG, Tay YL, Chua YH, Goh KM. Diversity of thermophiles in a Malaysian hot spring determined using 16S rRNA and shotgun metagenome sequencing. Front Microbiol. 2015;6:177.

268. Zakharova YR, Petrova DP, Galachyants YP, Bashenkhaeva MV, Kurilkina MI, Likhoshway YV. Bacterial and archaeal community structure in the surface diatom sediments of deep freshwater lake Baikal (eastern Siberia). Geomicrobiol J. 2018;35(8):635-47.

5 References

269.   Warren JR, Marshall B. Unidentified curved bacilli on gastric epithelium in active chronic gastritis. Lancet. 1983;1(8336):1273-5.

270.   Piscione M, Mazzone M, Di Marcantonio MC, Muraro R, Mincione G. Eradication of *Helicobacter pylori* and gastric cancer: A controversial relationship. Front Microbiol. 2021;12:630852.

271.   Bray F, Ferlay J, Soerjomataram I, Siegel RL, Torre LA, Jemal A. Global cancer statistics 2018: GLOBOCAN estimates of incidence and mortality worldwide for 36 cancers in 185 countries. CA Cancer J Clin. 2018;68(6):394-424.

272.   Blaser MJ. Ecology of *Helicobacter pylori* in the human stomach. J Clin Invest. 1997;100(4):759-62.

273.   Moodley Y, Linz B, Bond RP, Nieuwoudt M, Soodyall H, Schlebusch CM, *et al.* Age of the association between *Helicobacter pylori* and man. PLoS Pathog. 2012;8(5):e1002693.

274.   Hooi JKY, Lai WY, Ng WK, Suen MMY, Underwood FE, Tanyingoh D, *et al.* Global prevalence of *Helicobacter pylori* infection: Systematic review and meta-Analysis. Gastroenterology. 2017;153(2):420-9.

275.   Tacconelli E, Carrara E, Savoldi A, Harbarth S, Mendelson M, Monnet DL, *et al.* Discovery, research, and development of new antibiotics: The WHO priority list of antibiotic-resistant bacteria and tuberculosis. Lancet Infect Dis. 2018;18(3):318-27.

276.   Kelly DJ. The physiology and metabolism of the human gastric pathogen *Helicobacter pylori*. Adv Microb Physiol. 1998;40:137-89.

277.   Marais A, Mendz GL, Hazell SL, Megraud F. Metabolism and genetics of *Helicobacter pylori*: The genome era. Microbiol Mol Biol Rev. 1999;63(3):642-74.

278.   Kim IJ, Lee J, Oh SJ, Yoon MS, Jang SS, Holland RL, *et al. Helicobacter pylori* infection modulates host cell metabolism through VacA-dependent inhibition of mTORC1. Cell Host Microbe. 2018;23(5):583-93 e8.

279.   Chauhan N, Tay ACY, Marshall BJ, Jain U. *Helicobacter pylori* VacA, a distinct toxin exerts diverse functionalities in numerous cells: An overview. Helicobacter. 2018:e12544.

280.   Rokkas T, Ladas S, Liatsos C, Petridou E, Papatheodorou G, Theocharis S, *et al.* Relationship of *Helicobacter pylori* CagA status to gastric cell proliferation and apoptosis. Dig Dis Sci. 1999;44(3):487-93.

281.   Boonyanugomol W, Chomvarin C, Baik SC, Song JY, Hahnvajanawong C, Kim KM, *et al.* Role of cagA-positive *Helicobacter pylori* on cell proliferation, apoptosis, and inflammation in biliary cells. Dig Dis Sci. 2011;56(6):1682-92.

282.   Parsonnet J, Friedman GD, Orentreich N, Vogelman H. Risk for gastric cancer in people with CagA positive or CagA negative *Helicobacter pylori* infection. Gut. 1997;40(3):297-301.

283.   Vander Heiden MG, Cantley LC, Thompson CB. Understanding the Warburg effect: The metabolic requirements of cell proliferation. Science. 2009;324(5930):1029-33.

284.   Takahashi T, Matsumoto T, Nakamura M, Matsui H, Tsuchimoto K, Yamada H. *L*-lactic acid secreted from gastric mucosal cells enhances growth of *Helicobacter pylori*. Helicobacter. 2007;12(5):532-40.

285. Machuca MA, Johnson KS, Liu YC, Steer DL, Ottemann KM, Roujeinikova A. *Helicobacter pylori* chemoreceptor TlpC mediates chemotaxis to lactate. Sci Rep. 2017;7(1):14089.

286. Cover TL, Lacy DB, Ohi MD. The *Helicobacter pylori* Cag type IV secretion system. Trends Microbiol. 2020;28(8):682-95.

287. Ricci V, Giannouli M, Romano M, Zarrilli R. *Helicobacter pylori* gamma-glutamyl transpeptidase and its pathogenic role. World J Gastroenterol. 2014;20(3):630-8.

288. Shibayama K, Wachino J, Arakawa Y, Saidijam M, Rutherford NG, Henderson PJ. Metabolism of glutamine and glutathione *via* gamma-glutamyltranspeptidase and glutamate transport in *Helicobacter pylori*: Possible significance in the pathophysiology of the organism. Mol Microbiol. 2007;64(2):396-406.

289. Baj J, Forma A, Sitarz M, Portincasa P, Garruti G, Krasowska D*, et al. Helicobacter pylori* virulence factors-mechanisms of bacterial pathogenicity in the gastric microenvironment. Cells. 2020;10(1).

290. Huang Y, Wang QL, Cheng DD, Xu WT, Lu NH. Adhesion and invasion of gastric mucosa epithelial cells by *Helicobacter pylori*. Front Cell Infect Microbiol. 2016;6:159.

291. Bansil R, Turner BS. The biology of mucus: Composition, synthesis and organization. Adv Drug Deliv Rev. 2018;124:3-15.

292. Gupta N, Maurya S, Verma H, Verma VK. Unraveling the factors and mechanism involved in persistence: Host-pathogen interactions in *Helicobacter pylori*. J Cell Biochem. 2019;120(11):18572-87.

293. van Amsterdam K, van der Ende A. Nutrients released by gastric epithelial cells enhance *Helicobacter pylori* growth. Helicobacter. 2004;9(6):614-21.

294. Fraser DW, Tsai TR, Orenstein W, Parkin WE, Beecham HJ, Sharrar RG*, et al.* Legionnaires' disease: Description of an epidemic of pneumonia. The New England journal of medicine. 1977;297(22):1189-97.

295. Brown JS. Community-acquired pneumonia. Clin Med. 2012;12(6):538-43.

296. Burillo A, Pedro-Botet ML, Bouza E. Microbiology and Epidemiology of Legionnaire's Disease. Infect Dis Clin North Am. 2017;31(1):7-27.

297. Chauhan D, Shames SR. Pathogenicity and virulence of *Legionella*: Intracellular replication and host response. Virulence. 2021;12(1):1122-44.

298. Boamah DK, Zhou G, Ensminger AW, O'Connor TJ. From many hosts, one accidental pathogen: The diverse protozoan hosts of *Legionella*. Front Cell Infect Microbiol. 2017;7:477.

299. Molofsky AB, Swanson MS. Differentiate to thrive: Lessons from the *Legionella pneumophila* life cycle. Mol Microbiol. 2004;53(1):29-40.

300. Oliva G, Sahr T, Buchrieser C. The life cycle of *L. pneumophila*: Cellular differentiation is linked to virulence and metabolism. Front Cell Infect Microbiol. 2018;8(3).

301. Fonseca MV, Swanson MS. Nutrient salvaging and metabolism by the intracellular pathogen *Legionella pneumophila*. Front Cell Infect Microbiol. 2014;4:12.

5 References

302. Hoffmann C, Harrison CF, Hilbi H. The natural alternative: Protozoa as cellular models for *Legionella* infection. Cell Microbiol. 2014;16(1):15-26.

303. Guimaraes AJ, Gomes KX, Cortines JR, Peralta JM, Peralta RH. *Acanthamoeba* spp. as a universal host for pathogenic microorganisms: One bridge from environment to host virulence. Microbiol Res. 2016;193:30-8.

304. Nisar MA, Ross KE, Brown MH, Bentham R, Whiley H. *Legionella pneumophila* and protozoan hosts: Implications for the control of hospital and potable water systems. Pathogens. 2020;9(4).

305. Burstein D, Amaro F, Zusman T, Lifshitz Z, Cohen O, Gilbert JA, *et al.* Genomic analysis of 38 *Legionella* species identifies large and diverse effector repertoires. Nat Genet. 2016;48(2):167-75.

306. Price C, Jones S, Mihelcic M, Santic M, Abu Kwaik Y. Paradoxical pro-inflammatory responses by human macrophages to an *Amoebae* host-adapted *Legionella* effector. Cell Host Microbe. 2020;27(4):571-84 e7.

307. Lomma M, Dervins-Ravault D, Rolando M, Nora T, Newton HJ, Sansom FM, *et al.* The *Legionella pneumophila* F-box protein Lpp2082 (AnkB) modulates ubiquitination of the host protein parvin B and promotes intracellular replication. Cell Microbiol. 2010;12(9):1272-91.

308. Escoll P, Song OR, Viana F, Steiner B, Lagache T, Olivo-Marin JC, *et al. Legionella pneumophila* modulates mitochondrial dynamics to trigger metabolic repurposing of infected macrophages. Cell Host Microbe. 2017;22(3):302-16 e7.

309. Eylert E, Herrmann V, Jules M, Gillmaier N, Lautner M, Buchrieser C, *et al.* Isotopologue profiling of *Legionella pneumophila*: Role of serine and glucose as carbon substrates. J Biol Chem. 2010;285(29):22232-43.

310. Gillmaier N, Schunder E, Kutzner E, Tlapak H, Rydzewski K, Herrmann V, *et al.* Growth-related metabolism of the carbon storage poly-3-hydroxybutyrate in *Legionella pneumophila*. J Biol Chem. 2016;291(12):6471-82.

311. Heuner K, Eisenreich W. Crosstalk between metabolism and virulence of *Legionella pneumophila*. In: Unden G, Thines E, Schüffler A, editors. Host - Pathogen Interaction; Microbial metabolism, pathogenicity and antiinfectives: Wiley-VCH Verlag GmbH & Co. KGaA, Weinheim, Germany; 2016. p. 19-36.

312. Schreiber S, Konradt M, Groll C, Scheid P, Hanauer G, Werling HO, *et al.* The spatial orientation of *Helicobacter pylori* in the gastric mucus. Proc Natl Acad Sci U S A. 2004;101(14):5024-9.

313. Hirayama A, Kami K, Sugimoto M, Sugawara M, Toki N, Onozuka H, *et al.* Quantitative metabolome profiling of colon and stomach cancer microenvironment by capillary electrophoresis time-of-flight mass spectrometry. Cancer Res. 2009;69(11):4918-25.

314. Dunne C, Dolan B, Clyne M. Factors that mediate colonization of the human stomach by *Helicobacter pylori*. World J Gastroenterol. 2014;20(19):5610-24.

315. Steffens L, Pettinato E, Steiner TM, Mall A, König S, Eisenreich W, *et al.* High CO_2 levels drive the TCA cycle backwards towards autotrophy. Nature. 2021;592(7856):784-8.

316. Muchowska KB, Varma SJ, Chevallot-Beroux E, Lethuillier-Karl L, Li G, Moran J. Metals promote sequences of the reverse Krebs cycle. Nat Ecol Evol. 2017;1(11):1716-21.

317. Braakman R, Smith E. The emergence and early evolution of biological carbon-fixation. PLoS Comput Biol. 2012;8(4):e1002455.

318. Kunze M, Steiner T, Chen F, Huber C, Rydzewski K, Stämmler M*, et al.* Metabolic adaption of *Legionella pneumophila* during intracellular growth in *Acanthamoeba castellanii*. Int J Med Microbiol. 2021;311(4):151504.

319. Steiner TM, Lettl C, Schindele F, Goebel W, Haas R, Fischer W*, et al.* Substrate usage determines carbon flux *via* the citrate cycle in *Helicobacter pylori*. Mol Microbiol. 2021;116(3):841-60.

320. Ma EH, Verway MJ, Johnson RM, Roy DG, Steadman M, Hayes S*, et al.* Metabolic profiling using stable isotope tracing reveals distinct patterns of glucose utilization by physiologically activated CD8(+) T cells. Immunity. 2019;51(5):856-70 e5.

321. McCracken KW, Cata EM, Crawford CM, Sinagoga KL, Schumacher M, Rockich BE*, et al.* Modelling human development and disease in pluripotent stem-cell-derived gastric organoids. Nature. 2014;516(7531):400-4.

322. Dutta D, Clevers H. Organoid culture systems to study host-pathogen interactions. Curr Opin Immunol. 2017;48:15-22.

323. Alzeeb G, Metges JP, Corcos L, Le Jossic-Corcos C. Three-dimensional culture systems in gastric cancer research. Cancers 2020;12(10).

324. Lau HCH, Kranenburg O, Xiao H, Yu J. Organoid models of gastrointestinal cancers in basic and translational research. Nat Rev Gastroenterol Hepatol. 2020;17(4):203-22.

325. Bartfeld S, Bayram T, van de Wetering M, Huch M, Begthel H, Kujala P*, et al. In vitro* expansion of human gastric epithelial stem cells and their responses to bacterial infection. Gastroenterology. 2015;148(1):126-36 e6.

326. Schlaermann P, Toelle B, Berger H, Schmidt SC, Glanemann M, Ordemann J*, et al.* A novel human gastric primary cell culture system for modelling *Helicobacter pylori* infection in vitro. Gut. 2016;65(2):202-13.

327. Chakrabarti J, Zavros Y. Generation and use of gastric organoids for the study of *Helicobacter pylori* pathogenesis. Methods Cell Biol. 2020;159:23-46.

328. Wroblewski LE, Piazuelo MB, Chaturvedi R, Schumacher M, Aihara E, Feng R*, et al. Helicobacter pylori* targets cancer-associated apical-junctional constituents in gastroids and gastric epithelial cells. Gut. 2015;64(5):720-30.